Methodological Considerations and Clinical Relevance of Diffusion Tensor Imaging in Acute Stroke Prognosis

Eric Moulton

SORBONNE UNIVERSITÉ

École Doctorale Cerveau Cognition Comportement

Institut du Cerveau et de la Mœlle Épinière

Methodological Considerations and Clinical Relevance of Diffusion Tensor Imaging in Acute Stroke Prognosis

---

Par Eric MOULTON

Thèse de Doctorat de Neurosciences

Dirigée par le Dr. Charlotte ROSSO

Présentée et soutenue publiquement le 14 mars 2019

Devant un jury composé de:

Pr. KRAINIK Alexandre	Professeur des Universités	Rapporteur
Dr. JAILLARD Assia	Praticien Hospitalier-HDR	Rapporteur
Pr. SAMSON Yves	Professeur des Universités	Examinateur
Dr. RONDINA Jane	Research Associate	Examinateur
Dr. ROSSO Charlotte	Maître de Conférence Université-Praticien Hospitalier	Directrice de Thèse

Contents

Acknowledgements

First of all, I would like to express my sincere gratitude to my advisor Charlotte Rosso who kindly welcomed me into her lab for my Master's research project and PhD studies. You have given me invaluable advice, tools, and insights over these past five years, and your guidance has helped me grow and attain many personal and professional goals. I am extremely thankful to you for your involvement in my thesis work and for encouraging me to explore my own research interests during my doctoral studies.

I would also like to thank my thesis committee members, Alexandre Krainik, Assia Jaillard, Yves Samson, and Jane Rondina for taking the time to read this manuscript and agreeing to be part of the jury.

A special thanks to my colleagues and friends at Babinski and Paul Castaigne, notably Chiara Zavanone, Giulia Frasca Polara, Raphaël Lebouc, and Sara Leder who kindly allowed me to evaluate a number of their patients during their busy consultation hours. The work in this thesis would also not have been possible without Christine Pires's meticulous bookkeeping of all of the medical records. Finally, I would like to show my appreciation to Yves Samson for our rich discussions and his involvement in my scientific writing.

Many thanks to Marie Vidailhet and Stéphane Lehéricy and the entire MOVIT team for hosting me over the years.

Thanks also to all my colleagues and friends from the CENIR for your help during scanning and advice during team meetings. A particular mention goes out to Romain Valabregue who indulged me in my curiosity for data science, machine learning, and deep learning. Our discussions, collaborations, and data challenges have allowed me to accomplish so much during my time at the ICM, and for that, I am thankful.

My seemingly endless analyses could not have gone smoother without the help of my pals in IT, Ludovic Prévost and Maxime Kermarquer. Your patience, instruction, and great sense of humor was instrumental to the completion of my PhD.

My friends, especially from the salle 1.001, have been a source of inspiration, motivation, and – above all – amusement. In no particular order, Fatma, Olivier,

Fernando, Isaac, Sophie, Gizem, Maya, Benjamin, you have made my time at the ICM unforgettable. I would like to extend a special thanks to my one and only team member, Claire Kemlin. You have been a great source of support, and I truly cherish the time we spent together during our PhD.

Of course, none of this would have been possible without the loving support of my family. Thank you for believing in me and always encouraging me at every step of the way. My undergraduate and graduate studies have been the most enriching experience of my life, and I owe it all to you.

It goes without saying that I am eternally grateful to my wife Beatrice for being at my side throughout this journey. Thank you for always loving and encouraging my fascination with science.

Source of funding: This thesis would also not have been possible without the precious sources of financial aid. I therefore thank Edouard de Royère, the Fondation Philips, and the Fondation AVC.

List of Publications

Published Works

Moulton, E., Valabrègue, R., Díaz, B., Kemlin, C., Leder, S., Lehéricy, S., Samson, Y., Rosso, C., 2018. Comparison of spatial normalization strategies of diffusion MRI data for studying motor outcome in subacute-chronic and acute stroke. *Neuroimage* 183, 186–199.

Submitted Articles

Moulton, E., Valabrègue, Lehéricy, S., Samson, Y., Rosso, C. Multivariate prediction of long-term functional outcome of acute ischemic stroke with DTI. *NeuroImage: Clinical*. *In Revision*.

Moulton, E., Magno, S., Valabregue, S., Amor-Sahli, M., Pires, C., Lehéricy, S., Leger, A., Samson, Y., Rosso, C. Acute diffusivity biomarkers for prediction of motor and language outcome in mild-to-severe stroke patients. *Stroke*. *Submitted*.

Additional publications and contributions parallel to the current thesis

Kemlin, C., **Moulton, E.**, Leder, S., Houot, M., Meunier, S., Rosso C., Lamy JC. *In Prep*. Redundancy among parameters describing the input-output relation of motor evoked potentials.

Kemlin C., **Moulton E.**, Houot M., Lamy JC., Rosso C. *In Prep*. Are corticospinal structure and excitability independent to explain upper limb motor impairment after stroke?

Moulton, E., Bouhali, F., Monzalvo, K., Poupon, C., Zhang, H., Dehaene, S., Dehaene-Lambertz, G., Dubois, J. Connectivity between the Visual Word Form Area and the parietal lobe improves after the first year of reading instruction: a longitudinal MRI study in children. *Brain Structure and Function*. *In Revision*.

Rosso, C., Baronnet, F., Diaz, B., Le Bouc, R., Frasca Polara, G., **Moulton, E.J.**, Deltour, S., Leger, A., Crozier, S., Samson, Y., 2018. The silver effect of admission glucose level on excellent outcome in thrombolysed stroke patients. *J. Neurol.* 265, 1684–1689.

Moulton, E., Galléa, C., Kemlin, C., Valabregue, R., Maier, M.A., Lindberg, P., Rosso, C., 2017. Cerebello-Cortical Differences in Effective Connectivity of the Dominant and Non-dominant Hand during a Visuomotor Paradigm of Grip Force Control. *Front. Hum. Neurosci.* 11, 1–12.

Rosso, C., Perlbarg, V., Valabregue, R., Obadia, M., Kemlin-Méchin, C., **Moulton, E.**, Leder, S., Meunier, S., Lamy, J.C., 2017. Anatomical and functional correlates of cortical motor threshold of the dominant hand. *Brain Stimul.* 10, 952–958.

Kemlin, C., **Moulton, E.**, Samson, Y., Rosso, C., 2016. Do Motor Imagery Performances Depend on the Side of the Lesion at the Acute Stage of Stroke? *Front. Hum. Neurosci.* 10, 1–10.

Moulton, E., Amor-Sahli, M., Perlbarg, V., Pires, C., Crozier, S., Galanaud, D., Valabregue, R., Yger, M., Baronnet-Chauvet, F., Samson, Y., Dormont, D., Rosso, C., 2015. Axial diffusivity of the corona radiata at 24 hours post-stroke: A new biomarker for motor and global outcome. *PLoS One* 10, 1–16.

List of Tables

List of Figures

List of Abbreviations

ADC	**A**pparent **D**iffusion **C**oefficient
AD	**A**xial **D**iffusivity
ADL	**A**ctivities of **D**aily **L**iving
AF	**A**rcuate **F**asciculus
AHS	**A**phasia **H**andicap **S**core
ART	**A**phasia **R**apid **T**est
ASRS	**A**phasia **S**everity **R**ating **S**cale
BDAE	**B**oston **D**iagnostic **A**phasia **E**xamination
CST	**C**ortical **S**pinal **T**ract
dMRI	**d**iffusion **M**agnetic **R**esonance **I**maging
DTI	**D**iffusion **T**ensor **I**maging
DWI	**D**iffusion-**W**eighted **I**maging
FA	**F**ractional **A**nisotropy
FMA	**F**ugl-Meyer **M**otor **A**ssessment
FOD	**F**iber **O**rientation **D**istrubtion
IFG	**I**nferior **F**rontal **G**yrus
IFOF	**I**nferior **F**ronto-**O**ccipital **F**asciculus
ILF	**I**nferior **L**ongitudinal **F**asciculus
ITG	**I**nferior **T**emporal **G**yrus
M1	Primary **M**otor Cortex
MD	**M**ean **D**iffusivity
MRI	**M**agnetic **R**esonance **I**maging
mRS	**m**odified **R**ankin **S**cale
MTG	**M**iddle **T**emporal **G**yrus
NIHSS	**N**ational **I**nstitute of **H**ealth **S**troke **S**cale
PLIC	**P**osterior **L**imb of the **I**nternal **C**apsule
PMd	**D**orsal **Pre**motor Cortex
PMv	**V**entral **Pre**motor Cortex
ROI	**R**egion **O**f **I**nterest

RD	**R**adial **D**iffusivity
SMA	**S**upplementary **M**otor **A**rea
STG	**S**uperior **T**emporal **G**yrus
UF	**U**ncinate **F**asciculus
VBA	**V**oxel **B**ased **A**nalysis

Abstract

Three of the most common long-term outcome domains to predict following ischemic stroke are motor, language, and global outcome. While clinical variables, such as initial severity of the impairment, age, and lesion volume have proven good indicators of future outcome, the preservation of major white matter structures also plays a role in each of these outcome domains. One particular neuroimaging modality, diffusion tensor imaging (DTI), is sensitive to axonal damage following ischemia and can evaluate the integrity of important white matter bundles. Using a large cohort of patients who underwent a DTI protocol at 24 hours post-stroke, the current thesis sought to (1) investigate spatial normalization strategies in order to optimally process the available data, (2) establish which DTI parameter best captures axonal injury related to long-term global outcome, and (3) determine if DTI can bring to light simple and independent biomarkers of long-term motor and language outcome. First, our work showed that commonly used scalar-based *vs.* novel fiber orientation distribution (FOD)-based spatial normalization strategies performed similar for acute stroke data, yet in an independent dataset of subacute-chronic stroke patients, FOD-based registration yielded stronger anatomo-clinical correlations. Second, we established that axial diffusivity (AD) best captures acute axonal damage and that its evaluation in the corona radiata highly contributes to the prediction of the autonomy or dependence on external aid in patients at three months post-stroke. Third, we demonstrate that AD evaluated in the corticospinal tract as early as 24 hours post-stroke alone can predict motor outcome at the chronic stage. More importantly, we showed for the first time that the AD of the arcuate fasciculus is an independent marker of aphasia outcome. The work presented in this thesis supports the use of AD for quantifying early brain damage and also the importance of the corona radiata, corticospinal tract, and arcuate fasciculus for global, motor, and language outcome, respectively. These surrogate markers could be used not only to inform patients but also to evaluate the efficacy of neuroprotective therapies at the hyperacute stage or as a stratification means for future rehabilitative therapies.

Keywords: Biomarkers, diffusion MRI, diffusion tensor imaging, acute stroke, prediction, prognosis, motor outcome, language outcome, functional outcome, machine learning, corticospinal tract, arcuate fasciculus, spatial normalization.

Résumé

Prédire le plus tôt possible la récupération (notamment l'autonomie, le langage et la motricité) après un Accident Vasculaire Cérébral (AVC) est un défi de la recherche. En plus de la valeur prédictive établie de la sévérité initiale d'un déficit, de l'âge et du volume de l'infarctus, la préservation de certains faisceaux de matière blanche s'avère cruciale pour la récupération de chacune de ces fonctions. Une modalité d'Imagerie par Résonance Magnétique (IRM) nommée le tenseur de diffusion (DTI) est sensible aux changements microstructuraux des neurones suivant l'ischémie et peut donc quantifier l'intégrité de ces faisceaux. Les travaux de cette thèse reposent sur une cohorte de patients thrombolysés ayant eu une IRM à 24 heures post-AVC (et un DTI) et ont pour objectif de (1) comparer les stratégies de normalisation spatiale afin de mieux traiter les données, (2) établir quel paramètre du modèle du tenseur de diffusion reflète le mieux l'atteinte neuronale en lien avec la récupération globale, et (3) déterminer si l'évaluation des faisceaux de substance blanche sont des biomarqueurs indépendants de récupération des fonctions motrices et du langage à trois mois post-AVC. La première étude de cette thèse montre que deux types de normalisation spatiale – une basée sur les cartes scalaires et l'autre basée sur les cartes de distribution d'orientation de fibre (FOD) – donnent tous les deux des résultats similaires pour les images obtenues au stade aigu, mais la normalisation par les cartes de FOD fournit de meilleures corrélations anatomo-cliniques dans une cohorte de patients au stade subaigu-chronique. La deuxième étude met en valeur la diffusivité axiale (AD) comme étant le paramètre qui reflète le mieux l'atteinte axonale. De plus, son évaluation dans la couronne rayonnante contribue fortement à la prédiction de l'autonomie d'un patient à trois mois post-AVC. Enfin, la troisième étude démontre que l'AD du faisceau corticospinal seule peut prédire le handicap moteur au stade chronique. Plus important encore, nous démontrons pour la première fois que l'AD du faisceau arqué est un marqueur indépendent de l'aphasie à trois mois. Les travaux présentés dans cette thèse mettent en avant l'usage de l'AD pour la quantification de la sévérité de l'ischémie aigüe ainsi que l'importance respective de la couronne

rayonnante, du faisceau corticospinal et du faisceau arqué pour l'autonomie, le handicap moteur et l'aphasie à trois mois post-AVC. Ces marqueurs pourraient servir non seulement à informer les patients et leur proches mais aussi à évaluer l'efficacité de thérapies neuroprotectrices au stade hyperaigu ou bien comme un critère de stratification pour d'éventuels essais cliniques.

Keywords: Biomarqueurs, IRM de diffusion, tenseur de diffusion, accident ischémique cérébrale, prédiction, pronostic, récupération motrice, récupération de la parole, récupération globale, machine learning, faisceau corticospinal, faisceau arqué, normalisation spatiale.

Introduction

Cerebrovascular ischemia results from insufficient blood flow due to the obstruction of blood vessels in the brain and leads to rapid cellular necrosis. Depending on the affected populations of neurons, serious deficits can abruptly manifest, the most common being related to motor function or language processing. While the brain is capable of repairing itself, this process is highly imperfect, leaving patients with long-lasting impairments affecting their autonomy in everyday life.

Predicting motor and language outcome, as well as overall autonomy, has become one of the most important questions in stroke research. The initial severity of a given deficit has been shown to highly correlate to its final severity; however, clinical scales used to evaluate residual neurological function suffer from a poor specificity-sensitivity tradeoff. In particular, initially minor deficits will almost always resolve themselves in the long run, whereas patients with mild-to-severe deficits exhibit highly variable recovery trajectories, making their final outcomes difficult to predict.

Recent work has shown that the structural integrity of important white matter pathways are crucial for patient outcome. While motor outcome is highly dependent on the preservation of the corticospinal tract, language outcome relies on a wider network of white matter fasciculi, such as the arcuate fasciculus, inferior fronto-occipital fasciculus, inferior longitudinal fasciculus, and the uncinate fasciculus. Global outcome, on the other hand, is in large part the reflection of the cumulative damage to these important structures. Moreover, the fact that ischemic stroke affects white matter more than gray matter by a far larger percentage suggests that integrity of these long-range fasciculi could be effective biomarkers for outcome in mild-to-severe stroke patients.

Diffusion weighted imaging (DWI) is an imaging modality sensitive to the diffusion of water molecules both in the healthy brain and ischemic stroke and is thus optimal to probe the integrity of important white matter bundles. An extension of DWI, called diffusion tensor imaging (DTI), is capable of characterizing the diffusion of water in 3D space and yields several parametric maps, each providing complementary insights on the integrity of affected and unaffected neuronal populations.

DTI could therefore uncover essential biomarkers indicative of the kind of motor, language, and global outcome patients may expect.

The present thesis expands upon existing work using DTI at the acute stage for long-term outcome. However, a majority of this work has only investigated acute DTI for motor prediction, whereas the utility of DTI for global and language outcome remained undefined to the scientific community. To investigate these unresolved questions, we prospectively screened a large cohort of thrombolyzed patients from the Pitié-Salpêtrière Hospital for whom a follow-up DTI sequence 24 hours after admission has been systematically scheduled since September 2013. This dataset is truly unique of its kind, since few studies have been able to exploit DTI data at such an early time point. Because comparable datasets have so scarsely been reported in the literature, reliable procedures to analyze these images were not available to us at the onset of the current doctoral work. These available images therefore enabled us to elucidate open-ended methodological questions to pave the path for future investigations not only for our own studies but for future independent datasets once they become more readily available. Using the insights from an initial technical study, we were able to confidently probe the prognostic value of DTI at the acute stage of stroke for long-term global, motor, and language outcome in two subsequent studies. The flowchart showing patient inclusion from the original database to each of the three studies is shown below in Figure 1. The varying sample sizes of each study depended on the time at which each study was conceived and the respective inclusion criteria to respond to the precise questions at hand.

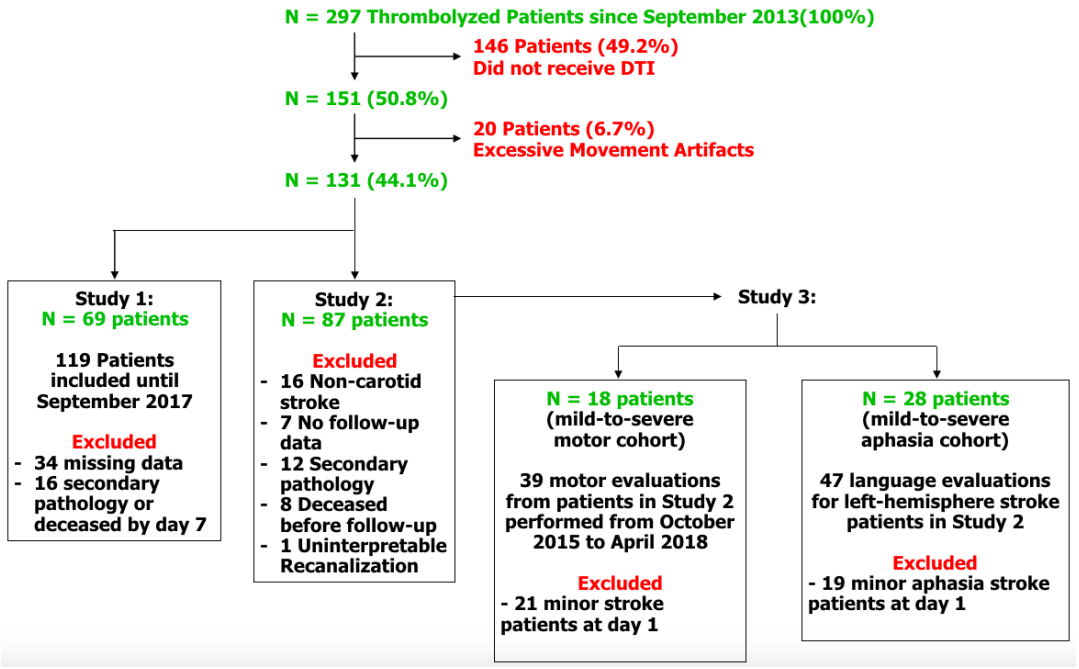

FIGURE 1: Patient inclusion flowchart for studies related to the current thesis. Three studies emerged from a database available at the Pitié-Salpêtrière Hospital. An initial methodological investigation allowed us to reliably prepare data for statistical analyses, and two subsequent investigations sought to probe the prognostic value of the diffusion tensor imaging sequence at 24 hours post-stroke for global, motor, and language outcome.

Taking advantage of recent advances in imaging processing, machine learning, and statistical analyses, the current doctoral thesis attemps to respond to the following three objectives:

- Determine a spatial normalization strategy for diffusion MRI data of acute stroke patients that preserves anatomical overlap of crucial white matter structures
- Compare machine-learning classification models constructed with DTI data in order to deduce which diffusion parameters accurately capture acute stroke damage related to long-term functional outcome.
- Conclude whether acute ischemic damage, quantified with DTI, can bring to light simple and independent biomarkers of long-term motor and language outcome in mild-to-severe stroke patients for whom outcome is more difficult to predict.

Part I presents the thesis background and contains four chapters as follows:

- **Chapter 1** provides an overview of ischemic stroke deficits and introduces the concept of predictive models for long-term outcome. The strengths and weaknesses of important prognostic models constructed with clinical data are presented. This chapter also argues that neuroimaging, especially DWI, is capable of improving upon already existing clinical models, especially for mild-to-severe stroke patients.

- **Chapter 2** presents the anatomical underpinnings of motor function and language processing in healthy individuals as well as the determinants of global outcome in stroke patients. Common measures of evalatuing motor, language, and global outcome are also presented.

- **Chapter 3** lays the foundations for DWI in addition to common models of water diffusion in the brain derived from this sequence. Diffusion parameters estimated from these models are given for various structures in the healthy brain as well as their evolution in ischemic stroke. Popular types of analyses using DWI data are also presented with a focus on group-level analyses and existing strategies for spatial normalization.

- **Chapter 4** reviews the state of the art surrounding the prognostic value of DWI in acute stroke for long-term outcome using the types of analyses outlined in chapter 3 and constitutes the core of the current thesis.

Part II constitutes the thesis work and contains three chapters:

- **Chapter 5** is a methodological study comparing sophisticated spatial normalization techniques for DWI data in both acute and subacute-chronic stroke. The study serves to contrast commonly used scalar-based techniques with novel strategies that take advantage of the rich 3D data provided by DWI. The results of this study, particularly for acute stroke patients, are used for the subsequent studies.

- **Chapter 6** presents a study comparing the accuracy of DTI parameter maps as well as lesion segmentations for predicting global outcome with a multivariate machine learning classification technique.

- **Chapter 7** reports a regression analysis between diffusion abnormalities in important white matter fasciculi for mild-to-severe stroke patients and fine-grained measures for long-term motor and language outcome. This analysis

is also complemented by a voxel-based analysis to show the specificity of the chosen fiber tracts used in the regression models.

Part III is dedicated to the general discussion and conclusion:

- **Chapter 8** finally concludes the thesis with a global discussion and perspectives on the true clinical relevance of diffusion tensor imaging at the acute stage of stroke.

Part I

Thesis Background

Chapter 1

Ischemic Stroke and Prognosis

Contents

1.1 Post-stroke Deficits and Recovery

Stroke is defined as the sudden onset of focal symptoms related to vascular origin[1]. It has recently moved from the third to the second cause of disability in the world, in terms of disability-adjusted life years, and is also a leading cause of years lost due to disability worldwide[2]. While stroke incidence, prevalence, mortality, and disability-adjusted life-years have declined in the past two decades, the absolute number of people affected or disabled from stroke has grown[3], mainly from improvements in stroke care and the increasing aging population.

Specifically, stroke encompasses three separate pathology types: ischemic stroke, intracerebral haemorrhage, and subarachnoid haemorrhage. Ischemic stroke represents more than 85% of all stroke occurrences[4] and will be the focus of the present dissertation. By definition, ischemic stroke is the result of insufficient blood flow due to the obstruction of blood vessels in the brain. After prolonged deprivation of oxygen and glucose, neural cells in the ischemic core begin to undergo necrosis following a cascade of pathological mechanisms. Massive neuronal death results in the sudden onset of neurological deficits[5] the nature of which depends on the affected neuronal populations and the functions they uphold[6].

The recovery process of lost neuronal function begins shortly after stroke onset and continues until the chronic stage[7] (i.e., more than 6 months post-stroke onset[8]). Throughout this period, the brain undergoes massive reorganization through the genesis of neurons, glia, and blood vessels in addition to functional and structural remapping of preserved brain tissue in an attempt to maximally recover lost neurological function. Neural remodeling can rely on nearby tissue with similar function either by strengthening diffuse synaptic connections or by creating new ones[7]. This biological process is most active during the first month of stroke[9] with most patients achieving maximum gains by 3-6 months post-stroke (Fig 1.1).

Despite the brain's best efforts to recover lost function, many patients are still burdened by debilitating sequellae at the chronic stage of stroke. Common impairments include motor function, language, and spatial attention. Motor deficits are the most frequent impairment from stroke with 50-80% of patients presenting with hemiparesis of the upper limb at the acute stage of stroke and about 40% at the chronic stage[10,11]. Aphasia is present in around 30-40% of left-hemisphere stroke cases at the acute stage, with longitudinal studies reporting only a small percentage that fully recover pre-stroke language abilities[12–14]. About 25-50% of patients present with symptoms relating to hemispatial neglect (usually following a stroke of the right hemisphere),

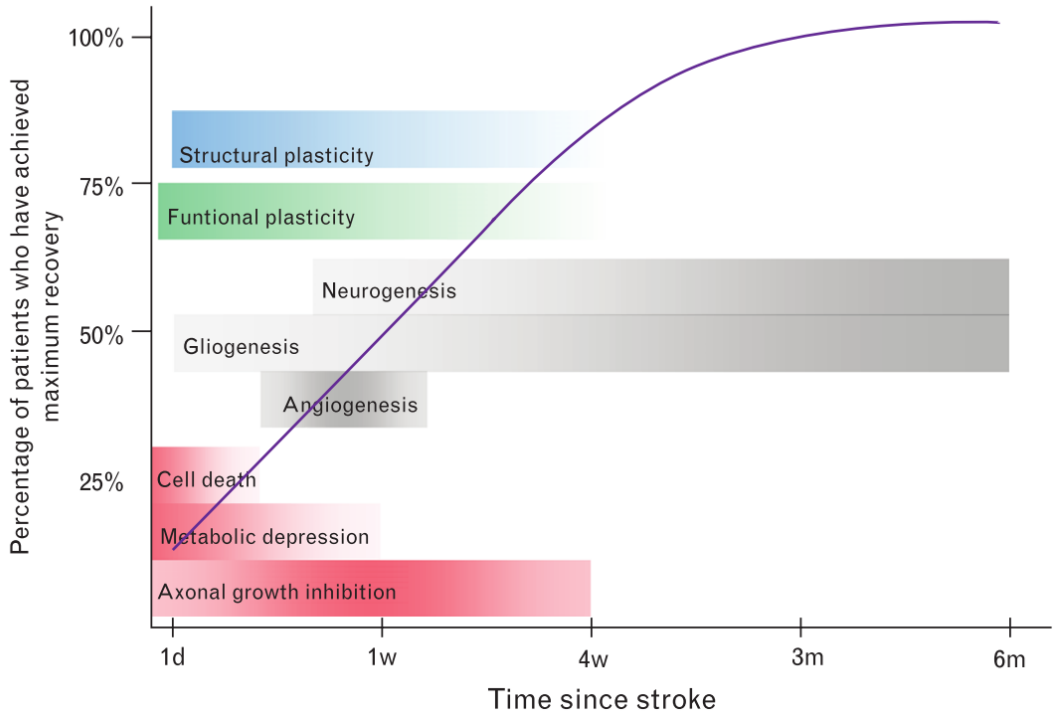

FIGURE 1.1: Time windows of brain plasticity and spontaneous neurological recovery following stroke.
Cellular and molecular processes result in neural death (red). Cell repair and genesis are active in the weeks following stroke. Finally, functional (green) and structural(blue) plasticity begin almost immediately following stroke onset and are maximal in the first month. Most patients achieve their maximum potential for recovery by 3 months post-stroke. Adapted from Stinear and Byblow[9]

with 75% of these patients experiencing persistent deficits in the chronic stage[15–18]. Finally, all of these factors have significant impacts on the autonomy of patients, as disabilities affecting basic activities of daily living (ADL) are present in more than 25% of stroke sufferers in the long term[1,11].

1.2 Prognosis, Biomarkers, and the Role of Neuroimaging

Beyond quantifying the prevalence of deficits at the population level, being able to explain and predict any impairment of individual stroke patients at any time is one of the highest priorities in stroke research[19]. Prognostic models can be used to predict anything from global stroke impairments, such as general autonomy or dependence on external aid, to precise domain-specific deficits, such as motor dexterity or strength, language comprehension or production, or spatial awareness. Effective models serve several purposes: (1) informing patients, family, caregivers, and clinicians, (2) planning the future course of rehabilitation therapy[20], and (3) determining

which patients can benefit from interventions aimed at promoting stroke recovery[21]. While the true underlying cause of any neurological impairment is ultimately the result of cellular damage and repair, direct measurements of such processes are difficult to obtain; therefore, finding substitute *biomarkers* of these mechanisms, capable of explaining present or future deficits, has been a developmental priority in stroke research[19]. In addition to clinical variables (e.g., age, sex, stroke severity scales, etc.), the vast majority of investigated biomarkers have been derived from radiological exams with magnetic resonance imaging (MRI) (e.g., lesion volume, lesion localization, non-invasive measures of brain function or structure, etc.).

Predictive models can be applied to and across any stage of stroke to describe different aspects of neurological impairments. In particular, the main concern of prognostic models is to find variables capable of explaining three important yet independent concepts: severity, outcome, and recovery. Stroke severity models are those in which both explanatory factors (i.e., independent variables) and measures of the degree of an impairment are acquired at the same time t post-stroke. Such models are useful for elucidating the underlying clinical or neural correlates responsible for the severity of a given deficit[22–24]. Due to the dynamic nature of spontaneous recovery, deficits of a given domain (e.g., motor, language, or cognition) may be explained by different factors at the hyperacute (0-24 hours), acute (1-7 days), subacute (1 week - 6 months), or chronic (>6 months) stage of stroke[8,19]. Outcome models, on the other hand, attempt to uncover explanatory factors obtained at some time t capable of explaining an impairment measured at some future time $t + \Delta t$. Finally, recovery models serve to explain the *change* in impairment from time t to time $t + \Delta t$. While related, there is a fundamental difference between outcome and recovery (Fig 1.2). This difference can be appreciated in patients with distinct recovery profiles: two patients may present with drastically different initial severities, yet both patients may end up reaching the same level of impairment at some future point. In this case, while one patient has *recovered* more than the other, both effectively have evolved toward the same *outcome*.

Different outcome and recovery profiles are largely due to patient-specific variations in cerebral reorganization. In fact, there has been considerable work showing that the outcome and recovery of patients in a particular neurological domain (e.g., motor, language, or cognition) are highly explained by the initial severity of the stroke[26,27] and the impairment itself[28,29].

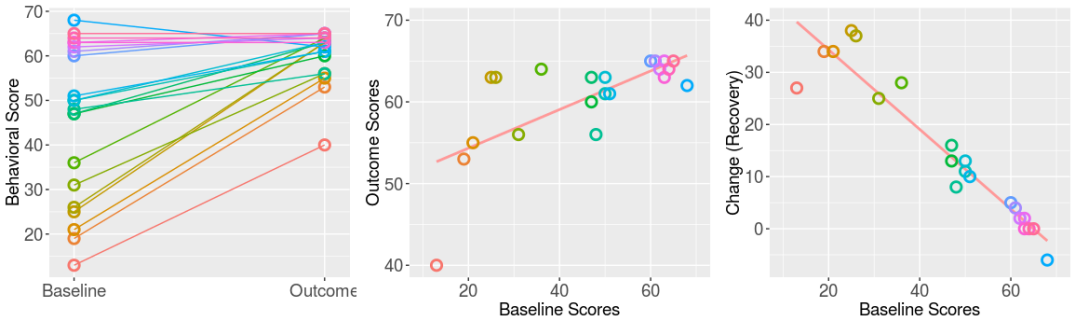

FIGURE 1.2: Outcome *vs.* Recovery.
(Left) Patients with different baseline impairments may evolve towards the same outcome (e.g., the yellow and light blue lines). (Middle) Outcome, given by the y-value in the leftmost graph, may be directly explained by a baseline measure. (Right) Recovery, given by the difference between outcome and baseline, may be explained by a baseline measure. Points of the same color refer to the same individual. Adapted from Hope et al. (2018)[25]

1.2.1 Initial severity as a Predictor of Outcome and Recovery

Early evaluation of a patient's deficit can therefore reveal the specific outcome and recovery potential to be attained within the period of spontaneous recovery. In other words, patients with more severe deficits have a higher *potential* to recover function and reach higher outcome endpoints, whereas patients with mild deficits recover less and reach slightly better outcome endpoints, simply because there is less progress to make. In fact, research has suggested that the vast majority of function regained by patients is determined by biological processes at play during spontaneous recovery[30,31].

At the broadest level, a general relationship between stroke severity and long-term functional outcome has been demonstrated with crude stroke-deficit rating scales and overall outcome scales. In the seminal paper of the National Institute of Health Stroke Severity (NIHSS) scale (see section 2.3), Brott et al. (1989)[32] reported that 3-month functional outcome was significantly correlated with stroke severity assessed at admission (Spearman's ρ=0.53) and at 7 days post stroke (ρ=0.71). Several subsequent studies report similar findings in that the NIHSS evaluted at day 5 or 7 predicts long-term outcome better than at admission or at day 1[33,34]. However, greater prognostic value can be obtained with the NIHSS at admission when combined with other clinical variables, such as the age of the patient and treatment received (e.g., recanalization therapy *vs.* none)[35,36].

Where these clinical variables truly excel is when outcome measures are situated at one extreme of the spectrum (i.e., near-to-perfect recovery *vs.* imperfect recovery

or death *vs.* survival). For example, the SPAN-100 trial constructed the SPAN score defined as the sum of the NIHSS at admission and the age of a patient. By dichotimizing this score at 100, the authors created two groups: a "positive" group for whom SPAN-100 < 100 and a "negative" group for whom SPAN-100 > 100. Their primary outcome measure was a composite score for quasi-perfect outcome (mRS of 0 or 1 AND NIHSS$\leq$1 AND Barthel index$\geq$95 AND and Glasgow Outcome Scale score of 1 at 3 months, see reference[37] for an explanation of these outcome measures). Highly skewed towards severely affected patients, the SPAN-100 score was able to correctly classify 93.5% of SPAN-100-negative patients in the less-than-perfect outcome group, but only 47.7% of SPAN-100-positive patients in the perfect outcome group. Similarly, Weimar et al. (2004)[27] showed that the NIHSS at admission and age correctly predicted mortality at 100 days post stroke with 91.5% specificity but only 57.9% sensitivity, showing that only extremely severe patients at admission have a high chance of mortality, but the mortality of all other patients is more variable.

These relationships have also been shown to be valid for multiple functional domains, including the upper[28,38,39] and lower[40] limbs as well as for aphasia[29,41] and visuopatial neglect[42]. For example, a study performed by Duncan et al. (1992)[38] analyzed motor function using the Fugl-Meyer score (see section 2.3) at admission and at 6 months post-stroke. The authors reported that all initially mild motor deficits remained mild at six months (average change in Fugl-Meyer score = 5.4), whereas the variability in outcome in all other patients was much larger (change for initially moderate motor deficits = 20.8; moderate-severe = 25.5; severe = 35.7). Similarly, Pedersen et al. (2004)[29] reported a significant relationship between aphasia severity at admission and 1 year post-stroke: while all mildly aphasic patients reached almost perfect outcome, severely aphasic patients at admission exhibited a wide range of outcome scores with some attaining perfect outcome and others improving very little.

The true predictive value of initial severity – be it global or domain-specific – therefore seems to be driven by those patients who present with very minor deficits shortly after stroke onset. For mild-to-severe deficits, on the other hand, outcome is much more difficult to predict. However, for these patients, several studies have shown that damage to crucial structures of, for instance, the motor or language system can determine the outcome patterns of the corresponding neurological functions for this difficult-to-predict population[43–45].

1.2.2 The Role of Neuroimaging in Prognostic Models

The potential for spontaneous neural plasticity is thus highly limited by both residual function (i.e., initial severity) *and* preserved brain regions. It is therefore essential for researchers to identify proper biomarkers capable of accurately quantifying and localizing stroke damage to important brain structures in order to understand global patterns as well as the patient-specific potential for reaching certain outcome endpoints[19]. Neuroimaging is a promising means of non-invasively investigating stroke size and topography in addition to the structure and function of lesioned and preserved brain regions. Imaging biomarkers are therefore strong candidates for providing more subtle and sensitive measures of damage to brain regions critical for the recovery of various neurological functions, such as sensorimotor, language, and cognition[19].

Neuroimaging biomarkers typically originate from two modalities: structural and functional. While brain function is generally studied with functional MRI, electroencephalography, or magnetoencephalography, structural imaging is accomplished with either classical anatomical MRI sequences (e.g., T1- or T2-weighted images) or diffusion MRI (dMRI). While each modality benefits from different temporal and spatial resolutions and thus reveals different aspects about structural and functional damage following stroke, the most interesting and widely used sequence in clinical settings remains dMRI. Indeed, already acquired in many hospitals, this sequence is an optimal candidate for finding effective and implementable biomarkers, which constitutes the essence of the current doctoral work. Precisely, the present thesis focuses on three of the most studied outcome domains in stroke research: (1) global outcome, (2) motor deficits, and (3) aphasia. The anatomical bases of these systems will be discussed in chapter 2, and the principles of dMRI will be detailed in chapter 3. Finally, chapter 4 will provide a review of the literature revolving around prognostic models using dMRI data acquired at the acute stage of stroke for long-term outcome.

Chapter 2

Outcome Domains and Measures

Contents

The three major outcome domains studied in the context of this doctoral work are motor, language, and global outcome. The present chapter serves to outline the neuroanatomy of the motor and language systems in the brain as well as the determinants of global outcome. Each section is thereafter followed by a description of the corresponding outcome measures used in the research contained in this manuscript.

2.1 Motor

The motor system is a large network of cortical and subcortical structures that relay messages for planning and executing movements. This section concentrates on the cortical regions and white matter pathways responsible for emitting and transmitting the final motor commands to skeletal muscle for volitional movement as well as standardized tests to evaluate their precision and performance.

2.1.1 Neuroanatomy of the Motor System

Volitional movement is generated by various motor cortices in the brain. The majority of motor commands originates in the primary motor cortex (M1), located along the posterior bank of the central sulcus and anterior surface of the precentral gyrus, extending until the paracentral lobule on the medial surface of the brain (Fig 2.1A). Secondary motor areas, such as the ventral (PMv), dorsal (PMd) premotor cortices, and the supplementary motor area (SMA) also contribute to motor output, albeit to a lesser degree[47,48]. These secondary motor areas influence muscle activity, either by indirectly modulating pyramidal neurons in M1[49,50] or directly projecting onto target muscles through the spinal cord[48]. The premotor cortices are mostly involved in the preparation and selection of motor programs driven by external cues[51], whereas the SMA plays a role in internally initiated movements[52]. A somatotopical organization exists along M1 and reflects the degree of motor control exerted by the brain. In particular, the cortical representation of distal muscles, such as those in the hands, legs, and feet occupy a larger surface than more proximal muscles, such as those in the trunk (Fig 2.1B).

Motor neurons in the cortex relay their activity to target muscles through two organized bundles of axons: the corticospinal tract (CST), originating from the upper half of M1, and the corticobulbar tract, stemming from the lateral surface of M1. The CST innervates muscles of the upper and lower limbs through relays in the spinal cord, whereas the corticobulbar tract outputs motor commands to the muscles of

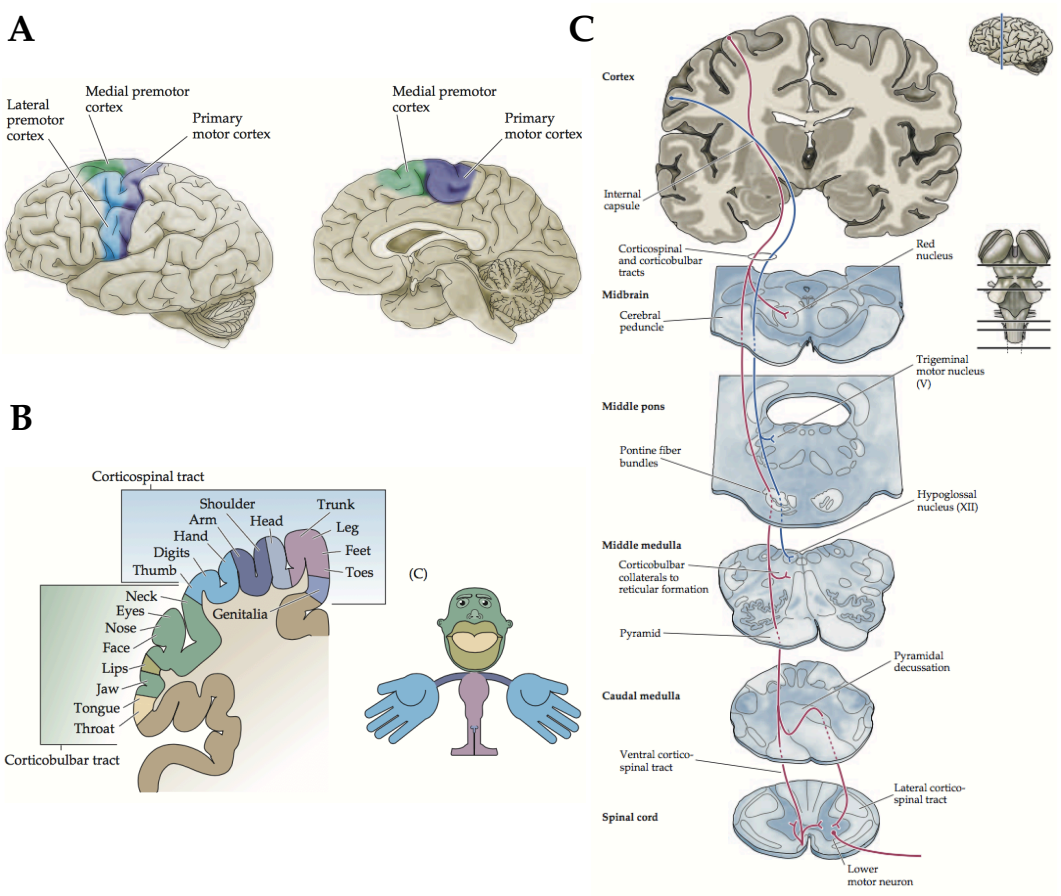

FIGURE 2.1: The cortical and white matter substrates of volitional movement. (A) The primary motor cortex (M1 - purple), The lateral premotor cortex (blue), composed of ventral (PMv) and dorsal (PMd) subparts, and the medial premotor cortex (green), also referred to as the Supplementary Motor Area (SMA). (B) The somatotopy of M1 known as Penfield's homunculus. (C) Trajectories of the corticospinal (CST) and corticobulbar tracts. Adapted from Purves et al. (2004)[46]

the neck and face through relays in the various nuclei of the brain stem (Fig 2.1C). Both the CST and corticobulbar tract descend through the corona radiata, posterior limb of the internal capsule (PLIC), and cerebral peduncles. In the caudal portion of the medulla, the vast majority of the CST fibers decussate and enter the lateral columns of the spinal cord. Neurons in M1 represent about 70% of the fibers in the CST, constituting the most important outflow of information for movement execution, and have thus been the primary object of investigation in motor stroke recovery[53,54].

Due to the somatotopical nature of M1, damage to these cortical areas or the fibers emanating from them can lead to deficits of specific body parts. For instance, a stroke lesion to the hand region area in M1 or the associated fibers at the level of the PLIC or cerebral preduncles can lead to deficits of the upper limb. Therefore, a large portion of

upper limb deficits can be explained by direct damage to CST fibers emanating from M1[54], with recent work highlighting the additive role of additional corticofugal[48,55–57] and corticocortical[49,50,58,59] fibers in motor-related plasticity.

2.1.2 Measures

There is currently a plethora of used measurement scales for evaluating motor recovery in stroke. In fact, a recent Cochrane Overview of interventions aimed at increasing upper limb function after stroke identified 208 assessment tools from 243 trials[60]. Interestingly, however, recent research has shown that different aspects of motor impairment, such as strength, coordination, and range of motion and function all covary to a considerable degree[61,62]. Presented in this section are the three motor outcome assessments used in the research for this thesis and are among the most commonly used in the literature[63].

The Fugl-Meyer Motor Assessment

The most common measure for body function is the Fugl-Meyer Motor Assessment (FMA)[64–66]. The FMA is a two-part numerical assessment of motor skill after stroke, which takes into account limb synergy and range of motion for both the upper and lower extremities[65]. In this doctoral thesis and as is commonly done[67], only the upper limb evaluation was used and is provided in Appendix A.

Various movements of the shoulder, forearm, and hand are attempted by a patient and graded on an ordinal scale from 0 to 2. A correct execution of the movement is graded 2; partial completion is graded 1; and absence of movement or incorrect form is graded 0. All scores are added to compute a final score, reflecting the overall motor status. A maximum score of 66 (or 60 without testing reflexes) corresponds to no impairment, and a minimum score of 0 corresponds to complete hemiplegia.

The Jebson-Taylor Test

The Jebsen-Taylor Test (JTT)[68] is a timed assessment of fine motor skills. Initially, seven tasks were proposed by the authors[68]: (1) writing a sentence, (2) turning over index cards, (3) picking up small objects, (4) picking up dried beans with a spoon, (5) stacking checker pieces, (6) picking up empty tin cans, and (7) picking up full tin cans. The work in this doctoral thesis as well as in other studies[62] omitted the first task due to its dependence on hand dominance and education level. Patients are

timed for each task with a maximum cutoff of 120 seconds. A total score is computed by adding the time for each task. Finally, a ratio of the scores from the affected and unaffected limb can be computed to represent a relative percentage of dexterity.

Grip Strength

Grip strength is a measure of the maximum force output during a five-finger grip. Usually while seated, patients grasp a dynamometer with their arm at a 90° angle and their elbow resting on a table. If patients are not able to maintain their arm upright, support can be provided by the examiner without influencing force production. In other studies[62] as well as in those in the present doctoral thesis, the average of three trials is computed for the affected and unaffected limb from which a ratio (i.e., affected/unaffected) can be calculated. The ratio represents the percentage of the force output of the affected hand with respect to the unaffected hand.

2.2 Language

The faculty of language comprises a large range of functions subserved by a vast network of cortical regions and their respective white matter connectivity[69]. The exact organization of the language system is by far more contentious than the motor network, both in terms of the cortical substrates[70] and their underlying connections[71–73], bringing into question the exact function(s) each element upholds[70,72]. This section serves to outline the major constituents of the language network pertinent to the work presented in this thesis.

2.2.1 Neuroanatomy of the Language System

The origin of the neural substrates for language production and comprehension date back to the 19th century with the discoveries of Paul Broca[74] and Carl Wernicke[75], respectively. While Paul Broca postulated that the seat of language production was in the left posterior portion of the inferior frontal gyrus (IFG), Carl Wernicke posited that language comprehension was localized to the left posterior superior temporal gyrus (STG). About a century later, Normand Geschwind provided a unified view of language processing by relating a series of deficits in aphasia as disconnections between these regions and emphasizing the importance of the left angular gyrus as a "way station" via an important white matter pathway, the arcuate fasciculus[76,77]. Several decades later, the advent of functional brain imaging contributed important

insights to the function of the language network and broadened the community's understanding thereof[70]. In 2007, Hickock and Poeppel expanded Geschwind's classical model by proposing a refined dorsal and ventral "dual-stream" theory to explain the cortical substrates for processing speech[78] (Fig 2.2).

According to this model, the two streams allow for parallel processing of different aspects of speech input and output. On one hand, the dorsal stream was posited to be largely left-lateralized in the brain and subtend auditory-to-motor mapping for functions such as speech repetition. These functions would mainly be subserved by (a) region in the Sylvian fissure at the boundary between the parietal and temporal lobe just anterior to the angular gyrus as described by Geschwind, (b) the region identified by Broca consisting of the pars triangularis and pars opercularis, and (c) dorsal premotor areas. On the other hand, the ventral stream would underpin conceptually driven speech production by bilaterally processing auditory inputs in

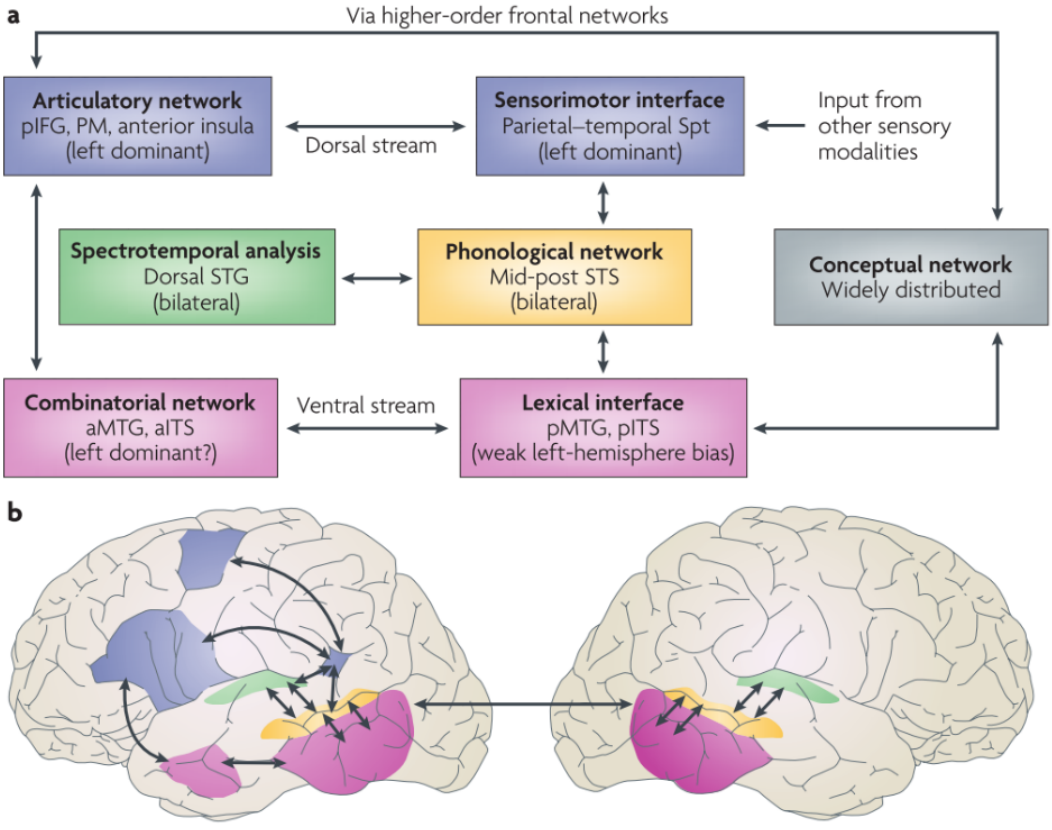

FIGURE 2.2: The dual stream model proposed by Hickok and Poeppel (2007). Prefixes: a, anterior; p, posterior. Abbreviations; IFG, inferior frontal gyrus; PM, premotor cortex; Spt, region in the Sylvian fissure at the parieto-temporal boundary; STG, superior temporal gyrus; STS, superior temporal sulcus; MTG, middle temporal gyrus; ITS, anterior inferior temporal sulcus. From Hickok and Poeppel (2007)[78]

the STG and mapping them to conceptual and semantic representations in the middle (MTG) and inferior (ITG) temporal gyri.

While considerable advances have clarified the cortical regions involved in language processing[70], their underlying connections and cortical terminations are still a source of controversy in the literature[71–73,79] due to contradictory results from diffusion tractography studies[80–85] and post-mortem dissections[79,86,87]. By virtue of the tight link between connectivity and function in the brain[88–90], different versions of the connectivity for each of these fiber tracts have resulted in revised models of their function within the language network and the possible deficits that may arise from lesions thereof[91–93]. Nevertheless, the presence of separate dorsal and ventral pathways is a recurrent finding in the literature, which has lead to a general consensus of their existence[72,94].

As for the dorsal stream, the major white matter tract is the arcuate fasciculus (AF), which classically connects Wernicke's and Broca's region[95]. Common variants of the composition of the AF include a "two segment" model[80], consisting of a phonological and lexical-semantic pathway, in addition to a "three segment" model, comprising a long, anterior, and posterior segment[86,96] (Fig 2.3). Depending on the assumed profile of connectivity, the AF has been posited to play a role in repetition and spontaneous speech by converting both auditory information (from the STG) and lexical-semantic information (from the MTG) to motor output in Broca's area (pars triangularis, pars opercularis) as well as in the PMv[71,92].

The ventral stream, on the other hand, is composed of many individual fiber pathways and is thus responsible for many functions revolving around language comprehension (Fig 2.3). Its main purpose is to extract meaning from acoustic-phonological input, integrate it with semantic hubs in the temporal lobe, and transfer them to regions in the frontal lobe[72]. The three main pathways of the ventral stream are the inferior fronto-occipital fasciculus (IFOF), the inferior longitudinal fasciculus (ILF), and the uncinate fasiculus (UF)[72]. The IFOF is a long bundle with caudal terminations in the occipital pole, certain parts of the superior parietal lobe, and the ventral occipito-temporal cortex[97]. It courses through the external capsule and fans out rostrally to parts of the medial, lateral, and dorsal frontal lobe[84]. Similar to the IFOF, the ILF's most caudal terminations are located in the inferior occipital gyrus and ventral occipito-temporal cortex; however, the ILF projects laterally to the temporal pole and medially to the anterior fusiform gyrus, parahippocampal gyrus, and amygdala. Finally, the UF can be portrayed as a relay between the ILF

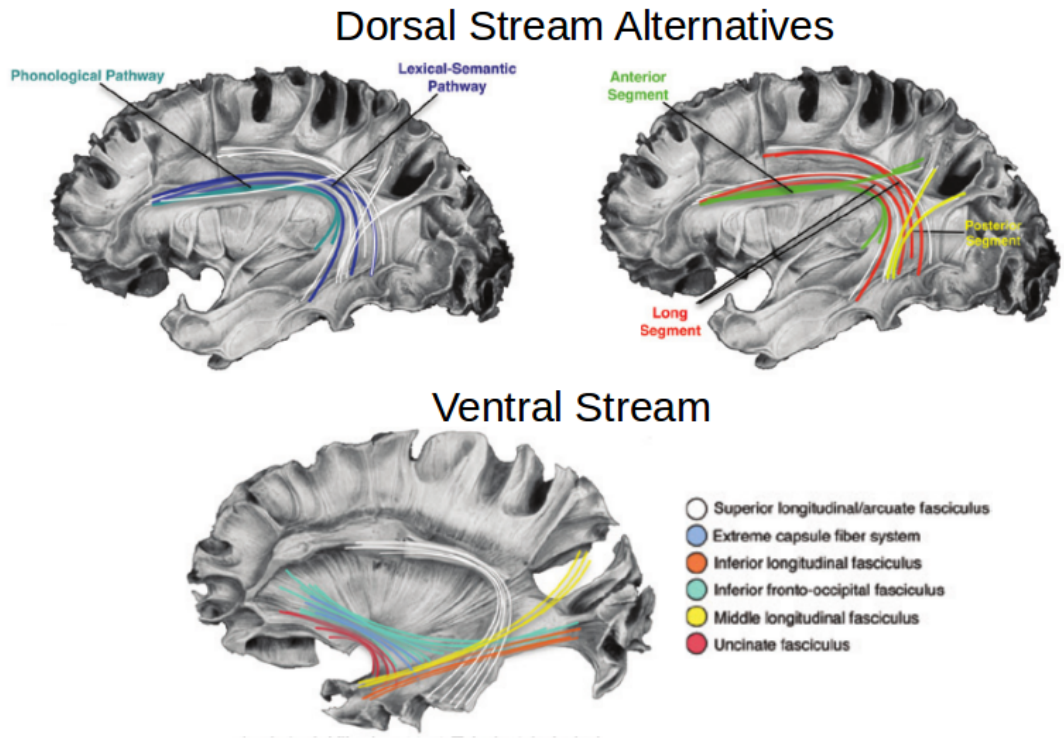

FIGURE 2.3: White matter pathways of the dorsal and ventral stream. Top Left: a two-segment version of the arcuate fasciculus (AF) connectivity according to Glasser et al. (2008)[80]. Top Right: a three-segment version of the AF connectivity according to Catani et al. (2005)[100]. Bottom: Proposed pathways of the ventral stream. Figure adapted from Dick et al. (2014)[72].

and frontal lobe by linking the anterior temporal lobe[98] with the ventral and medial frontal cortex, including the pars orbitalis[99].

Disentangling the role in semantic processing of each of these pathways has been the subject of debate in recent research due to the considerable degree of shared connectivity. Certain authors have claimed that the IFOF is the main "direct" pathway subserving the ventral stream through semantic processing for language and can compensate for damage to an "indirect" pathway composed of the ILF and UF[93]. Due to their shared connectivity between the extrastriate cortex, visual word form areas of the fusiform territory, and frontal regions, these pathways share roles in object recognition, picture naming, proper name retrieval, and reading.

The division of labor proposed by various dual stream models is often observed in anatomo-behavioral studies of aphasia. Speech production deficits are largely due to damage to dorsal pathway regions[45,101], whereas language comprehension and semantic processing deficits are far more related to ventral stream damage[69,99]. However, purely isolated production or comprehension deficits are rarely seen in

practice can also be compensated by the other preserved stream[91,92]. That being said, patients with the most disabling aphasia are usually those with damage to regions at the crossroads of both pathways[102–104].

2.2.2 Measures

Due to the multifaceted nature of language, standardized tests are often lengthy and detailed in an attempt to dissociate the various aspects of aphasia and are thus difficult to obtain in clinical settings or at the patient's bedside[105]. However, like motor deficits as explained above, recent research has shown that even for cognitive functions as complex as language, there is a high level of correlation between scores from different behavioral batteries[61]. Indeed, a dimensionality analysis on language tests[17] and lesion-deficit maps[69,94] in large cohorts have revealed that overall aphasia can reliably be expressed by a single factor, whereas more detailed structure (e.g., speech comprehension/semantics/ventral pathway *vs.* production/phonology/dorsal pathway) becomes evident through an additional independent factor[106]. Due to the consistency between such scores, therefore, the following section selectively presents two measures of aphasia severity, a commonly used in-depth standardized battery able to capture production and comprehension abilities and an in-house bedside evaluation for global aphasia used at the Pitié-Salpêtrière Hospital.

The Boston Diagnostic Aphasia Evaluation

The Boston Diagnostic Aphasia Evaluation (BDAE)[107] is a language battery for the diagnosis of aphasia and the evaluation of perceptual (auditory, visual, and gestural), processing functions (comprehension, analysis, problem-solving), and response modalities (writing, articulation, and manipulation). In its original version, the BDAE is composed of eight sections for assessing fluency, auditory comprehension, naming, oral reading, repetition, automatic speech, reading comprehension, and writing. The BDAE exists in a short form yet still requires 30-45 minutes to administer. The Aphasia Severity Rating Scale (ASRS) is an associated global measure of functional language ability assessed on a 6-point scale with a lowest possible score of 0, corresponding to no intelligible speech and no comprehension, to a best possible score of 5, referring to no perceptible language disorders (Appendix B).

The Aphasia Rapid Test

The Aphasia Rapid Test (ART) is a bedside assessment conceived by Azuar et al. (2013) at the Pitié-Salpêtrière Hospital to rate aphasia severity in stroke patients in less than 3 minutes[108]. The ART is a NIHSS-like 26-point scale with higher scores indicating greater impairment (Appendix C), and its reproducibility, sensitivity, and high predictive value have already been demonstrated[108]. The assessment is based on 6 items, consisting of simple comprehension tasks (rated from 0-5 points), word and sentence repetition (0-8 points), object naming (0-6 points), semantic fluency of animals (0-4 points), and dysarthria evaluation (0-3 points).

The Aphasia Handicap Score

Complementary to the ART and similar to the modified Rankin Score (see section 2.3 hereafter), a global aphasia score, termed the Aphasia Handicap Score (AHS), can be determined as well. The AHS is a five-point scoring system for disability in verbal communication (Appendix D) and highly correlates with the ASRS[108]. The AHS score and corresponding functions are as follows: 0 = normal communication, 1 = minor difficulties of language without disability (no impact on normal life), 2 = mild-language related disability (without restrictions in the autonomy of verbal communication in daily life), 3 = moderate language-related disability (restricted autonomy of verbal communication), 4 = severe language-related disability (lack of effective verbal communication), 5 = mutism or total loss of verbal expression and comprehension.

2.3 Stroke severity and Global Outcome

Stroke severity refers to crude measurements that encompass the overall degree of present stroke deficits. While non-specific and sometimes inaccurate with respect to the true deficit, their use and interpretation is nevertheless rather intuitive. Moreover, the slight sacrifice of accuracy has highly contributed to their reproducibility across treatment sites, making them indispensable for patient evaluation and clinical trials[109]. On the other hand, global outcome (also referred to as functional outcome) reflects a patient's autonomy and ability to perform activities of daily living (ADL) and is usually evaluated as a long-term outcome measure[66].

2.3.1 Neural Underpinnings

Due to the non-specific nature of global outcome scales, neural correlates of such measures are distributed throughout the brain, covering a large range of neurological functions, such as motor, language, and neglect[110–114] (Fig 2.4). In one of the first studies investigating stroke infarct location on functional outcome, Cheng et al. (2014) found that lesions to the white matter corresponding to the CST or AF were associated with worse outcome in patients. In fact, these regions are usually found at the intersection of long-range pathways, causing simultaneous multiple disconnections[112,114,115]. The level of autonomy of patients therefore decreases with the increasing number of deficits arising from a higher number of affected white matter tracts.

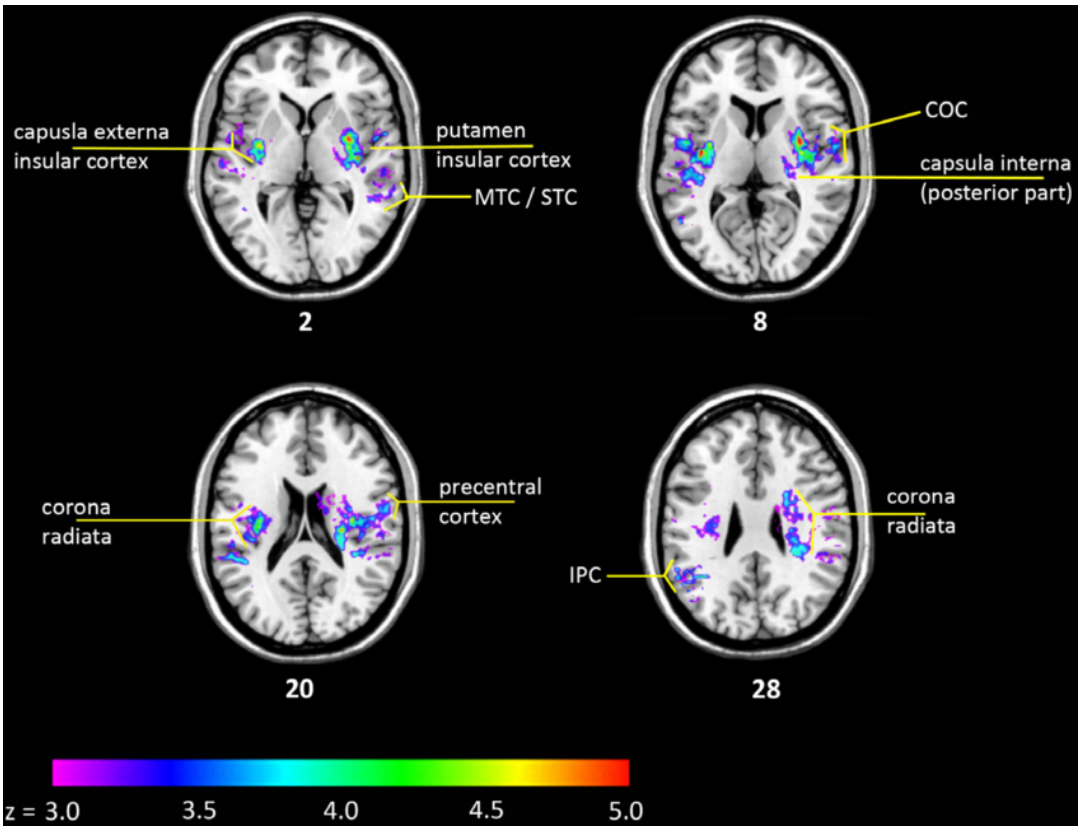

FIGURE 2.4: Annotated statistical maps of lesioned areas associated with global outcome.
Colored regions correspond to worse clinical outcome. Z-coordinates in MNI space are given below each slice. The colorbar shows the Z-score thresholded at 1% False Discovery Rate separately for each hemisphere. COC, central opercular cortex; IPC, inferior parietal cortex; MTC, middle temporal cortex; STC, superior temporal cortex. Figure from Cheng et al. (2014)[110].

2.3.2 Measures

The most common measures of stroke severity and global outcome are the National Institute of Health Stroke Scale (NIHSS) and the modified Rankin Scale (mRS)[66,116].

The National Institute of Health Stroke Scale

The NIHSS is a scale composed of 15 items for different neurological functions: consciousness, gaze, vision, facial palsy, upper and lower motor function, ataxia, tactile sensation, language, dysarthria, and spacial neglect (Appendix E). Each function is assessed with a 3- or 4-point ordinal scale (5 for motor items) where 0 indicates no impairment. The NIHSS has become such a universal and important measure of stroke severity that most clinical trials require it to adjust outcome measures or use it as an outcome measure in and of itself[109].

The modified Rankin Scale

The most common outcome measure of functional outcome is the modified Rankin Scale (mRS). The mRS is a 7 point scale ranging from no sequellae (mRS=0) to death (mRS=6) (Appendix F). Despite the coarse scale and non-specificity to certain neurological deficits, the mRS can provide a practitioner with an overall idea of the status of a stroke patient, and single-point changes are clinically relevant[117]. Rather than an ordinal variable, certain studies have employed a dichotimized version of the mRS, each with different cutoffs: (1) mRS 0-1 *vs.* 2-6 distinguishes patients who are able to perform all ADL as before the stroke from those for whom certain tasks are no longer feasible, and (2) mRS 0-2 *vs.* 3-6 regroups patients who are autonomous in their daily lives from those who require assistance on external aid.

Chapter 3

Diffusion Modeling in the Brain and Analyses

Contents

In this chapter and before discussing the state-of-the-art research related to this doctoral work, I herein provide the technical basis of diffusion MRI image acquisition, modeling, and analysis.

3.1 Origin of the Diffusion Signal in MRI

Diffusion Magnetic Resonance Imaging (dMRI) is a non-invasive imaging modality sensitive to the natural diffusion of water molecules *in-vivo* and has become an indispensable tool not only for neuroscience in general but also for stroke research[118]. The principle of dMRI, laid out as early as the mid-1980s[119], consists in a small adaptation to conventional anatomical imaging sequences, such as a spin-echo sequence, in order to render it sensitive to the diffusion of water molecules (Fig 3.1)[120].

In a conventional spin-echo sequence, for example, the magnetic moments of water molecules in a region of the brain are first excited by a 90° magnetic pulse, then refocused by a 180° pulse. Finally, some time later, the water molecules re-emit the absorbed energy as radiofrequency waves with coherent phases, which can thereafter

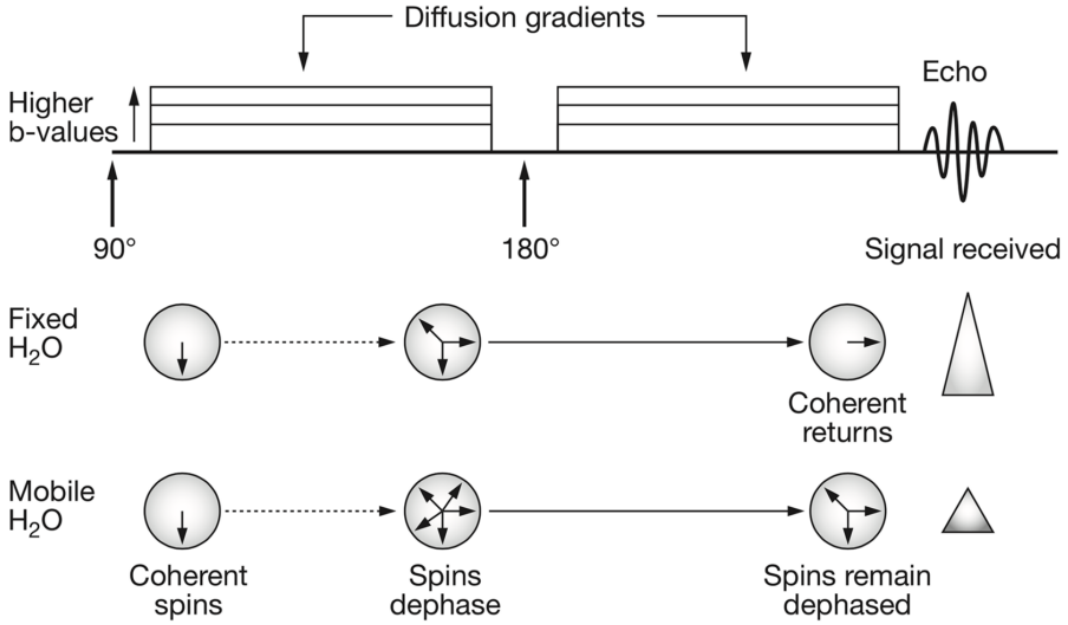

FIGURE 3.1: A spin-echo diffusion sequence.
Diffusion gradient strength and duration is determined by the b-value. For stationary water molecules, the two diffusion gradients effectively cancel each other out, resulting in coherent spin phases, as in a normal spin-echo sequence. For mobile water molecules, the difference in diffusion gradients will cause a loss in phase coherence, resulting in signal attenuation. From Bastiani and Roebroeck (2015)[121].

be converted into an image. For a diffusion-weighted imaging (DWI) sequence, only the insertion of two spatially varying *diffusion* gradients before and after the 180° pulse are required[120] (Fig 3.1). The spatially varying magnitude of the magnetic field from the first gradient serves to label a water molecule's position along a specific axis. The molecule is then free to diffuse for some time after which the second gradient is applied with the same duration and direction after the 180° pulse so as to undo the "labeling" effect of the first gradient. If the molecule has not moved from its original position along the axis of the diffusion gradients, the effect of the two gradients is effectively canceled, and the signal will remain unchanged with respect to a conventional, non-diffusion-weighted imaging sequence. On the other hand, if the molecule has moved from its original position, the difference in strengths of the two gradient pulses will induce a decoherent phase, and the resulting signal will be attenuated with respect to a non-diffusion-encoding sequence (Fig 3.1).

It can be shown that the signal from diffusion decays as an exponential function of the strength and duration of the gradient pulses, summarized in a term called the *b*-value, times the magnitude of observed diffusion along the direction of the diffusion-encoding gradient, called the apparent diffusion coefficient (ADC)[122]. The *b*-value is given by the Stejskal and Tanner equation:

$$b = \gamma^2 G^2 \delta^2 (\Delta - \delta/3) \tag{3.1}$$

where γ is the gyromagnetic constant, G is the magnitude of the diffusion gradient, δ is the duration of the diffusion gradients, and Δ is the time interval between the onsets of both diffusion gradients. By comparing a non-DWI sequence to a DWI sequence, one can show that the natural logarithm of the relative signals becomes linear in b·ADC as shown in the following equation

$$\ln\left[\frac{S(b)}{S(0)}\right] = -b \cdot \mathrm{ADC} \tag{3.2}$$

where *S(b)* is the signal due to diffusion along a specific axis encoded by b, *S(0)* is the signal without diffusion-encoding gradients (b=0 s/mm^2) and ADC refers to the observed magnitude of diffusion of water, given the local environment (e.g., brain tissue). Since the gradient information contained in b is fixed by the experimenter, the ADC can be deduced from the relative signal attenuation.

In DWI, voxel sizes in traditional imaging protocols are typically on the order of a few millimeters, yet free water diffuses only on the order of a few micrometers

on these time scales[124]. In the end, the observed signal attenuation reflects the contribution of all microscopic displacements – both *inter-* and *intra*-voxel – of the water molecules present in a given region of the brain. However, the goal of dMRI is not to measure inherent physical properties of water but to deduce properties of the local microstructure that are reflected through the diffusion of water[124]. In fact, water in the brain diffuses through a complex architecture of axons, cell bodies, glia, and capillaries, which is ultimately captured in the ADC term from equation 3.2. Naturally, therefore, in a given region of the brain, the physical obstacles presented by highly organized axons give rise to different ADC measurements depending on the direction of the diffusion-encoding gradients (Fig 3.2). Water diffusion in such regions is said to be anisotropic. In fact, diffusion is less restricted along the axis of fibers and can be 3 to 6 times faster than in the plane perpendicular to fiber orientation due to a highly organized architecture of hydrophobic cellular membranes, myelin sheaths, and extracellular tortuosity[125].

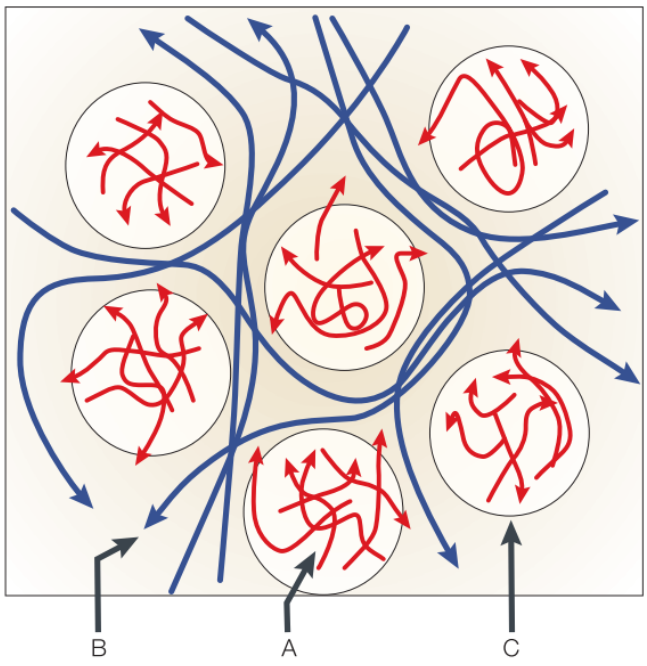

FIGURE 3.2: Different types of water diffusion in the brain.
Diffusion takes place in (A) the intra-cellular space, (B) in the tortuous pathways of the extra-cellular space, or (C) even through cellular membranes or myelin. Adapted from LeBihan (2003)[123].

3.2 Diffusion Models

The diffusion process in the brain can be represented with many models, each with its own level of complexity. This section serves to outline three major models of water diffusion in the brain and the types of inferences one can make about the underlying microstructure in relation to ischemic stroke from the hyperacute to chronic stages.

3.2.1 Isotropic Apparent Diffusion Coefficient

As mentioned in the previous section, the ADC term in equation 3.2 represents the apparent diffusion through local tissue and varies considerably depending on the direction of the applied diffusion gradients[126]. However, it is often desirable to obtain images that are both diffusion-sensitive but direction-independent in order to extract reliable and reproducible information about the local microstructure[122,126–128] The simplest means of removing the effect of white matter anisotropy is to obtain an "isotropic" diffusion weighted (DW) image by taking the average or sum of three diffusion-weighted images with three orthogonal diffusion-encoding gradients (Fig 3.3). From this "isotropic" DW image, a corresponding "isotropic" ADC map, sometimes referred to as trace ADC maps or diffusion trace images, can be obtained with equation 3.2. Diffusion trace images represent quantitative maps that reflect the

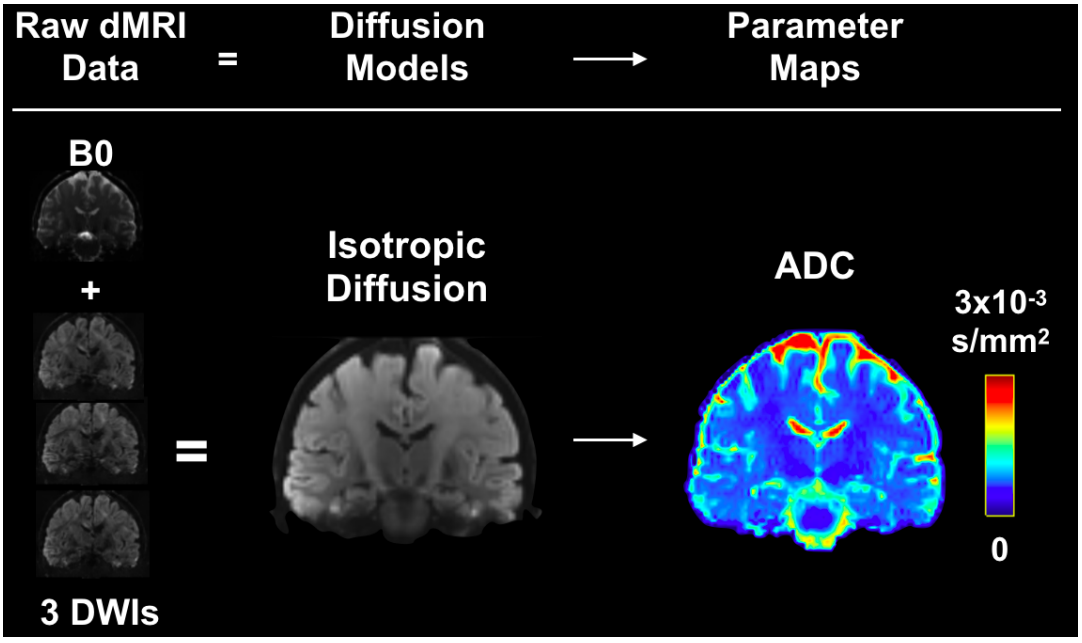

FIGURE 3.3: Isotropic apparent diffusion coefficient model.
At least one non-diffusion-weighted (B0) and three DWIs are required for an isotropic diffusion model yielding apparent diffusion coefficient (ADC) maps.

average diffusivity. The practice of acquiring "isotropic" ADC maps in clinical routine for the detection of acute stroke lesions[129] is so diffuse that the term ADC has become synonymous with isotropic ADC maps. Therefore, for the remainder of the current thesis, ADC refers to isotropic ADC maps unless otherwise noted. The time course of normal and pathological ADC values in ischemic stroke will be elaborated in section 3.4.

3.2.2 Diffusion Tensor Imaging

A more accurate means of studying anisotropic diffusion is with the diffusion tensor imaging (DTI) model. Indeed, while isotropic ADC images bypass certain flaws of direction-sensitive uni-directional ADC maps, they are not capable of fully characterizing diffusion in all directions[130]. DTI is a simple model which represents the diffusion profile in 3D space as a 3×3 tensor, which has a geometrical interpretation as an ellipsoid[120,127]. Instead of estimating direction-dependent apparent diffusion coefficients, DTI serves to estimate a diffusion tensor $\mathbf{D}$ with a simple adjustment to equation 3.2 as follows:

$$\ln\left[\frac{S(\mathbf{b})}{S(0)}\right] = -\|\mathbf{b}\|\,\hat{\mathbf{r}}^{\top}\mathbf{D}\hat{\mathbf{r}} \tag{3.3}$$

where $\mathbf{b}$ is the vector equivalent of the b-factor that now also encodes for the direction of the diffusion gradients $\hat{\mathbf{r}}$, and $\mathbf{D}$ is the symmetric diffusion tensor as shown below

$$\mathbf{D} = \begin{bmatrix} D_{xx} & D_{xy} & D_{xz} \\ D_{yx} & D_{yy} & D_{yz} \\ D_{zx} & D_{zy} & D_{zz} \end{bmatrix}$$

The goal of DTI is to estimate each element of the diffusion tensor $\mathbf{D}$. Since there are six unknowns in $\mathbf{D}$, at least six noncollinear diffusion-encoding measurements in addition to a diffusion-unweighted ($\mathbf{b}$=0) image must be acquired. In practice, diffusion is sampled along many more directions to more reliably estimate the elements of $\mathbf{D}$ due to noise[131]. Then, the coefficients of $\mathbf{D}$ can be estimated with, for example, an Ordinary Least Squares regression by rewriting equation 3.3 as such:

$$\ln\left[\frac{S(\mathbf{b})}{S(0)}\right] = \mathbf{M}\mathbf{c} \tag{3.4}$$

where $\ln\left[\frac{S(\mathbf{b})}{S(0)}\right]$ is a N×1 column vector of the measured diffusion signals along N different gradient directions encoded in **b**, **M** is a N×6 matrix of the different unit vectors describing the N directions along which diffusion is sampled, and **c** is a 6×1 column vector of the six unknown diffusion tensor coefficients to be estimated. The diffusion coefficients can thus be fit for every voxel in an image. These coefficients in each voxel are all measured with respect to the laboratory reference frame; however, by diagonalizing the diffusion matrices, we can represent each tensor in its own local reference frame where its axes are coincident with the major directions of the local diffusion ellipsoid. The resulting whole-brain eigenvalue maps λ_1, λ_2, and λ_3 (where $\lambda_1 > \lambda_2 > \lambda_3$) represent the magnitude of diffusion along these axes , and the eigenvector maps $\mathbf{e}_1$, $\mathbf{e}_2$, and $\mathbf{e}_3$ show the direction of the major and minor axes.

Several scalar maps can be calculated with the eigenvalue maps, each characterizing a different aspect of the underlying diffusion behavior and microstructure[120,127] (Fig 3.4). Fractional Anisotropy (FA) describes the fraction of the total diffusivity that can be attributed to pure anisotropic diffusion and is given by the following equation:

$$\mathrm{FA} = \sqrt{\frac{3}{2} \cdot \frac{(\lambda_1 - \hat{\lambda})^2 + (\lambda_2 - \hat{\lambda})^2 + (\lambda_3 - \hat{\lambda})^2}{\lambda_1^2 + \lambda_2^2 + \lambda_3^2}} \tag{3.5}$$

,

where $\hat{\lambda}$ is the average of the three eigenvalues, also referred to as the Mean Diffusivity (MD). MD is thus related to the trace of the diffusion tensor, given by $\frac{1}{3}\mathrm{Tr}(\mathbf{D})$. As the name indicates, MD is the mathematical equivalent to trace ADC maps or diffusion trace images described previously in section 3.2.1. However, diffusion trace images typically do not benefit from as high a precision as MD maps, which are optimally estimated from the diffusion tensor by solving equation 3.4. It is also possible to investigate the λ_1 map alone, as this represents the magnitude of diffusivity along the major axis of the diffusion tensor. For white matter regions where fibers are high aligned, water molecules would selectively and preferentially diffuse along these axons. The λ_1 map is therefore often referred to as the axial diffusivity (AD). Likewise, we can consider the diffusivity in the plane perpendicular to AD by taking the average of the remaining eigenvalues, λ_2 and λ_3, often termed radial diffusivity (RD). The time course of normal and pathological DTI parameters in ischemic stroke will be elaborated in section 3.4.

While DTI presents several advantages over simple ADC mapping, it is of paramount importance to recognize that a literal interpretation of this model and

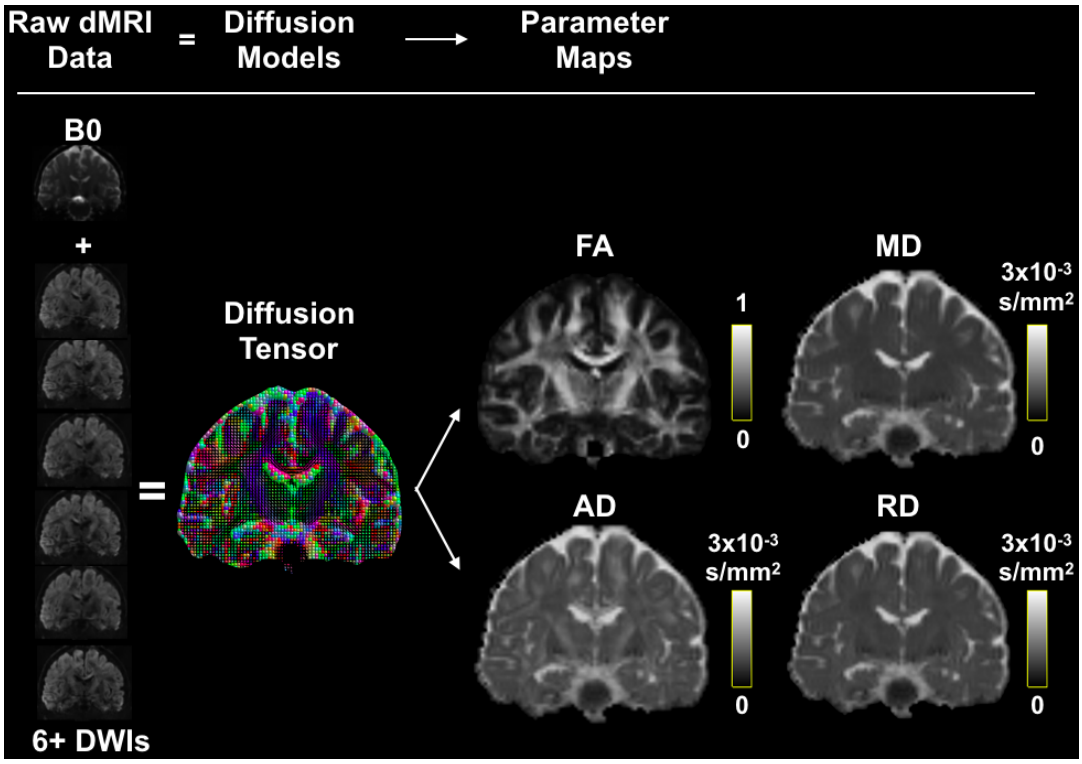

FIGURE 3.4: Diffusion tensor imaging model in the brain.
At least one non-diffusion-weighted (B0) and six DWIs are required for a Diffusion Tensor Imaging model yielding Fractional Anisotropy (FA), Mean Diffusivity (MD), Axial Diffusivity (AD), and Radial Diffusivity (RD) maps. The directions for diffusion tensors are mediolateral for red, anteroposterior for green and superoinferior for blue.

the resulting parameter maps are based on the assumption of a single fiber population in a given voxel. However, a recent study has estimated that up to 90% of the white matter contains multiple fiber orientations[132]. In these "crossing-fiber" regions, DTI parameters, such as FA, highly differ from regions where a single fiber population dominates[132,133]. Therefore, extreme care needs to be taken when relating DTI parameters with the properties of the underlying fibers[134–136].

3.2.3 Fiber Orientation Distribution

Despite the utility and wide-spread use of DTI in studying fiber microstructure and orientation, its invalidity in regions of crossing fibers created a need for more sophisticated techniques to properly characterize the full underlying profile of the diffusion of water[136]. The past two decades have witnessed the emergence of new techniques to model the diffusion process with more precision (see Dell'Acqua et al. (2018) for a review[136]), One particularly successful method is to estimate what is referred to as the fiber orientation distribution (FOD).

The FOD gives the fraction of total fibers within a sample that are aligned along a given direction characterized by (θ,ϕ) in a spherical coordinate system[137]. Several steps are necessary in order to infer fiber orientations from the diffusion signal; however, the process is rather intuitive. Equation 3.2 implies that the observed signal will be strong in directions where diffusion is low, but weak in directions where diffusion is high. Hypothetically speaking, by measuring diffusion in all conceivable directions, a typical shape of the signal from a generic single-fiber population would generate 3D surfaces as shown in figure 3.5. Indeed, by plotting the radius as a function of the strength of the diffusion signal in all orientations (θ,ϕ), the orientation of the fiber can be easily deduced: (1) along the fiber axis, the radius is small (low signal) due to high diffusivity along the fiber, and (2) in a plane normal to the fiber axis, the radius is larger (stronger signal) due to low diffusivity perpendicular to the fiber. If we assume that all fiber populations yield the same response function with respect to their respective fiber orientation, the signal resulting from the presence of two fibers in the same regions of space will be nothing other than the linear superposition of their respective response functions. The following simple relationship can thus be established:

$$S(\theta, \phi) = F(\theta, \phi) \otimes R(\theta) \tag{3.6}$$

where $S(\theta, \phi)$ is the measured signal along a given direction, $F(\theta, \phi)$ is the underlying FOD, and $R(\theta)$ is the canonical "response function" for a single fiber population, and $\otimes$ is the convolution operator.

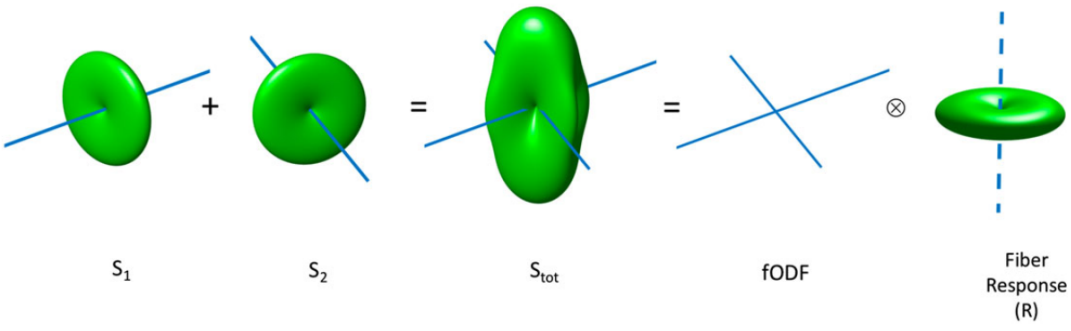

FIGURE 3.5: A schematic representation of spherical convolution. Each underlying fiber (blue line) yields a "canonical" signal S represented by the radius of the green surface from the origin. The observed signal in a voxel is simply the linear superposition of the response functions (R) from all present fibers, represented by the fiber orientation distribution function (fODF) or (FOD). Adapted from Dell'Acqua (2018)[136].

Since the signal is often represented in the spherical coordinate system, it can be easily reconstructed in the spherical harmonic basis. Indeed, similar to how a sound wave can be reconstructed with a linear superposition of sine and cosine waves, the diffusion signal measured in a many directions can be reconstructed with a set of spherical basis functions. With this approach, the goal is to infer the underlying FOD by undoing the convolution operation in equation 3.6 (i.e., through deconvolution). If one assumes a fixed response function defined *a priori*, then the only unknowns to estimate are the coefficients of the spherical harmonic functions to linearly reconstruct the measured signal.

To perfectly reconstruct the continuous FOD function would require an infinite number of spherical harmonics; however, in practice, only a few components are needed to adequately estimate the FOD. The number of spherical harmonic components in the FOD used to reconstruct the diffusion signal is governed by the maximum degree, denoted by ℓ_{max}. As ℓ_{max} increases, the number and angular precision of fiber populations which can be accurately reconstructed both increase, at the expense of more unknown coefficients to estimate, which, in turn, require more DW images[138]. Due to certain properties of the DWI signal, the minimum number of DW images required to estimate the number of spherical harmonics up to degree ℓ_{max} is given by $n = \frac{1}{2}(\ell_{max}+1)(\ell_{max}+2)$[138]. To properly resolve two fiber populations (e.g., crossing fibers) in a given voxel, it is recommended to estimate FODs with at least a ℓ_{max} of 4, corresponding to a minimum of 15 directions. However, in practice, diffusion should be sampled along more directions in order to accurately estimate the shape of the underlying FOD[138].

3.3 Tractography

A major application of modeling the diffusion signal with diffusion tensors or FODs is diffusion tractography, a technique for reconstructing entire fiber bundles in the brain[139]. The process consists of (1) starting at a single point in the brain, called a seed point, (2) observing the local fiber orientation, and (3) moving in that direction some short distance Δ, called the step-size. This process is repeated at each step to trace out the fiber's trajectory, until various termination criteria are met such as (A) a fiber reaching a pre-defined endpoint, for instance, the edge of the brain, gray matter, or CSF, (B) an area of small FOD amplitude, (C) or sharp changes in fiber orientation[139].

The resulting virtual fiber is also called a streamline, in order to distinguish the mathematical nature of the object from a true biological fiber.

The manner in which the streamline proceeds throughout the brain volume depends on two popular frameworks called deterministic tractography and probabilistic tractography[140]. While deterministic tractography results in a streamline that faithfully follows the direction of maximum diffusivity (given by the primary eigenvector in DTI or the peaks of the FOD shape), probabilistic tractography can use the FOD or tensor model as a probability distribution to choose the direction in which a streamline most likely proceeds. As the name indicates, deterministic tractography will always yield the same result for a given configuration of initial seed points, whereas streamlines in probabilistic tractography can differ. The advantage of probabilistic tractography is that streamlines are more disperse due to the probabilistic nature of the algorithm; by creating many seed points, the true underlying pathway is presumed to be where the majority of streamlines pass[141]. Since FODs can resolve

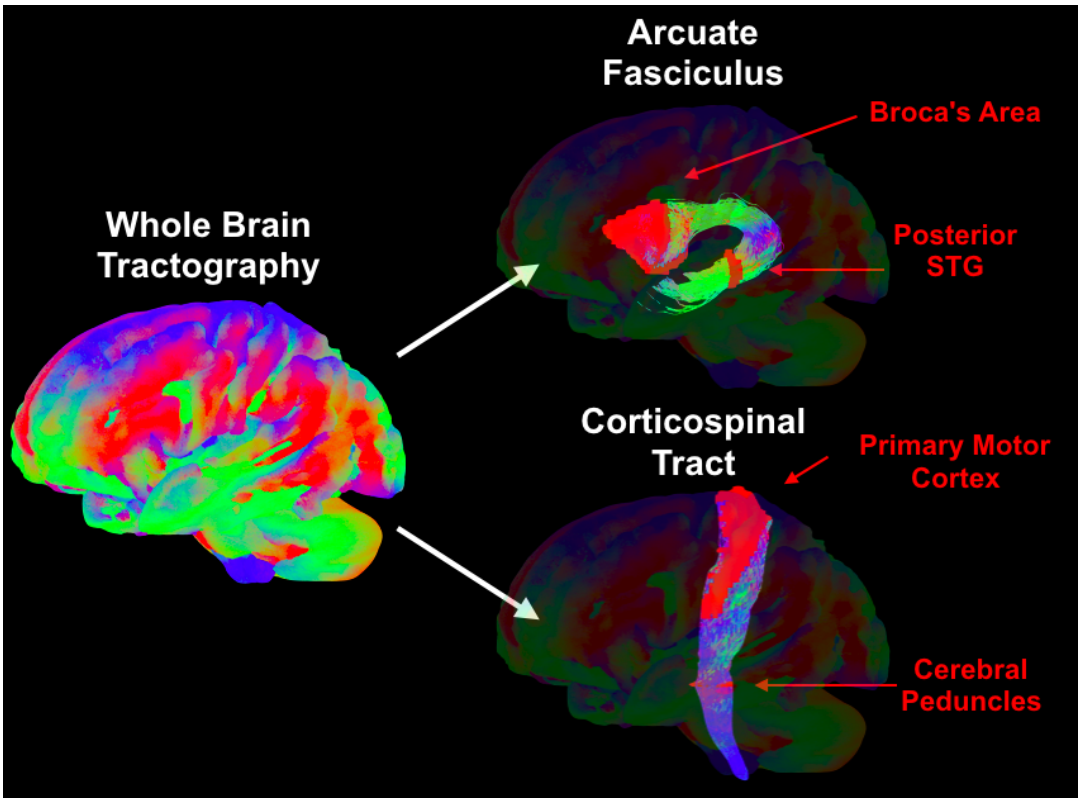

FIGURE 3.6: Virtual fiber dissection with tractography.
Shown here is an example of whole-brain tractography done on a healthy subject. Regions of interest (red) are placed according to the anatomy of the pathway of interest. Streamline colors are given by the primary diffusion axis: mediolateral for red, anteroposterior for green and superoinferior for blue. STG, superior temporal gyrus.

multiple fibers in a single region, FOD-based tractography in a probabilistic framework has been repeatedly shown to accurately reconstruct intersecting major white matter tracts in the brain, especially in the lesioned brain[139,141].

The virtual dissection of known fiber pathways typically requires that the user draw inclusion regions of interest (ROIs) at areas that the fiber pathway traverses based on *a priori* anatomical knowledge. For longer tracts, several inclusion ROIs are drawn to better extract relevant fibers. Likewise, exclusion ROIs can be used to filter out erroneous fibers. One strategy consists in using one of the inclusion ROIs to generate seed points and using the other ROIs to filter out aberrant fibers not part of the targeted pathway. The second strategy consists of creating seed points in all voxels in the brain, a process referred to as whole brain tractography, and subsequently dissecting the tract with the pertinent ROIs (Fig 3.6).

3.4 Evolution of Diffusion MRI Parameters in Ischemic Stroke

3.4.1 Diffusion MRI Parameters in the Healthy Brain

Understanding the evolution of the various diffusion parameters in ischemic stroke is important for determining the sensitivity of each one for quantifying neuronal damage and thus its relationship with future outcome. At baseline, the individual values of FA, MD/ADC, AD, and RD depend on the spatial organization and fiber density and also vary as a function of age[142]. A stable reference point is the cerebrospinal fluid (CSF): mostly composed of water and thus rather isotropic, CSF values of FA are rather low (around 0.01-0.15), and MD, AD, and RD values are on average about 3.0×10^{-3}s/mm^2 [143]. Grey matter, which is marginally more anisotropic than the CSF, has a FA spread of 0.05-0.25 due to a slightly larger AD (0.8-1.0$\times10^{-3}$s/mm^2) than RD (0.6-0.8$\times10^{-3}$s/mm^2)[143]. Diffusion values in the white matter vary the most according to the local fiber number and density. For example, the average FA of the corticospinal tract is around 0.50-0.55, with MD/AD/RD values around 0.75-0.80/1.35-1.45/0.55-0.66$\times10^{-3}$s/mm^2 [142,144]. On the other hand, the tightly packed fibers of the genu of the corpus callosum yield average FA values of 0.80-0.90 and MD/AD/RD values around 0.60-0.65/1.40-1.45/0.20-0.25$\times10^{-3}$s/mm^2 [142,144]. Due to the spatial dependence of diffusion properties in the white matter, most studies investigate relative changes of diffusion parameters in the lesion with respect to control regions-of-interest (ROIs), usually consisting of the contralesional homologous region. By presuming that the contralesional ROI is representative of the infarcted

area before stroke onset, the evolution of diffusion properties in the lesion can be represented as changes from a baseline measure (Fig 3.7).

3.4.2 Diffusion MRI Parameters in Ischemic Lesions and Their Evolution

Within 30 minutes of vessel occlusion from stroke, cytotoxic edema drives an inflow of water into neurons, increasing intracellular fluid and thus decreasing extracellular space[145]. Swollen neurons result in water restriction in the axoplasm as well as an increased tortuosity in the extracellular environment. Ultimately, this mechanism is responsible for the hallmark sign of stroke, that is, a hypersignal in DWI and a decrease in ADC, which are visible on MRI as early as 30 minutes after occlusion[146]. In fact, the decrease in ADC/MD at this hyperacute stage of stroke (<7 hours) is driven by significant decreases in AD by 37% and RD by 45% with respect to baseline[147,148]. The stronger decrease in RD *vs.* AD results in elevated FA (by a factor of 1.1[146,149], which has also been observed on MRI in humans as early as 2-7 hours post-stroke[146,148,150,151].

The acute and early sub-acute phase (i.e., 24 hours to 1 month post-stroke) is characterized by an increase in RD following the end of cytotoxic edema and the onset of the breakdown of myelin sheaths[145,147]. AD, on the other hand, remains

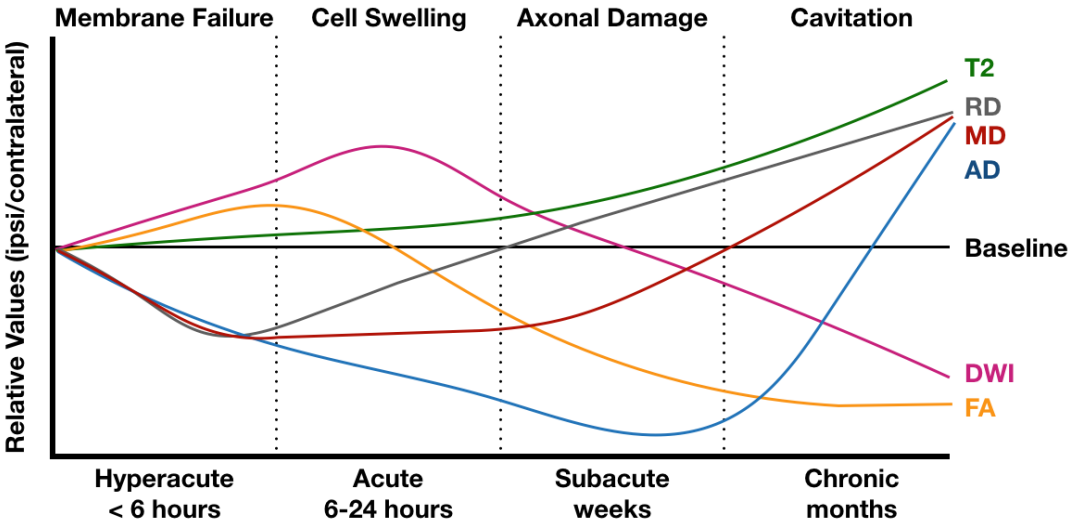

FIGURE 3.7: Illustrative evolution of diffusion MRI parameters in ischemic stroke lesions.
The evolution of each parameter in the ipsilesional hemisphere is relative to the unchanging signal of the contralesional unaffected hemisphere. T2, hyperintensity on non-diffusion-weighted images; RD, radial diffusivity; MD, mean diffusivity; AD, axial diffusivity; DWI, diffusion weighted image; FA, fractional anisotropy.

decreased throughout this time due to permanent axonal damage following the initial ischemia, only to normalize and subsequently increase around 2-3 weeks post-stroke due to lesion cavitation[147,152]. Within the first 2 weeks post-stroke, therefore, the stable decrease in AD and steadily increasing RD give rise to an early normalization of FA around 24-36 hours post-stroke and a steady subsequent reduction of FA as of 3-5 days post-stroke until cavitation has been achieved several weeks later[146,147,150,153]. Likewise, during the same period, MD normalizes at about 2 weeks post-stroke[154–157] and continues to increase until cavitation.

Beyond local changes within the infarct core, remote effects can also be observed due to a process referred to as Wallerian degeneration[158]. Following neuronal injury within an ischemic lesion, anterograde degeneration of the distal parts of neurons takes place with the disintegration of the axonal skeleton and degradation of myelin sheaths. For example, Wallerian degeneration of the CST following a stroke of the middle cerebral artery typically reaches the cerebral peduncles at around 1 week post-stroke. This process has been corroborated by several studies reporting quasi-normal FA of the cerebral peduncles at 80 hours post-stroke[159] but significant observable decreases in FA[157,160], ADC[161], and AD[162] around 1 week. In similar studies performed in patients after 1 week and well into the chronic stage (i.e., > 1 year post-stroke), a decreased AD can be reliably observed in distal portions of the CST due to microstructral obstacles following axonal breakdown, whereas a permanent increase in RD can be observed due to the degradation of myelin sheaths[157,160]. Ultimately, this results in a perpetual decrease in FA not only within the lesion but also along the entire affected pathway.

3.5 Types of Analyses in Diffusion MRI

In many studies on stroke outcome with diffusion MRI, investigators typically aim to establish the existence of correlations between early brain damage and future outcome. Brain damage can be inferred and characterized by various means with the previously described diffusion models and the resulting parameter maps. Currently, there is no gold-standard for this practice; therefore, the current section serves to outline the two most common strategies for relating early brain damage from stroke and future clinical scores in addition their strengths and weaknesses: region-of-interest and tract-specific analyses. Figure 3.8 serves as a reference for this section.

3.5.1 Region-of-Interests Analyses in Native Space

As mentioned in section 3.2.2, dMRI-derived parameter maps can provide information about the microstructure of white matter fibers in the brain and thus abnormalities due to ischemic stroke. One of the simplest methods to characterize stroke damage reflected through diffusion changes is to calculate the average value within a region-of-interest (ROI) (Fig 3.8). Drawing ROIs by hand directly on a subject's image (i.e, in native space) requires expert knowledge in neuroanatomy and also strong *a priori* hypotheses regarding the outcome measure and the chosen structure[163–165].

3.5.2 Tract-Specific Analyses in Native Space

Several tract-specific types of analysis are possible with tractography:
(A) The most direct measure is the number of streamlines that successfully reconstruct a tract. Indeed, since severe strokes are known to create white matter disconnections in the brain, a loss of streamlines for certain pathways with respect to the contralesional hemisphere or healthy controls usually reflects a loss of function[166–169]. However, particular care is required when analyzing the absolute number of streamlines as it is also determined by the size of the ROI used to generate seed points as

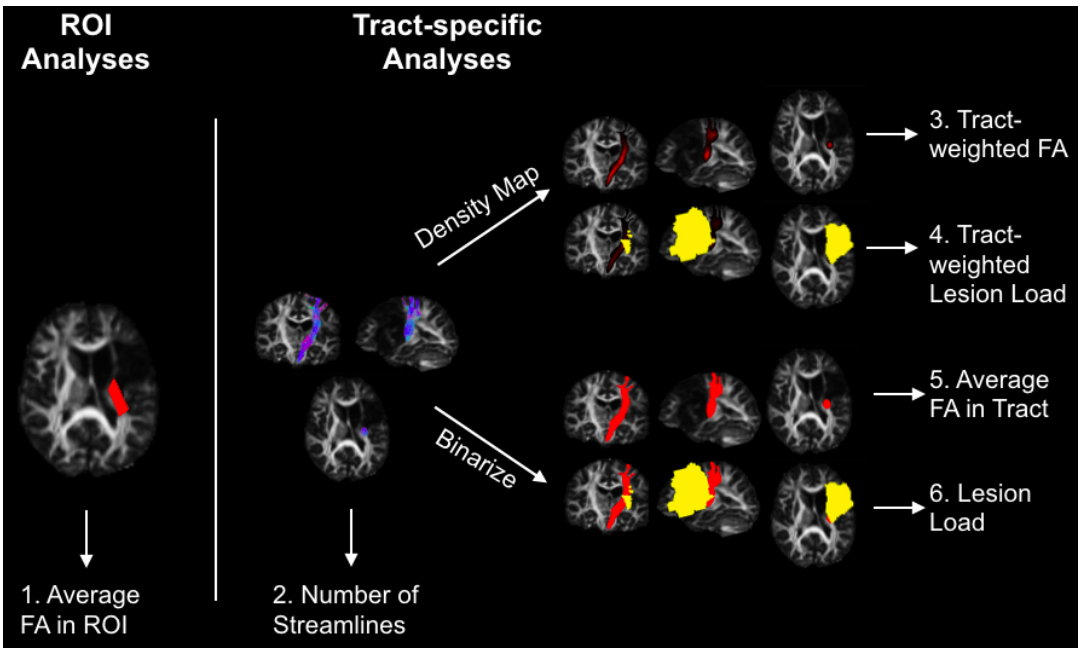

FIGURE 3.8: Common analyses with diffusion MRI.
Left: Regions of Interest (ROIs) serve to extract the average value of a parameter of interest. Shown here is a ROI in the posterior limb of the internal capsule overlaid on a FA map of a chronic stroke patient. Right: Various tract-specific analyses exist after virtual dissection of a pathway with tractography.

well as voxel size (smaller voxels yield more seeds for a fixed ROI volume).
(B) Second, a set of streamlines constituting a reconstructed pathway can be converted into a *density* image in which each voxel reflects the number of streamlines passing through it. Alternatively, the image can be binarized to create a "mask" simply depicting the spatial location of a tract. In this framework, the entire tract becomes a ROI from which average parameters can be extracted. In the case of density maps, the contribution of each voxel in the average is weighted by the number of streamlines passing through it, since areas where tract density is high are presumed to have a higher probability of belonging to the tract in question[139].
(C) Third, one can also calculate the percent of a tract intersected by a patient's hand drawn lesion mask, referred to as lesion load[39,45,170].

The greatest benefit of the previously described ROI and tract-specific analyses is the specificity to each patient. However, in certain cases, various problems may arise[171]. For manually drawn ROIs, the operator bias can severely hinder the reproducibility of reported results, and severe stroke may sometimes obscure the exact boundaries of certain structures. For tract-specific analyses using tractography-derived masks, reconstructed pathways – and thus parameter extraction – is limited to the parts of the tract where neuronal integrity is most preserved and spared by stroke[164]. More serious lesions may result in the failure to recover any streamlines, preventing investigators from attributing a tract-specific measure for these patients or forcing them to assign a default value of 0[172,173]. In any case, both methods can be time consuming if the study sample is rather large.

3.5.3 ROI and Tract-Specific Analysis in a Common Space with Spatial Normalization

To lessen the time burden of processing images in large cohorts, many researchers resort to conducting analyses in a common space through spatial normalization. With this procedure, a single ROI can be drawn on a standard imaging template, and tract probability maps can be constructed by considering the spatial overlap of warped tracts reconstructed in healthy individuals[174] or directly within the imaging template[175,176]. The same ROI or tract mask/probability map in a standard space can thus be used to extract the average parameter of interest from all warped images. This approach has gained significant momentum in the past decade[54], resulting in the creation of many public imaging "reference" templates[175,177,178], atlases of long-range tracts[83,174] or ROIs for various brain regions[179].

The process of spatial normalization consists in deforming a "source" image $\mathcal{I}$ to resemble a "reference" image $\mathcal{J}$. More precisely, one attempts to establish a spatial transformation ϕ that maps each voxel $\mathbf{x}$ in image $\mathcal{I}$ to the corresponding location $\mathbf{x'}$ in image $\mathcal{J}$ by minimizing some cost function $\mathcal{C}$, which describes the similarity between both images[180]. After successful spatial normalization of a cohort to a standard imaging template image, the same voxel for all images at location $\mathbf{x'}$ in the standard space corresponds – within some error – to the same anatomical landmark.

3.5.4 Voxel-based Analyses in a Common Space

Spatial normalization naturally paves the way for a set of analyses called voxel-based analyses (VBAs). In general, for VBAs, images of a cohort are grouped together in a 4D volume where the first 3 dimensions correspond to the size of the image (x,y,z), and the 4th dimension is determined by the sample size N (Fig 3.9). Due to the anatomical correspondence between spatially normalized images, all voxels (i,j,k)

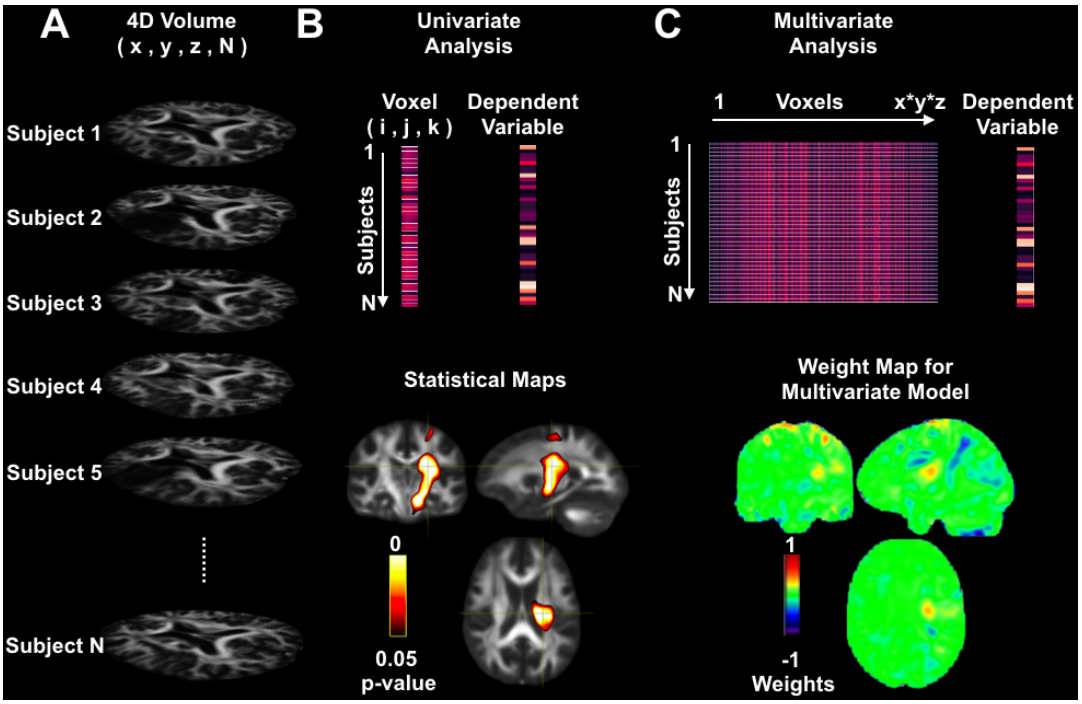

FIGURE 3.9: Voxel-based analyses.
(A) Images in a cohort are stored as a 4D file where the first 3 dimensions correspond to the size of the image, and the 4th dimension is determined by the sample size N. (B) Univariate analyses are independent statistical analyses performed at every voxel with a dependent variable. (C) Multivariate analyses transform the input volume (x,y,z,N) to a 2D data matrix (N,x*y*z) in which all voxels are used as features for machine learning algorithms, the output of which can be a weight map for classifiers or decoders. Weight maps adapted from Rondina et al. (2017)[181].

map to the same anatomical area. Therefore, the results of voxel-wise analyses can be mapped back onto the brain in order to make inferences on the underlying structures at a specific location. The major advantage of VBAs over ROI or tract-based analyses is the absence of *a priori* assumptions concerning the choice of a given structure or isolated tracts for posited structure-function relations.

Two types of frameworks are common for VBAs: mass univariate analyses at every voxel[182] or multivariate machine learning analyses[183,184] (Fig 3.9). In mass univariate analyses, independent statistical tests are performed at every voxel (i,j,k) by extracting their values for every subject (along the 4^{th} dimension). The output of such analyses are statistical maps that show the significant relationships between brain regions and a given dependent variable. Multivariate analyses, on the other hand, take the entire 4D volume and transform it into a 2D data matrix of size (N,x*y*z) in which all voxels are used as features for a given machine learning algorithm[184]. The output of these models are typically weight maps for classifiers or decoders[185].

One advantage of multivariate machine learning techniques is that they can account for complex interactions between distant brain regions, unlike in univariate analyses where every voxel is considered independent from one another[186]. However, a major downside of multivariate analyses is that they require large amounts of data to be reliable due to the disproportionate number of features (i.e., voxels) to subjects[187]. This imbalance is commonly referred to as the curse of dimensionality and can hinder the performance of multivariate models. Univariate analyses, on the other hand, can perform reasonably well with smaller sample sizes.

In light of the descriptions of the most common methods for analyzing diffusion MRI data, Table 3.1 provides a summary of each method's pros and cons.

Analysis	Native	Common
All types	Pro: • Specific to a patient's brain morphology Con: • Operator Bias • Requires expert knowledge in neuroanatomy • Time-consuming	Pro: • Time efficient Con: • Registration mismatches • Lesion-healthy template dissimilarities
ROI	Pro: • – Con: • Stroke may blur boundaries • *A priori* assumptions needed for selected ROI	Pro: • – Con: • Does not match patient's brain morphology • Difficulty in finding publically available atlases for ROIs of specific structures (e.g., PMv, PMd)
Tract-based	Pro: • Patient-specific tract morphology may be a property of interest Con • Restrained to parts of the tract with the highest neuronal integrity • Automatic assignment of 0 for non-reconstructible tracts • *A priori* assumptions needed for selected tract	Pro: • Can evaluate changes for patients with non-reconstructible tracts Con: • Unable to disentangle lesion from remote effects (e.g., Wallerian Degeneration) • Normalization may not take into account infarct-induced changes to tract trajectory
Voxel-based	Pro: • Analysis not possible Con: • Analysis not possible	Pro: • No *a priori* assumptions for anatomo-behavioral relations Con: • –

TABLE 3.1: A comparison of the pros and cons of different common analyses with diffusion MRI data performed in a patient's native space or in a common space. PMv = ventral premotor cortex, PMd = dorsal premotor cortex.

3.6 Advances in Normalization Techniques and Stroke Patient Images

For all the reasons exposed in the table, we chose in this thesis to analyze our acute stroke images in a common space. However, working in a common space required a careful consideration of the available options regarding normalization strategies of dMRI data within the scientific community.

3.6.1 Normalization Strategies

Many studies that conduct analyses in a common space resort to one of the two following normalization strategies: (1) directly warping FA images to a FA template[48,59,188,189] or (2) coregistering dMRI data to a high-resolution anatomical image (e.g., T1-weighted), normalizing said image to a standard space, and applying the warp field to dMRI-derived parameter maps[172,190,191]. However, T1-weighted images are completely insensitive to the complex fiber architecture of the white matter, and FA provides no information on the orientation of the underlying neural fibers (Fig 3.10). Using scalar images such as these for spatial normalization may not result in proper overlap of white matter regions between subjects. Recently, researchers have proposed more powerful registration algorithms, based on the entire diffusion tensor or FOD, and thus result in better alignment of major white matter pathways with respect to scalar-based registration.

Two recently developed software packages that optimize registration between diffusion tensor images and FOD images are DTI-TK[192] and MRtrix3[176], respectively. While a specific comparison of tensor *vs.* FOD registration has not been done, each software has been shown to perform better than FA-based registration in aligning well-known fiber bundles of the white matter in healthy subjects[176,193]. However, the superiority of FOD/DTI over FA-based registration has yet to be proven in stroke images and could also depend on the age of the stroke lesion. Indeed, as detailed in section 3.4, diffusion parameters drastically change throughout the different stages of stroke and could influence the behavior of FOD/DTI-based registration models, which have only been evaluated in healthy subjects. Therefore, considering that (1) the efficacy of ROI, tract-based, and voxel-based analyses performed in a common space highly depends on the quality of the non-linear warping and (2) white matter structures play an integral role in stroke outcome, these recent findings suggest that such registration techniques could be highly beneficial for studies investigating white

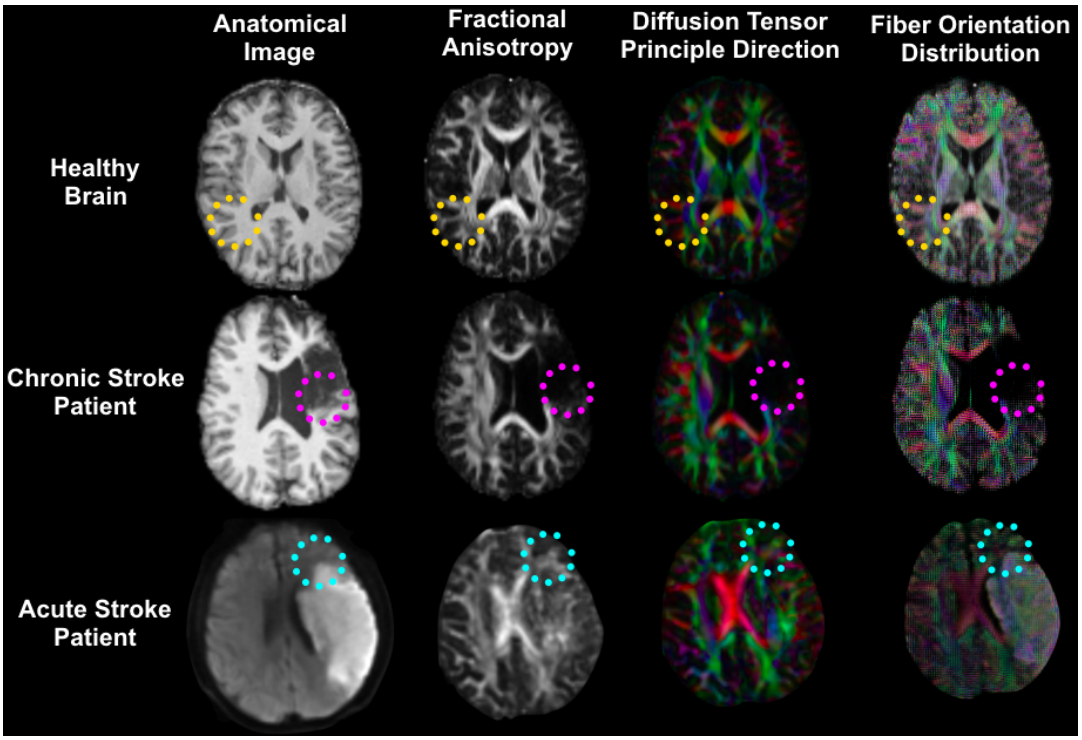

FIGURE 3.10: Sensitivity of imaging modalities to fiber orientation. Top: Different common imaging modalities capture the complex architecture of white matter in healthy individuals at varying degrees of sensitivity. From least to highest, T1-weighted, Fractional Anisotropy, Diffusion Tensors, and Fiber Orientation Distributions (FOD). The yellow dotted circle highlights an area where multiple fiber populations cross. Lesioned tissue appears abnormal on different imaging modalities for chronic (middle) and acute (bottom) stroke patients. The pink and turquoise dotted circles highlight a chronic and acute stroke lesion and the adjacent tissue, respectively. The directions for diffusion tensors and FODs are mediolateral for red, anteroposterior for green and superoinferior for blue.

matter in stroke using analyses conducted in a standard space. However, a proper comparison of their effectiveness with commonly used scalar techniques in stroke subjects is merited.

3.6.2 To Mask the Lesion or Not?

Regardless of the normalization strategy chosen, an important hurdle for registering stroke images is accounting for the large dissimilarities between lesioned regions in a patient's image and the corresponding areas in a template (Fig 3.10). In general, registration algorithms attempt to maximize the similarity between the patient's image and the template by overly distorting the lesion during non-linear warping, usually by shrinking the lesion[194–196]. By masking the lesion from the

similarity calculation, such distortions can be lessened in order to obtain a more accurate normalization[194,196,197]. A more advanced technique proposed by Nachev et al. (2008)[198], called enantiomorphic normalization, consists in replacing lesioned tissue by contralesional homologous healthy tissue before performing normalization. While a vast majority of this work has investigated the practice of "lesion-masking" at the chronic stage and on T1 or FA images[194,196–198], its effect on diffusion tensor or FOD images in either acute or chronic stroke had yet to be elucidated before the present doctoral thesis. Moreover, due to the differential changes in diffusion properties at each stage of stroke, different normalization strategies might have different effects for such populations. Therefore, in order to select the most appropriate strategy to normalize stroke data and, considering that the existing literature did not provide an adequate solution, we decided to first conduct a methodological study to elucidate this question (see chapter 5 in Part II - Thesis Work).

Chapter 4

Prognostic Value of Diffusion MRI at the Acute Phase for Long-term Outcome

Contents

As described in chapter 1, one of the main goals of stroke research is to be able to predict future outcome as soon as possible, even as early as 24 hours post stroke. While clinical data are robust predictors, they suffer from a poor specificity-sensitivity trade-off in patients with mild-to-severe stroke. The added value of neuroimaging could therefore be found especially within this subpopulation. In a clinical setting, DWI is the MRI modality of choice as this sequence is acquired routinely for the diagnosis and monitoring of ischemic stroke patients. In research, the use of early DWI data to predict long-term outcome relies on three major types of analyses: (1) clinical models incorporating lesion volume, (2) analyzing the effect of lesion location with voxel-based analyses (VBAs), and (3) studying region-of-interest (ROI) or tract-specific properties. The present chapter serves to review recent, important studies seeking to use early DWI data obtained within 1 week post-stroke in order to explain mid- or long-term outcome past 1 month post-stroke. For each analysis, significant contributions will be discussed first for motor, then language, and finally global outcome. Moreover, the sections detailing recent studies resorting to VBA, ROI and tract-specific studies will encompass all imaging modalities derived from DWI sequences (e.g., lesion segmentations, ADC, or DTI-derived parameters). Finally, it is worth noting that a fourth type of analysis exists with DWI data: tractography. While certain studies have used tractography in the native space of acute stroke patients to investigate long-term outcome, (1) the majority of them were performed at the early developmental stages of dMRI, when tractography algorithms were not well developed and imaging sequences were long with coarse spatial resolution and low angular resolution; (2) sample sizes of these studies are rather low; and (3) it has not proven to be a rather successful predictor of outcome when performed at the acute stage but harbors greater predictive value at the subacute and chronic stages. For these reasons, I have chosen to not discuss these studies in the context of the present thesis.

4.1 Lesion Volume

Arguably the most impactful contribution of DWI is the highly sensitive detection of acute ischemia for emergency management of stroke[199]. By manually delineating the presence of hypersignal regions on DW images, one can obtain a rather accurate estimation of the volume of the lesion. Due to the known relationship between *final*

lesion volume and outcome scores, clinicians and researchers were naturally interested in the additive prognostic value of *acute* lesion volume in addition to important clinical values, such as early stroke severity and age[200–202]. Thijs et al. (2000)[200] were among the first to report that DWI lesion volume measured within 48 hours of symptom onset was an independent predictor (with respect to early NIHSS and age) of autonomy *vs.* dependency assessed with a Barthel Index cutoff at 85. In two studies by Johnston and colleagues, lesion volume did not yield clinically important increases in predicting excellent outcome or death better than clinical variables, whether they were measured upon admission[201] or at day 5[202]. However, in these studies, their outcome criteria were more skewed towards patients with very good outcome assessed as a Barthel Index score of > 95 or mRS 0-1. Yoo and colleagues[26], on the other hand, reported in a cohort of 54 patients that all those with DWI lesion volumes < 72cm^3 had good outcome using a mRS cutoff at 2, yielding a better model than NIHSS alone. While achieving a specificity of 100%, the same model only predicted poor outcome with a sensitivity of 61.9%. Similar trends have been observed between lesion volume and with more fine outcome scales in the motor[203,204] and language[204,205] domains; however, the size of the lesion likely contributes differently to prognosis. For instance, since motor function primarily relies on intact fibers of a single anatomical tract, the CST, location is arguably more important than volume[170,206]. On the other hand, language function is subserved by several fiber bundles in the brain which play a compensatory role when one is damaged[91,92]. Persistent aphasia is therefore often the result of large lesions simultaneously affected several fiber bundles[104,115], attributing a more important role to lesion volume than for motor function.

4.2 Lesion Location

Beyond mere lesion load, segmented lesions from DW images – or other anatomical imaging modalities – provide valuable information on an infarct's spatial distribution and the precise regions that are affected. Lesion topography is therefore a rich, patient-specific measure, which can shed light on the determinants of post-stroke outcome in individual functional domains[204,207,208].

With regards to the objectives of the current thesis – that is, early imaging for long-term prognosis – certain methodological considerations regarding lesion-behavior relationships should be addressed. Lesion topography can be associated to long-term outcome using either (1) a binary mask of the segmented lesion, or (2) parameter

maps capable of quantifying brain damage by reflecting biological processes, such as DTI parameter maps. The fundamental difference between both methods lies in their dependency on infarct chronicity.

Concerning the use of lesion segmentations, the spatial extent of stroke lesions between the acute and chronic stage has been shown to correlate quite well (r=0.84, p<0.0001)[209], despite acute lesion size significantly overestimating the extent of the final infarct[210]. It thus becomes difficult to disentangle the prognostic value of binary segmentations of acute *vs.* chronic lesions when the dependent variable remains chronic outcome in both cases. Indeed, most studies investigating the relationship between chronic lesion topography with long-term outcome often make inferences that transcend infarct chronicity[47,181,211,212]; in other words, if a lesion-function relationship is observed at the chronic stage, similarly infarcted tissue in the acute stage should yield comparable long-term deficits[213]. Karnath et al. (2017)[214] addressed this exact question by performing lesion-symptom mapping using structural images and behavioral scores at both the acute (<5 days) and chronic stage (mean$\pm$standard deviation: 409$\pm$202 days). They obtained the same results with either acute *or* chronic images to explain chronic outcome (on the condition that patients who recovered be included in the analysis). For this reason, this section will discuss pertinent lesion-behavior studies performed to address the anatomical correlates of chronic outcome or recovery (i.e., transient vs. persistent deficits), regardless of the time point of imaging.

With respect to DTI parameter maps, microstructural differences within infarcted tissue drastically change from the acute to the subacute and chronic stages, as described in section 3.4. Consequently, when one is interested in the prognostic value of early imaging parameters (such as those from DTI), *only* images acquired at the acute stage should be used. Diffusion indices used at alternative time points may be indicative of neural repair processes unique to later stages of stroke. For example, one study by Chen et al. (2008) sought to relate DTI parameters of the anterior, knee, and posterior limbs of the internal capsule and muscle strength in nine stroke patients scanned between 2 hours and 14 days post stroke (mean$\pm$standard deviation = 5.0$\pm$5.7 days). However, this time period is when DTI parameters are most dynamic due to different cellular and molecular processes involved in neural repair. This particular study hence suffers from severe methodological flaws, and the proposed structure-function relationships should be interpreted with extreme caution. For these reasons, only pertinent studies having acquired DTI data within 1 week will be

discussed here.

4.2.1 Motor Outcome

Most voxel-wise studies on motor deficits from stroke have been performed at the chronic stage. One such study by Lo et al. (2010)[47] revealed that motor ability assessed by the Jebsen-Taylor Test (JTT) and Upper Extremity Fugl-Meyer (UE-FM) scale was highly correlated with damage to the corona radiata where several corticofugal fibers descend from the primary motor and sensory cortices as well as the premotor cortex. A very detailed study by Ramsey and colleagues (2017)[204] had imaging data of 132 patients within 2 weeks post-stroke and behavioral data at 3 months post-stroke. Controlling for lesion size, age, education level, physiotherapy dose, and baseline behavioral measurements, they showed that lesions (characterized by binary lesion segmentation) involved in the deep white matter of the corona radiata were significantly correlated with worse motor outcome. A third study by Liu et al. (2017)[215] acquired DTI data in patients within 1 week post-stroke and motor evaluations with the UE-FM at baseline and 3 months post-stroke. The longitudinal data allowed them to retrospectively identify patients for whom recovery was proportional to their initial severity (PROP) and severely impaired patients that recovered poor function (POOR). A voxel-wise analysis revealed that within 1 week post stroke, MD in the PLIC, corona radiata, and cerebral peduncles but not FA was able to distinguish between PROP and POOR groups. Furthermore, MD in the posterior limb of the interal capsule (PLIC) and corona radiata but not FA was able to predict motor improvements. That MD but not FA was sensitive to detect group level differences as well as predict future recovery is in line with the time course of diffusion parameters within the first week of stroke. At this time, MD remains decreased due to axonal damage (reflected by decreases in AD), whereas FA normalizes at this time. At the chronic stage, however, other studies have found relationships between FA and motor abilities. For instance, Wang et al. (2018)[216] scanned 18 chronic stroke patients (29 weeks post-stroke) and found that lower FA in regions of the corpus callosum, internal capsule, cortico-pontine-cerebellar and superior longitudinal fasciculus were correlated with motor performance. Two other studies reported a lack of correlation between diffusion abnormalitites and motor performance at the chronic stage, but the sample sizes were rather low (N=11[173],N=10[217]).

4.2.2 Language Outcome

Language encompasses a plethora of abilities related to speech production and comprehension and can be evaluated by testing different skills, such as articulation, prosody, phonematic structure, speech repetition, speech comprehension, picture naming, reading, and semantic differentiation[218]. These skills are usually attributed to one of the two streams of language, with faculties of speech production (e.g., fluency, object naming, repetition, naming-sentence-completion, etc.) being more associated with the dorsal stream and faculties of speech comprehension (e.g., phonemic errors, phonological errors, semantics, etc.) being more associated with the ventral stream. Indeed, due to the many abilities that language comprises, whole-brain exploratory analyses on the anatomical correlates of language abilities are abundant[214]. A major finding of these studies is that a wide variety of aphasia symptoms seems to be specific to the left hemisphere peri-sylvian regions[94]. One noteworthy study by Fridriksson et al. (2016) performed lesion-symptom analyses for many aspects of language processing and investigated the principle components of the spatial distribution of the resulting statistical maps. They found that the first principle component reflected global aphasia severity due to lesion distributions across the peri-sylvian territory, whereas the classical ventral and dorsal streams naturally emerged in the second principle component[94] (Fig 4.1). These results are corroborated by findings

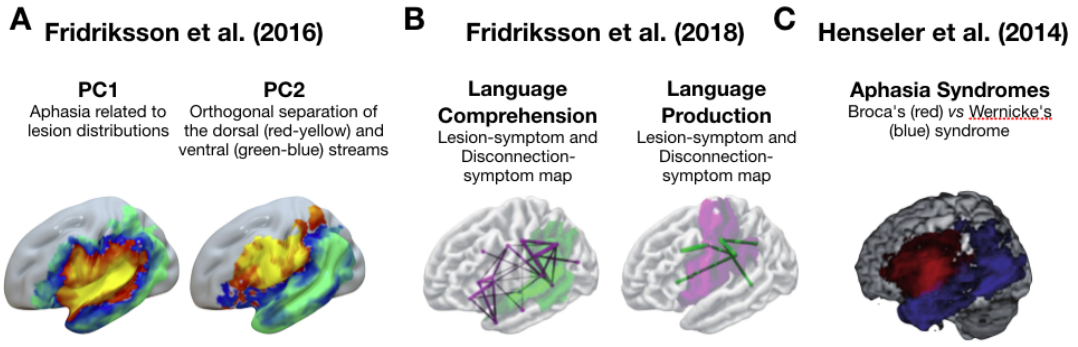

FIGURE 4.1: Lesion-symptom components of aphasia.
Major studies revealing the reflection of the dorsal and ventral streams of language processing in aphasia through principle component analysis (PCA). (A) Fridriksson et al. (2016)[94] investigated the major spatial variations of lesion-symptom maps, which revealed the emergence of the two language streams in the second principle component (PC2). Colors represent the loadings of the principle components onto the lesion-symptom data. (B) Fridriksson et al. (2018)[69] computed lesion-symptom and disconnection-symptom maps on components reflecting language production and language comprehension. Purple and green colors represent the Z-scores for lesion-symptom and disconnection-symptom analyses. (C) Henseler et al. (2014)[218] performed a lesion-symptom analysis on scores for similarity to Broca's (red) and Wernicke's (blue) aphasia.

from the same team[69] using lesion-symptom (and disconnection-symptom) mapping for measures of speech production and comprehension, which were derived from a principle component analysis of a large set of language evaluations (Fig 4.1). Similarly, Henseler et al. (2014)[218] found comparable results with a language battery that can associate probabilites for classifying Broca's and Wernicke's aphasias: they found that the classical syndromes based on a characterization of language deficits mapped well to the respective vascular territories (but brain regions governing specific symptoms were overlapping and crossed the Broca-Wernicke borders) (Fig 4.1).

In terms of studies with early imaging data to predict chronic outcome, Ramsey et al. (2017)[204] also investigated language recovery in the same cohort as described in section 4.2.1. Using lesion location from brain imaging performed within 2 weeks post stroke, they showed that worse aphasia (quantified by the first principle component of a set of language evaluations) at 3 months was associated with lesions of the superior and medial temporal gyri and the white matter corresponding to posterior regions of the arcuate fasciculus, which improved prediction beyond lesion size, age, education level, physiotherapy dose, and baseline behavioral measurements. Three studies[219–221] using acute DWI data to uncover determinants of acute aphasia showed that semantic errors and comprehension performance were associated to damage of cortical and subcortical regions of the ventral stream, whereas repetition errors were localized to regions of the dorsal stream (specifically due to damage to the arcuate fasciculus[221]), consistent with lesion-symptom analyses performed at the chronic stage. Finally, a study by Zavanone et al. (2018) highly aligns with the objectives of the current thesis. Using ADC maps at day 1 post-stroke, they conducted a voxel-wise correlation analysis with ART scores assessed at 6 months post-stroke. They found that lower ADC values in the posterior STG, MTG, and the underlying white matter significantly correlated with worse aphasia outcome. This study is the first to report a significant link between acute changes in diffusivity with chronic language outcome, which has been declared a developmental priority by the scientific community[19].

4.2.3 Global Outcome

Concerning global outcome, several important studies have taken advantage of the diffuse use of the modified Rankin Score (mRS) to study the correlates of long-term functional outcome. Moreover, all of these studies have acquired imaging data within 3 days post-stroke onset and clinical outcome scores at least 3 months afterwards (> 1 month for one study[110]). A rather encouraging finding is the strong convergence of

these studies regarding the link between damage to deep white matter (especially the corona radiata and the periventricular white matter) and functional outcome assessed with the mRS despite slight differences in methodology: while Cheng et al (2014)[110], Wu et al. (2015)[111], Payabvash et al. (2017)[222], and Munsch et al. (2016)[223] used binary lesion segmentations and the mRS as an ordinal variable, Rosso et al (2011)[112] and Cuingnet et al. (2011)[114] used continous ADC values to classify patients with good (mRS 0-2) and poor (mRS 3-5) outcome (Fig 4.2).

Through a tractography analysis, Rosso et al. (2015) demonstrated that this crucial region corresponds to the crossroads of major white matter bundles, such as the corticospinal tract, the arcuate fasciculus, and the corpus callosum. Of note, methodological considerations for lesion-symptom mapping of the mRS were raised in two studies[111,113] that performed similar analyses but controlled for sex, age, and lesion volume. With this correction, they showed that a relationship between stroke location and outcome was only found in the left hemisphere, whereas these clinical

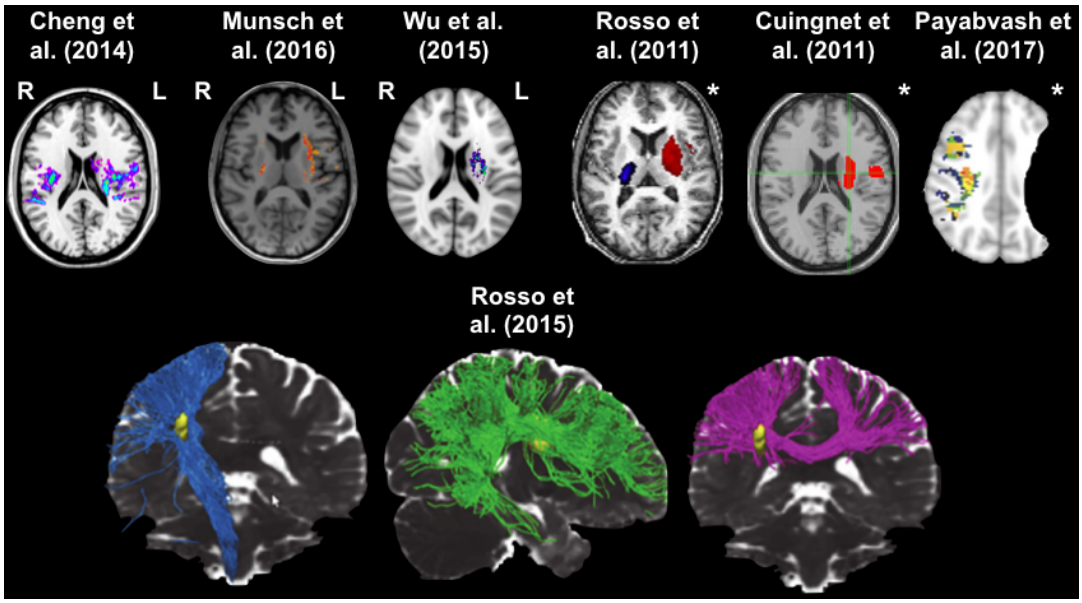

FIGURE 4.2: Lesion location and global outcome.
Concordant evidence from several studies has demonstrated a link between damage to the deep white matter and long-term functional outcome. For each study, significant voxels are shown for a specific slice as reported by the authors. Cheng et al (2014)[110], Munsch et al. (2016)[223], and Wu et al. (2015)[111] analyzed right (R) and left (L) lesions separately. Rosso et al. (2011)[112], Cuingnet et al. (2011)[114], and Payabvesh et al. (2017)[222] analyzed all lesions in the same hemisphere(*). Using a tractography analysis, Rosso et al. (2015) showed that these critical areas correspond to the crossroads of major white matter bundles, such as the corticospinal tract (Blue), the arcuate fasciculus (Green), and the corpus callosum (Purple). Blue region for Rosso et al. (2011) corresponds to the location of the corticospinal tract. L=Left; R=Right.

variables could independently explain variations in outcome in right-hemisphere stroke.

4.3 ROI or Tract-specific Analyses to Predict Outcome

4.3.1 Motor Outcome

The corticospinal tract has received the most attention in the literature due to its critical role in motor output[54]. Outside of dMRI studies, lesion load to the CST has proven a valuable marker for future outcome. For example, Zhu et al. (2010)[170] showed that, for a cohort of chronic stroke patients, a regression model constructed with lesion size and CST lesion load (weighted by fiber density) accounted for 72.7% of the variance in UE-FM scores. These results were corroborated by Feng et al. (2015)[206] who demonstrated that a regression model for lesion load also evaluated at the acute stage and the UE-FM at 3 months explained around 69% of the variance in an independent cohort, and 47% of severely impaired subjects in a subgroup analysis. Moreover, they showed that the lesion load of the CST correlated with motor outcome better than the initial impairment.

The CST has also been studied with diffusion MRI at the acute stage. Spampinato et al. (2017) used DTI – among other methods – to evaluate the microstrutural integrity of the CST in 17 stroke patients 1-4 days after stroke for whom they had UE-FM scores at 3 months post-stroke. They reported significant correlations with the ratio of the MD (ρ=0.65) and AD (ρ=0.55) of the affected:unaffected CST, but not with FA (ρ=0.08). Another study by Groisser et al. (2014) extracted DTI parameters from the CST in 10 acute stroke patients (3-7 days post-stroke) to investigate motor outcome evaluated by grip strength and other outcome measures. They found the highest correlations between the difference of AD between the affected and unaffected CST and 6-7 month motor outcome. Moreover, they showed that this correlation remained significant even after controlling for initial impairment. With the same patients, they also evaluated the neuronal integrity of the CST at 1-2 months and found that it was ΔFA that correlated the best with 6-7 month outcome. These results corroborate findings from Puig et al. (2013) who evaluated the FA in the cerebral peduncles in 70 patients at <12 hours, 3 days, and 30 days for motor outcome at 2 years post-stroke but only found correlations with FA at 30 days. Unfortunately, the authors did not report analyses with other DTI parameters, such as AD or MD. Yu et al. (2009) recorded DTI parameters in the cerebral peduncles 1-7 days and 13-20

days post stroke and found no correlation for 1 year motor outcome with either time point. On the other hand, the differences in FA observed between both time points highly correlated with the motor NIHSS and another motor evaluation at one year post-stroke. The neural integrity of alternative motor fibers, such as fronto-parietal association fibers[58], descending corticofugal fibers from the premotor cortex[48,57] and cerebello-cortical fibers[49], and their relationship with residual motor function have been studied at the chronic stage with dMRI; however, no studies have investigated the predictive value of these fibers at the acute stage.

In summary, despite the difficulty of obtaining lengthy DTI data shortly after stroke onset, there is a slowly developing corpus of literature on the predictive value of acute DTI for 3-month motor outcome. There are conflicting results around the predictive value of DTI parameters acquired at the acute stage in either the CST or ROIs thereof for long-term outcome; however, a possible reason for the discrepency between these results may be the variable time points at which patients were scanned (e.g., 1-4 days for Spampinato et al. (2017), 3-7 days for Groisser et al. (2014), <12 hours or 3 days for Puig et al. (2013), 1-7 days for Yu et al. (2009)). Indeed, DTI parameters quickly evolve during this period of neural repair and degradation following acute stroke[147]. Scanning patients at such different time points may capture distinct phases of microstructural dynamics, which could severely hinder correlational analyses. That being said, there is a strong consensus that FA evaluated at the acute stage is not a sensitive biomarker for neuronal damage and hence future outcome. On the other hand, relative changes in the diffusivity (i.e., AD or MD) of motor structures seem to harbor higher predictive values for motor outcome.

4.3.2 Language Outcome

There has been considerably less work on the prognostic value of diffusion MRI at the acute stage for long-term language outcome than for motor outcome. Nevertheless, there is growing evidence to support the clinical relevance of the integrity of the arcuate fasciculus. At the chronic stage, damage to the arcuate fasciculus has been shown to correlate with rate, informativeness, efficiency of speech[45], fluency[224,225], and other various measures of speech[226]. One notable study by Hillis et al. (2018)[101] acquired acute DWI scans <48 hours post-stroke and found that lesion load to the posterior STG and the AF was highly predictive of improvement in object naming 6 months afterwards. As for DTI studies, one at the chronic stage reported lower FA in the AF, IFOF, ILF, and UF. Moreover, FA of the AF correlated with naming and

sentence construction, whereas FA of the ILF and IFOF correlated with comprehension of single words. One study having acquired DTI data at 2 days post-stroke reported that the FA of the AF was not able to distinguish between aphasic and non-aphasic patients at discharge. Unfortunately, this study did not report information on any other diffusivity parameter, such as AD or MD.

Currently, there are no studies relating early diffusion changes and future language outcome in pre-defined ROIs. While Zavanone et al. (2018)[227], as described in section 4.2.2, found that decreases in ADC in the STG, MTG, and underlying white matter to be predictive of 6 month aphasia severity using a whole-brain analysis, there has yet to be a rigorous investigation of acute diffusion abnormalities in well establish language tracts or regions of interest. While whole-brain and ROI analyses are complementary for elucidating the underpinnings of aphasia outcome, a single tract or set of regions are easy biomarkers to implement in clinical practice and could be readily deployed in large-scale trials. As mentioned above, identifying crucial structures at the early phases of stroke constitutes a developmental priority in stroke research[19].

4.3.3 Global Outcome

As discussed in section 4.2.3, voxel-based analyses have found that global outcome is determined by a large set of regions due to the cumulative effect of motor, language, and cognitive impairments. Certain studies have therefore investigated the lesion load of many ROIs and their relationship to global outcome. Forkert et al. (2015)[228], Payabvash et al. (2017)[229], Habegger et al. (2018)[203] used ROIs from several available public atlases and found that the preservation of regions, such as the corona radiata, insula, caudate nucleus, the corticospinal tract, somatosensory cortex, and superior longitudinal fasciculus was crucial for outcome. As for diffusion studies, Rosso et al. (2011)[230] tested the importance of grey and white matter motor structures (M1, putamen, SMA, cerebellum, CST) involved in functional outcome with ADC measurements at admission and 24 hours post-stroke. They found that the putamen at 2 hours post-stroke and the CST at day 1 classified outcome better than lesion volume. In a similar study, Moulton et al. (2015)[231] studied diffusion changes at different levels of the CST (M1, the corona radiata, PLIC, and cerebral peduncles). They found that AD decreases were more pronounced in the corona radiata and that such asymmetries were correlated with the mRS at 3 months more than any other

part of the CST or DTI parameter. Of note, the FA of no regions correlated with future outcome.

4.4 Remarks on Acute DTI

In conclusion, in this chapter, we have seen a variety of analyses centered around DWI data for the prognosis of motor, language, and global outcome in acute stroke. Two major points emerge from the literature: (1) damage to important white matter structures is a strong correlate of outcome, and (2) it is crucial to account for dynamic changes in diffusivity within the first week of stroke. In fact, both VBAs and ROI/tract-based analyses have brought to light the importance of changes in MD/ADC or AD but *not* FA within relevant fiber bundles for motor, language, and global outcome within the first week of stroke. The correlations between changes within these structures and future outcome are rather high and cover the entire range of impairments, suggesting that, indeed, DWI is a useful modality for early prognosis (i.e., at day 1 post-stroke) of long-term outcome.

Finally, another important limitation of these studies concerns the lack of comparison with the predictive value of clinical variables, such as initial severity and age. While it is important to first demonstrate that early changes in diffusivity of important white matter structures correlate with outcome, the true significance of these variables is determined by their independence of clinical scores that are already known to predict outcome.

Part II

Thesis Work

Chapter 5

Study I: Comparison of Spatial Normalization Strategies of Diffusion MRI Data for Studying Motor Outcome in Subacute-Chronic and Acute Stroke

Contents

5.1 Overview of Study

The first study of my doctoral work served to establish an imaging processing pipeline in order to warp all of my data to a common reference space. As we saw in chapter 3, spatially warped images allow for both tract-specific analyses using common tract templates in addition to voxel-based analyses. The majority of my imaging data being derived from diffusion MRI sequences, it was important to consider not only commonly used scalar normalization strategies but also more novel normalization techniques based on complex diffusion models, such as the diffusion tensor or the fiber orientation distribution (FOD). DTI and FOD-based registration have already shown to yield significantly better overlaps in healthy individuals; however, a systematic comparison in stroke patients had yet to be performed. Moreover, since my imaging data contained ischemic lesions, which severely alters the diffusion signal in the brain, another interesting aspect to analyze was the practice of "lesion masking". Lesion masking is a method of reducing problematic distortions of abnormal tissue during the normalization process. At the time of conception of the study, no DTI-based registration had a readily implementable lesion masking function; therefore, we were not able to include it in our analysis. Finally, as we saw in chapter 3, diffusion within the lesion is drastically different at the acute stage compared to the subacute-chronic stage. We therefore thought it interesting for the scientific communinity to include a cohort of subacute-chronic stroke patients (minimum 1 month post-stroke) scanned in a parallel study in order to verify if strategies differed with the time between stroke onset and imaging.

Our primary question was the following: what is the effect of normalization strategy and lesion masking in acute stroke and subacute-chronic stroke? To answer this question, we required a means to evaluate the quality of the studied normalization techniques. For this, we took advantage of well-established structure-function relationships as outlined in chapter 4: (1) in subacute-chronic stroke, the fractional anisotropy (FA) of the corticopsinal tract (CST) correlates with motor performance, and (2) in acute stroke, axial diffusivity (AD) of the CST correlates with acute motor outcome. We therefore presumed that the most successful normalization strategy would be that which best overlays a patient's CST with the corresponding region in the imaging template. Better voxel-wise anatomical correspondence would thus result in a more accurate extraction of FA or AD in the CST, which, in turn, would yield better correlations between motor scores.

5.2 Article

The supplementary materials for this article are found in Appendix G

NeuroImage 183 (2018) 186–199

Contents lists available at ScienceDirect

NeuroImage

journal homepage: www.elsevier.com/locate/neuroimage

Comparison of spatial normalization strategies of diffusion MRI data for studying motor outcome in subacute-chronic and acute stroke

Eric Moulton [a], Romain Valabregue [a,b], Belén Díaz [c], Claire Kemlin [a], Sara Leder [c], Stephane Lehéricy [a,d], Yves Samson [a,c], Charlotte Rosso [a,c,*]

[a] INSERM U 1127, CNRS UMR 7225, Sorbonne Universités, UPMC Univ Paris 06 UMR S 1127, Institut du Cerveau et de la Moelle épinière, ICM, F-75013, Paris, France
[b] Centre de Neuro-Imagerie de Recherche, CENIR, Paris, France
[c] AP-HP, Urgences Cérébro-Vasculaires, Hôpital Pitié-Salpêtrière, Paris, France
[d] AP-HP, Department of Neuroradiology, Hôpital Pitié-Salpêtrière, Paris, France

ARTICLE INFO

Keywords:
Diffusion MRI
Corticospinal tract
Stroke
Motor outcome
Spatial normalization

ABSTRACT

A common means of studying motor recovery in stroke patients is to extract Diffusion Tensor Imaging (DTI) parameters from the corticospinal tract (CST) and correlate them with clinical outcome scores. To that purpose, conducting group-level analyses through spatial normalization has become a popular approach. However, the reliability of such analyses depends on the accuracy of the particular registration strategy employed. To date, most studies have employed scalar-based registration using either high-resolution T1 images or Fractional Anisotropy (FA) maps to warp diffusion data to a common space. However, more powerful registration algorithms exist for aligning major white matter structures, such as Fiber Orientation Distribution (FOD)-based registration. Regardless of the strategy chosen, automatic normalization algorithms are prone to distortions caused by stroke lesions. While lesion masking is a common means to lessen such distortions, the extent of its effect on tract-related DTI parameters and their correlation with motor outcome has yet to be determined. Here, we aimed to address these concerns by first investigating the effect of common T1 and FA-based registration as well as novel FOD-based registration algorithms with and without lesion masking on lesion load and DTI parameter extraction of the CST in datasets typically acquired for subacute-chronic and acute stroke patients. Second, we studied how differences in these procedures influenced correlation strength between CST damage (through DTI parameters) and motor outcome. Our results showed that, for high-quality subacute-chronic stroke data, FOD-based registration captured significantly higher lesion loads and significantly larger FA asymmetries in the CST. This was also associated with significantly stronger correlations in motor outcome with respect to T1 or FA-based registration methods. For acute data acquired in a clinical setting, there were few observed differences, suggesting that commonly employed FA-based registration is appropriate for group-level analyses.

1. Introduction

In the past 20 years, the number and sample sizes of studies investigating the role of the corticospinal tract (CST) in motor outcome with diffusion MRI (dMRI) have increased substantially with time, especially in the last decade (Koch et al., 2016). As a result, performing analyses in a common space through spatial normalization is becoming a popular choice. Conducting group-level analyses using a common template for the CST presents several advantages over individual analyses in subjects' native spaces without compromising lesion-behavior relationships (Park et al., 2013; Vargas et al., 2013). The most obvious benefit is the quickness with which large cohorts can be processed for statistical analysis. Second, less expertise is required to properly reconstruct the CST based on hand-drawn regions of interest for tractography. Third, in patients with severe lesions for whom CST reconstruction failed, a template allows for the evaluation of dMRI parameters and their relation to motor outcome (Park et al., 2013).

Despite the appealing aspects of group-level analyses in a common space, the efficacy of such procedures highly depends on the quality of the non-linear warping for matching the template image with the anatomy of the studied subject. To date, most studies often employ one of the two following normalization strategies: (1) directly warping Fractional

* Corresponding author. Urgences Cérébro-Vasculaires, 47-83 Boulevard de l'Hôpital, 75013, Paris, France.
E-mail address: charlotte.rosso@aphp.fr (C. Rosso).

https://doi.org/10.1016/j.neuroimage.2018.08.002
Received 19 April 2018; Received in revised form 2 July 2018; Accepted 3 August 2018
Available online 4 August 2018

List of abbreviations

AD	axial diffusivity
ANOVA	analysis of variance
ANTs	Advanced Normalization Tools
CI	confidence interval
CST	corticospinal tract
dMRI	diffusion magnetic resonance imaging
DTI	diffusion tensor imaging
DWI	diffusion weighted imaging
FA	fractional anisotropy
FLAIR	fluid-attenuated inverse recovery
FOD	fiber orientation distribution
JTT	Jebson-Taylor Test
MPRAGE	magnetization-prepared rapid gradient-echo
MRI	magnetic resonance imaging
MSMT-CSD	multi-shell multi-tissue constrained spherical deconvolution
MVC	maximum voluntary contraction
NIHSS	National Institute of Health Stroke Scale
RGB	red green blue
SD	standard deviation
SE	standard error
TE	echo time
TI	inversion time
TR	repetition time
UE-FM	upper extremity Fugl-Meyer
wLL	weighted lesion load

Anisotropy (FA) images to a FA template (Archer et al., 2017; Kunimatsu et al., 2003; Lindenberg et al., 2012; Schulz et al., 2012) or (2) co-registering dMRI data to a high-resolution anatomical image (e.g. T1-weighted), normalizing said image to a standard space, and applying the deformation fields to dMRI-derived parameter maps (Hirai et al., 2016; Newton et al., 2006; Phan et al., 2013). However, T1-weighted images are completely insensitive to the complex fiber architecture of the white matter, and FA provides no information on the orientation of the underlying neural fibers. Using scalar images such as these for spatial normalization may not result in proper overlap of white matter regions between subjects. Recently, researchers have proposed more powerful registration algorithms, which take into account the local, complex diffusion profile and thus result in better alignment of major white matter pathways with respect to scalar-based registration. One such method, available in the MRtrix3 package (http://www.mrtrix.org) uses Fiber Distribution Orientation (FOD) images to register diffusion weighted images (Raffelt et al., 2011). FODs are mathematical constructs calculated from dMRI data which represent the partial volume of underlying neuronal fibers as a function of orientation in the spherical harmonic basis functions $Y(l,m)$, expressed by the associated Legendre polynomials P_l^m, where l is the degree and m is the order (Tournier et al., 2004). The number of spherical harmonic components in the FOD used to reconstruct the diffusion signal is governed by the maximum degree, also called *lmax*. As *lmax* increases, the number and angular precision of fiber populations which can be accurately reconstructed both increase, provided there are enough diffusion-encoding directions (Tournier et al., 2013). While FOD-based registration has been shown to be superior to registration of FA images in healthy subjects (Raffelt et al., 2011), its efficacy has yet to be tested in stroke patients.

In this study, we were interested in evaluating the following common and novel spatial normalization strategies in subacute-chronic but also acute stroke patients: (1) direct normalization of FA images, (2) warping of FA images through T1 normalization, and (3) FOD registration. While there is no established method for determining the "success" of a normalization strategy, in the context of stroke imaging, an optimal normalization should preserve well-established relationships between dMRI-derived parameters of CST damage and subacute-chronic and acute motor outcomes. Here, we investigated the effect of normalization strategy on two important Diffusion Tensor Imaging (DTI) parameters, Fractional Anisotropy (FA) and Axial Diffusivity (AD) (Basser, 1995; Basser et al., 1994; Pierpaoli and Basser, 1996). FA has been shown to robustly reflect damage to the CST at the subacute-chronic stage (Boyd et al., 2017; Puig et al., 2017; Rosso et al., 2013; Stinear and Ward, 2013). In contrast, at the acute stage of stroke (i.e., within a week of stroke onset), AD - and not FA - has shown to be a better predictor of subacute and chronic outcome (Doughty et al., 2016; Groisser et al., 2014; Moulton et al., 2015; Spampinato et al., 2017).

Regardless of the normalization strategy chosen, an important hurdle for registering stroke images is accounting for the large dissimilarities between lesioned regions in a patient's image and the corresponding areas in a template. In general, registration algorithms attempt to maximize the similarity between the patient's image and the template by overly distorting the lesion during non-linear warping, usually by shrinking the lesion (Brett, 2001; Renard et al., 2016; Ripollés et al., 2012). By masking the lesion from the similarity calculation, such distortions can be lessened in order to obtain a more accurate normalization (Andersen et al., 2010; Brett, 2001; Nachev et al., 2008; Ripollés et al., 2012). This beneficial effect of lesion masking has been largely studied with anatomical images, such as T1-weighted images; however, only a few studies have investigated its effect on dMRI-derived images, such as FA maps (Andersen et al., 2010; Brett, 2001; Nachev et al., 2008; Renard et al., 2016; Ripollés et al., 2012). Moreover, most of this work has solely investigated the effect of lesion masking on the volume of normalized lesions, but, to our knowledge, only one study has explored the effect of lesion masking on the extraction of tract-related dMRI parameters from chronic stroke images (Archer et al., 2017). Here, we sought to bridge the gap between the spatial extent of the lesion and DTI parameter extraction in the CST. We therefore performed the aforementioned normalization strategies with and without lesion masking and evaluated the direct effect of lesion masking by testing the correlations between differences – due to lesion masking – in lesion load and DTI parameter extraction of the CST.

Our goals were to (1) study the effect of lesion masking with common, scalar as well as FOD-based registration on lesion overlap and DTI parameter extraction in a template CST and (2) determine which registration strategy yielded the highest correlation(s) between well-established DTI parameters of the CST and motor outcome. We examined these goals at two different stages of stroke (subacute-chronic and acute phases) where the challenges are different for two reasons: (A) at the subacute-chronic stage, large lesions are often characterized by cerebrospinal fluid-filled cavities surrounded by gliosis, causing atrophy and stretching of the lateral ventricles (Skriver et al., 1990). On the other hand, at the acute stage (day 1 post-stroke), infarcted tissue is swollen from cytotoxic edema, causing local mass effects (Liang et al., 2007; Skriver et al., 1990) but has yet to completely degrade the underlying white matter fibers. Second, (B) DTI parameter dynamics differ at the subacute-chronic and acute stage causing some to be more affected than others (Bhagat et al., 2006; Lansberg et al., 2001; Puig et al., 2013).

We hypothesized that lesion masking should yield differences in lesion load of the CST and that this should have a direct effect on DTI parameter extraction and correlations with motor outcome. Furthermore, we hypothesized that scalar *vs.* FOD-based registration should yield differences in correlation strength due to each strategy's sensitivity to the underlying white matter architecture.

2. Methods and materials

2.1. Subjects

2.1.1. Subacute-chronic stroke cohort (N = 40)

Forty stroke patients (14 female, mean ± SD age = 63.0 ± 12.8 years) were included in this study. Stroke patients spanned the early subacute to the chronic stage (median time [IQR] since stroke = 105.5 [47.5–275.75] months). Data were extracted from a parallel study (Core protocol: NCT 02284087) and were collected before the intervention stage of the study. Patients were recruited according the following inclusion criteria: (1) no history of neurological or psychiatric disorders determined through an interview with a trained neurologist, (2) Mini-Mental Status Examination score greater or equal to 27, (3) age older than 18 years, (4) no contra-indications for MRI, and (5) presence of an upper-limb deficit (Fugl-Meyer Score < 60) with some preserved hand movement (maximum voluntary contraction > 0 N). All subjects from this cohort were examined and scanned at the Brain and Spine Institute (Institut du Cerveau et de la Moelle Epinière).

On the day of scanning, patients underwent a motor function evaluation by a trained physiotherapist. The evaluation consisted of the (1) Upper Extremity Fugl-Meyer (UE-FM) Scale (Fugl-Meyer et al., 1975), (2) the Jebson-Taylor Test (JTT) (Jebsen et al., 1969), and (3) a grip-force evaluation of the maximum voluntary contraction (MVC) using a dynamometer (MIE, Medical Research Ltd., http://www.mie- uk.com/pgripmyo/index.html). Similar to other studies (Park et al., 2013; Rondina et al., 2017), we evaluated residual motor ability with a composite motor score by taking the first principle component of the following measures: (1) the raw UE-FM score, (2) the ratio of the affected/unaffected JTT total times (rJTT), and (3) the ratio of the affected/unaffected MVC (rMVC). The first principle component accounted for 88.2% of the total variance in the three scores and correlated strongly with the UE-FM (Pearson's r [95% Confidence Interval] = 0.96 [0.93; 0.98]), the rJTT (r = −0.96 [-0.98;-0.92]), and the rMVC (r = 0.89 [0.81; 0.94]) (p < 0.0001).

From the same protocol, 24 healthy controls (10 females, mean ± SD age = 31.7 ± 10.4 years, Supplementary Materials) were included in this study to create the different image templates for normalization. Inclusion criteria for healthy participants were (1) no history of neurological or psychiatric disorders, (2) Mini-Mental State Examination ≥ 27, (3) age older than 18 years, (4) no contraindications to MRI, and (5) no use of psychoactive medication or recreational drugs.

The study was approved by the appropriate legal and ethical authority (CPP Ile de France VI— Pitié-Salpêtrière, Paris, France). Written informed consent was obtained from all participants.

2.1.2. Acute stroke data (N = 69)

Sixty-nine acute stroke patients (36 females, mean ± SD age = 71.9 ± 15.4 years) were studied retrospectively from the Urgences Cérébrovasculaires at the Hôpital de la Pitié Salpêtrière (subsample in Moulton et al., 2015). Inclusion criteria for this cohort were: (1) MRI-demonstrated ischemic stroke of the carotid territory, (2) thrombolysis treatment within 4.5 h after stroke onset, (3) follow-up MRI access at 24 h post-stroke, and (4) availability of day 7 National Institute of Health Stroke Scale (NIHSS) data.

The sum of NIHSS items 5 and 6 of the contralesional limbs acquired on day 7 (herein referred to as NIHSS7 MOT) was used in the correlation analysis for short outcome. As these data were acquired in a purely clinical setting for emergency acute stroke management and studied retrospectively, no imaging data for healthy controls are available.

2.2. Image acquisition

The diffusion MRI sequences detailed below reflect imaging protocols typically acquired in today's research and clinical settings.

2.2.1. Subacute-chronic stroke cohort

Anatomical and diffusion MRI data were obtained with a 3T scanner (Siemens, VERIO) with a 32-channel head coil. The MRI protocol included a sagittal **T1-weighted MPRAGE** image (TR = 2300 ms, TE = 4.18 ms, matrix size = 176 × 256, slice number = 256, voxel size = 1 × 1 × 1 mm^3, acquisition time = 4:44 min), a **Fluid-Attenuated Inverse Recovery (FLAIR)** sequence (TR = 9000 ms, TE = 128 ms, TI = 2500 ms, matrix size = 320 × 320, slice number = 26, voxel size = 0.75 × 0.75 × 5.5 mm^3, acquisition time = 3:20 min), and a **multi-shell Diffusion Weighted Imaging (DWI)** sequence (3 b-value shells obtained with both posterior to anterior (PA) and anterior to posterior (AP) phase encoding: 60 non-collinear diffusion encoding gradients at b = 1500 s/mm^2, 30 at b = 700 s/mm^2, and 8 at b = 300 s/mm^2, TR = 4000 ms, TE = 87.8 ms, matrix size = 110 × 110, slice number = 66, voxel size = 2 × 2 × 2mm^3, acquisition time = 16:16 min).

2.2.2. Acute stroke cohort

Twenty-four hours after admission to the emergency stroke unit, patients underwent a follow-up MRI with a General Electric 3T MRI scanner with an 8-channel coil. The following DWI sequences were used for the current analysis: (1) An **averaged 3-direction DWI** (b = 1000 s/mm^2, TR = 11700 ms, TE = 72.3 ms, matrix size = 256 × 256, slice number = 48, voxel size = 0.94 × 0.94 × 3mm^3, acquisition time = 0:59 min) and (2) a **30-direction DWI** (2 b = 0 s/mm^2 images followed by 30 non-collinear diffusion-encoding gradients at b = 1000 s/mm^2, TR = 12000 ms, TE = 82.3 ms, matrix size = 256 × 256, slice number = 44, voxel size = 1.09 × 1.09 × 3mm^3, acquisition time = 6:36 min).

2.3. Image preprocessing

We used a series of preprocessing steps from multiple image processing packages to optimally clean and prepare our data for both scalar and FOD-based registration.

2.3.1. Anatomical MRI

T1-weighted anatomical images were only available for the subacute-chronic stroke cohort. T1-weighted anatomical images for the subacute-chronic stroke cohort underwent a bias correction and were segmented into grey matter (GM), white matter (WM), cerebrospinal fluid (CSF) and non-brain tissue using SPM12 in Matlab (http://www.fil.ion.ucl.ac.uk/spm/software/spm12/) (Ashburner and Friston, 2005). A brain mask for brain extraction was constructed with the mathematical and morphological operations in the following order: (1) thresholding the GM, WM, and CSF probability maps at 10%, (2) summing the thresholded maps, (3) binarizing, (4) filling holes, and (5) computing a morphological closing using a 5 mm spherical structuring element to smooth the edges.

2.3.2. Diffusion MRI

DWI images underwent the following preprocessing steps: (1) denoising (Veraart et al., 2016a, 2016b) (2) susceptibility distortion correction using FSL's TOPUP (Andersson et al., 2003; Smith et al., 2004) and EDDY with slice interpolation for slices with significant signal drop (Andersson et al., 2016; Andersson and Sotiropoulos, 2016), and (3) bias-field correction (Smith et al., 2004; Zhang et al., 2001) (https://fsl.fmrib.ox.ac.uk). Diffusion MRI data for the acute stroke group did not undergo TOPUP as they were acquired with only one phase-encoding direction; however, they were processed with EDDY with slice interpolation in order to salvage the maximum number of usable DWI volumes as well as to optimize movement correction (Andersson et al., 2016). All preprocessed DWI volumes were visually inspected after EDDY slice interpolation, and any excessively artifacted volumes were removed. All diffusion weighted volumes for the subacute-chronic stroke cohort were of sufficiently good quality or corrected by preprocessing strategies, whereas 21 (30.4%) patients of the acute stroke cohort had varying amounts of overly artifacted data, requiring the removal of certain volumes (Median = 2, Interquartile range = 2–7, Range = 1–12).

Fractional Anisotropy (FA) and Axial Diffusivity (AD) maps were calculated from a tensor model estimated using FSL's DTIFIT (Basser et al., 1994; Smith et al., 2004). Fiber Orientation Distribution (FOD) volumes were computed by estimating response functions for the GM, WM, and CSF tissues (Dhollander et al., 2016) for multi-shell multi-tissue constrained spherical deconvolution (MSMT-CSD) using a *lmax* of 4 (Jeurissen et al., 2014). Of note, the MSMT-CSD model on the acute stroke cohort (with 2 b-values) output response functions only for two tissue classes, the white matter and CSF, without disentangling the contribution of the gray matter (Jeurissen et al., 2014). A *lmax* value of 4 was chosen for the MSMT-CSD model for two reasons: (1) FOD-based registration accuracy does not improve when spherical harmonic coefficients *Y(l,m)* beyond a *lmax* of 4 are used (Raffelt et al., 2011) and (2) the removal of corrupted volumes from the 30-direction DWI sequence in our acute stroke cohort prevented us from estimating higher order FODs. Nevetheless, a low number of diffusion-encoding directions with a clinical b-value of 1000 s/mm^2 and a *lmax* of 4 are acceptable parameters for computing FODs, especially for the purpose of image registration (Raffelt et al., 2011; Tournier et al., 2013; Wilkins et al., 2015). Finally, we performed FOD intensity normalization (MRtrix3's *mtnormalize*) in order to increase registration accuracy between FOD volumes from different imaging protocols due to the sum of squares metric (see section 2.6).

We calculated brain masks from the mean b = 0 s/mm^2 volume using FSLs Brain Extraction Tool (Smith, 2002) and eroded them with a 6 × 6 × 6mm^3 kernel in order to remove the remaining thin "halo" of bright voxels around FA maps. All brain masks and FA maps were visually inspected.

2.4. Creation of the study-specific templates and tractography

We created three study-specific templates from the healthy control cohort as reference images for our non-linear registration strategies: (1) a FOD template, (2) a FA template, and (3) a T1 template (Fig. 1, Supplementary Materials). Briefly, we first created a FOD template through iterative non-linear warping and averaging of FOD volumes using MRtrix's *population_template* function (http://www.mrtrix.org). The following warps were applied to the FA and coregistered T1 volumes for the corresponding templates (Fig. 1). The CST was manually dissected from whole-brain tractography performed on the FOD template (Geyer et al., 2000; Newton et al., 2006) (Fig. 1, Supplementary Materials).

2.5. Lesion segmentation and masking

To perform the chosen registration strategies with lesion masking, it was necessary to accurately contour the acute and subacute-chronic lesions and coregister them onto the appropriate images (i.e., FA and T1, when available) in their native spaces.

Subacute-chronic lesions were manually segmented on the FLAIR sequence by identifying hypersignal (gliosis) and hyposignal regions (cavitary lesions) (Fig. 2). Subacute and chronic lesions were transferred to diffusion space images by coregistering the FLAIR images to the corresponding FA maps with an affine transformation and a trilinear interpolation thresholded at 0.25. This transformation served for masking the lesions for registration of the FA and FOD images. As for the T1 images, to correct for distortions in the DWI sequence, we first needed to estimate a non-linear transformation between FA maps and the T1 images for patients - as we did for healthy controls and as in (Schulz et al., 2015) (see Supplementary Materials) - in order to estimate a transformation for normalizing FA maps to the template space, passing through T1 space. We therefore reused this transformation to transfer the lesion into T1 space for lesion masking during normalization.

Acute lesions were manually segmented by identifying hypersignal regions on the 3-direction DWI sequence image (Fig. 2). Acute lesions were then transferred to diffusion space by coregistering the averaged 3-direction DWI sequence to the FA maps using an affine transformation and a trilinear interpolation thresholded at 0.25. This transformation served for masking the lesions for registration of the FA and FOD images.

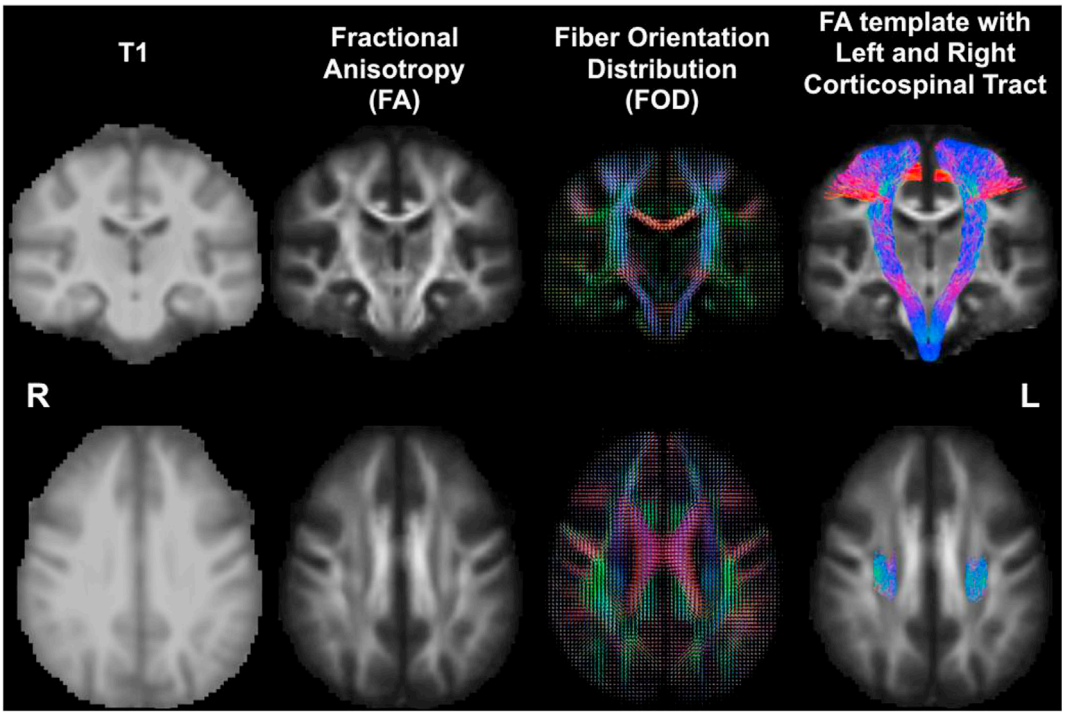

Fig. 1. Templates built from healthy controls and used for spatial registration. Top row: a representative coronal slice of the templates where the corticospinal (CST) tract descends from the motor cortex into the cerebral penduncles. Bottom row: a representative axial slice of the template where the CST intersects other white matter pathways, leading to local changes in Fractional Anisotropy (FA) invisible on the T1. RGB color code of the FOD template refers to the principle direction of diffusion in the lateral-medial, anterior-posterior, and inferior-superior directions, respectively. Right column: streamlines of the manually dissected CST from tractography performed directly on the FOD template overlaid on the FA map. Streamlines on the coronal slice are those from the entire reconstructed CST. Images are presented in the neuroradiological convention (right is left).

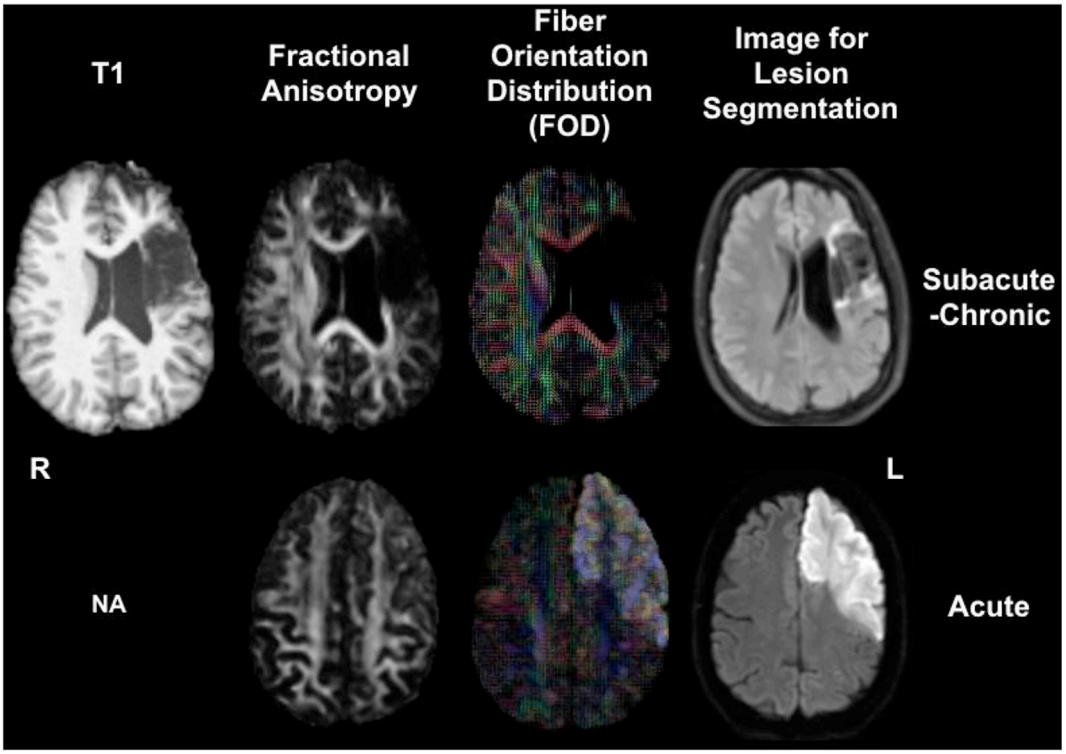

Fig. 2. Appearance of lesioned tissue on different imaging modalities for subacute-chronic and acute stroke. Image slices are from two representative patients from the subacute-chronic (top) and the acute (bottom) stroke cohort. From left to right, the T1-weighted, Fractional Anisotropy (FA), and Fiber Orientation Distribution (FOD) images used for normalization to the templates in Fig. 1. Lesion segmentation was performed on the FLAIR (top-right) or the averaged 3-direction Diffusion-Weighted Image (bottom-right) for the subacute-chronic and acute stroke cohorts, respectively. Note the prominent effects of the subacute-chronic lesion on all imaging modalities, whereas the acute stroke lesion is unnoticeable on the FA map, and the principle directions of diffusion are preserved in the FOD image. T1-weighted images were not available (NA) for the acute stroke cohort. Images are presented in the neuroradiological convention (right is left).

2.6. Registration strategies

In this study, we used both scalar and FOD-based registration for subacute-chronic and acute diffusion MRI data. Registration between native images and the templates were performed both with and without lesion masking. For scalar-based registration (i.e., for registering T1 and FA maps), we opted for Advanced Normalization Tools (ANTs) with default parameters using the mutual information metric for both rigid and affine steps and the cross-correlation metric for the non-linear step.

For FOD-based registration, we used symmetric diffeomorphic registration of fiber orientation distributions as provided by MRtrix3's *mrregister*. In FOD-based registration, the number of spherical harmonic coefficients *Y(l,m)* (governed by the parameter *lmax*) used to drive registration may differ. Here, we tested *lmax* values of 2 and 4. While it has been shown that a *lmax* of 4 yields the most accurate registration in normal, healthy adults (Raffelt et al., 2011), it is known that stroke can cause long-range significant changes in affected pathways in both DTI parameters, as well as the principle direction of diffusivity (Pierpaoli et al., 2001). For this reason, we chose to also evaluate the performance of FOD-based registration using a *lmax* of 2 with the hypothesis that such a strategy might be more robust to distal stroke effects on the FOD orientations. The only readily available registration metric for *mrregister* at the time of publication is the sum-of-squares. Consequently, this registration strategy is restrictively optimal between FOD images derived from similar protocols using a shared, average response function with proper intensity normalization and bias-field correction as is done in other within-group studies (de Manzano and Ullén, 2018). In our study, we were not able to use a shared, average response function as the number of unique b-values (i.e., shells) was different for the acute and subacute-chronic cohort. Nevertheless, in order to circumvent this issue as much as possible, we incorporated intensity normalization and bias-field correction to our image processing pipeline. Furthermore, as a precautionary measure, we incorporated additional subsampling steps (i.e., scaling from 0.1 to 1.0 in increments of 0.1) in the FOD registration algorithm for a smoother registration.

2.7. Effect of registration strategy and lesion masking on DTI parameter extraction and lesion load

As a first step, we established whether registration strategies affected the raw extraction of diffusion parameters in the CST before computing ratios and correlations. In particular, we investigated the influence of strategy and lesion masking on the diffusion parameters of the CST in the unaffected and affected hemisphere as well as their ratio. We studied the FA of the CST in the subacute-chronic stroke cohort and the AD of the CST in the acute stroke cohort. To this end, we applied the deformation fields estimated with each strategy to the native FA and AD maps and computed tract-density-weighted averages of these parameters, $\overline{P}$, of both the affected and unaffected hemisphere with the following equation:

$$\overline{P} = \frac{\sum_{i \in D} P(i) * D(i)}{\sum_{i \in D} D(i)} \quad (1)$$

where *P(i)* is the value of the parameter (FA or AD) in voxel *i* of the CST density map *D* and *D(i)* is the CST streamline density at voxel *i*. The parameter of interest from both hemispheres was converted to a ratio ($\overline{P}_{\text{affected}}/\overline{P}_{\text{unaffected}}$) noted here as rFA or rAD.

In addition, we analyzed the effect of lesion load per strategy to study the impact of lesion masking and normalization strategy on the spatial extent of infarcted tissue in the CST. We warped native lesion segmentations into the common space using the deformation fields for each

strategy with a nearest neighbor interpolation. We then computed a weighted lesion load (wLL) with the following equation:

$$wLL = \frac{\sum_{i \in D} L(i)^* D(i)}{\sum_{i \in D} D(i)} \quad (2)$$

where *L(i)* is equal to 1 if a lesion is present in voxel *i* of the CST density map *D* and 0 if not, and *D(i)* is the CST streamline density at voxel *i*. By weighting lesion load by streamline density, we can take into account the narrowing in of the CST in the posterior limb of the internal capsule and the cerebral peduncles (Zhu et al., 2010).

All statistics were performed using the R programming software (R Core Team, 2016; www.r-project.org). We performed repeated measures ANOVA to find systematic differences in the dependent variables, $\overline{P}_{\text{affected}}$, $\overline{P}_{\text{unaffected}}$, $\overline{P}_{\text{ratio}}$, and wLL, with within-subject factors MASKING and STRATEGY (Lawrence, 2015). If Mauchly's test of sphericity indicated that the assumption of sphericity was violated, degrees of freedom and p-values were reported using Greenhouse-Geisser correction. We proceeded with post-hoc t-tests when the main effect of a factor or interaction term was significant. We also computed individual paired t-tests in the following manner. First, we fixed registration strategy and compared lesion masking *vs.* no lesion masking (e.g., FOD-*lmax4* with lesion masking *vs.* FOD-*lmax4* without lesion masking). Second, we fixed the lesion masking factor and compared strategies (e.g., FOD-*lmax4* with lesion masking *vs.* ANTs-FA with lesion masking). This resulted in 16 pairs of correlation coefficients for the subacute-chronic stroke cohort and 9 for the acute stroke cohort.

Finally, to determine if differences in lesion load – due to lesion masking – had an effect on the observed asymmetries in DTI parameters, we performed Spearman rank correlations between the difference in lesion load and the difference in $\overline{P}_{\text{ratio}}$. The aforementioned post-hoc t-tests, individual paired t-tests, and correlations were Bonferroni-corrected for multiple comparisons.

2.8. Comparison of registration strategy by correlation strength

For the subacute-chronic stroke cohort, we computed Spearman rank correlations between the rFA of the CST and the composite motor score (see section 2.1.1). For the acute stroke cohort, we computed Spearman rank correlations between rAD of the CST with day 7 NIHSS total motor score. Confidence intervals were calculated by bootstrapping with 10,000 iterations. We analyzed the FA of the CST in the subacute-chronic stroke cohort and the AD of the CST in the acute stroke cohort, as these are the DTI parameters which best characterize CST damage at these two stages in stroke. However, the correlation analysis with the other DTI parameters (Radial Diffusivity-RD, Mean Diffusivity-MD) can be found in the Supplementary Materials.

In order to demonstrate that the difference between two Spearman correlation coefficients (i.e. $\rho_a - \rho_b = \Delta\rho$) is statistically significant, we ran permutation tests with 10,000 iterations to reconstruct the sampling distribution of the null hypothesis, $H_0 : \rho_a = \rho_b$ (two-tailed) (Nieuwenhuis et al., 2011; Roser et al., 2015). In the subacute-chronic cohort, there were 8 correlation coefficients (4 registration strategies with and without lesion masking), and in the acute cohort, there were 6 correlation coefficients (3 registration strategies with and without lesion masking). We performed the same pairwise comparisons as with the repeated measures ANOVA. First, we fixed registration strategy and compared lesion masking *vs.* no lesion masking. Second, we fixed the lesion masking factor and compared strategies.

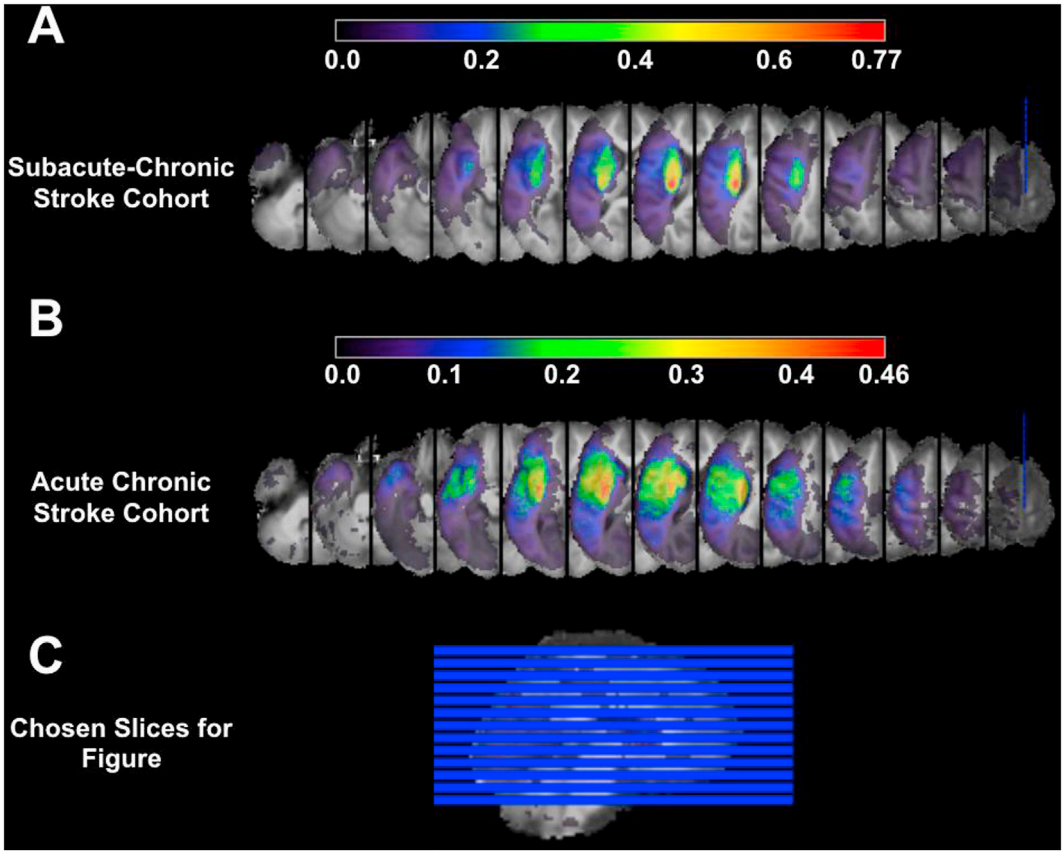

Fig. 3. Lesion probability maps from the subacute-chronic (A) and acute stroke cohorts (B) overlaid on selected slices of the T1 template (C). The two color maps reflect the percentage of lesioned voxels for the acute and subacute-chronic cohorts, respectively. Right-sided lesions were flipped onto the left hemisphere, and normalization was performed again to warp the lesion.

3. Results

3.1. Patients

3.1.1. Subacute-chronic stroke cohort

Patients had overall severe to moderate deficits (mean ± SD Fugl-Meyer = 44 ± 16) with reduced grip strength (rMVC = 0.50 ± 0.31) and slower movements with the affected hand (rJTT = 6.94 ± 8.62). Lesions for the subacute-chronic cohort were of variable size (mean ± SD lesion volume = 25.6 ± 44.3 mL) located at different levels along the corticospinal tract, consistent with their deficit (Fig. 3A). Maximum overlap for this cohort (75.0–77.5% of subjects depending on normalization strategy, N = 30–31, Fig. 3A) was located in the white matter of the inferior corona radiata and superior portion of the posterior limb of the internal capsule, like in similar studies investigating motor outcome in stroke (Schulz et al., 2017a).

3.1.2. Acute stroke cohort

At day 1, 47.8% (n = 33) of patients had no proximal limb deficits (NIHSS1 MOT = 0), and the remaining patients exhibited varying motor deficit severity (NIHSS1 MOT = 4.6 ± 2.7). At day 7, 6 additional patients fully recovered proximal limb function (NIHSS7 MOT = 0), and the remaining patients still exhibited a large spread of motor deficit severity (NIHSS7 MOT = 4.5 ± 2.9). Acute stroke lesions were also of variable size (38.7 ± 61.0 mL). Maximum lesion overlap for this cohort was in the putamen, external capsule, and the caudate nucleus (43.5%–46.4% of subjects depending on normalization strategy, N = 30–32, Fig. 3B), reflecting typical lesions of the middle cerebral artery territory of a clinical population, as was the case for the majority of the acute stroke patients (Phan et al., 2005).

3.2. Effect of registration strategy and lesion masking on DTI parameter extraction

Presented below are the results of the repeated measures ANOVA investigating the effects of STRATEGY and MASKING on DTI parameters extracted from the corticospinal tract (CST) of the unaffected and affected hemisphere as well as their ratio and lesion load. Tests of statistical significance are provided in the Supplementary Materials.

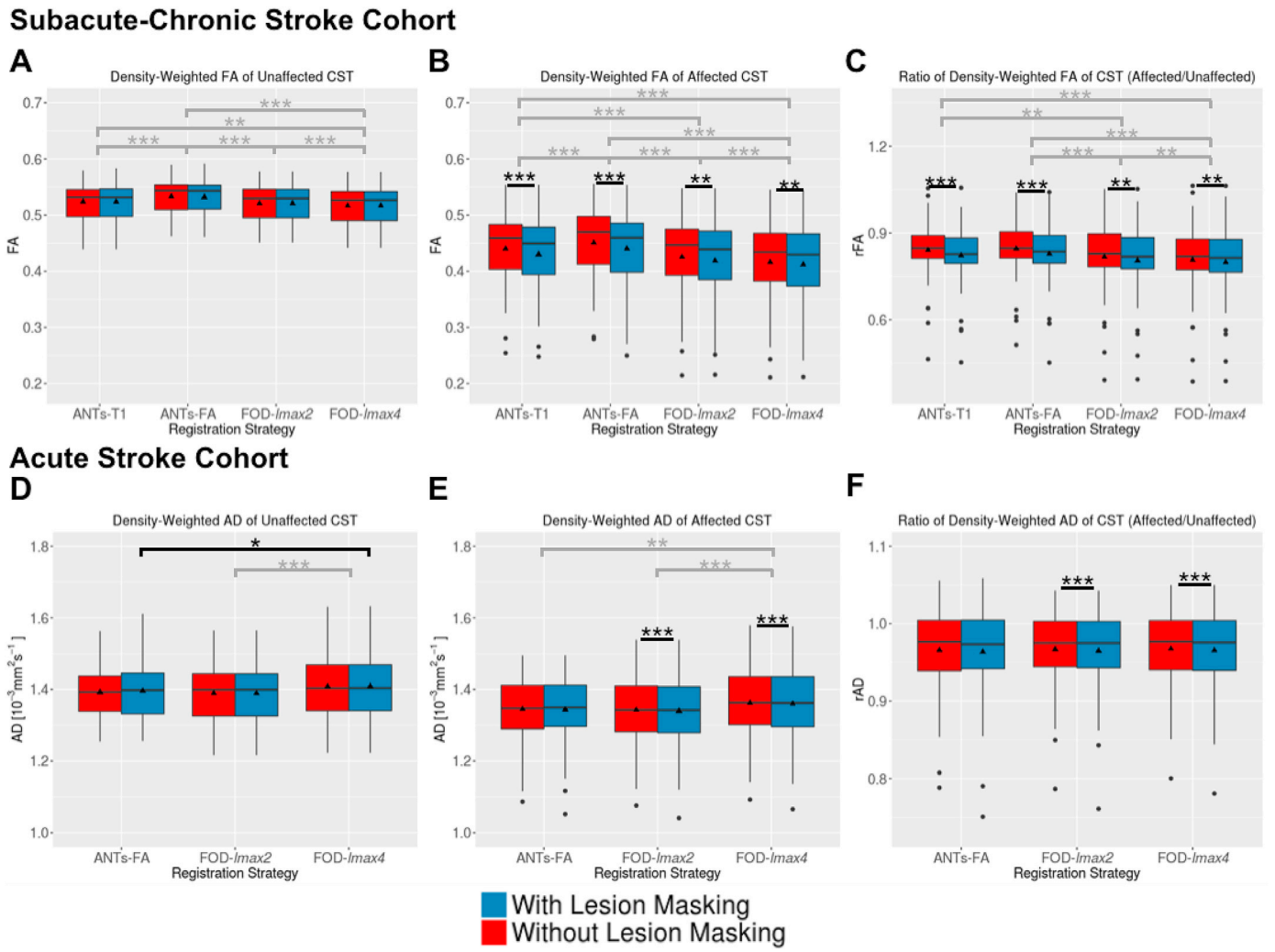

Fig. 4. Effect of registration strategy and lesion masking on DTI parameter extraction of the corticospinal tract (CST). Fractional Anisotropy (FA) of the subacute-chronic stroke cohort (top row) and Axial Diffusivity (AD) of the acute stroke cohort (bottom row) of the unaffected (left column) and affected (middle column) CST as well as the ratio (right column). Boxes display the median and interquartile range, whiskers show the range of values, dots reflect outliers, and triangles represent the mean value. For tidiness, black-colored comparisons reflect significant differences between two registration strategies (hooks over interquartile lines), whereas grey-colored comparisons reflect significant differences between two software packages for both lesion masking and without lesion masking (hooks in between blue and red boxplots). Black bars at the top of the whiskers reflect significant differences for lesion masking for a given software. *p < 0.05, **p < 0.001, ***p < 0.0001 Bonferroni-corrected from individual paired t-tests.

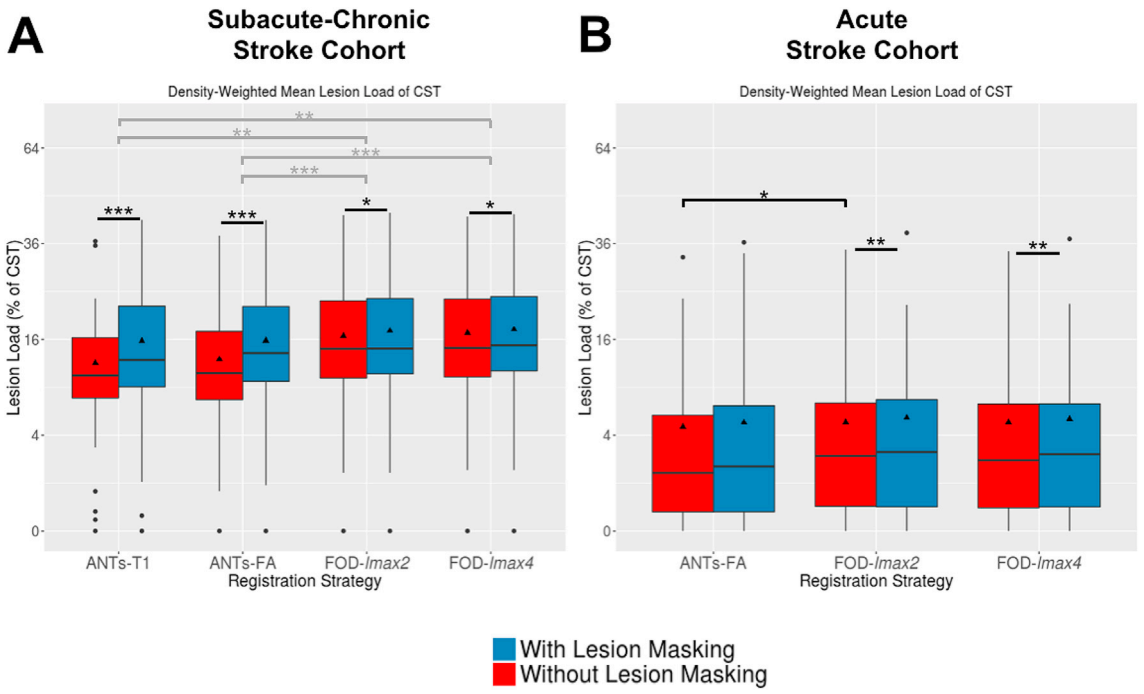

Fig. 5. Lesion load analysis. Lesion load for the subacute-chronic stroke cohort (A) and the acute stroke cohort (B). Note that the y-axis scales as y^2 to facilitate visualization between both groups. Boxes display the median and interquartile range, whiskers show the range of values, dots reflect outliers, and triangles represent the mean value. For tidiness, black-colored comparisons reflect significant differences between two registration strategies (hooks over interquartile lines), whereas grey-colored comparisons reflect significant differences between two software packages for both lesion masking and without lesion masking (hooks in between blue and red boxplots). Black bars at the top of the whiskers reflect significant differences for lesion masking for a given software. *$p < 0.05$, **$p < 0.001$, ***$p < 0.0001$ Bonferroni-corrected from individual paired t-tests.

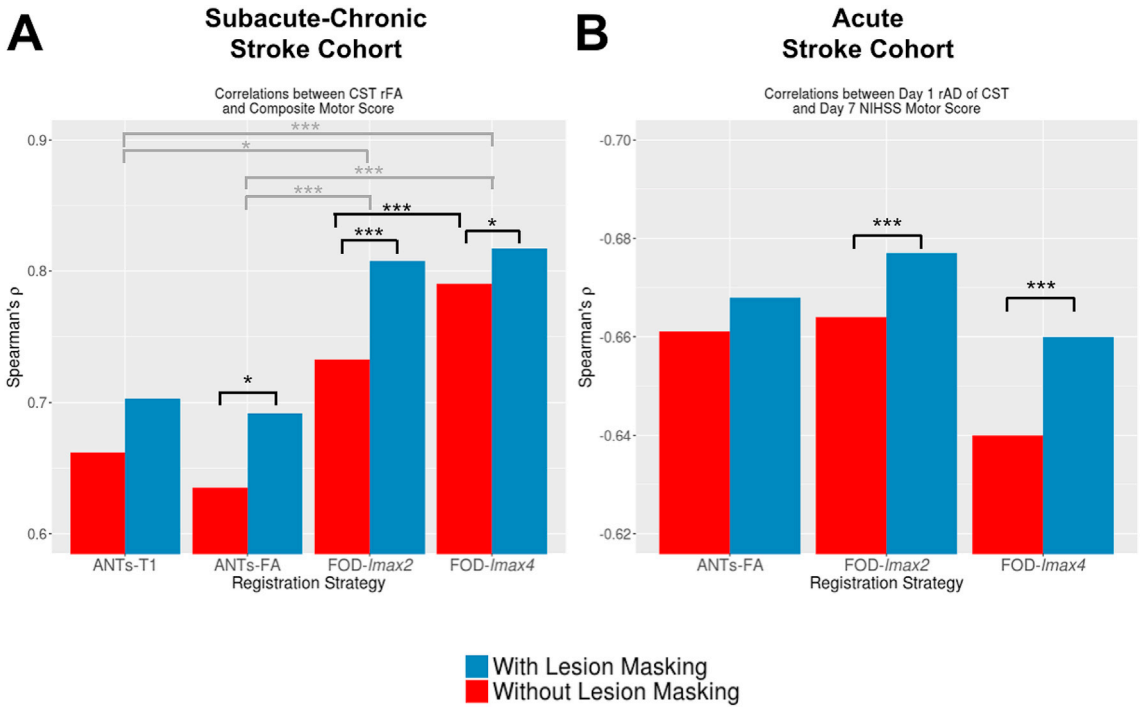

Fig. 6. Spearman correlations between clinical scores and DTI parameters of the CST for each registration strategy. (A) Correlations were performed between ratios of the Fractional Anisotropy (rFA = affected/unaffected) and the composite motor score for the subacute-chronic stroke cohort. (B) Correlations were performed between ratios of day 1 post-stroke Axial Diffusivity (rAD) and the NIHSS motor score at day 7 post-stroke. Spearman's ρ for each correlation is shown on the y-axis and each strategy with lesion masking (blue) and without lesion masking (red) is shown on the x-axis. For tidiness, black-colored comparisons reflect significant differences between two registration strategies (hooks over center of bars), whereas grey-colored comparisons reflect significant differences between two software packages for both lesion masking and without lesion masking (hooks in between blue and red bars). Permutation test significance: *$p < 0.05$, **$p < 0.001$, ***$p < 0.0001$.

3.2.1. Subacute-chronic stroke cohort

3.2.1.1. FA values. In the unaffected hemisphere, significant differences in FA were observed depending on the registration STRATEGY ($F(1.9,74.2) = 44.3$, $p < 0.001$), and there was neither an effect of MASKING ($F(1,39) = 2.8$, $p = 0.10$; Fig. 4A) nor significant interaction ($F(1.7,65.6) = 3.3$, $p = 0.051$). Methods yielded different values of FA of the CST (mean ± SD) with the following hierarchy: ANTs-FA (0.532 ± 0.033) > ANTs-T1 (0.524 ± 0.033) = FOD-*lmax2* (0.521 ± 0.035) > FOD-*lmax4* (0.516 ± 0.036).

In the affected hemisphere, significant differences in FA were also observed depending on STRATEGY ($F(1.4,54.8) = 66.3$, $p < 0.001$) and MASKING ($F(1,39) = 40.5$, $p < 0.001$; Fig. 4B) with a significant STRATEGY*MASKING interaction ($F(2,84.9) = 7.9$, $p < 0.001$). Post hoc t-tests revealed that the hierarchy of FA values in the affected hemisphere was the following: ANTs-FA (0.445 ± 0.067) > ANTs-T1 (0.435 ± 0.067) > FOD-*lmax2* (0.422 ± 0.076) > FOD-*lmax4* (0.414 ± 0.076). FA values were consistently lower when lesion masking was employed. Also, post-hoc t-tests for the interaction term revealed that lesion masking had the smallest effect on FOD-*lmax4* than on any other strategy (Supplementary Materials).

Finally, ratios of the FA were also different depending on STRATEGY ($F(1.3,49.8) = 27.6$, $p < 0.001$) with a significant main effect of MASKING ($F(1,39) = 36.5$, $p < 0.001$; Fig. 4C) and a significant STRATEGY*MASKING interaction ($F(2.2,85.3) = 6.3$, $p = 0.002$). The hierarchy for rFA values was the following: ANTs-FA (0.836 ± 0.116) = ANTs-T1 (0.831 ± 0.118) > FOD-*lmax2* (0.811 ± 0.136) > FOD-*lmax4* (0.802 ± 0.139). rFA values were always lower when lesion masking was employed. Lesion masking had the smallest effect on FOD-*lmax4* than on any other strategy (Supplementary Materials).

3.2.1.2. Lesion load of the CST. For weighted lesion load (wLL) of the CST, significant effects for STRATEGY ($F(1.4,54.8) = 37.3$, $p < 0.001$), MASKING ($F(1,39) = 47.2$, $p < 0.001$), and a STRATEGY*MASKING interaction ($F(2.0,78.5) = 16.0$, $p < 0.001$) were observed (Fig. 5A). The hierarchy of lesion load was the following: ANTs-FA ($14.4 \pm 8.9\%$) = ANTs-T1 ($14.1 \pm 9.3\%$) < FOD-*lmax2* ($17.0 \pm 10.2\%$) < FOD-*lmax4* ($17.4 \pm 10.2\%$). wLL was always higher when lesion masking was employed. Lesion masking had the smallest effect on FOD-*lmax2* and FOD-*lmax4*, both of which were smaller than the effect on ANTs-FA and ANTs-T1 (Supplementary Materials).

Our data showed that the additional lesion load from masking *vs*. no masking correlated significantly with decreases in FA from masking *vs*. no masking for all strategies ($p < 0.05$, Supplementary Materials).

3.2.2. Acute stroke cohort

3.2.2.1. AD values. In the unaffected hemisphere, registration strategy yielded different values of AD of the CST ($F(1.3,85.6) = 15.2$, $p < 0.001$) with no effect of MASKING ($F(1,68) = 2.0$, $p = 0.16$; Fig. 4D) and no significant interaction ($F(1.0,68.1) = 1.8$, $p = 0.18$). In this case, the hierarchy of AD values in the acute stroke cohort was different than for the FA of the subacute-chronic stroke cohort. In particular, FOD-*lmax4* had higher AD values (mean ± SD: $1.408 \pm 0.084 \times 10^{-3} mm^2 s^{-1}$) than both ANTs-FA ($1.393 \pm 0.071 \times 10^{-3} mm^2 s^{-1}$) and FOD-*lmax2* ($1.389 \pm 0.075 \times 10^{-3} mm^2 s^{-1}$) which yielded similar values.

In the affected hemisphere, registration strategy had the same effect on the hierarchy of AD values of the unaffected CST ($F(1.3,87.2) = 24.6$, $p < 0.001$; Fig. 4E): FOD-*lmax4* ($1.361 \pm 0.105 \times 10^{-3} mm^2 s^{-1}$) followed by ANTs-FA ($1.344 \pm 0.093 \times 10^{-3} mm^2 s^{-1}$) and FOD-*lmax2* ($1.341 \pm 0.098 \times 10^{-3} mm^2 s^{-1}$), with ANTs-FA and FOD-*lmax2* yielding similar AD values. Also, on average, AD values were lower with lesion masking. The interaction term was not significant ($F(1.0,70.5) = 2.4$, $p = 0.12$).

As for the ratio of AD in the CST, there was a significant effect of MASKING ($F(1,68) = 11.6$, $p < 0.001$; Fig. 4F) with no difference between strategies ($F(1.5,99.6) = 0.5$, $p = 0.54$), or interaction ($F(1.0,70.1) = 0.1$, $p = 0.88$). On average, the rAD with lesion masking was lower than with masking.

3.2.2.2. Lesion load of the CST. Concerning lesion load, there was a significant effect of STRATEGY ($F(1.1,75.2) = 4.3$, $p = 0.04$) and MASKING ($F(1,68) = 12.7$, $p < 0.001$, Fig. 5B) with no interaction ($F(1.1,74.2) = 0.3$, $p = 0.6$). Post hoc t-tests revealed that there was only a significant difference between ANTs-FA ($5.0 \pm 7.2\%$) and FOD-*lmax2* ($5.3 \pm 7.1\%$), both of which were similar to FOD-*lmax4* (5.3 ± 7.0). wLL was higher when lesion masking was employed.

Finally, changes in lesion load also correlated with changes in AD for the acute stroke cohort ($p < 0.001$, Supplementary Materials).

3.3. Correlation analysis between CST integrity and motor outcome

For the subacute-chronic stroke cohort, correlations between the composite motor score and the rFA of the CST were highly significant for each registration method (Fig. 6A, Table 1). The more severe the motor deficit was (low composite motor score), the more pronounced the FA asymmetry was (low rFA). We observed significantly different correlations between the composite motor score and rFA depending on registration strategy. Lesion masking improved the correlation strength significantly for ANTs-FA, FOD-*lmax2*, and FOD-*lmax4* with a marginally significant effect for ANTs-T1 ($p = 0.062$). For registration strategies where lesion masking was employed, there was no significant difference between (a) ANTs-T1 and ANTs-FA or (b) FOD-*lmax2* and FOD-*lmax4*. All other comparisons between strategies with lesion masking were significant ($p < 0.0001$), with FOD-*lmax4* yielding the highest correlation strength and ANTs-FA and ANTs-T1 yielding the lowest, resulting in a max improvement in correlation strength of $\Delta\rho = 0.125$. Differences in strategies without lesion masking were similar to those with lesion masking (Fig. 6A, Supplementary Materials).

For the acute stroke cohort, correlations between the day 7 NIHSS motor score and day 1 rAD of the CST were highly significant (Table 1, Fig. 6B). The only observed significant differences were due to lesion masking *vs.* no lesion masking for FOD-*lmax2* ($p < 0.0001$) and FOD-*lmax4* ($p < 0.0001$); however, the differences in correlation coefficient were rather small ($\Delta\rho = 0.013$, 0.019 respectively).

4. Discussion

We evaluated both scalar *vs*. FOD-based registration strategies with and without lesion masking in dMRI data for tract-based correlations in subacute-chronic and acute stroke patients. For multi-shell datasets in subacute-chronic stroke populations, our results showed that normalization strategy had a strong effect on FA asymmetry and lesion load calculated from a corticospinal tract (CST) template. These different parameters thereafter yielded significantly different correlations in motor outcome with FOD-based registration with lesion masking outperforming common FA/T1-scalar registration. As for the acute stroke cohort, registration strategies performed equally well with a minor effect of lesion masking for FOD-based registration.

4.1. Registration effects on DTI parameter extraction

In the subacute-chronic stroke cohort, FOD-based registration yielded the lowest FA values for both the affected and unaffected hemisphere, whereas ANTs-FA yielded the highest. At first sight, it may seem counterintuitive that there be differences in the unaffected hemisphere. However, these observations may be explained by each registration algorithm's cost function (Irfanoglu et al., 2016). Here, FA-based registration is more precise when aligning the CST according to its FA values,

Table 1
Subacute-chronic and acute stroke cohort tract-based correlations. Spearman's ρ is given for the correlations between the ratio of the Fractional Anisotropy (for the subacute-chronic cohort) or Axial Diffusivity (for the acute cohort) extracted with each normalization strategy and the respective motor outcome scores with the bootstrapped 95% confidence interval (CI). All correlations are statistically significant $p \leq 0.0002$.

Strategy	Lesion Masking	Subacute-Chronic Stroke ρ (CI)	Acute cohort ρ (CI)
ANTs-T1	Yes	0.703 (0.470; 0.839)	–
	No	0.662 (0.409; 0.823)	–
ANTs-FA	Yes	0.692 (0.458; 0.841)	−0.668 (−0.776;-0.513)
	No	0.635 (0.362; 0.813)	−0.660 (−0.778;-0.500)
FOD-*lmax2*	Yes	0.808 (0.637; 0.901)	−0.677 (−0.785;-0.528)
	No	0.733 (0.518; 0.864)	−0.664 (−0.776;-0.509)
FOD-*lmax4*	Yes	0.817 (0.647; 0.907)	−0.658 (−0.769;-0.501)
	No	0.790 (0.618; 0.888)	−0.639 (−0.758;-0.470)

whereas diffusion-based registration is better at aligning the CST according to its diffusion orientation and amplitude (Irfanoglu et al., 2016; Wang et al., 2011). ANTs-FA is therefore incentivized to warp high FA values towards the center of the CST where densely-packed fibers aggregate and low FA values towards the edge of the tract or areas of crossing fibers in the centrum semiovale and corona radiata, where CST fiber density is low (Jones, 2008; Jones et al., 2013; Puig et al., 2017) (Figs. 1 and 7). Since we calculated density-weighted FA, ANTs-FA could have attributed more weight to high FA values and less to low FA values. On the other hand, FOD-based registration is more sensitive to the different axes of diffusivity. For example, in the crossroads of the fiber pathways within the corona radiata, the principle axis of diffusivity primarily reflects descending fibers of the CST (Moulton et al., 2015). Therefore, even FODs with spherical harmonic coefficients up to a *lmax* of 2 – which are mostly sensitive to a single direction – can capture descending CST fibers. Consequently, there is less bias towards warping high FA values of patients with high FA values in the template. These factors likely had the effect of capturing the whole anatomy of the CST for FOD-based registration, be it at the crossroads of several pathways (i.e., low FA) or at the center (i.e., high FA). Ultimately, this leads to a lower FA value for FOD-based registration than for FA-based registration. In line with this idea, T1-based registration had FA values in between those of ANTs-FA and FOD-*lmax2*/FOD-*lmax4*. This is likely explained by the T1 images' blindness to elevated FA regions in combination with the imprecision in overlap with the underlying white matter architecture (Zhang et al., 2006).

On the affected side, as expected, FA was reduced for all methods likely from the lesion itself and Wallerian degeneration (Beaulieu et al., 1996; Lindberg et al., 2007; Puig et al., 2010; Thomalla et al., 2004; Yu et al., 2009). Furthermore, we observed a similar hierarchy in FA values as on the unaffected side (Fig. 7). This is likely due to the same reason as for the unaffected side, namely the effect of each normalization's cost function; however, here, distal effects of the lesion likely played an additional role. Indeed, even outside the masked lesion, ANTs-FA will ignore pathological (low) FA of the CST, preferring FA values resembling those of the healthy subjects from which the template was made.

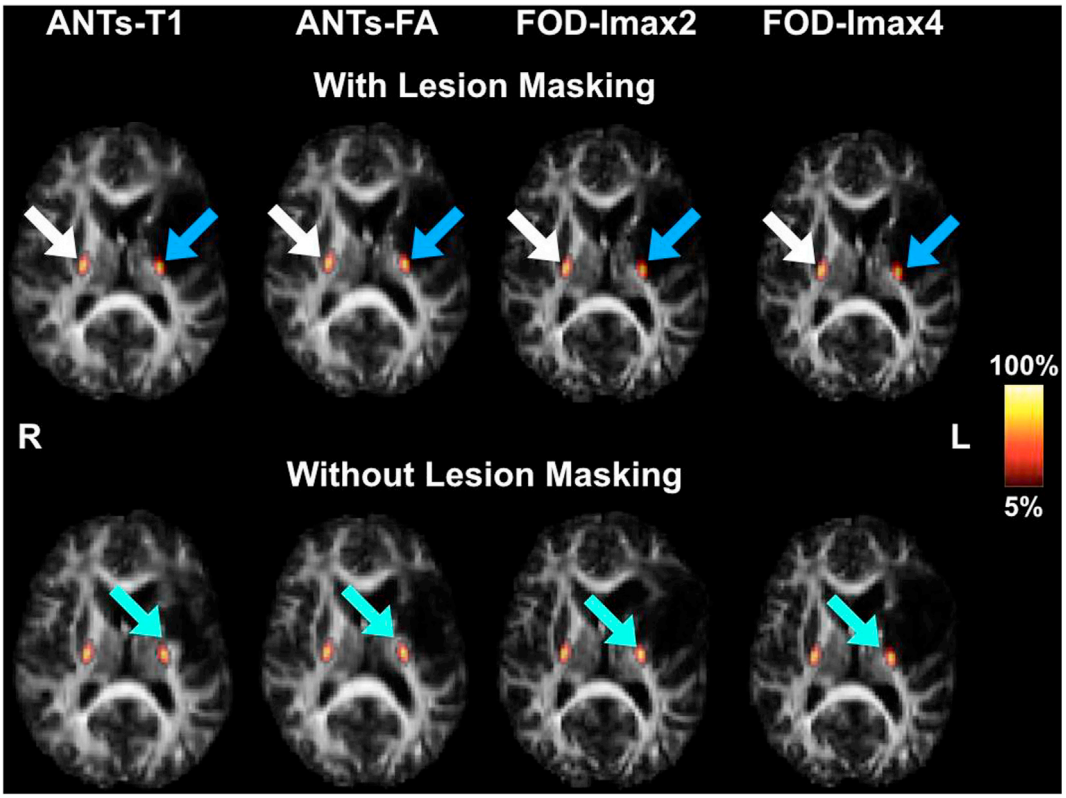

Fig. 7. Effects of scalar vs. FOD-based registration in subacute-chronic stroke. Image slice is from a representative chronic stroke patient. From left to right, the normalized FA maps using warp fields with strategies ANTs-T1, ANTs-FA, FOD-*lmax2*, and FOD-*lmax4*. Top row: Normalization with lesion masking. Bottom row: Normalization without lesion masking. The colorbar shows the percentage of the maximum tract density. White arrows point to the posterior limb of the internal capsule (PLIC) of the unaffected hemisphere, showing larger normalized PLICs for scalar-based registration and smaller PLICs for FOD-based registration. Blue arrows highlight white matter tissue of the PLIC close to the lesion when lesion masking is applied; visually, ANTs-FA results in the lowest lesion overlap, whereas FOD-*lmax4* yields the most. Turquoise arrows show varying degrees of distortions when the lesion is not masked during normalization; as can be seen, scalar-based registration causes most of the PLIC to be filled by high-FA perilesional white matter, whereas FOD-based registration is less sensitive to the lesion.

FOD-based registration, on the other hand, may be more likely to capture remnants of the CST, thereby retaining the pathological FA of the affected side in the weighted average and thus reflecting true FA asymmetries brought on by subacute-chronic stroke lesions. However, one concern in the interpretation of these results is the potential bias from weighting the averages of DTI parameters by fiber density. On the other hand, binarizing tracts by thresholding comes with its own methodological issues. In particular, thresholding at a low fiber density/probability allows one to conserve diffuse tracts near the upper cortex at the risk of false positives in inferior portions of the CST, whereas high thresholds allow for the removal of more false positives at the risk of eliminating the upper CST from the region of interest. To bypass this compromise, we reran the analysis using the publicly available binary CST-M1 mask from the sensorimotor area tract template (SMATT), which was constructed using a novel slice-wise thresholding technique as described in Archer et al. (2018) (Supplementary Materials). We found that the overall trends remained unchanged, albeit with a marked decrease in correlation strength. Despite the potential confounds of density-weighted DTI measurements (Archer et al., 2018), density weighting has been shown to be superior in quantifying acute stroke damage to the CST (Hirai et al., 2016) and can account for the important deficits that occur when compacted portions of the CST are lesioned (Vargas et al., 2013; Zhu et al., 2010).

More crucial than the absolute value of FA for which we do not have the ground truth, the parameter of clinical importance is the asymmetry. In fact, our data showed that FOD-*lmax4* registration yielded the largest FA differences between the affected and unaffected side (FA_{aff}-$FA_{unaff} = -0.105$), whereas ANTs-FA yielded the lowest FA differences (FA_{aff}-$FA_{unaff} = -0.087$). The relative proportion of FA_{aff}/FA_{unaff} was therefore highest for FOD-based registration, corroborating the notion that FOD-based registration is more sensitive to underlying FA asymmetries of the CST.

As for the acute stroke cohort, registration strategy had little effect on parameter extraction, a stark contrast from the subacute-chronic stroke cohort. Unfortunately, we are not able to perfectly disentangle the contributions of the nature of early stroke lesions and the limitations in the DWI protocol to these results. Concerning the effect of registration for the acute stroke cohort, that all registration strategies performed equally well likely stems from the low angular resolution of the DWI protocol which was acquired in a purely clinical setting and at day 1 post-stroke, no less. These are truly difficult circumstances for obtaining clean data, as can be seen by the large percentage of patients (30.4%) who needed manual removal of corrupted images. These data reflect the maximally feasible scanning time for day 1 post-stroke onset patients, making the improvement of the angular resolution of the dMRI imaging sequence quite difficult. Whereas 30 diffusion-encoding directions is sufficient to reliably estimate FA values (Sharman et al., 2011), it pales in comparison to the high angular resolution of the subacute-chronic stroke cohort for FOD estimation, undoubtedly resulting in more orientation errors and increased false-positive and false-negative rates of the FODs (Wilkins et al., 2015). This likely prevented FOD-based registration from surpassing FA-based registration as was the case for the subacute-chronic stroke cohort and other studies (Raffelt et al., 2011). That being said, the contribution of the spherical harmonic functions up to a *lmax* of 4 do not require many diffusion-encoding directions to stably model the diffusion signal (Tournier et al., 2013). Moreover, a *lmax* of 4 has been shown to be optimal for FOD-based registration (Raffelt et al., 2011). Finally, MRtrix has been shown to be a top-performing tool for estimating FODs with constrained spherical deconvolution for clinical datasets even with a low number of directions at a relative low b-value of 1000 s/mm^2 (Wilkins et al., 2015). Although we were mathematically able to perform FOD-based registration with the recommended *lmax* value of 4 with the acute stroke data, the less-than-optimally estimated FODs undoubtedly hindered the full potential of FOD-based registration. In fact, although not significant, FOD-*lmax4* yielded weaker correlations than FOD-*lmax2* and ANTs-FA, on average. This likely arose from overfitting noise with the 15 free parameters using a *lmax* of 4 *vs.* the 6 free parameters using a *lmax* of 2.

4.2. Lesion masking effects on DTI parameter extraction and lesion overlap

Expectedly, lesion masking produced no effect in the unaffected hemisphere for DTI parameter extraction or lesion load, but only in the affected hemisphere, attesting to the local nature of non-linear warping (Andersen et al., 2010; Brett, 2001). In our study, lesion masking resulted in significantly larger lesion loads of the CST (Fig. 7), corroborating previous findings that lesion masking prevents volume reduction of infarcted tissue through normalization (Brett, 2001; Renard et al., 2016). Furthermore, lesion masking always yielded decreased FA values in the affected CST in subacute-chronic stroke. In fact, our data showed that the marked changes in FA of the subacute-chronic stroke cohort were, in part, the result of the additional lesion load resulting from masking the lesion during normalization.

In acute stroke, lesion masking only affected AD measures for FOD-based normalization and not FA-based normalization. Such differential effects of lesion masking on lesion load likely reflect the fact that, at day 1 post stroke, FA values are pseudonormal (see Fig. 2). FA-based registration therefore is not as affected by lesioned tissue than at the subacute-chronic stages, where FA values both at the core of the lesion and distally through Wallerian degeneration are drastically reduced (Beaulieu et al., 1996; Lindberg et al., 2007; Puig et al., 2010; Thomalla et al., 2004; Yu et al., 2009). On the other hand, in acute stroke, cytotoxic edema causes extreme reductions in diffusivity (Bhagat et al., 2008, 2006; Feng et al., 2015; Liang et al., 2007; Moulton et al., 2015; Sotak, 2002). Despite superficially preserving the local directions of diffusivity in the FOD maps, edema causes fiber density to be over-estimated as can be seen in Fig. 2, directly affecting registration, albeit by a small amount.

4.3. Effect of registration strategy on correlations between CST integrity and motor outcome

In the subacute-chronic stroke group, FOD-*lmax4* yielded the strongest correlations between FA asymmetries and motor outcome. Here, we argue that FOD-*lmax4* is, in fact, truly capable of better aligning the entirety of the affected CST, both directly and indirectly affected by stroke, better than FA or T1-based registration (Raffelt et al., 2011), thus capturing true asymmetries. While stroke can cause long-range significant changes in both DTI parameters as well as the principle orientations of diffusivity (Pierpaoli et al., 2001), FODs altered by stroke may still be able to capture remnants of the CST, leading to better anatomical overlap as in healthy subjects. Indeed, the fact that lesion masking in FOD-based registration had a smaller effect on rFA extraction than in scalar-based registration corroborates this idea. Importantly, as explained in section 4.1, FOD-based registration is not driven by the same parameter as that used for motor outcome correlations. Consequently, FOD-based registration is less likely to misrepresent FA of the affected side and accurately capture remnants of the CST, yielding larger lesion loads and thus FA reductions. That these FA asymmetries then correlate the most strongly with motor outcome become attests to a more anatomically accurate normaliza-tion with FODs.

Despite FOD-based registration yielding the strongest correlations with motor outcome, normalization with ANTs-FA and ANTs-T1 still yielded significant correlations. Our results, in no way, therefore, cast doubt on previous studies that employed similar techniques. Rather, this new, innovative method can improve existing models of recovery based on asymmetries in CST FA, including those which have investigated the role of alternate corticofugal or corticocortical pathways in motor outcome in a common space (Schulz et al., 2017a, 2017b, 2012). These pathways are often very close to the fibers originating in the primary motor cortex; suboptimal normalization can therefore lead to improper overlap of the various corticofugal and/or corticocortical pathways and thus different correlation strengths. Notably, more sensitive measures of

CST damage (via better correlations from FOD-based registration) leave less variance to be explained by other pathways. This effect might particularly alter model outcome when the contribution of such alternate pathways is close to the threshold of significance, once adjusted for CST damage (Schulz et al., 2017a, 2017b, 2012). Our data suggest that, when the acquisition protocol permits, FOD-based registration should be considered the reference technique when normalizing subacute-chronic stroke dMRI data to a common template.

As for the acute stroke cohort, registration strategy had little effect on parameter correlation strength. We attribute this result in part to the nature of acute stroke lesions as well as to the limitations in the imaging protocol as previously discussed. Nevertheless, most clinical studies having performed group-level analyses in acute stroke rarely acquired more than 30 diffusion-encoding directions (Doughty et al., 2016; Moulton et al., 2015; Puig et al., 2011). Until acquisition acceleration techniques can be incorporated in clinical dMRI sequences, our data suggest that FA-based registration remains an adequate technique for normalization of dMRI data in acute stroke.

4.4. Limitations

The most important limitation to our study was the different protocols for our acute and subacute-chronic stroke cohort. In particular, our acute stroke cohort did not have T1-weighted images. However, in clinical practice for emergency thrombolysis treatment, it is not customary to acquire high-resolution T1 images as they are lengthy and do not provide clinically relevant information to medical doctors for acute management of stroke. Second, the number of diffusion-encoding directions and b-value of the acute DWI sequence were both inferior to that of the subacute-chronic stroke cohort and thus to the templates derived from the healthy controls. It is therefore conceivable that such a disparity in imaging protocol artifactually drove the findings about the acute stroke cohort. We therefore reran the entire analysis using new templates constructed from separate healthy control images acquired with similar imaging parameters in the same MRI machine as the acute stroke cohort ($TR = 14s$, $TE = 83.2$, voxel size $= 1.09 \times 1.09 \times 3mm^3$, no phase encoding, 30 directions, $b = 1000\ s/mm^2$). We found that the results remained globally unchanged for both the acute and subacute-stroke cohort, implying that our registration was robust to the imaging template and that our conclusions remain valid (Supplementary Materials). Nevertheless, only a few studies have published imaging data using DTI models at the acute stroke stage (Doughty et al., 2016; Groisser et al., 2014; Moulton et al., 2015; Puig et al., 2011; Spampinato et al., 2017). Instead of comparing acute *vs.* subacute-chronic stroke, this study serves to suggest optimal registration strategies for datasets typically acquired in today's clinical and research settings. As image acquisition acceleration techniques become available in the future, similar data should be reanalyzed with more directions, or possibly higher b-values (Xie et al., 2015) for stroke cohorts at any stage.

Second, we note that our healthy controls are younger than the studied stroke patients ($p < 0.0001$) and that there are well-known changes in dMRI parameters with age (Lebel et al., 2012). Nevertheless, the healthy controls used to construct our templates are similar to those for existing open source FA and FOD templates, such as the IIT Human Brain Atlas v4.1 (https://www.nitrc.org/projects/iit/) (Varentsova et al., 2014).

Third, we limited our comparison to T1, FA, and FOD-based registration using ANTs and MRtrix despite the availability of other software aimed at registering DWI data, such as other commonly used scalar-based (Klein et al., 2009), tensor-based (Irfanoglu et al., 2016; Zhang et al., 2006), surface-based (Esteban et al., 2016), streamline-based (Garyfallidis et al., 2015), or based on whole DWI datasets (Afzali et al., 2017; Zhang et al., 2014). We limited our registration algorithms to ANTs and MRtrix for the following reasons: (1) These two packages have been openly available to the general public for many years and do not require study-specific file formats or data architecture. (2) One important factor we wished to evaluate was lesion masking vs. no lesion masking. It was therefore crucial that this feature be readily implemented in the studied algorithms and appropriate for stroke lesions. At the time of publication, this feature was not available for two popular tensor-based registration software packages, DTI-TK (Zhang et al., 2006) and MED-INDRIA (Yeo et al., 2009), whereas a third, DR-TAMAS (Irfanoglu et al., 2016), utilized a lesion masking algorithm unsuitable for subcortical stroke lesions. Nevertheless, DTI-based registration remains a promising avenue for registration in stroke imaging and should be evaluated in the future studies when appropriate lesion masking schemes become available. (3) We deemed streamline based registration an unsuitable candidate due to the strong white matter disconnections known to be caused by stroke (Grefkes and Fink, 2014); moreover, this would have required personalized tractography in all 109 patients' native spaces, which defeated the purpose of this study. (4) ANTs and MRtrix's *mrregister* are both based on the same underlying symmetric diffeomorphic non-linear registration (Avants et al., 2008; Raffelt et al., 2011), making the comparison of each strategy's performance less ambiguous. (5) Finally, we chose ANTs for our scalar based registration due to its superiority over other commonly used techniques for registering T1 and FA images (Irfanoglu et al., 2016; Klein et al., 2009; Tustison et al., 2014) and because it has already shown to perform well with lesion masking in chronic stroke (Ripollés et al., 2012).

Lastly, we did not investigate the effect of virtual lesions superimposed on healthy dMRI data on registration accuracy as in Brett (2001), Nachev et al. (2008), Renard et al. (2016) due to the high-dimensional complex models that are FODs. Unlike T1 or FA images where subacute-chronic ischemic lesions resemble simple hypointense regions, their effect on FOD shape has not been explored and is difficult to artificially reproduce. Indeed, due to the complex shape of FODs, which may reflect spared fiber populations, it is imperative that any virtual lesion be consistent with the surrounding healthy tissue when superimposed on a healthy brain. Not only is this procedure challenging, but it also highly restricts the reusability of virtually lesioned FODs in different areas of the brain where the direction of diffusion needs to be consistent along major white matter pathways. Second, unlike chronic stroke, acute stroke lesions contain restricted water diffusion due to cytotoxic edema, yielding large FOD shapes that have a completely different and under-investigated diffusion profile. For these reasons, we did not investigate enantiomorphic normalization as described in Nachev et al. (2008), which has proven effective in normalizing T1 stroke images (Nachev et al., 2008). Indeed, the amplitude and complex directional information of the FODs make the implementation of enantiomorphic normalization in FOD-based registration far from straight-forward. As explained previously, simply swapping lesioned regions with the homologous healthy side may lead to discontinuities along the interface of the superimposed lesion and the salvaged, surrounding white matter. Concerning virtual lesions reflecting acute stroke damage, at the acute stage, FA is pseudonormal in the lesion (Doughty et al., 2016; Moulton et al., 2015), making it difficult to create useful FA virtual lesions.

5. Conclusion

Our study is unique in that we contrasted commonly used and novel, FOD-based registration strategies for typical datasets in subacute-chronic and acute stroke. We have demonstrated that for high angular resolution diffusion imaging in subacute-chronic stroke, FOD-based registration to a template with lesion masking is the optimal method determining lesion load and DTI correlates of motor outcome in a common space. While this strategy could be used by many existing data sets, no study to our knowledge has yet taken advantage of this strategy. This normalization method should serve as a reference procedure for conducting future group-level analyses for effective biomarkers of stroke recovery in the white matter (Boyd et al., 2017; Carey et al., 2015). As for acute stroke data acquired in clinical routine, traditional scalar-based normalization methods are still appropriate until image acquisition acceleration

techniques can become readily available, allowing for a denser sampling of diffusion space.

Acknowledgments

The Pitié-Salpêtrière registry was supported by the French Ministry of Health grant EVALUSINV PHRC AOM 03 008. The research leading to these results has received funding from “Investissements d'avenir” ANR-10-IAIHU-06. We also thank Sophie Sébille for her remarks on the manuscript.

Appendix A. Supplementary data

Supplementary data related to this article can be found at https://doi.org/10.1016/j.neuroimage.2018.08.002.

References

Afzali, M., Fatemizadeh, E., Soltanian-Zadeh, H., 2017. Sparse registration of diffusion weighted images. Comput. Meth. Progr. Biomed. 151, 33–43. https://doi.org/10.1016/j.cmpb.2017.08.003.

Andersen, S.M., Rapcsak, S.Z., Beeson, P.M., 2010. Cost function masking during normalization of brains with focal lesions: still a necessity? Neuroimage 53, 78–84. https://doi.org/10.1016/j.neuroimage.2010.06.003.

Andersson, J.L.R., Graham, M.S., Zsoldos, E., Sotiropoulos, S.N., 2016. Incorporating outlier detection and replacement into a non-parametric framework for movement and distortion correction of diffusion MR images. Neuroimage 141, 556–572. https://doi.org/10.1016/j.neuroimage.2016.06.058.

Andersson, J.L.R., Skare, S., Ashburner, J., 2003. How to correct susceptibility distortions in spin-echo echo-planar images: application to diffusion tensor imaging. Neuroimage 20, 870–888. https://doi.org/10.1016/S1053-8119(03)00336-7.

Andersson, J.L.R., Sotiropoulos, S.N., 2016. An integrated approach to correction for off-resonance effects and subject movement in diffusion MR imaging. Neuroimage 125, 1063–1078. https://doi.org/10.1016/j.neuroimage.2015.10.019.

Archer, D.B., Patten, C., Coombes, S.A., 2017. Free-water and free-water corrected fractional anisotropy in primary and premotor corticospinal tracts in chronic stroke. Hum. Brain Mapp. 38, 4546–4562. https://doi.org/10.1002/hbm.23681.

Archer, D.B., Vaillancourt, D.E., Coombes, S.A., 2018. A template and probabilistic atlas of the human sensorimotor tracts using diffusion MRI. Cerebr. Cortex 28, 1685–1699. https://doi.org/10.1093/cercor/bhx066.

Ashburner, J., Friston, K.J., 2005. Unified segmentation. Neuroimage 26, 839–851. https://doi.org/10.1016/j.neuroimage.2005.02.018.

Avants, B.B., Epstein, C.L., Grossman, M., Gee, J.C., 2008. Symmetric diffeomorphic image registration with cross-correlation: evaluating automated labeling of elderly and neurodegenerative brain. Med. Image Anal. 12, 26–41. https://doi.org/10.1016/j.media.2007.06.004.

Basser, P.J., 1995. Inferring microstructural features and the physiological state of tissues from diffusion-weighted images. NMR Biomed. 8, 333–344.

Basser, P.J., Mattiello, J., LeBihan, D., 1994. Estimation of the effective self-diffusion tensor from the NMR spin echo. J. Magn. Reson. B 103, 247–254.

Beaulieu, C., Does, M.D., Snyder, R.E., Allen, P.S., 1996. Changes in water diffusion due to Wallerian degeneration in peripheral nerve. Magn. Reson. Med. 36, 627–631. https://doi.org/10.1002/mrm.1910360419.

Bhagat, Y.A., Emery, D.J., Shuaib, A., Sher, F., Rizvi, N.H., Akhtar, N., Clare, T.L., Leatherdale, T., Beaulieu, C., 2006. The relationship between diffusion anisotropy and time of onset after stroke. J. Cerebr. Blood Flow Metabol. 26, 1442–1450. https://doi.org/10.1038/sj.jcbfm.9600294.

Bhagat, Y.A., Hussain, M.S., Stobbe, R.W., Butcher, K.S., Emery, D.J., Shuaib, A., Siddiqui, M.M., Maheshwari, P., Al-Hussain, F., Beaulieu, C., 2008. Elevations of diffusion anisotropy are associated with hyper-acute stroke: a serial imaging study. Magn. Reson. Imaging 26, 683–693. https://doi.org/10.1016/j.mri.2008.01.015.

Boyd, L.A., Hayward, K.S., Ward, N.S., Stinear, C.M., Rosso, C., Fisher, R.J., Carter, A.R., Leff, A.P., Copland, D.A., Carey, L.M., Cohen, L.G., Basso, D.M., Maguire, J.M., Cramer, S.C., 2017. Biomarkers of stroke recovery: consensus-based core recommendations from the stroke recovery and rehabilitation roundtable. Int. J. Stroke 12, 480–493. https://doi.org/10.1177/1747493017714176.

Brett, M., 2001. Spatial normalization of brain images with focal lesions using cost function masking. Neuroimage 14, 486–500. https://doi.org/10.1006/nimg.2001.0845.

Carey, L.M., Crewther, S., Salvado, O., Lindén, T., Connelly, A., Wilson, W., Howells, D.W., Churilov, L., Ma, H., Tse, T., Rose, S., Palmer, S., Bougeat, P., Campbell, B.C.V., Christensen, S., Macaulay, S.L., Favaloro, J., O' Collins, V., Mcbride, S., Bates, S., Cowley, E., Dewey, H., Wijeratne, T., Gerraty, R., Phan, T.G., Yan, B., Parsons, M.W., Bladin, C., Barber, P.A., Read, S., Wong, A., Lee, A., Kleinig, T., Hankey, G.J., Blacker, D., Markus, R., Leyden, J., Krause, M., Grimley, R., Mahant, N., Jannes, J., Sturm, J., Davis, S.M., Donnan, G.A., 2015. STroke imAging pRevention and treatment (START): a longitudinal stroke cohort study: clinical trials protocol. Int. J. Stroke 10, 636–644. https://doi.org/10.1111/ijs.12190.

de Manzano, Ö., Ullén, F., 2018. Same genes, different brains: neuroanatomical differences between monozygotic twins discordant for musical training. Cerebr. Cortex 28, 387–394. https://doi.org/10.1093/cercor/bhx299.

Dhollander, T., Raffelt, D., Connelly, A., 2016. Unsupervised 3-tissue response function estimation from single-shell or multi-shell diffusion MR data without a co-registered T1 image. In: ISMRM Workshop on Breaking the Barriers of Diffusion MRI, p. 5.

Doughty, C., Wang, J., Feng, W., Hackney, D., Pani, E., Schlaug, G., 2016. Detection and predictive value of fractional anisotropy changes of the corticospinal tract in the acute phase of a stroke. Stroke 47, 1520–1526. https://doi.org/10.1161/STROKEAHA.115.012088.

Esteban, O., Zosso, D., Daducci, A., Bach-Cuadra, M., Ledesma-Carbayo, M.J., Thiran, J.P., Santos, A., 2016. Surface-driven registration method for the structure-informed segmentation of diffusion MR images. Neuroimage 139, 450–461. https://doi.org/10.1016/j.neuroimage.2016.05.011.

Feng, W., Wang, J., Chhatbar, P.Y., Doughty, C., Landsittel, D., Lioutas, V.A., Kautz, S.A., Schlaug, G., 2015. Corticospinal tract lesion load: an imaging biomarker for stroke motor outcomes. Ann. Neurol. 78, 860–870. https://doi.org/10.1002/ana.24510.

Fugl-Meyer, A.R., Jääskö, L., Leyman, I., Olsson, S., Steglind, S., 1975. The post-stroke hemiplegic patient. 1. a method for evaluation of physical performance. Scand. J. Rehabil. Med. 7, 13–31. https://doi.org/10.1038/35081184.

Garyfallidis, E., Ocegueda, O., Wassermann, D., Descoteaux, M., 2015. Robust and efficient linear registration of white-matter fascicles in the space of streamlines. Neuroimage 117, 124–140. https://doi.org/10.1016/j.neuroimage.2015.05.016.

Geyer, S., Matelli, M., Luppino, G., Zilles, K., 2000. Functional neuroanatomy of the primate isocortical motor system. Anat. Embryol. https://doi.org/10.1007/s004290000127.

Grefkes, C., Fink, G.R., 2014. Connectivity-based approaches in stroke and recovery of function. Lancet Neurol. https://doi.org/10.1016/S1474-4422(13)70264-3.

Groisser, B.N., Copen, W.A., Singhal, A.B., Hirai, K.K., Schaechter, J.D., 2014. Corticospinal tract diffusion abnormalities early after stroke predict motor outcome. Neurorehabilitation Neural Repair 28, 751–760. https://doi.org/10.1177/1545968314521896.

Hirai, K.K., Groisser, B.N., Copen, W.A., Singhal, A.B., Schaechter, J.D., 2016. Comparing prognostic strength of acute corticospinal tract injury measured by a new diffusion tensor imaging based template approach versus common approaches. J. Neurosci. Meth. 257, 204–213. https://doi.org/10.1016/j.jneumeth.2015.09.005.

Irfanoglu, M.O., Nayak, A., Jenkins, J., Hutchinson, E.B., Sadeghi, N., Thomas, C.P., Pierpaoli, C., 2016. DR-TAMAS: diffeomorphic registration for tensor accurate alignment of anatomical structures. Neuroimage 132, 439–454. https://doi.org/10.1016/j.neuroimage.2016.02.066.

Jebsen, R.H., Taylor, N., Trieschmann, R.B., Trotter, M.J., Howard, L.A., 1969. An objective and standardized test of hand function. Arch. Phys. Med. Rehabil. https://doi.org/10.1002/acr.20631.

Jeurissen, B., Tournier, J.D., Dhollander, T., Connelly, A., Sijbers, J., 2014. Multi-tissue constrained spherical deconvolution for improved analysis of multi-shell diffusion MRI data. Neuroimage 103, 411–426. https://doi.org/10.1016/j.neuroimage.2014.07.061.

Jones, D.K., 2008. Studying connections in the living human brain with diffusion MRI. Cortex 44, 936–952. https://doi.org/10.1016/j.cortex.2008.05.002.

Jones, D.K., Knösche, T.R., Turner, R., 2013. White matter integrity, fiber count, and other fallacies: the do's and don'ts of diffusion MRI. Neuroimage 73, 239–254. https://doi.org/10.1016/j.neuroimage.2012.06.081.

Klein, A., Andersson, J., Ardekani, B.A., Ashburner, J., Avants, B., Chiang, M.C., Christensen, G.E., Collins, D.L., Gee, J., Hellier, P., Song, J.H., Jenkinson, M., Lepage, C., Rueckert, D., Thompson, P., Vercauteren, T., Woods, R.P., Mann, J.J., Parsey, R.V., 2009. Evaluation of 14 nonlinear deformation algorithms applied to human brain MRI registration. Neuroimage 46, 786–802. https://doi.org/10.1016/j.neuroimage.2008.12.037.

Koch, P., Schulz, R., Hummel, F.C., 2016. Structural connectivity analyses in motor recovery research after stroke. Ann. Clin. Transl. Neurol. 3, 233–244. https://doi.org/10.1002/acn3.278.

Kunimatsu, A., Aoki, S., Masutani, Y., Abe, O., Mori, H., Ohtomo, K., 2003. Three-dimensional white matter tractography by diffusion tensor imaging in ischaemic stroke involving the corticospinal tract. Neuroradiology 45, 532–535. https://doi.org/10.1007/s00234-003-0974-4.

Lansberg, M.G., Thijs, V.N., O'Brien, M.W., Ali, J.O., de Crespigny, a J., Tong, D.C., Moseley, M.E., Albers, G.W., 2001. Evolution of apparent diffusion coefficient, diffusion-weighted, and T2-weighted signal intensity of acute stroke. AJNR. Am. J. Neuroradiol. 22, 637–644.

Lawrence, M.A., 2015. Ez: Easy Analysis and Visualization of Factorial Experiments. R package version 4.3.

Lebel, C., Gee, M., Camicioli, R., Wieler, M., Martin, W., Beaulieu, C., 2012. Diffusion tensor imaging of white matter tract evolution over the lifespan. Neuroimage 60, 340–352. https://doi.org/10.1016/j.neuroimage.2011.11.094.

Liang, D., Bhatta, S., Gerzanich, V., Simard, J.M., 2007. Cytotoxic edema: mechanisms of pathological cell swelling. Neurosurg. Focus 22, E2.

Lindberg, P.G., Skejø, P.H.B., Rounis, E., Nagy, Z., Schmitz, C., Wernegren, H., Bring, A., Engardt, M., Forssberg, H., Borg, J., 2007. Wallerian degeneration of the corticofugal tracts in chronic stroke: a pilot study relating diffusion tensor imaging, transcranial magnetic stimulation, and hand function. Neurorehabilitation Neural Repair 21, 551–560. https://doi.org/10.1177/1545968307301886.

Lindenberg, R., Zhu, L.L., Rüber, T., Schlaug, G., 2012. Predicting functional motor potential in chronic stroke patients using diffusion tensor imaging. Hum. Brain Mapp. 33, 1040–1051. https://doi.org/10.1002/hbm.21266.

Moulton, E., Amor-Sahli, M., Perlbarg, V., Pires, C., Crozier, S., Galanaud, D., Valabregue, R., Yger, M., Baronnet-Chauvet, F., Samson, Y., Dormont, D., Rosso, C., 2015. Axial diffusivity of the corona radiata at 24 hours post-stroke: a new biomarker for motor and global outcome. PLoS One 10, 1–16. https://doi.org/10.1371/journal.pone.0142910.

Nachev, P., Coulthard, E., Jäger, H.R., Kennard, C., Husain, M., 2008. Enantiomorphic normalization of focally lesioned brains. Neuroimage 39, 1215–1226. https://doi.org/10.1016/j.neuroimage.2007.10.002.

Newton, J.M., Ward, N.S., Parker, G.J.M., Deichmann, R., Alexander, D.C., Friston, K.J., Frackowiak, R.S.J., 2006. Non-invasive mapping of corticofugal fibres from multiple motor areas - relevance to stroke recovery. Brain 129, 1844–1858. https://doi.org/10.1093/brain/awl106.

Nieuwenhuis, S., Forstmann, B.U., Wagenmakers, E.J., 2011. Erroneous analyses of interactions in neuroscience: a problem of significance. Nat. Neurosci. https://doi.org/10.1038/nn.2886.

Park, C.-H., Kou, N., Boudrias, M.-H., Playford, E.D., Ward, N.S., 2013. Assessing a standardised approach to measuring corticospinal integrity after stroke with DTI. NeuroImage. Clin. 2, 521–533. https://doi.org/10.1016/j.nicl.2013.04.002.

Phan, T.G., Donnan, G.A., Wright, P.M., Reutens, D.C., 2005. A digital map of middle cerebral artery infarcts associated with middle cerebral artery trunk and branch occlusion. Stroke 36, 986–991. https://doi.org/10.1161/01.STR.0000163087.66828.e9.

Phan, T.G., Van Der Voort, S., Chen, J., Beare, R., Ma, H., Clissold, B., Ly, J., Foster, E., Thong, E., Srikanth, V., 2013. Impact of corticofugal fibre involvement in subcortical stroke. BMJ Open 3. https://doi.org/10.1136/bmjopen-2013-003318.

Pierpaoli, C., Barnett, A., Pajevic, S., Chen, R., Penix, L.R., Virta, A., Basser, P., 2001. Water diffusion changes in Wallerian degeneration and their dependence on white matter architecture. Neuroimage 13, 1174–1185. https://doi.org/10.1006/nimg.2001.0765.

Pierpaoli, C., Basser, P.J., 1996. Toward a quantitative assessment of diffusion anisotropy. Magn. Reson. Med. 36, 893–906.

Puig, J., Blasco, G., Daunis-I-Estadella, J., Thomalla, G., Castellanos, M., Figueras, J., Remollo, S., van Eendenburg, C., Sánchez-González, J., Serena, J., Pedraza, S., 2013. Decreased corticospinal tract fractional anisotropy predicts long-term motor outcome after stroke. Stroke 44, 2016–8. https://doi.org/10.1161/STROKEAHA.111.000382.

Puig, J., Blasco, G., Schlaug, G., Stinear, C.M., Daunis-i-Estadella, P., Biarnes, C., Figueras, J., Serena, J., Hern?ndez-P?rez, M., Alberich-Bayarri, A., Castellanos, M., Liebeskind, D.S., Demchuk, A.M., Menon, B.K., Thomalla, G., Nael, K., Wintermark, M., Pedraza, S., 2017. Diffusion tensor imaging as a prognostic biomarker for motor recovery and rehabilitation after stroke. Neuroradiology. https://doi.org/10.1007/s00234-017-1816-0.

Puig, J., Pedraza, S., Blasco, G., Daunis-I-Estadella, J., Prados, F., Remollo, S., Prats-Galino, A., Soria, G., Boada, I., Castellanos, M., Serena, J., 2011. Acute damage to the posterior limb of the internal capsule on diffusion tensor tractography as an early imaging predictor of motor outcome after stroke. AJNR. Am. J. Neuroradiol. 32, 857–863. https://doi.org/10.3174/ajnr.A2400.

Puig, J., Pedraza, S., Blasco, G., Daunis-I-Estadella, J., Prats, A., Prados, F., Boada, I., Castellanos, M., Sánchez-González, J., Remollo, S., Laguillo, G., Quiles, a M., Gómez, E., Serena, J., 2010. Wallerian degeneration in the corticospinal tract evaluated by diffusion tensor imaging correlates with motor deficit 30 days after middle cerebral artery ischemic stroke. AJNR. Am. J. Neuroradiol. 31, 1324–1330. https://doi.org/10.3174/ajnr.A2038.

R Core Team, 2016. R: a Language and Environment for Statistical Computing.

Raffelt, D., Tournier, J.D., Fripp, J., Crozier, S., Connelly, A., Salvado, O., 2011. Symmetric diffeomorphic registration of fibre orientation distributions. Neuroimage 56, 1171–1180. https://doi.org/10.1016/j.neuroimage.2011.02.014.

Renard, F., Urvoy, M., Jaillard, A., 2016. Bayesian stroke lesion estimation for automatic registration of DTI images. In: MICCAI, Brain Lesion Workshop, pp. 91–103. https://doi.org/10.1007/978-3-319-30858-6_9.

Ripollés, P., Marco-Pallarés, J., de Diego-Balaguer, R., Miró, J., Falip, M., Juncadella, M., Rubio, F., Rodriguez-Fornells, A., 2012. Analysis of automated methods for spatial normalization of lesioned brains. Neuroimage 60, 1296–1306. https://doi.org/10.1016/j.neuroimage.2012.01.094.

Rondina, J.M., Park, C., Ward, N.S., 2017. Brain regions important for recovery after severe post-stroke upper limb paresis. J. Neurol. Neurosurg. Psychiatry 88, 737–743. https://doi.org/10.1136/jnnp-2016-315030.

Roser, B., Wang, W., Eliassen, H., Hibert, E., 2015. Comparison of dependent pearson and spearman correlation coefficients with and without correction for measurement error. J. Biometrics Biostat. 6. https://doi.org/10.4172/2155-6180.1000226.

Rosso, C., Valabregue, R., Attal, Y., Vargas, P., Gaudron, M., Baronnet, F., Bertasi, E., Humbert, F., Peskine, A., Perlbarg, V., Benali, H., Lehéricy, S., Samson, Y., 2013. Contribution of corticospinal tract and functional connectivity in hand motor impairment after stroke. PLoS One 8 e73164. https://doi.org/10.1371/journal.pone.0073164.

Schulz, R., Koch, P., Zimerman, M., Wessel, M., Bönstrup, M., Thomalla, G., Cheng, B., Gerloff, C., Hummel, F.C., 2015. Parietofrontal motor pathways and their association with motor function after stroke. Brain 138, 1949–1960. https://doi.org/10.1093/brain/awv100.

Schulz, R., Park, C.-H., Boudrias, M.-H., Gerloff, C., Hummel, F.C., Ward, N.S., 2012. Assessing the integrity of corticospinal pathways from primary and secondary cortical motor areas after stroke. Stroke 43, 2248–2251. https://doi.org/10.1161/STROKEAHA.112.662619.

Schulz, R., Park, E., Lee, J., Chang, W.H., Lee, A., Kim, Y.-H., Hummel, F.C., 2017a. Interactions between the corticospinal tract and premotor-motor pathways for residual motor output after stroke. Stroke STROKEAHA 117, 016834. https://doi.org/10.1161/STROKEAHA.117.016834.

Schulz, R., Park, E., Lee, J., Chang, W.H., Lee, A., Kim, Y.H., Hummel, F.C., 2017b. Synergistic but independent: the role of corticospinal and alternate motor fibers for residual motor output after stroke. NeuroImage Clin 15, 118–124. https://doi.org/10.1016/j.nicl.2017.04.016.

Sharman, M.A., Cohen-Adad, J., Descoteaux, M., Mess??, A., Benali, H., Lehericy, S., 2011. Impact of outliers on diffusion tensor and Q-ball imaging: clinical implications and correction strategies. J. Magn. Reson. Imag. 33, 1491–1502. https://doi.org/10.1002/jmri.22577.

Skriver, E.B., Olsen, T.S., McNair, P., 1990. Mass effect and atrophy after stroke. Acta Radiol. 31, 431–438. https://doi.org/10.1177/028418519003100502.

Smith, S.M., 2002. Fast robust automated brain extraction. Hum. Brain Mapp. 17, 143–155. https://doi.org/10.1002/hbm.10062.

Smith, S.M., Jenkinson, M., Woolrich, M.W., Beckmann, C.F., Behrens, T.E.J., Johansen-Berg, H., Bannister, P.R., De Luca, M., Drobnjak, I., Flitney, D.E., Niazy, R.K., Saunders, J., Vickers, J., Zhang, Y., De Stefano, N., Brady, J.M., Matthews, P.M., 2004. Advances in functional and structural MR image analysis and implementation as FSL. Neuroimage S208–S219. https://doi.org/10.1016/j.neuroimage.2004.07.051.

Sotak, C.H., 2002. The role of diffusion tensor imaging in the evaluation of ischemic brain injury - a review. NMR Biomed. 15, 561–569. https://doi.org/10.1002/nbm.786.

Spampinato, M.V., Chan, C., Jensen, J.H., Helpern, J.A., Bonilha, L., Kautz, S.A., Nietert, P.J., Feng, W., 2017. Diffusional kurtosis imaging and motor outcome in acute ischemic stroke. Am. J. Neuroradiol. 1–7. https://doi.org/10.3174/ajnr.A5180.

Stinear, C.M., Ward, N.S., 2013. How useful is imaging in predicting outcomes in stroke rehabilitation? Int. J. Stroke 8, 33–37. https://doi.org/10.1111/j.1747-4949.2012.00970.x.

Thomalla, G., Glauche, V., Koch, M.A., Beaulieu, C., Weiller, C., Röther, J., 2004. Diffusion tensor imaging detects early Wallerian degeneration of the pyramidal tract after ischemic stroke. Neuroimage 22, 1767–1774. https://doi.org/10.1016/j.neuroimage.2004.03.041.

Tournier, J.-D.D., Calamante, F., Gadian, D.G., Connelly, A., 2004. Direct estimation of the fiber orientation density function from diffusion-weighted MRI data using spherical deconvolution. Neuroimage 23, 1176–1185. https://doi.org/10.1016/j.neuroimage.2004.07.037.

Tournier, J.D., Calamante, F., Connelly, A., 2013. Determination of the appropriate b value and number of gradient directions for high-angular-resolution diffusion-weighted imaging. NMR Biomed. 26, 1775–1786. https://doi.org/10.1002/nbm.3017.

Tustison, N.J., Avants, B.B., Cook, P.A., Kim, J., Whyte, J., Gee, J.C., Stone, J.R., 2014. Logical circularity in voxel-based analysis: normalization strategy may induce statistical bias. Hum. Brain Mapp. 35, 745–759. https://doi.org/10.1002/hbm.22211.

Varentsova, A., Zhang, S., Arfanakis, K., 2014. Development of a high angular resolution diffusion imaging human brain template. Neuroimage 91, 177–186. https://doi.org/10.1016/j.neuroimage.2014.01.009.

Vargas, P., Gaudron, M., Valabrègue, R., Bertasi, E., Humbert, F., Lehéricy, S., Samson, Y., Rosso, C., 2013. Assessment of corticospinal tract (CST) damage in acute stroke patients: comparison of tract-specific analysis versus segmentation of a CST template. J. Magn. Reson. Imag. 37, 836–845. https://doi.org/10.1002/jmri.23870.

Veraart, J., Fieremans, E., Novikov, D.S., 2016a. Diffusion MRI noise mapping using random matrix theory. Magn. Reson. Med. 76, 1582–1593. https://doi.org/10.1002/mrm.26059.

Veraart, J., Novikov, D.S., Christiaens, D., Ades-aron, B., Sijbers, J., Fieremans, E., 2016b. Denoising of diffusion MRI using random matrix theory. Neuroimage 142, 394–406. https://doi.org/10.1016/j.neuroimage.2016.08.016.

Wang, Y., Gupta, A., Liu, Z., Zhang, H., Escolar, M.L., Gilmore, J.H., Gouttard, S., Fillard, P., Maltbie, E., Gerig, G., Styner, M., 2011. DTI registration in atlas based fiber analysis of infantile Krabbe disease. Neuroimage 55, 1577–1586. https://doi.org/10.1016/j.neuroimage.2011.01.038.

Wilkins, B., Lee, N., Gajawelli, N., Law, M., Leporé, N., 2015. Fiber estimation and tractography in diffusion MRI: development of simulated brain images and comparison of multi-fiber analysis methods at clinical b-values. Neuroimage 109, 341–356. https://doi.org/10.1016/j.neuroimage.2014.12.060.

Xie, S., Zuo, N., Shang, L., Song, M., Fan, L., Jiang, T., 2015. How does B-value affect HARDI reconstruction using clinical diffusion MRI data? PLoS One 10. https://doi.org/10.1371/journal.pone.0120773.

Yeo, B.T.T., Vercauteren, T., Fillard, P., Peyrat, J.-M., Pennec, X., Golland, P., Ayache, N., Clatz, O., 2009. DT-REFinD: diffusion tensor registration with exact finite-strain differential. IEEE Trans. Med. Imag. 28, 1914–1928. https://doi.org/10.1109/TMI.2009.2025654.

Yu, C., Zhu, C., Zhang, Y., Chen, H., Qin, W., Wang, M., Li, K., 2009. A longitudinal diffusion tensor imaging study on Wallerian degeneration of corticospinal tract after motor pathway stroke. Neuroimage 47, 451–458. https://doi.org/10.1016/j.neuroimage.2009.04.066.

Zhang, H., Yushkevich, P.A., Alexander, D.C., Gee, J.C., 2006. Deformable registration of diffusion tensor MR images with explicit orientation optimization. Med. Image Anal. 10, 764–785. https://doi.org/10.1016/j.media.2006.06.004.

Zhang, P., Niethammer, M., Shen, D., Yap, P.T., 2014. Large deformation diffeomorphic registration of diffusion-weighted imaging data. Med. Image Anal. 18, 1290–1298. https://doi.org/10.1016/j.media.2014.06.012.

Zhang, Y., Brady, M., Smith, S., 2001. Segmentation of brain MR images through a hidden Markov random field model and the expectation-maximization algorithm. IEEE Trans. Med. Imag. 20, 45–57. https://doi.org/10.1109/42.906424.

Zhu, L.L., Lindenberg, R., Alexander, M.P., Schlaug, G., 2010. Lesion load of the corticospinal tract predicts motor impairment in chronic stroke. Stroke 41, 910–915. https://doi.org/10.1161/STROKEAHA.109.577023.

5.3 Conclusion

Our results showed that, for high-quality **subacute-chronic** stroke data, FOD-based registration captured significantly larger FA asymmetries in the CST. This was also associated with significantly stronger correlations in motor outcome with respect to T1 or FA-based registration methods. For acute data acquired in a clinical setting, there were few observed differences, suggesting that commonly employed FA-based registration is appropriate for group-level analyses. Concerning the acute stroke group, we were unable to conclude if the lack of differences were attributable to the lower angular resolution of the DWI sequence or inherent diffusion properties of acute ischemic stroke.

On a global level, FOD-based registration instead of commonly used FA-based registration seems to robustly capture damage to important white matter structures and should be considered a reference procedure for future studies. While the same clear-cut conclusions could not be extended to the acute stroke cohort, these unresolved questions could constitute the basis for future investigations. The major unsolved question of the first study is whether a higher angular resolution of the acute stroke cohort imaging protocol could have lead to a better performance of FOD with respect to FA-based registration. Indeed, the clinical DTI protocol of our acute stroke cohort only benefited from diffusion-weighted images along 30 directions, which, while mathematically sufficient to estimate FODs, are less than what is commonly acquired in research imaging centers. On the other hand, if obtaining more diffusion-weighted images is not logistically feasible in practice, there exists several DTI-based registration techniques which appear to be a promising alternative for datasets of low angular resolution, such as those obtained in our clinical practice. Indeed, here, 30 directions are more than adequate to reliably estimate the diffusion tensor and could thus drive a more accurate registration than with FODs. However, today's most popular DTI-based registration techniques do not benefit from easily implementable lesion masking strategies and could thus constitute the focus of future research. In any case, considering that FA and FOD-based registration yielded similar results for our acute stroke cohort and that the corresponding DWI protocol did not benefit from a high angular resolution, we chose to use FA-based registration for the subsequent investigations in the current thesis.

Finally, these results not only served for the remaining studies of the present doctoral work but also contributed to an independent research project outside the context of this thesis. A parallel study by Kemlin et al. (*In Prep*) at the Institut du

Cerveau et de la Mœlle Epinière sought to determine the independent contributions of the structural integrity of the corticospinal tract – evaluted with the FOD-based registration method outlined in this chapter – and other electrophysiological and clinical variables for upper limb motor impairments at the subacute-chronic stage of stroke. Our proposed method allowed the authors to accurately quantify the neuronal integrity of the corticospinal tract and evaluate the amount of variance in upper limb motor impairment explained by this variable in relation to others.

Chapter 6

Study II: Multivariate Prediction of Functional Outcome using Lesion Topography Characterized by Acute Diffusion Tensor Imaging

Contents

6.1 Overview of Study

Now that a proper registration strategy had been established for the acute stroke imaging data, we were able to proceed to a voxel-based analysis for evaluating the prognostic value of early DTI for long-term global outcome. In particular, the conception of the second study arose from the most common functional outcome score available in our acute stroke cohort, the modified Rankin Score (mRS), which, as detailed in section 2.3.2, is a measure of the level of patient autonomy in everyday life. Previous studies have already demonstrated the relationship between stroke location and functional outcome using primarily binary manual lesion segmentations. However, as detailed in chapter 3, Diffusion Tensor Imaging (DTI) constitutes a powerful means of quantifying the degree of acute ischemia and may be more suitable for characterizing stroke topography. Indeed, each patient experiences different degrees of neuronal damage depending on different factors, such as the duration of ischemia and the success of recanalization therapy. DTI could thus be more sensitive to patient-specific neuronal damage, whereas lesion segmentations treat all visible infarcts on a "all-or-nothing" basis. Moreover, DTI is able to capture remote effects outside the visible lesion, whereas any analysis performed with lesion segmentations is restrained to these regions. We wondered whether using DTI-derived imaging parameters could improve prediction models over those constructed with lesion segmentation and thus provide valuable insight on critical brain areas important for long-term outcome. Using the normalization strategies established in the first study in addition to the large cohort of acute stroke patients enabled us to take advantage of more powerful multivariate machine learning techniques to elucidate this question.

The major objective of the second study was to determine which DTI parameter best captures acute axonal damage in relation to long-term functional outcome. To do so, we used machine-learning classifiers called support vector machines (SVM) to build prognostic models with different imaging modalities – in combination with lesion volume, age, recanalization status, and thrombectomy treatment – in order to predict good (modified Rankin Score - mRS $\leq$ 2) and poor (mRS > 2) outcome. Our hypothesis was that the parameter that best captured microstructural damage from stroke would also predict patient outcome with the highest accuracy. Then, by inspecting the feature weights of the best classifier, we could deduce which brain regions are most important for long-term global outcome. The specific goals of the second study were thus: (1) to evaluate the predictive power of the four classical DTI parameter maps – fractional anisotropy, mean diffusivity, axial diffusivity, and radial

diffusivity – at the acute stage of stroke as well as lesion segmentations in classifying good *vs.* poor outcome classifiers and (2) infer which brain regions contributed the most to predicting functional outcome by investigating the weights of the SVM classifer.

6.2 Article

The supplementary materials for this article can be found in Appendix H

Title: Multivariate Prediction of Functional Outcome using Lesion Topography Characterized by Acute Diffusion Tensor Imaging

Author names and affiliations:

Eric Moulton[1], Romain Valabregue[1,2], Stephane Lehéricy[1-4], Yves Samson[1,5], Charlotte Rosso[1,3,5]

(1) Institut du Cerveau et de la Moelle épinière, ICM, Inserm U 1127, CNRS UMR 7225, Sorbonne Université, F-75013, Paris, France

(2) Centre de Neuro-Imagerie de Recherche, CENIR, ICM, Paris, France

(3) ICM team Movement Investigation and Therapeutics

(4) AP-HP, Department of Neuroradiology, Hôpital Pitié-Salpêtrière, Paris, France

(5) AP-HP, Urgences Cérébro-Vasculaires, Hôpital Pitié-Salpêtrière, Paris, France

Corresponding author:

Charlotte Rosso

Urgences Cérébro-Vasculaires, 47-83 Boulevard de l'Hôpital 75013 Paris

Phone: +33 1 42161854 Fax: +33 1 42161839 E-mail: charlotte.rosso@gmail.com

Declaration of interest: none

Abstract

The relationship between stroke topography and functional outcome has largely been studied with binary manual lesion segmentations. However, stroke topography may be better characterized by continuous variables capable of reflecting the severity of ischemia, which may be more pertinent for long-term outcome. Diffusion Tensor Imaging (DTI) constitutes a powerful means of quantifying the degree of acute ischemia and its potential relation to functional outcome. Our aim was to investigate whether using more clinically pertinent imaging parameters with powerful machine learning techniques could improve prediction models and thus provide valuable insight on critical brain areas important for long-term outcome. Eighty-seven thrombolyzed patients underwent a DTI sequence at 24 hours post-stroke. Functional outcome was evaluated at 3-months post-stroke with the modified Rankin Score and was dichotomized into good (mRS ≤ 2) and poor (mRS > 2) outcome. We used support vector machines to classify patients into good *vs.* poor outcome and evaluate the accuracy of different models built with fractional anisotropy, mean diffusivity, axial diffusivity, radial diffusivity asymmetry maps, and lesion segmentations in combination with lesion volume, age, recanalization status, and thrombectomy treatment. SVM classifiers built with axial diffusivity maps yielded the best accuracy of all imaging parameters (median [IQR] = 82.8 [79.3-86.2]%), compared to that of lesion segmentations (76.7 [73.3-82.8]%) when predicting 3-month functional outcome. Model weights revealed a strong contribution of clinical variables, notably – in descending order – lesion volume, thrombectomy treatment, and recanalization status, in addition to the deep white matter at the crossroads of major white matter tracts. Axial diffusivity is a more appropriate imaging marker to characterize stroke topography for predicting long-term outcome than binary lesion segmentations.

1. Introduction

While clinical variables such as initial stroke severity, age, and lesion volume are useful in determining long-term outcome assessed by the modified Rankin Score (mRS), recent work has shed light on the independent predictive power of early ischemic stroke topography (Cheng et al., 2014; Duncan et al., 2000; Rosso et al., 2011; Wu et al., 2015; Yoo et al., 2010). In particular, damage to deep white matter at the crossroads of major white matter pathways has been shown to play a critical role in the level of autonomy patients can expect after an ischemic stroke (Rosso et al., 2011). In the majority of these studies, lesion topography is often represented as binary segmentations of abnormal regions on clinical diffusion weighted imaging (DWI) or FLAIR sequences. However, at the acute stage, the mere presence or absence of a lesion (binary segmentation) might be less informative than continuous variables capable of reflecting the severity of ischemia, which could be more pertinent for long-term outcome. The diffusion tensor imaging (DTI) model can reliably quantify tissue microstructure and thus constitutes a powerful means of evaluating the degree of ischemia at the acute stage of stroke (Beaulieu, 2002; Sotak, 2002). While, fractional anisotropy (FA) has proven a noteworthy biomarker at the subacute-chronic stage, there is now substantial evidence that axial diffusivity (AD) instead of FA is able to accurately reflect acute axonal damage related to subacute and chronic motor and global outcome (Doughty et al., 2016; Groisser et al., 2014; Liu et al., 2018; Moulton et al., 2015; Spampinato et al., 2017). Whether the severity of ischemia assessed with continuous DTI parameter maps and the presence or absence of an infarct using binary lesion segmentations harbor different prognostic values, however, remains to be elucidated.

Studying the effect of stroke topography on functional outcome using machine learning techniques has become increasingly popular due to their ability to account for complex interactions between brain regions (Price et al., 2017). Unlike commonly used mass-univariate analyses such as Voxel-based Lesion Symptom Mapping (VLSM) (Bates et al., 2003), multivariate methods can represent the relation of damage at every voxel to all other voxels. These methods are therefore highly adapted for predicting multifaceted clinical outcome scores, such as the mRS, which can reflect deficits covering several functional domains, namely motor, language, and spatial attention (Cheng et al., 2014). The relationship between functional outcome, evaluated by the mRS, and stroke topography has already been studied with both univariate and multivariate analyses using lesion segmentations (Cheng et al., 2014; Ernst et al., 2018; Munsch et al., 2016; Wu et al., 2015) and also with apparent diffusion coefficient (ADC) maps (Cuingnet et al., 2011; Rosso et al., 2011) acquired at the acute stage; however, to our knowledge, no whole-brain study has been performed with acute DTI images. In this study, we take advantage of a large dataset of thrombolyzed stroke patients who underwent a DTI imaging protocol at 24 hours post-stroke and a sophisticated machine learning pipeline to evaluate the prognostic value of DTI-derived parameters and lesion segmentations.

Our goals were to (1) evaluate the predictive power of the DTI-derived parameter maps generated at the acute stage as well as lesion segmentations in classifying good *vs.* poor outcome using support vector machine (SVM) classifiers, (2) determine if certain DTI maps yield better classification rates than lesion segmentations, and (3) infer which brain regions contribute the most to functional outcome by investigating the weights of the best performing model. We predicted that classification accuracy would differ among the four classical DTI parameters, considering the varying degrees to which each one reflects acute stroke damage. Furthermore, we hypothesized that the severity (i.e., continuous changes in diffusivity) rather than the presence or absence of ischemia (i.e., binary lesion segmentation) would be able to better capture brain damage affecting long-term functional outcome. Finally, in concordance with previous findings, we expected damage to deep white matter to play an influential role in distinguishing good *vs.* poor outcome, due to the simultaneous multiple disconnections that may arise at the intersection of long-range pathways.

2. Materials and Methods

2.1. Patients

Two hundred ninety-seven patients were retrospectively screened from September 1, 2013 until April 30th, 2018 at the Urgences Cérébrovasculaires at the Hôpital de la Pitié Salpêtrière. Inclusion criteria for this cohort were: (1) MRI-demonstrated ischemic stroke of the carotid territory, (2) thrombolysis treatment within 4.5 h after stroke onset, (3) follow-up MRI access at 24 hours post-stroke, (4) interpretable recanalization status, and (5) clinical assessment using the modified Rank Score (mRS) at 3-months post-stroke. Thrombolytic treatment was administered according to the American Stroke Stroke Association and the European Stroke Organization guidelines (0.9 mg/kg, maximal dose 90 mg)(Jauch et al., 2013). Patients with bilateral lesions were deemed suitable for analysis if clinical symptoms were lateralized to one hemisphere (e.g., unilateral hemiparesis, aphasia without neglect, etc.). For these patients, the affected hemisphere was considered as that which caused clinical symptoms. Exclusion criteria were (1) overly artifacted imaging data, (2) dependence on external aid before the stroke (i.e., pre-stroke mRS > 2) or the reoccurrence of stroke before the 3-month follow-up, (3) death before the 3-month follow-up.

A mRS score was recorded at the 3-month follow-up through a physical examination with a neurologist at our hospital or through a structured telephone interview. The primary outcome measure of this study was a dichotomized mRS score for good (mRS ≤ 2) and poor (mRS > 2) outcome. Descriptive statistics consisted of median and interquartile ranges (IQR). All imaging and clinical data were obtained during routine clinical workup in our stroke center. According to French legislation, explicit informed

consent was therefore waived. The study was approved by the Pitié-Salpêtrière Hospital Ethics Committee.

2.2. Image Acquisition

Imaging data used in this study are from our emergency stroke unit in which we examined patients with typical DWI sequences but also a DTI protocol. Twenty-four hours after admission, patients underwent a follow-up MRI with a 3T MR750 MRI scanner (General Electric) with an 8-channel coil. The following DWI sequences were used for the current analysis: (1) an averaged 3-direction DWI (b=1000 s/mm^2, TR=11700ms, TE=72.3ms, matrix size=256×256, slice number=48, voxel size=0.94×0.94×3mm^3, acquisition time=0:59 min) and (2) a 30-direction DWI (2 b=0 s/mm^2 images followed by 30 non-collinear diffusion-encoding gradients at b=1000 s/mm^2, TR=12000ms, TE=82.3ms, matrix size=256×256, slice number=44, voxel size=1.09×1.09×3mm^3, acquisition time=6:36 min).

2.3. Image Processing

Image processing served to prepare data for classification in a common reference space and was performed using a pipeline optimal for diffusion MRI data at the acute stroke stage as previously described (Moulton et al., 2018). In brief, after correcting for (1) denoising (Veraart et al., 2016a, 2016b) (2) eddy currents and head motion using FSL's EDDY with slice interpolation for slices with significant signal drop (Andersson et al., 2016; Andersson and Sotiropoulos, 2016), and (3) bias-field correction (Zhang et al., 2001), FA, AD, mean diffusivity (MD), and radial diffusivity (RD) maps were calculated from a tensor model estimated using FSL's DTIFIT (Basser et al., 1994; Smith et al., 2004), and brains were skull stripped (Smith, 2002). Lesion segmentation was performed by identifying hypersignal regions on the 3-direction DWI sequence image and co-registered to the DTI maps. To process all images in the same hemisphere, both native and flipped DTI maps as well as lesion segmentations were registered to an in-house healthy-subject FA template using Advanced Normalization Tools (ANTs) with lesion masking (Supplementary Materials).

In stroke imaging, it is common practice to analyze relative differences between the affected and unaffected hemispheres rather than absolute values of the affected hemisphere alone. To this end, we kept all affected hemispheres to the same side and constructed laterality index (LI) maps, hereafter referred to as asymmetry maps, using the normalized native and flipped DTI maps with the following equation at each voxel: (affected-unaffected)/(affected+unaffected). The LI is a score between -1 and 1 for which the negative range indicates smaller values on the affected side and the positive range indicates larger values on the affected side. Acute stroke is largely characterized by strong decreases in diffusivity with respect to the unaffected hemisphere, which can be seen as negative values on the MD, AD, or RD asymmetry maps (Fig. 1). We also applied a modest 2 mm Gaussian smoothing to the asymmetry maps to compensate for imperfections in normalization while conserving the specificity of each region (Samper-

González et al., 2018). Since asymmetry maps are highly symmetrical, our analysis can be reliably restrained to one hemisphere. Moreover, relative differences in diffusivity are more pronounced in white matter than grey matter regions (Bhagat et al., 2008; Muñoz Maniega et al., 2004; Yang et al., 1999). With these considerations, we restricted our analysis to a hemispheric white matter mask by thresholding the FA template at 0.2 and manually filling in potential holes in the mask, such as those in the basal ganglia.

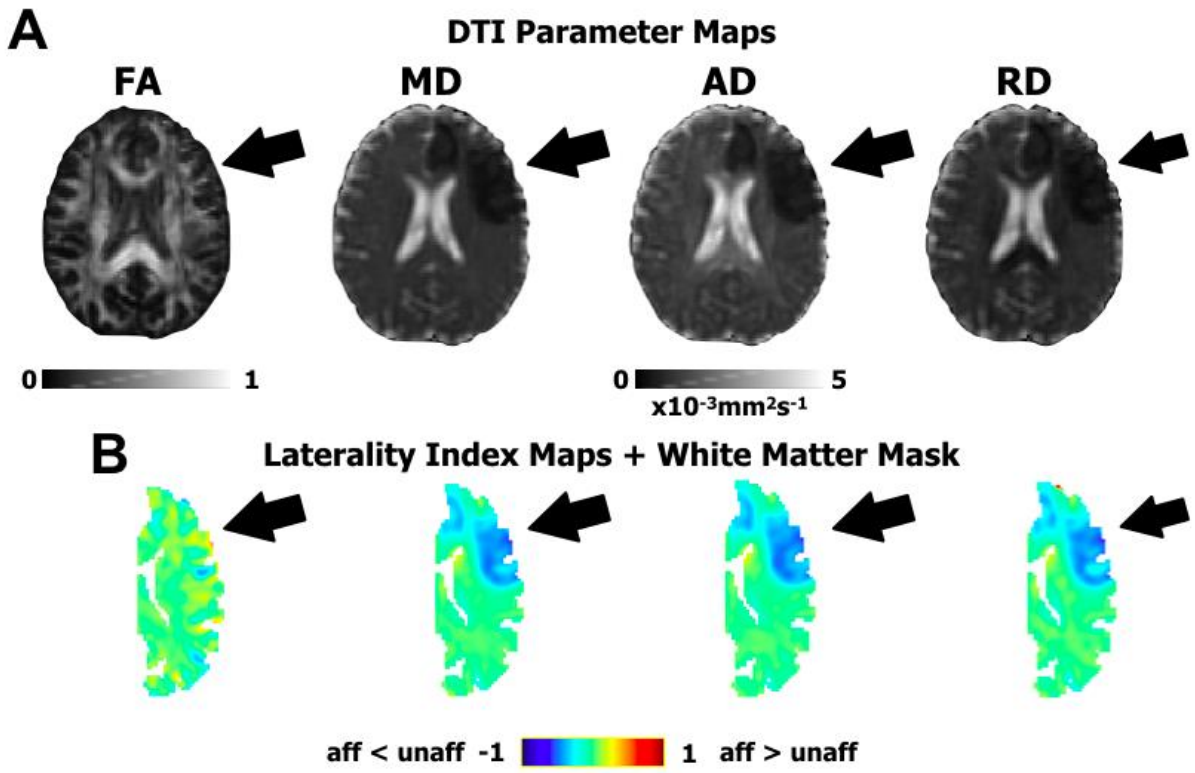

Figure 1. Diffusion Tensor Imaging (DTI) features

A. The four DTI parameter maps for a representative acute stroke patient. From left to right: Fractional Anisotropy (FA), Mean Diffusivity (MD), Axial Diffusivity (AD), and Radial Diffusivity (RD). B. The corresponding Laterality Index (LI) or asymmetry maps in a white matter mask used to create prediction models. The black arrow indicates the presence of acute ischemia, shown as an area of low diffusivity on MD, AD, and RD maps and negative regions on the respective LI maps. Acute ischemia is poorly seen on the FA map.

2.4. Model Estimation and Validation

We sought to classify patients into good *vs.* poor outcome at 3 months post-stroke with imaging data at 24 hours post-stroke and baseline clinical variables using a support vector machine (SVM) as implemented in scikit-learn in Python (Abraham et al., 2014). SVMs are useful machine learning

techniques used in neuroimaging (See Lemm et al., (2011) for a detailed explanation of SVMs and Rondina et al., (2017) for an illustrative application to stroke imaging), have already proven effective in explaining various categories of stroke-related deficits, and are compatible with structural imaging data (Cuingnet et al., 2011; Mah et al., 2014; Mateos-Pérez et al., 2018; Rondina et al., 2016; Yourganov et al., 2015; Zhang et al., 2014). Here, we estimated and validated classification models using different imaging modalities (i.e., DTI-derived asymmetry maps or lesion segmentations) along with important clinical variables considered to be independent predictors of stroke outcome, notably recanalization status, thrombectomy treatment, age, and lesion volume. Recanalization status (complete or not) and thrombectomy treatment (received or not) were treated as binary variables. As in similar studies (Wu et al., 2015), we did not include baseline NIHSS as a feature since it already reflects the extent of brain damage and can be predicted from stroke topography (Phan et al., 2010).

In machine learning and neuroimaging, there is often a disproportionate ratio of features (here, voxels) for available observations (i.e., patients). This imbalance is commonly referred to as the curse of dimensionality and can hinder the predictive power of multivariate models. Therefore, we introduced a principle component analysis (PCA) step for imaging data in our model construction pipeline in order to reduce the dimensionality of our data (Figure 2). In fact, PCA presents a double advantage in machine learning analyses with stroke patients. The most obvious advantage is that the number of features will be, at most, one less than the number of observations (when there are more features than observations). The second advantage of PCA stems from the fact that, in stroke, lesioned voxels do not arise randomly but co-occur according to the vascular tree (Mah et al., 2014). At the population level, therefore, recurrent patterns of diffusivity asymmetries and stroke lesions will be present across patients and can form a new basis for explaining them. In other words, we can describe diffusivity asymmetries or lesioned voxels by a weighted sum of representative patterns of these parameters instead of tens of thousands of voxels (38,807 in our case). These weights in PCA-space then become the features for our classifier. While previous studies have fixed the number of components based on *a priori* explained variance criteria (Corbetta et al., 2015; Siegel et al., 2016), we decided to introduce the number of principle components to retain as a hyper-parameter to be optimized as explained below.

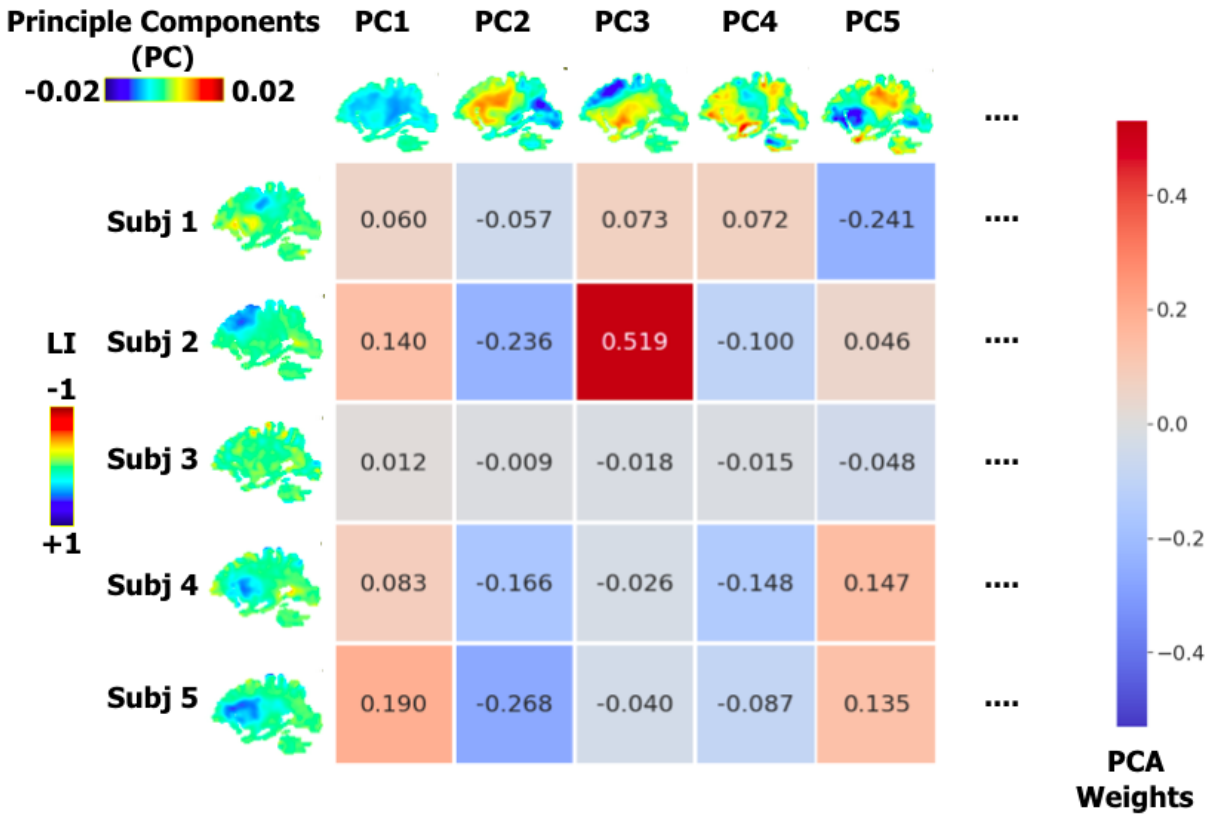

Figure 2. Dimensionality reduction with Principle Component Analysis (PCA).
PCA allows for the reconstruction of each subject's (subj) imaging data through a linear combination of principle components (PC), which reflect representative patterns over the studied population. The coefficients of each PC used to reconstruct each subject's imaging data become the features for the classifier. For illustrative purposes, shown here is the PCA analysis for AD asymmetry maps (LI) over the whole cohort, whereas independent PCAs are performed for each cross-validation split.

We employed repeated stratified nested cross-validation (CV) for the unbiased construction and evaluation of our classifiers, according to the recommendations in Varoquaux et al. (2017) (Supplementary Figure 1). In our nested CV, an inner 2-fold CV loop first builds models with optimized hyperparameters (here, number of principle components and L2-regularization constant), and an outer 3-fold CV loop then yields unbiased evaluations of the constructed model. With this CV scheme, we ensured not only an equal partition of our data set in all loops but also a balanced proportion of good:poor class observations. Furthermore, models were constructed with a misclassification penalty weighted by class balance. To bypass the computational time required to determine the optimal set of hyperparameters, for each inner CV loop, we randomly chose 60 candidate values from a discrete uniform distribution for possible principle components (1-87) and a reciprocal distribution for regularization constants (1×10^{-3} to 1×10^{6}). Random searches over parameter space have been found to be as good as or better than systematic grid searches with significant gains in computational time (Bergstra and Bengio, 2012). In our

case, using 60 candidate values ensured that we had a 95% chance of being within a 5% interval of the best parameter set. This procedure was repeated 500 times in order to obtain a reliable point-estimate of model accuracy with an associated confidence interval. For each imaging modality, we herein summarize classification accuracy, sensitivity, and specificity as the median with the interquartile range (IQR) over CV splits. In order to demonstrate that model accuracy significantly differed from chance, we ran permutation tests with 1,000 iterations to reconstruct the sampling distribution of the underlying null hypothesis.

To gain insight on the underlying anatomical determinants of long-term outcome, we inspected the model of the imaging modality that yielded the highest median classification accuracy. For this model, we projected the SVM model weights back onto the brain from PCA-space and calculated the average over all CV folds (Rondina et al., 2017; Varoquaux et al., 2017). The resulting map reflected the relative importance of each brain region in classifying groups. We created a region of interest (ROI) composed of the largest connected component of voxels with the strongest weights (95^{th} percentile) associated with larger decreases in diffusivity or higher lesion incidence in patients with poor outcome, depending on the winning model. We then used this ROI to investigate the involvement of well-known long-range white matter tracts in functional outcome in a tractography analysis using a whole-brain connectome performed on the in-house template (Moulton et al., 2018) (Supplementary Materials).

3. Results

3.1. Patient Cohort

Out of the prospective 297 patients, 87 were retained for the final analysis (Figure 3, Table 1). Maximum lesion overlap was in the putamen, external capsule, and caudate nucleus (35-40%, N=31–36), reflecting typical lesions of the middle cerebral artery territory of a clinical population(Phan et al., 2005) (Supplementary Figure 2).

Age (years)	71.1 [57.1-80.8]
Female N (%)	39 (44.8%)
NIHSS Admission (N=87)	11.5 [7.3-20.0]
NIHSS Day 1 (N=85)	4.5 [2.0-12.0]
NIHSS Day 7 (N=62)	2.0 [0.0-9.5]
Time to MRI (min) (N=87)	110.0 [78.0-170.0]
Time to rtPA (min) (N=87)	140.0 [110.8-202.3]
DWI Lesion Volume (mL) (N=87)	12.4 [4.2-45.1]
Received Thrombectomy N (%)	32 (36.8%)
Complete Recanalization N (%)	62 (71.3%)
Pure MCA stroke N (%)	81 (92.0%)
Mixed MCA-ACA stroke N (%)	2 (2.3%)
Mixed MCA-PCA stroke N (%)	4 (4.6%)
Mixed MCA-ICA stroke N (%)	1 (1.1%)
Left Lesions N (%)	58 (66.6%)
Good Outcome (mRS ≤ 2) N (%)	61 (70.1%)

Table 1. Patient cohort descriptive statistics.

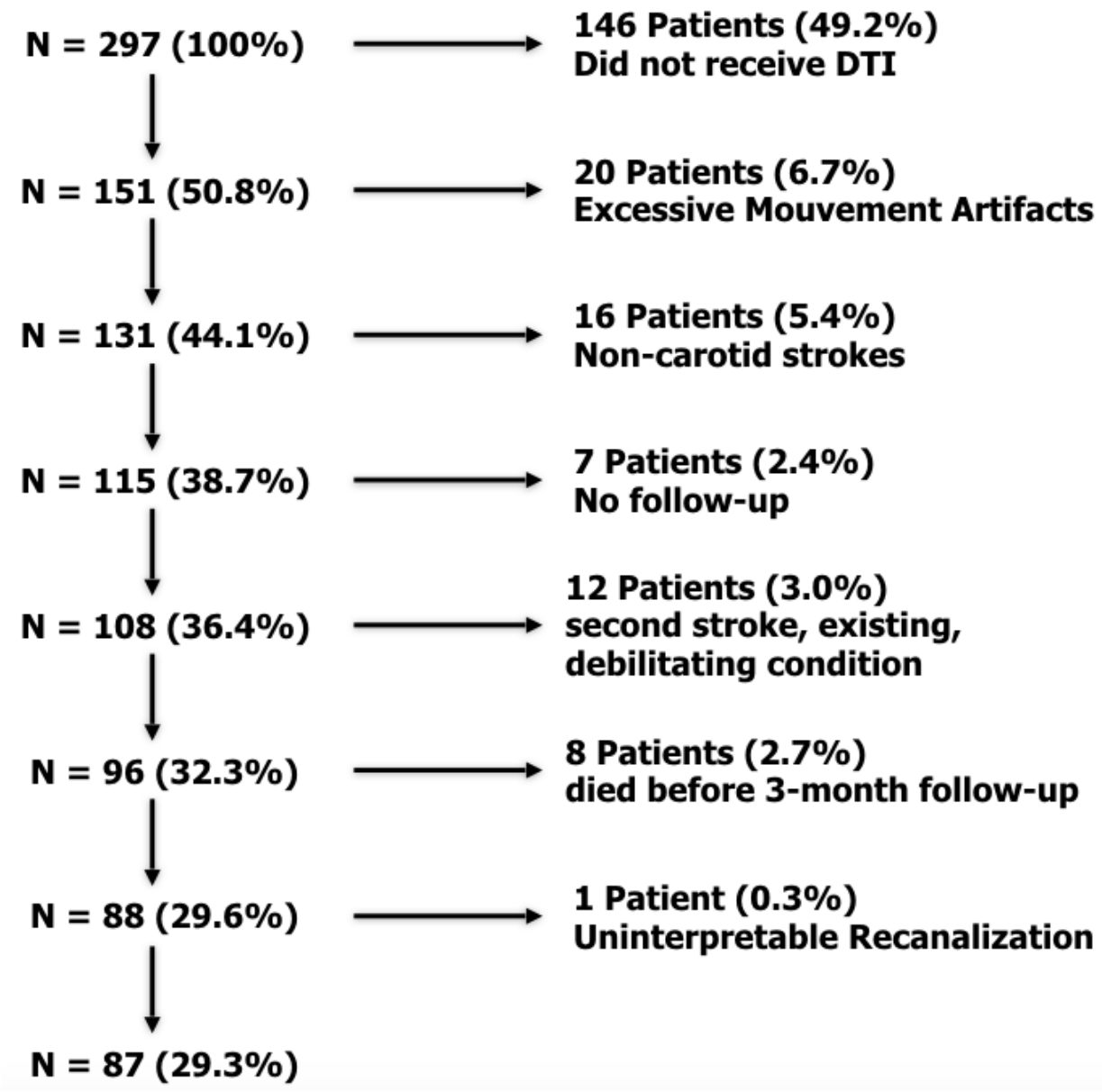

Figure 3. Patient inclusion flowchart.

3.2. Model Evaluation

Model performance differed for each imaging modality (Table 2). In particular, AD asymmetry maps yielded the highest median accuracy (82.8%), sensitivity (80.0%), and specificity (84.0%). MD asymmetry maps performed slightly less well, closely followed by RD. Finally, classifiers with lesion segmentation and FA performed the worst, both yielding median accuracies of 76.7%. In other words, a model based on AD maps would result in a false prediction for one out of every six patients in a clinical setting, whereas, a model based on FA maps or lesion segmentation would result in a false prediction for one out of every four patients. All model accuracies were statistically significant ($p<0.003$).

Imaging Modality	Model Evaluation			Model Construction	
	Accuracy (%)	Sensitivity (%)	Specificity (%)	Number of Principle Components	Variance of Data Explained by PCs (%)
FA	76.7 [72.4-80.0]*	66.7 [57.1-80.0]	80.0 [76.2-83.3]	17 [9-24]	53.2 [38.2-64.1]
MD	80.0 [75.9-86.2]*	77.8 [66.7-88.9]	82.6 [79.2-86.4]	17 [9-25]	82.3 [70.3-87.8]
AD	82.8 [79.3-86.2]*	80.0 [66.7-88.9]	84.0 [80.0-88.2]	15 [8-24]	77.5 [66.0-85.0]
RD	79.3 [72.4-82.8]*	71.4 [60.0-83.3]	81.0 [77.3-85.7]	18 [9-26]	89.0 [81.2-93.4]
Lesion Segmentation	76.7 [73.3-82.8]*	66.7 [57.1-80.0]	81.8 [77.3-85.0]	15 [7-23]	80.7 [65.5-89.2]

Table 2. Model evaluation and construction.

The median and interquartile range is shown over cross-validation splits for SVM models constructed with different imaging modalities. The number of principle components and explained variance thereof refer to automatically tuned hyper-parameters. Permutation test significant *p<0.003

Each type of model found different numbers of principle components optimal for classification (Table 2). Models built with AD, MD, RD asymmetry maps and lesion segmentations retained principle components explaining the variance of much of the data (77.5%-89.0%). On the other hand, classifiers with FA asymmetry maps retained only 53.2% of the variance in the data.

For the winning model constructed with AD asymmetry maps, the clinical variable with the strongest influence on outcome was lesion volume (indicating that smaller lesion volumes were associated with good prognosis), followed by thrombectomy treatment (receiving thrombectomy treatment resulted in good outcome) and less so by recanalization status (patients with complete recanalization had good outcome) (Figure 4). As for imaging data, the strongest SVM weights formed a large cluster in the deep MCA territory (Figure 4). The tractography analysis revealed that this region largely corresponded to the deep white matter at the crossroads of corticofugal and long-range associative pathways, such as the corticospinal tract, the corpus callosum, the long, anterior, and posterior segments of the arcuate fasciculus, the second and third branches of the superior longitudinal fasciculus, and the frontal aslant tract (Figure 5).

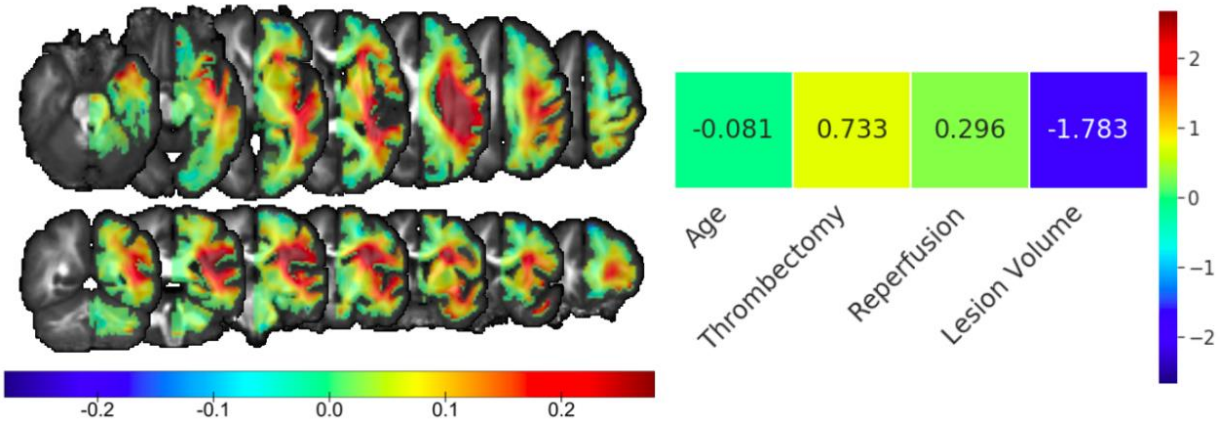

Figure 4. Model weights of the SVM classifier using AD asymmetry maps and clinical variables. For imaging data, the weights represent the relative relevance of each brain region in classifying good *vs.* poor outcome on axial (top) and coronal (bottom) slices. Positive values indicate relatively lower AD asymmetries for patients with poor outcome compared with those with good outcome, and vice-versa. Separate color bars are used for the SVM weights of the imaging data and clinical variables due to the differences in scale.

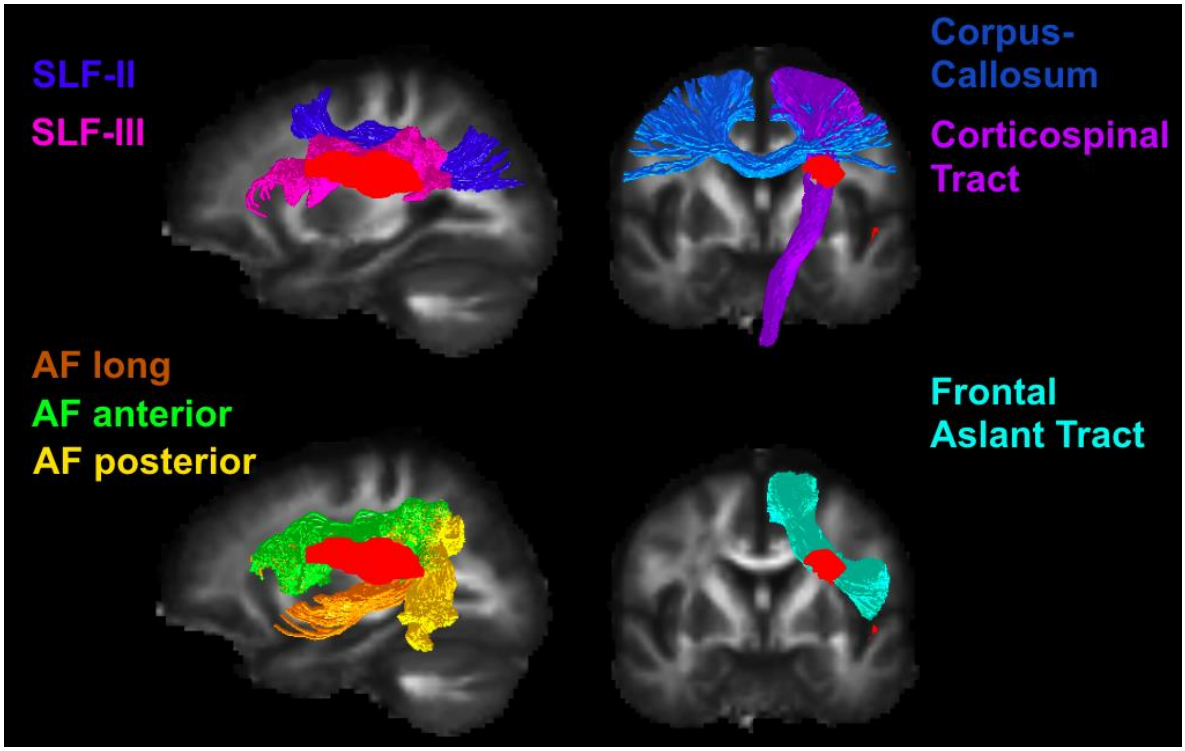

Figure 5. Tractography analysis from most influential regions for functional outcome.
The most influential areas of lower axial diffusivity for patients with poor outcome (red cluster). Major corticofugal and long-range associative tracts pass through this critical area, notably, the second and third branch of the superior longitudinal fasciculus (SLF), the corpus callosum, the corticospinal tract, the long, anterior, and posterior segments of the arcuate fasciculus (AF), and the frontal aslant tract.

4. Discussion

We used early DTI in combination with baseline clinical data in a large cohort of acute stroke patients to power a sophisticated machine learning pipeline aimed at classifying good *vs.* poor functional outcome. We found that AD was able to best classify long-term outcome, much better than FA or commonly used lesion segmentations. As expected, we found a strong contribution from clinical variables, notably – in decreasing order – lesion volume, thrombectomy treatment, and recanalization status. In addition, we found that the most influential brain areas on outcome were highly concordant with previous studies, supporting the validity of our results.

The novelty of our study lies within the systematic availability of DTI data at 24 hours post-stroke to investigate the effect of stroke topography on long-term outcome. This unique data set differs from similar studies performed at the acute phase which have primarily resorted to clinical DWI or FLAIR sequences for lesion segmentation to address this question (Cheng et al., 2014; Ernst et al., 2018; Munsch et al., 2016; Wu et al., 2015). Moreover, while other studies have evaluated the predictive value of

acute DTI biomarkers with correlation analyses (Groisser et al., 2014; Liu et al., 2018; Moulton et al., 2015; Spampinato et al., 2017), to our knowledge, this is the first study to use whole-brain DTI data in a multivariate framework for classifying functional outcome. Interestingly, in our study, we found that not only did AD asymmetry maps result in the highest classification accuracies of all DTI parameters, but they also outperformed commonly used binary lesion segmentations by 6.1%, resulting in an improvement of false prediction ratio of 1/4 to 1/6. It is important to note that, considering the current study design, there was no *a priori* reason for all models to not achieve the same classification rate if not for the data driving them. Indeed, each model was given the same clinical scores along with the same partitions of imaging data over cross-validation loops and was free to optimize its own hyper-parameters to maximize accuracy. From this perspective, all imaging modalities were on an equal footing. The only limiting factor for each classifier, therefore, was the relevance – or lack thereof – of the imaging features used to train it. We can therefore conclude that there was truly something unique about the clinical pertinence of AD – compared to other candidate imaging parameters and beyond baseline clinical scores – in characterizing acute ischemia and its relationship to future outcome.

The superior classification performance of AD over other imaging modalities corroborates previous studies having reported higher correlations between acute AD abnormalities of the corticospinal tract and future motor and global outcome with respect to other DTI parameters (Groisser et al., 2014; Liu et al., 2018; Moulton et al., 2015; Spampinato et al., 2017). Acute changes in AD likely reflect increased intracellular viscosity from direct axonal damage as supported by recent DTI-immunohistology studies or neuronal beading (Baron et al., 2015; Budde and Frank, 2010; Sun et al., 2006). Moreover, from the acute to subacute stage, AD and RD follow different trajectories. While AD monotonically decreases over this time period partly from cell necrosis and axonal degeneration, RD first decreases, in part, due to cytotoxic oedema only to then increase following the deterioration of myelin sheaths (Liang et al., 2007). This switch in dynamics of RD happens within days post stroke onset, limiting its ability to characterize the degree of ischemia and thus its predictive power. The same limitations therefore apply to FA since it takes into account both AD and RD.

The most noteworthy result of our analysis is that continuous DTI variables, in particular AD, performed better than binary lesion segmentations, which have been the primary means for stroke topography characterization. This result has important repercussions for the long-debated independent role of stroke topography *vs.* baseline clinical variables. For example, using voxel-based lesion symptom mapping (VLSM), two studies reported that, once corrected for lesion volume, lesion location was no longer related to the 3-month follow-up mRS in the right hemisphere but remained so in the left hemisphere (Ernst et al., 2018; Wu et al., 2015). Similarly, Munsch et al., (2016) used VLSM to identify eloquent brain regions associated with the 3-month mRS; in a separate analysis, they showed that the number of overlapping voxels between patients' lesions and the previously found eloquent cluster was not an independent predictor of good *vs.* poor outcome. While these studies have provided evidence that

stroke location may not be as important as baseline clinical variables in predicting long-term outcome, our findings suggest that these previously reported negative results may arise from inadequately characterizing stroke topography with simple lesion segmentation. Furthermore, unlike models with binary lesion segmentations, which are constrained to areas of high infarct incidence, whole-brain diffusion maps can also take into account abnormalities at a distance from the lesion. In light of these considerations, right hemisphere and perhaps additional left hemisphere regions may still in fact highly contribute to long-term stroke outcome, if represented by more sensitive imaging markers.

Our SVM models with AD asymmetry maps revealed a spatially heterogeneous set of weights for classification. In particular, the weights corresponding to larger decreases in diffusivity for poor *vs.* good recovery formed a cluster in the white matter at the crossroads of many major fiber tracts governing motor, language, and attention, in concordance with many previous findings (Cheng et al., 2014; Cuingnet et al., 2011; Ernst et al., 2018; Munsch et al., 2016; Rosso et al., 2011; Wu et al., 2015). Importantly, this critical region was established through the contribution of different lesion topographies accounting for 77.5% of the variance in AD asymmetry maps, as identified with PCA. An interpretation of this result is that functional outcome is mostly governed by a subset of reoccurring lesion patterns, rather than individual voxels. In other words, it is the similarity between the spatial extent of a patient's lesion and these critical patterns that ultimately determines autonomy *vs.* dependence on external aid at 3-months post-stroke, supporting the significance of lesion topography (Corbetta et al., 2015). In fact, this procedure likely enabled us to overcome the fixed set of lesion patterns specific to our cohort and capture global lesion topographies that generalize to a typical population.

A caveat of our study was our inability to disentangle the contribution of lesion side. Indeed, machine learning techniques require large datasets to build reliable models and evaluate their performance in an unbiased way (Varoquaux, 2018). For this reason, we were obliged to keep all lesions in the same hemisphere to maximize the amount of usable data. As mentioned, previous studies have highlighted differential effects of lesion topography for left *vs.* right lesions, either from a symptomatology (Cheng et al., 2014) or a clinical relevance (Ernst et al., 2018; Munsch et al., 2016; Wu et al., 2015) point-of-view. While our approach prevented us from further investigating this, our study provides a serious argument to revisit certain conclusions of these studies, since most of them have been performed with lesion segmentations. Moreover, our tractography analysis revealed a crucial role of fiber tracts involved in well-recognized lateralized functions, such as the arcuate fasciculus for language (Marchina et al., 2011; Rosso et al., 2015) and the SLF-II for neglect (Thiebaut de Schotten et al., 2014), suggesting that our model captured important structures of stroke topography for both left and right hemispheres.

A second limitation could be our restrained analysis to the white matter and inclusion of patients with stroke of the carotid territory. However, in a general clinical population, as in ours, infarcts of the carotid territory represent more than 85% of all stroke and mostly occur in subcortical structures where

DTI is most informative and important diffusion changes take place in response to acute ischemia (Bhagat et al., 2008; Muñoz Maniega et al., 2004; Phan et al., 2005; Yang et al., 1999).

5. Conclusion

In summary, this is the first study to investigate the effect of stroke topography on functional outcome evaluated with both DTI and lesion segmentations in a machine learning framework. Our study highlights the added benefit of axial diffusivity in addition to the limitations of binary lesion segmentation for quantifying acute ischemic stroke topography and its relation to long-term outcome. Our results have important implications for salvaging brain areas critical for functional outcome and can aid clinicians in weighing the costs, benefits, and risks for thrombolysis or thrombectomy treatments at the acute stroke stage.

Acknowledgements

Sources of Funding

The Pitié-Salpêtrière registry was supported by the French Ministry of Health grant EVALUSINV PHRC AOM 03 008. The research leading to these results has received funding from “Investissements d'avenir” ANR- 10-IAIHU-06 and ANR-11-INBS-0006.

Disclosures

None

References

Abraham, A., Pedregosa, F., Eickenberg, M., Gervais, P., Muller, A., Kossaifi, J., Gramfort, A., Thirion, B., Varoquaux, G.G., Mueller, A., Kossaifi, J., Gramfort, A., Thirion, B., Varoquaux, G.G., 2014. Machine learning for neuroimaging with scikit-learn. Front. Neuroinform. 8, 1–10. https://doi.org/10.3389/fninf.2014.00014

Andersson, J.L.R., Graham, M.S., Zsoldos, E., Sotiropoulos, S.N., 2016. Incorporating outlier detection and replacement into a non-parametric framework for movement and distortion correction of diffusion MR images. Neuroimage 141, 556–572. https://doi.org/10.1016/j.neuroimage.2016.06.058

Andersson, J.L.R., Sotiropoulos, S.N., 2016. An integrated approach to correction for off-resonance effects and subject movement in diffusion MR imaging. Neuroimage 125, 1063–1078. https://doi.org/10.1016/j.neuroimage.2015.10.019

Baron, C.A. lla., Kate, M., Gioia, L., Butcher, K., Emery, D., Budde, M., Beaulieu, C., 2015. Reduction of Diffusion-Weighted Imaging Contrast of Acute Ischemic Stroke at Short Diffusion Times. Stroke. 46, 2136–2141. https://doi.org/10.1161/STROKEAHA.115.008815

Basser, P.J., Mattiello, J., LeBihan, D., 1994. Estimation of the effective self-diffusion tensor from the NMR spin echo. J. Magn. Reson. B 103, 247–54.

Bates, E., Wilson, S.M., Saygin, A.P., Dick, F., Sereno, M.I., Knight, R.T., Dronkers, N.F., 2003. Voxel-based lesion–symptom mapping. Nat. Neurosci. 6, 448–450. https://doi.org/10.1038/nn1050

Beaulieu, C., 2002. The basis of anisotropic water diffusion in the nervous system - a technical review. NMR Biomed. 15, 435–55. https://doi.org/10.1002/nbm.782

Bergstra, J., Bengio, Y., 2012. Random Search for Hyper-Parameter Optimization. J. Mach. Learn. Res. 13, 281–305. https://doi.org/10.1162/153244303322533223

Bhagat, Y. a, Hussain, M.S., Stobbe, R.W., Butcher, K.S., Emery, D.J., Shuaib, A., Siddiqui, M.M., Maheshwari, P., Al-Hussain, F., Beaulieu, C., 2008. Elevations of diffusion anisotropy are associated with hyper-acute stroke: a serial imaging study. Magn. Reson. Imaging 26, 683–93. https://doi.org/10.1016/j.mri.2008.01.015

Budde, M.D., Frank, J.A., 2010. Neurite beading is sufficient to decrease the apparent diffusion coefficient after ischemic stroke. Proc. Natl. Acad. Sci. 107, 14472–14477. https://doi.org/10.1073/pnas.1004841107

Cheng, B., Forkert, N.D., Zavaglia, M., Hilgetag, C.C., Golsari, A., Siemonsen, S., Fiehler, J., Pedraza, S., Puig, J., Cho, T.H., Alawneh, J., Baron, J.C., Ostergaard, L., Gerloff, C., Thomalla, G., 2014. Influence of stroke infarct location on functional outcome measured by the modified rankin scale. Stroke 45, 1695–1702. https://doi.org/10.1161/STROKEAHA.114.005152

Corbetta, M., Ramsey, L., Callejas, A., Baldassarre, A., Hacker, C.D., Siegel, J.S., Astafiev, S. V, Rengachary, J., Zinn, K., Lang, C.E., Connor, L.T., Fucetola, R., Strube, M., Carter, A.R., Shulman, G.L., 2015. Common behavioral clusters and subcortical anatomy in stroke. Neuron 85, 927–941. https://doi.org/10.1016/j.neuron.2015.02.027

Cuingnet, R., Rosso, C., Chupin, M., Lehéricy, S., Dormont, D., Benali, H., Samson, Y., Colliot, O., 2011. Spatial regularization of SVM for the detection of diffusion alterations associated with stroke outcome. Med. Image Anal. 15, 729–737. https://doi.org/10.1016/j.media.2011.05.007

Doughty, C., Wang, J., Feng, W., Hackney, D., Pani, E., Schlaug, G., 2016. Detection and Predictive Value of Fractional Anisotropy Changes of the Corticospinal Tract in the Acute Phase of a Stroke. Stroke 47, 1520–1526. https://doi.org/10.1161/STROKEAHA.115.012088

Duncan, P.W., Jorgensen, H.S., Wade, D.T., 2000. Outcome measures in acute stroke trials: a systematic review and some recommendations to improve practice. Stroke 31, 1429–38.

Ernst, M., Boers, A.M.M., Forkert, N.D., Berkhemer, O.A., Roos, Y.B., Dippel, D.W.J., van der Lugt, A., van Oostenbrugge, R.J., van Zwam, W.H., Vettorazzi, E., Fiehler, J., Marquering, H.A., Majoie, C.B.L.M., Gellissen, S., MR CLEAN trial investigators (www.mrclean-trial.org), 2018. Impact of Ischemic Lesion Location on the mRS Score in Patients with Ischemic Stroke: A Voxel-Based Approach. AJNR. Am. J. Neuroradiol. 1–6. https://doi.org/10.3174/ajnr.A5821

Groisser, B.N., Copen, W.A., Singhal, A.B., Hirai, K.K., Schaechter, J.D., 2014. Corticospinal tract diffusion abnormalities early after stroke predict motor outcome. Neurorehabil. Neural Repair 28, 751–60. https://doi.org/10.1177/1545968314521896

Jauch, E.C., Saver, J.L., Adams, H.P., Bruno, A., Connors, J.J., Demaerschalk, B.M., Khatri, P., McMullan, P.W., Qureshi, A.I., Rosenfield, K., Scott, P.A., Summers, D.R., Wang, D.Z., Wintermark, M., Yonas, H., 2013. Guidelines for the Early Management of Patients With Acute Ischemic Stroke: A Guideline for Healthcare Professionals From the American Heart Association/American Stroke Association. Stroke 44, 870–947. https://doi.org/10.1161/STR.0b013e318284056a

Lemm, S., Blankertz, B., Dickhaus, T., Müller, K.R., 2011. Introduction to machine learning for brain imaging. Neuroimage 56, 387–399. https://doi.org/10.1016/j.neuroimage.2010.11.004

Liang, D., Bhatta, S., Gerzanich, V., Simard, J.M., 2007. Cytotoxic edema: mechanisms of pathological cell swelling. Neurosurg. Focus 22, E2.

Liu, G., Peng, K., Dang, C., Tan, S., Chen, H., Xie, C., Xing, S., Zeng, J., 2018. Axial diffusivity changes in the motor pathway above stroke foci and functional recovery after subcortical infarction. Restor. Neurol. Neurosci. 36, 173–182. https://doi.org/10.3233/RNN-170747

Mah, Y.H., Husain, M., Rees, G., Nachev, P., 2014. Human brain lesion-deficit inference remapped. Brain 137, 2522–2531. https://doi.org/10.1093/brain/awu164

Marchina, S., Zhu, L.L., Norton, A., Zipse, L., Wan, C.Y., Schlaug, G., 2011. Impairment of speech production predicted by lesion load of the left arcuate fasciculus. Stroke 42, 2251–2256. https://doi.org/10.1161/STROKEAHA.110.606103

Mateos-Pérez, J.M., Dadar, M., Lacalle-Aurioles, M., Iturria-Medina, Y., Zeighami, Y., Evans, A.C., 2018. Structural neuroimaging as clinical predictor: A review of machine learning applications. NeuroImage Clin. 20, 506–522. https://doi.org/10.1016/j.nicl.2018.08.019

Moulton, E., Amor-Sahli, M., Perlbarg, V., Pires, C., Crozier, S., Galanaud, D., Valabregue, R., Yger, M., Baronnet-Chauvet, F., Samson, Y., Dormont, D., Rosso, C., 2015. Axial diffusivity of the corona

radiata at 24 hours post-stroke: A new biomarker for motor and global outcome. PLoS One 10, 1–16. https://doi.org/10.1371/journal.pone.0142910

Moulton, E., Valabrègue, R., Díaz, B., Kemlin, C., Leder, S., Lehéricy, S., Samson, Y., Rosso, C., Valabregue, R., Díaz, B., Kemlin, C., Leder, S., Lehéricy, S., Samson, Y., Rosso, C., 2018. Comparison of spatial normalization strategies of diffusion MRI data for studying motor outcome in subacute-chronic and acute stroke. Neuroimage 183, 186–199. https://doi.org/10.1016/j.neuroimage.2018.08.002

Muñoz Maniega, S., Bastin, M.E., Armitage, P. a, Farrall, A.J., Carpenter, T.K., Hand, P.J., Cvoro, V., Rivers, C.S., Wardlaw, J.M., 2004. Temporal evolution of water diffusion parameters is different in grey and white matter in human ischaemic stroke. J. Neurol. Neurosurg. Psychiatry 75, 1714–8. https://doi.org/10.1136/jnnp.2003.033852

Munsch, F., Sagnier, S., Asselineau, J., Bigourdan, A., Guttmann, C.R., Debruxelles, S., Poli, M., Renou, P., Perez, P., Dousset, V., Sibon, I., Tourdias, T., 2016. Stroke location is an independent predictor of cognitive outcome. Stroke 47, 66–73. https://doi.org/10.1161/STROKEAHA.115.011242

Phan, T.G., Chen, J., Donnan, G., Srikanth, V., Wood, A., Reutens, D.C., 2010. Development of a new tool to correlate stroke outcome with infarct topography: A proof-of-concept study. Neuroimage 49, 127–133. https://doi.org/10.1016/j.neuroimage.2009.07.067

Phan, T.G., Donnan, G.A., Wright, P.M., Reutens, D.C., 2005. A digital map of middle cerebral artery infarcts associated with middle cerebral artery trunk and branch occlusion. Stroke 36, 986–991. https://doi.org/10.1161/01.STR.0000163087.66828.e9

Price, C.J., Hope, T.M., Seghier, M.L., 2017. Ten problems and solutions when predicting individual outcome from lesion site after stroke. Neuroimage 145, 200–208. https://doi.org/10.1016/j.neuroimage.2016.08.006

Rondina, J.M., Filippone, M., Girolami, M., Ward, N.S., 2016. Decoding post-stroke motor function from structural brain imaging. NeuroImage Clin. 12, 372–380. https://doi.org/10.1016/j.nicl.2016.07.014

Rondina, J.M., Park, C.H., Ward, N.S., 2017. Brain regions important for recovery after severe post-stroke upper limb paresis. J. Neurol. Neurosurg. Psychiatry 88, 737–743. https://doi.org/10.1136/jnnp-2016-315030

Rosso, C., Colliot, O., Valabrègue, R., Crozier, S., Dormont, D., Lehéricy, S., Samson, Y., 2011. Tissue at risk in the deep middle cerebral artery territory is critical to stroke outcome. Neuroradiology 53, 763–71. https://doi.org/10.1007/s00234-011-0916-5

Rosso, C., Vargas, P., Valabregue, R., Arbizu, C., Henry-Amar, F., Leger, A., Lehéricy, S., Samson, Y., 2015. Aphasia severity in chronic stroke patients: a combined disconnection in the dorsal and ventral language pathways. Neurorehabil. Neural Repair 29, 287–95. https://doi.org/10.1177/1545968314543926

Samper-González, J., Burgos, N., Bottani, S., Fontanella, S., Lu, P., Marcoux, A., Routier, A., Guillon, J., Bacci, M., Wen, J., Bertrand, A., Bertin, H., Habert, M.-O., Durrleman, S., Evgeniou, T., Colliot, O., 2018. Reproducible evaluation of classification methods in Alzheimer's disease: Framework and

application to MRI and PET data. Neuroimage 183, 504–521. https://doi.org/10.1016/j.neuroimage.2018.08.042

Siegel, J.S., Ramsey, L.E., Snyder, A.Z., Metcalf, N. V, Chacko, R. V, Weinberger, K., Baldassarre, A., Hacker, C.D., Shulman, G.L., Corbetta, M., 2016. Disruptions of network connectivity predict impairment in multiple behavioral domains after stroke. Proc. Natl. Acad. Sci. U. S. A. 113, E4367-76. https://doi.org/10.1073/pnas.1521083113

Smith, S.M., 2002. Fast robust automated brain extraction. Hum. Brain Mapp. 17, 143–155. https://doi.org/10.1002/hbm.10062

Smith, S.M., Jenkinson, M., Woolrich, M.W., Beckmann, C.F., Behrens, T.E.J., Johansen-Berg, H., Bannister, P.R., De Luca, M., Drobnjak, I., Flitney, D.E., Niazy, R.K., Saunders, J., Vickers, J., Zhang, Y., De Stefano, N., Brady, J.M., Matthews, P.M., 2004. Advances in functional and structural MR image analysis and implementation as FSL. Neuroimage 23 Suppl 1, S208-19. https://doi.org/10.1016/j.neuroimage.2004.07.051

Sotak, C.H., 2002. The role of diffusion tensor imaging in the evaluation of ischemic brain injury - a review. NMR Biomed. 15, 561–9. https://doi.org/10.1002/nbm.786

Spampinato, M.V., Chan, C., Jensen, J.H., Helpern, J.A., Bonilha, L., Kautz, S.A., Nietert, P.J., Feng, W., 2017. Diffusional Kurtosis Imaging and Motor Outcome in Acute Ischemic Stroke. Am. J. Neuroradiol. 1–7. https://doi.org/10.3174/ajnr.A5180

Sun, S.-W., Liang, H.-F., Le, T.Q., Armstrong, R.C., Cross, A.H., Song, S.-K., 2006. Differential sensitivity of in vivo and ex vivo diffusion tensor imaging to evolving optic nerve injury in mice with retinal ischemia. Neuroimage 32, 1195–204. https://doi.org/10.1016/j.neuroimage.2006.04.212

Thiebaut de Schotten, M., Tomaiuolo, F., Aiello, M., Merola, S., Silvetti, M., Lecce, F., Bartolomeo, P., Doricchi, F., 2014. Damage to White Matter Pathways in Subacute and Chronic Spatial Neglect: A Group Study and 2 Single-Case Studies with Complete Virtual “In Vivo” Tractography Dissection. Cereb. Cortex 24, 691–706. https://doi.org/10.1093/cercor/bhs351

Varoquaux, G., 2018. Cross-validation failure: Small sample sizes lead to large error bars. Neuroimage 180, 68–77. https://doi.org/10.1016/j.neuroimage.2017.06.061

Varoquaux, G., Raamana, P.R., Engemann, D.A., Hoyos-Idrobo, A., Schwartz, Y., Thirion, B., 2017. Assessing and tuning brain decoders: Cross-validation, caveats, and guidelines. Neuroimage 145, 166–179. https://doi.org/10.1016/j.neuroimage.2016.10.038

Veraart, J., Fieremans, E., Novikov, D.S., 2016a. Diffusion MRI noise mapping using random matrix theory. Magn. Reson. Med. 76, 1582–1593. https://doi.org/10.1002/mrm.26059

Veraart, J., Novikov, D.S., Christiaens, D., Ades-aron, B., Sijbers, J., Fieremans, E., 2016b. Denoising of diffusion MRI using random matrix theory. Neuroimage 142, 394–406. https://doi.org/10.1016/j.neuroimage.2016.08.016

Wu, O., Cloonan, L., Mocking, S.J.T., Bouts, M.J.R.J., Copen, W.A., Cougo-Pinto, P.T., Fitzpatrick, K., Kanakis, A., Schaefer, P.W., Rosand, J., Furie, K.L., Rost, N.S., 2015. Role of Acute Lesion Topography in Initial Ischemic Stroke Severity and Long-Term Functional Outcomes. Stroke 46,

2438–2444. https://doi.org/10.1161/STROKEAHA.115.009643

Yang, Q., Tress, B.M., Barber, P. a., Desmond, P.M., Darby, D.G., Gerraty, R.P., Li, T., Davis, S.M., Barber, ; P Alan, Desmond, P.M., Darby, D.G., Gerraty, R.P., Li, T., Davis, S.M., 1999. Serial Study of Apparent Diffusion Coefficient and Anisotropy in Patients With Acute Stroke. Stroke 30, 2382–2390. https://doi.org/10.1161/01.STR.30.11.2382

Yoo, A.J., Barak, E.R., Copen, W. a, Kamalian, S., Gharai, L.R., Pervez, M. a, Schwamm, L.H., González, R.G., Schaefer, P.W., 2010. Combining acute diffusion-weighted imaging and mean transmit time lesion volumes with National Institutes of Health Stroke Scale Score improves the prediction of acute stroke outcome. Stroke. 41, 1728–35. https://doi.org/10.1161/STROKEAHA.110.582874

Yourganov, G., Smith, K.G., Fridriksson, J., Rorden, C., 2015. Predicting aphasia type from brain damage measured with structural MRI. Cortex 73, 203–215. https://doi.org/10.1016/j.cortex.2015.09.005

Zhang, Y., Brady, M., Smith, S., 2001. Segmentation of brain MR images through a hidden Markov random field model and the expectation-maximization algorithm. IEEE Trans. Med. Imaging 20, 45–57. https://doi.org/10.1109/42.906424

Zhang, Y., Kimberg, D.Y., Coslett, H.B., Schwartz, M.F., Wang, Z., 2014. Multivariate lesion-symptom mapping using support vector regression. Hum. Brain Mapp. 35, 5861–5876. https://doi.org/10.1002/hbm.22590

6.3 Conclusion

Axial diffusivity maps yielded the best accuracy of all imaging parameters (82.8%), compared to that of lesion segmentations (76.7%) when predicting 3-month functional outcome. Model weights revealed a strong contribution of clinical variables, notably – in descending order – lesion volume, thrombectomy treatment, and recanalization status, in addition to the deep white matter at the crossroads of major white matter tracts. This study confirms that axial diffusivity is a more appropriate imaging marker to characterize acute stroke damage for predicting long-term outcome than commonly used binary lesion segmentations. Moreover, our study supports the importance of the deep white matter, notably within the corona radiata, and the many major long-range fiber bundles that pass through it.

The second study made use of all available DTI parameter maps in addition to classically used lesion segmentations to predict long-term global outcome. This study contributed two important conclusions to the scientific community. First, we showed that whole-brain axial diffusivity maps are capable of yielding generalizable predictions of long-term global outcome. Second, we demonstrated the limitations of making predictions of brain damage characterized by simple lesion segmentations. Due to the difficulty of obtaining DTI data at early times post-stroke, the vast majority of studies have used lesion segmentations on rapidly acquired anatomical MRI in order to relate the spatial extent of ischemic lesions to outcome. However, the results of this study suggest that the severity of acute ischemia, captured specifically by the continuous values of AD, reflects damage unique to given patients and their associated outcome. Of note, we did not evaluate the contribution of the day 1 NIHSS score as it is already encoded in the topography of the stroke. We did, however, control for other important clinical variables that could affect the magnitude of diffusion, such as thrombectomy treatment and recanalization status. Nevertheless, AD highlighted important brain regions for the prognosis of long-term global outcome, which resulted in the best predictions. As described in section 3.4, while AD, mean diffusivity (MD), and radial diffusivity (RD) are all decreased at 24 hours post-stroke, only AD remains consistenly decreased, whereas radial diffusivity (RD) – and thus mean diffusivity (MD) – begin to increase through demyelination. The monotonic evolution of AD (i.e., always decreasing), with respect to the dynamic behavior of RD and MD at the hyperacute-acute phase, likely explains why AD was able to classify patients better than MD or RD. In any case, these diffusivity measures all yielded better predictions than lesion segmentations or fractional anisotropy (FA). Our results therefore have

important implications not only for finding future biomarkers of the outcome of any functional domain – be it global, motor, or language – but also for understanding the underlying physiopathology of acute ischemic damage and thus the neural correlates of long-term outcome.

Chapter 7

Study III: Acute Diffusivity Biomarkers for Prediction of Motor and Language Outcome in Mild-to-Severe Stroke patients

Contents

7.1 Overview of Study

The results of the second study enabled us to ascertain that AD is the most appropriate DTI parameter for quantifying early acute stroke damage related to long-term outcome. While a few previous studies have already shown that acute AD is an independent predictor of long-term motor outcome, patient recruitment in these investigations has been at quite variable intervals following stroke onset, ranging over the first week post-stroke (1-7 days) when diffusion parameters rapidly evolve. In other words, there was a need to investigate the earliest moment at which DTI can yield effective predictions – that is, day 1 post stroke. Moreover, studies having investigated the effect of acute DTI and baseline clinical variables with long-term motor outcome suffered from small sample sizes.

In the third study, therefore, we sought to determine if changes in AD, measured as early as 24 hours post-stroke in a consistent manner, could independently predict motor outcome evaluated at 3 months post-stroke. Furthermore, we were also interested to see if the predictive value of AD extended to a theretofore unexplored functional domain: language. However, as explained in chapter 1, clinical variables such as initial severity, age, and – to a lesser degree – lesion volume are also powerful predictors of domain-specific outcomes. However, the relationship between these important variables and outcome is mainly driven by minor stroke patients, who generally evolve towards good recovery. On the other hand, this relationship is more questionable for mild-to-moderate stroke patients. We therefore focused on this subset of patients for whom outcome is more difficult to predict.

Because any predictive model should be easily implementable and reproducible for wide-range clinical trials, we first conducted simple tract-specific analyses. Here, we extracted changes in AD from a set of major white matter fasciculi known to be involved in motor and language function and included them in a regression analysis to predict clinical outcome scores at 3 months post-stroke. Since this initial analysis relies on strong hypothesis-driven assumptions, we complemented the regression analysis with data-driven mass univariate voxel-wise regressions to determine if the same, additional, or altogether new regions were associated with long-term outcome. Specifically, our goals were to (1) determine if changes in AD and in which major white matter fasciculi within the motor and language networks were independent predictors of outcome in these two domains in mild-to-severe acute stroke patients, and (2) conduct similar mass univariate voxel-wise regression analyses with whole-brain AD maps in order to determine the specificity of the anatomical regions

corresponding to the *a priori* choices of fasciculi.

7.2 Article

The supplementary materials for this article can be found in Appendix I

Title: Acute diffusivity biomarkers for prediction of motor and language outcome in mild-to-severe stroke patients

Author names and affiliations:

Eric Moulton[1], Serena Magno[1], Romain Valabregue[1,2], Melika Amor-Sahli[4] Christine Pires[5], Stéphane Lehéricy[1-4], Anne Leger[5], Yves Samson[1,5], Charlotte Rosso[1,3,5]

(1) Institut du Cerveau et de la Moelle épinière, ICM, Inserm U 1127, CNRS UMR 7225, Sorbonne Université, F-75013, Paris, France

(2) Centre de Neuro-Imagerie de Recherche, CENIR, ICM, Paris, France

(3) ICM team Movement Investigation and Therapeutics

(4) AP-HP, Department of Neuroradiology, Hôpital Pitié-Salpêtrière, Paris, France

(5) AP-HP, Urgences Cérébro-Vasculaires, Hôpital Pitié-Salpêtrière, Paris, France

Corresponding author:

Charlotte Rosso

Urgences Cérébro-Vasculaires, 47-83 Boulevard de l'Hôpital 75013 Paris

Phone: +33 1 42161854 Fax: +33 1 42161839 E-mail: charlotte.rosso@gmail.com

Declaration of interest: none

Abstract

Early severity of stroke symptoms – especially in mild-to-severe stroke patients – are imperfect predictors of long-term motor and aphasia outcome. Motor function and language processing heavily rely on the preservation of important white matter fasciculi in the brain. Axial diffusivity (AD) from the diffusion tensor imaging (DTI) model has been repeatedly shown to accurately reflect acute axonal damage and is thus optimal to probe the integrity of important white matter bundles and their relationship with long-term outcome. Our aim was to investigate the independent prognostic value of the AD of white matter tracts in the visuomotor and language network evaluated at 24 hours post-stroke for motor and language outcome at 3 months post-stroke. Eighteen (motor cohort) and twenty-eight (aphasia cohort) thrombolyzed patients with initial mild-to-severe stroke or aphasia underwent a DTI sequence at 24 hours post-stroke. Motor and language outcome was evaluated at 3 months post-stroke with a composite motor score and the aphasia handicap scale (AHS). We first used stepwise regression to determine which clinical (age, initial motor or aphasia severity, and lesion volume) and imaging (ratio of affected/unaffected AD of motor and language fasciculi) factors were related to outcome. Second, in order to determine the specificity of our *a priori* choices of fasciculi, we performed voxel-based analyses to determine if the same, additional, or altogether new regions were associated with long-term outcome. The ratio of AD in the corticospinal tract was the sole predictor of long-term motor outcome, and the ratio of AD in the arcuate fasciculus – along with age and initial aphasia severity – was an independent predictor of 3-month aphasia outcome. White matter regions overlapping with these fasciculi naturally emerged in the corresponding voxel-based analyses. AD of the corticospinal tract and arcuate fasciculus are effective biomarkers of long-term motor and aphasia outcome, respectively.

1. Introduction

Finding surrogate markers of long-term motor and aphasia outcome as early as a few days following cerebral ischemia has become one of the most important topics in stroke research (Boyd et al., 2017). The initial severity of motor and language deficits has been shown to highly correlate to their status at the chronic stage of stroke; however, clinical scales used to evaluate residual neurological function suffer from a poor specificity-sensitivity tradeoff. In particular, initially minor deficits will almost always resolve themselves in the long run, whereas patients with mild to severe impairments exhibit highly variable recovery trajectories, making their final outcomes difficult to predict (Pedersen et al., 2004; Prabhakaran et al., 2008). While other clinical factors such as age and lesion volume can refine prognostic models, notably for aphasia prediction (El Hachioui et al., 2013; Plowman et al., 2012), recent work has shown that the structural integrity of important white matter pathways in the motor and language systems are crucial for patient outcome (Byblow et al., 2015; Feng et al., 2015; Groisser et al., 2014; Marchina et al., 2011; Ramsey et al., 2017). In particular, motor outcome of the upper limb is highly dependent on the preservation of the corticospinal tract, whereas language outcome relies on a wider network of white matter fasciculi, such as the arcuate fasciculus, inferior fronto-occipital fasciculus, inferior longitudinal fasciculus, and uncinated fasciculus (Roelofs, 2014; Ueno et al., 2011; Zavanone et al., 2018).

Diffusion weighted imaging (DWI) is an imaging modality sensitive to the diffusion of water molecules both in the healthy brain and ischemic stroke and is thus optimal to probe the integrity of important white matter bundles. Diffusion tensor imaging (DTI), an extension of DWI, is capable of characterizing the diffusion of water in 3D space and yields several parametric maps, each providing complementary insights on the integrity of affected and unaffected neural populations. Of the four classical DTI parameters, fractional anisotropy (FA), mean diffusivity (MD), axial diffusivity (AD), and radial diffusivity (RD), AD has been repeatedly shown to most accurately reflect acute axonal damage related to subacute and chronic motor and functional outcome (Doughty et al., 2016; Groisser et al., 2014; Liu et al., 2018; Moulton et al., 2019, 2015; Spampinato et al., 2017). Acute changes in AD likely reflect increased intracellular viscosity from direct axonal damage as supported by recent DTI-immunohistology studies or neuronal beading (Baron et al., 2015; Budde and Frank, 2010; Sun et al., 2006). Groisser et al. (2018) scanned 10 stroke patients at 3-7 days post-stroke with DTI and evaluated their motor outcome with a grip force and dexterity assessment at 2 and 6 months. They found that early decreases in AD of the CST highly correlated with chronic motor outcome, even after adjusting for initial impairment and lesion volume. On the other hand, no study has yet confirmed these findings in a larger cohort or examined the predictive value of AD in language fasciculi on long-term aphasia outcome. In fact, to date, there have been no established predictors of long-term aphasia outcome from biomarkers assessed in the hyperacute period (<24h), and finding such markers has been declared a developmental priority (Boyd et al., 2017).

In this study, we attempted to determine if acute changes in AD in major white matter fasciculi of the motor network and the language network – evaluated at even earlier time points compared to previous studies (i.e., 24 hours post-stroke) – could predict not only motor but also aphasia outcome at 3 months post-stroke, independently from important clinical variables, such as age, lesion volume, and initial impairment. To do so, we retrospectively studied thrombolyzed stroke patients from our emergency stroke unit who systematically undergo a DTI imaging protocol at 24 hours post-stroke. Because any predictive model should be easily implementable and reproducible for wide-range clinical trials, we first conducted simple tract-specific analyses by extracting changes in AD from a set of major white mater bundles and inserted them in a regression analysis along with clinical variables (hypothesis-driven analysis). Next, in order to validate our choices of white matter tracts, we complemented the regression analysis with mass univariate voxel-wise regressions to determine if the same, additional, or altogether new regions were associated with long-term outcome (data-driven analysis).

Our goals were to (1) determine if changes in AD and in which major white matter fasciculi within the motor and language networks were independent predictors of outcome in these two domains in mild-to-severe acute stroke patients, and (2) conduct similar mass univariate voxel-wise regression analyses with whole-brain AD maps in order to determine the specificity of the anatomical regions corresponding to the *a priori* choices of fasciculi. We predicted that (A), in concordance with previous work, changes in AD would significantly contribute to the prediction of long-term motor and also language outcome – beyond important clinical variables, such as age, lesion volume, and initial impairment – and (B) that the specific fasciculi chosen *a priori* in the first analysis – namely, those that significantly contributed to motor and language outcome – would also emerge in the whole-brain analysis.

2. Materials and Methods

2.1. Patients

Patients were retrospectively screened from October 1, 2015 until April 30th, 2018 at the Urgences Cérébrovasculaires at the Hôpital de la Pitié Salpêtrière. Inclusion criteria common to both cohorts were: (1) MRI-demonstrated ischemic stroke of the carotid territory, (2) thrombolysis treatment within 4.5 h after stroke onset, (3) follow-up MRI access at 24 hours post-stroke, and (4) a clinical assessment at 3-months post-stroke with either a motor or language evaluation according to the patients' deficits. Since we were interested in predicting mild-to-severe patients at the acute stage, we only considered patients with a day 1 NIHSS > 4 for patients in the motor outcome cohort and a day 1 Aphasia Rapid Test (ART) > 4 (see section 2.2) for patients in the aphasia outcome cohort. Only patients with lesions to the left hemisphere were considered for the aphasia outcome cohort. Thrombolytic treatment was administered according to the American Stroke Association and the European Stroke Organization guidelines (0.9 mg/kg, maximal dose 90 mg)(Jauch et al., 2013). Patients with bilateral lesions were

deemed suitable for analysis if clinical symptoms were lateralized to one hemisphere (e.g., unilateral hemiparesis, aphasia without neglect, etc.). For these patients, the affected hemisphere was considered as that which caused clinical symptoms. Exclusion criteria were (1) overly artifacted imaging data, (2) dependence on external aid before the stroke (i.e., pre-stroke mRS > 2) or the reoccurrence of stroke before the 3-month follow-up, (3) death before the 3-month follow-up. All imaging and clinical data were obtained during routine clinical workup in our stroke center. According to French legislation, explicit informed consent was therefore waived. The study was approved by the Pitié-Salpêtrière Hospital Ethics Committee.

2.2. Evaluation of Initial Impairment

Initial stroke severity was evaluated with the National Institute of Health Stroke Scale (NIHSS) upon admission to our stroke clinic and at day 1 post-stroke. The day 1 NIHSS motor item of the upper limb (UL-NIHSS) was also recorded as a proxy for initial motor impairment. Initial aphasia severity was evaluated with the ART (Azuar et al., 2013). The ART is a NIHSS-like 26-point scale with higher scores indicating greater impairment. It is based on 6 items, consisting of simple comprehension tasks (rated from 0-5 points), word and sentence repetition (0-8 points), object naming (0-6 points), semantic fluency of animals (0-4 points), and dysarthria evaluation (0-3 points). The reproducibility, sensitivity, and high predictive value of the ART score have been published, and its external validation has recently been reported in Portuguese and Indian populations (Azuar et al., 2013; Jayakumar et al., 2018; Tábuas-Pereira et al., 2018).

2.3. Three-month Evaluation

The motor evaluation consisted of the (1) the Jebson-Taylor Test (JTT) (Jebsen et al., 1969), and (2) a grip-force evaluation for the maximum voluntary contraction (MVC) using a dynamometer (MIE, Medical Research Ltd., http://www.mie- uk.com/pgripmyo/index.html). Similar to other studies (Moulton et al., 2018; Park et al., 2013; Rondina et al., 2017), we evaluated residual motor ability with a composite motor score by taking the first principle component of the following measures: the ratio of the affected/unaffected JTT total times (rJTT) and the ratio of the affected/unaffected MVC (rMVC). The first principle component accounted for 86.9% of the total variance between the two scores. In our study, a higher motor composite score corresponded to a more severe deficit.

Aphasia outcome was assessed at 3 months post-stroke using the Aphasia Handicap Score (AHS) (Azuar et al., 2013). The AHS is a five-point scoring system for disability in verbal communication similar to the modified Rankin Scale. 0 = normal communication, 1 = minor difficulties of language without disability (no impact on normal life), 2 = mild-language related disability (without restrictions in the autonomy of verbal communication in daily life), 3 = moderate language-related disability (restricted autonomy of verbal communication), 4 = severe language-related disability (lack of effective verbal

communication), 5 = mutism or total loss of verbal expression and comprehension. There is a strong inverse relation with the AHS and the Boston Diagnosis Aphasia Examination aphasia severity rating scale (ASRS). For example, a AHS score of 0 corresponds to a ASRS score of 5, whereas a AHS score of 5 corresponds to a ASRS score of 0 (see Azuar et al. (2013) for a detailed description as well as the reproducibility and comparison with the ASRS). Here, the AHS was analyzed as a continuous variable.

2.4. MRI acquisition and processing

2.4.1. Acquisition

Imaging data used in this study are from our emergency stroke unit in which we examined patients with typical DWI sequences but also a DTI protocol. Twenty-four hours after admission, patients underwent a follow-up MRI with a 3T MR750 MRI scanner (General Electric) with an 8-channel coil. The following DWI sequences were used for the current analysis: (1) an averaged 3-direction DWI (b=1000 s/mm^2, TR=11700ms, TE=72.3ms, matrix size=256×256, slice number=48, voxel size=0.94×0.94×3mm^3, acquisition time=0:59 min) and (2) a 30-direction DWI (2 b=0 s/mm^2 images followed by 30 non-collinear diffusion-encoding gradients at b=1000 s/mm^2, TR=12000ms, TE=82.3ms, matrix size=256×256, slice number=44, voxel size=1.09×1.09×3mm^3, acquisition time=6:36 min).

2.4.2. Image processing

2.4.2.1. Preprocessing and spatial normalization

Image processing served to prepare data for spatial normalization to a study-specific diffusion imaging template as outlined in Moulton et al. (2018). In brief, after correcting for (1) denoising (Veraart et al., 2016a, 2016b), (2) eddy currents and head motion using FSL's EDDY with slice interpolation for slices with significant signal drop (Andersson et al., 2016; Andersson and Sotiropoulos, 2016), and (3) bias-field correction (Zhang et al., 2001), FA and AD maps were calculated from a tensor model estimated using FSL's DTIFIT (Basser et al., 1994; Smith et al., 2004), and brains were skull stripped (Smith, 2002). Lesion segmentation was performed by identifying hypersignal regions on the 3-direction DWI sequence image in order to calculate the volume of the lesion.

Warped images were used in a tract-specific analysis to extract average diffusion values from various left- and right-hemisphere fasciculi for a regression analysis (section 2.4.3). For our voxel-based analyses, we required that both affected and unaffected hemispheres be fixed to the same side in order to calculate voxel-wise asymmetry maps (see section 2.4.4). To this end, both original (unflipped) and flipped FA maps were registered to an in-house healthy-subject FA template using Advanced Normalization Tools (ANTs) with lesion masking. The corresponding warp fields were thereafter applied to the original and flipped AD maps (Supplementary Materials).

2.4.3. Tractography

Whole-brain tractography was performed on an in-house Fiber Orientation Distribution (FOD) imaging template constructed from healthy individuals as described in Moulton et al. (2018) (Supplementary Materials). Adhering to the procedures outlined in Rojkova et al. (2016) and Catani and Thiebaut de Schotten (2008), we virtually dissected the left and right (1) second and (2) third branches of the superior longitudinal fasciculus (SLF) and (3) the CST as part of the motor network in addition to the left and right (A) arcuate fasciculus (AF), (B) inferior fronto-occipital fasiculus (IFOF), (C) inferior longitudinal fasciculus (ILF), and (D) the uncinate fasciculus (UNC) as part of the language network. The SLF-II and SLF-III were included for analysing motor outcome in addition to the CST due to their important role in reaching and reach-to-grasp movements (Budisavljevic et al., 2016), which are necessary for good performance on the JTT evaluation. Moreover, microstructural changes assessed with DTI in such parieto-frontal connections have shown to play a role in residual motor function at the chronic stage, beyond damage to the CST (Schulz et al., 2015).

For the regression analyses, we extracted density-weighted AD values from the affected and unaffected fasciculi of the visuomotor and language networks from which ratios of the affected/affected AD (rAD) were computed (Moulton et al., 2018).

2.4.4. Construction of asymmetry maps for voxel-based analyses

To process all images in the same hemisphere for the voxel-based analyses, we warped both the original and flipped AD maps. Indeed, in stroke imaging, it is common practice to analyze relative differences between the affected and unaffected hemispheres rather than absolute values of the affected hemisphere alone. To this end, we kept all affected hemispheres to the same side (here, the left-hemisphere) and constructed laterality index (LI) maps, hereafter referred to as asymmetry maps, using the normalized original and flipped DTI maps with the following equation at each voxel: (affected-unaffected)/(affected+unaffected). The LI is a score between -1 and 1 for which the negative range indicates smaller values on the affected side and the positive range indicates larger values on the affected side. Particularly, acute stroke is largely characterized by strong decreases in AD with respect to the unaffected hemisphere.

AD asymmetry maps were smoothed with a 6 mm Gaussian kernel to compensate for imperfections in normalization while conserving the specificity of each region. Since all of the information of asymmetry maps is contained in one hemisphere, our analysis can be reliably restrained to one side. Moreover, relative differences in diffusivity are more pronounced in white matter than grey matter regions (Bhagat et al., 2008; Muñoz Maniega et al., 2004; Yang et al., 1999). With these considerations, we restricted our

analysis to the left cerebral white matter mask from the Harvard-Oxford Atlas by registering our study-specific FA template to the FMRIB58_FA template as provided by the FSL software using ANTs.

2.5. Statistics

Descriptive statistics are reported as the mean and interquartile range (IQR). Proportions were tested different from 50% with exact binomial tests. Between-group differences were tested with a Wilcoxon Rank-Sum test. Testing differences in behavioral and imaging measures between the affected and unaffected side were accomplished with a paired Wilcoxon Signed-Rank test. These statistical tests were performed using the R programming software (R Core Team, 2016; www.r-project.org).

For motor and aphasia outcomes, we ran two stepwise regressions, a purely "clinical" model with only clinical scores, and a mixed "radiological-clinical" model with both clinical and tract-specific measures of rAD. Dependent variables for the motor and language models were the motor composite score and the AHS at 3 months, respectively. Clinical independent variables consisted of age, lesion volume, and initial impairment (i.e., day 1 UL-NIHSS for motor models and day 1 ART for language models). Radiological variables were the rAD values of the visuomotor fasciculi for motor outcome and the rAD values of the language fasciculi for aphasia outcome as described in section 2.4.3. For all models, variables significant at $p<0.05$ were retained in the final regression models. Explained variance is reported as the adjusted R^2 of the final model. Step-wise regression models were run using MedCalc (version 12.5.0, Belgium, 2013).

To ensure that our *a-priori* choice of radiological variables (i.e., fasciculi) in the step-wise regression analyses were valid, we ran two mass univariate ordinary least squares regression analyses using permutation testing for family-wise error (FWE) corrected p-values as implemented in Nilearn v0.5.0 in Python (Abraham et al., 2014). Similar to the step-wise regression analyses, the dependent variables were the motor composite score and the AHS, and the corresponding independent variables were the AD asymmetry maps. In concordance with the step-wise regression analyses, we sought to determine in which regions significantly lower AD at day 1 post-stroke was associated with more severe deficits at 3 months post-stroke, correcting each linear model by the following confounding variables: (1) age, (2), lesion volume, and (3) the day 1 UL-NIHSS or ART for the motor and aphasia outcome models, respectively. Cluster location is reported according to the JHU white-matter tractography atlas (Laboratory of Brain Anatomical MRI, Johns Hopkins University).

3. Results

3.1. Patient Cohorts

Eighteen patients (9 female, 65.5 [50.0;77.7] years-old) were included in the motor analysis, and twenty-eight (13 female, 69.6 [53.3;78.9] years-old) were included in the language analysis (Table 1). Ten

patients (4 female, 64.7 [50.0-75.4] years-old) were common to both groups. Upon removal of these patients, groups did not differ in day 1 NIHSS (p=0.8), age (p=0.9), or lesion volume (p=0.6). All differences in clinical scores and AD between the affected and unaffected side were significant except for the rAD of the ILF in the language cohort. The motor cohort had a significantly higher rate of left hemisphere lesions than right lesions (p<0.01). In both groups, the highest infarct incidence was in the insular and central opercular cortex (Figure 1).

	Motor Group (N=18)		**Language Group (N=28)**
Day 1 Clinical variables			
Females N (%)	9 (50%)	**Females N (%)**	13 (46%)
Left hemisphere lesions N (%)	15 (83%)**	**Left hemisphere lesions N (%)**	28 (100%)**
Age (years)	65.5 [50.0;77.7]	**Age (years)**	69.6 [53.3;78.9]
Lesion volume (mL)	42.6 [25.8;74.5]	**Lesion volume (mL)**	41.3 [20.5;72.2]
Day 1 NIHSS	10.0 [7.0;13.5]	**Day 1 NIHSS**	11.0 [7.0;18.3]
Day 1 UL-NIHSS	1.00 [1.00;2.75]	**Day 1 ART**	22.0 [14.5;24.0]
Day 1 Radiological Variables			
rAD CST	0.98 [0.94;1.00]*	**rAD AD**	0.94 [0.81;0.97]*
rAD SLF-II	0.98 [0.95;1.00]*	**rAD IFOF**	0.97 [0.93;1.01]*
rAD SLF-III	0.92 [0.89;0.98]*	**rAD ILF**	0.99 [0.95;1.03]
		rAD UNC	0.95 [0.88;0.97]*
Month 3 Evaluation			
Month 3 rMVC	0.85 [0.58;0.98]*	**Month 3 AHS**	1 [1;3]
Month 3 rJTT	1.14 [1.01;1.44]*		
Motor Composite Score	-0.37 [-0.63;0.32]		

Table 1: Motor and language cohort. *p<0.05 according to a paired Wilcoxon signed-rank test between the affected and unaffected side. **p<0.05 according to an exact binomial test.

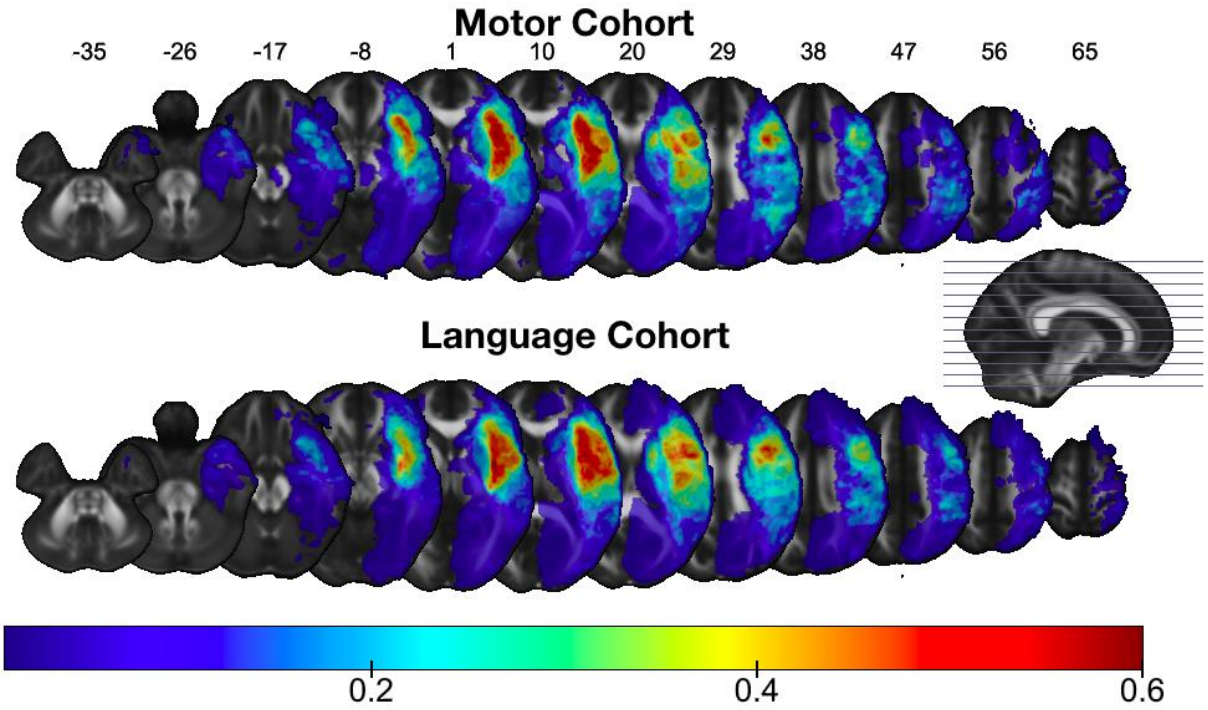

Figure 1: Lesion probability maps for the motor (top) and language (bottom) cohorts overlaid on the FMRIB58_FA template. The color map reflects the percentage of lesioned voxels. For the motor cohort, all lesions are fixed to the left hemisphere. Axial slice coordinates are given in MNI space.

3.2. Prediction of 3-month outcome using clinical and tract-specific measures

The only independent clinical predictor of long-term motor outcome was lesion volume, explaining 25.6% of the variance in motor impairment. Age and day 1 UL-NIHSS were not significantly associated with motor outcome. The inclusion of tract-specific measures revealed the rAD of the CST to be the sole independent predictor ($p=0.0003$), explaining 28.1% more variance than clinical variables for a total of 53.7% of explained variance in motor impairments at 3 months.

For language, the step-wise regression yielded a clinical model retaining only day 1 ART ($p<0.001$) for aphasia outcome, explaining 53.7% of the variance in outcome. On the other hand, after introducing radiological variables, the step-wise regression retained the rAD of the AF ($p=0.013$), age ($p=0.037$), and day 1 ART ($p=0.002$), explaining an additional 12.9% of the variance for a total of 66.6% of explained variance in aphasia severity at 3 months.

To verify that the motor and language fasciculi were specific to this functional domain, we reran the same step-wise regressions and included the rAD measures of all fasciculi. The models remained unchanged.

3.3. Prediction of 3-month outcome using voxel-based analyses with AD asymmetry maps

Four clusters corresponding to regions of lower AD asymmetries and more severe motor outcome of the upper limb emerged from the voxel-based analysis. There was a predominantly large cluster in the deep white matter of the corona radiata, the underlying white matter of the precentral and postcentral gyri and superior parietal lobe (Figure 2). Smaller clusters were found in the ventral temporal lobe as well as in the frontal and occipital poles.

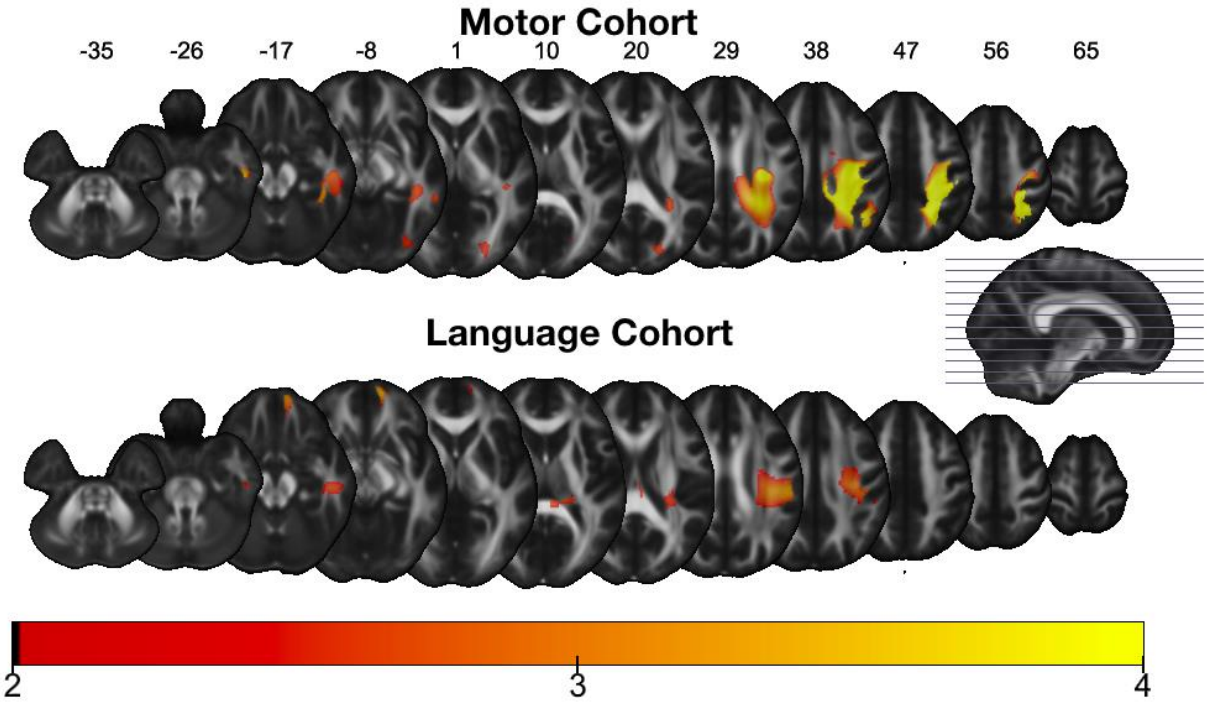

Figure 2. Clusters of reduced AD at day 1 post-stroke significantly associated with more sever motor impairments of the upper limb (top) and aphasia severity (bottom) at 3 months post-stroke overlaid on the FMRIB58_FA template. Both correlations are corrected for age, lesion volume, and initial impairment. For the motor cohort, all AD asymmetry maps were processed in the left hemisphere. Axial slice coordinates are given in MNI space. The color map shows the T statistic of the general linear model. All voxels are FWE-corrected at $p<0.05$.

As for the language analysis, three significant clusters corresponding to regions of lower axial diffusivity asymmetries and more severe aphasia outcome were found in the white matter of the AF as well as in the ventral temporal lobe, corresponding to waypoints of the ILF, and the frontal pole at the terminations of the IFOF and UNC (Figure 2).

4. Discussion

Combining acute DTI data in combination with baseline clinical scores measured at day 1 post-stroke, we found that acute changes in AD of the CST was an independent predictor of chronic motor impairment and – to our knowledge, for the first time – demonstrated that AD of the AF was also an independent predictor of aphasia outcome at 3 months in mild-to-severe stroke patients. Moreover, these tract-specific results were confirmed in a subsequent voxel-based analysis in which – without any *a priori* assumptions – white matter regions corresponding to these same fasciculi naturally emerged and remained significant even after adjusting for age, lesion volume, and initial impairment. The novelty of our study lies within the systematic availability of DTI data at 24 hours post-stroke to investigate the prognostic value of acute changes in axial diffusivity for long-term motor and aphasia outcome. Concordant with previous studies, we have confirmed that acute changes in AD of the CST are independent predictors of long-term motor outcome (Groisser et al., 2014), yet we have demonstrated this relationship to be valid at the very early time point of 24 hours post-stroke. More interestingly, our results suggest that the asymmetry in AD of the AF could serve as an effective biomarker of future aphasia outcome, responding to a developmental priority of the stroke imaging community.

4.1. Diffusion determinants of motor outcome

The step-wise regression revealed the CST, but not parieto-frontal pathways of the visuomotor network, to be independent predictors of long-term motor outcome. While the corresponding voxel-based analysis revealed a cluster highlighting, in part, the white matter of the CST, the cluster also extended far posteriorly to the white matter underlying the post-central gyrus and the superior parietal lobe. The posterior part of the cluster likely encompassed a portion of these parieto-frontal fasciculi, yet their correlations to future motor impairment were not independent of damage to the CST. Interestingly, however, the cluster largely overlapped white matter regions of ascending thalamocortical fibers extending until to the postcentral gyrus, which constitute the anatomical substrates for somatosensory perception (Meyer et al., 2016). Generally speaking, motor performance heavily relies on sensory and proprioceptive feedback loops within the somatosensory system in order to adjust and correct on-going movements (Scott, 2004), which are crucial factors for motor outcome in stroke patients (Meyer et al., 2014). It would be interesting for future studies to explicitly relate somatosensory deficits and acute changes in axial diffusivity for long-term motor outcome.

Surprisingly, the initial motor impairment was not an independent predictor of motor outcome. However, unlike the acute aphasia evaluation, we did not use a specific scale but the upper limb motor item of the NIHSS. The UL-NIHSS is scored from 0 to 4 and is easily obtained at day one. The long-term motor assessment was accomplished with sensitive measures of dexterity and strength output; however, the regression model only accounted for 53.7% of the variance. In this case, the unexplained variability in motor outcome might in fact be explained by missing clinical or imaging features. For example, an evaluation of motor impairment at the acute stage more refined than UL-NIHSS may have accounted for additional differences in motor outcome, yet these measures are rather difficult to obtain in clinical practice, especially at day 1 post-stroke onset. Similarly, tract-specific measures of somatosensory pathways could have improved the proposed prognostic model.

4.2. Specificity of the arcuate fasciculus for long-term aphasia outcome

As for language outcome, our tract-based analysis revealed the AF and no other language-related tract to be an independent predictor of aphasia outcome. Moreover, our voxel-based analysis suggests that damage to the dorsal portion of the AF drove the strong correlation between this tract and future language outcome. While there were two other clusters, one within the white matter of the ventral temporal lobe and a thin cluster in the frontal lobe, which are part of the ventral language pathways, the rAD of the ventral language pathways did not survive the statistical significance from the step-wise regression, and it is unclear if the latter was driven by mismatches in normalization at the grey-white matter interface.

In any case, our tract-based and voxel-based analyses having highlighted the importance of the AF suggest that the AHS reflects functions related to the dorsal stream of language processing. Traditionally, the AF is posited to primarily underpin repetition in language production (Hickok and Poeppel, 2007), which has been corroborated by several studies (Cloutman et al., 2009; Fridriksson et al., 2010; Kümmerer et al., 2013). However, more recent models have attributed a wider range of functions to the AF for spontaneous speech (Dick and Tremblay, 2012; Glasser and Rilling, 2008; Roelofs, 2014). Since the AHS reflects functional daily use of language, which is highly weighted by communication skills related to spontaneous speech, it is perhaps unsurprising that the AF correlate so well with this global measure of aphasia. In fact, several previous studies have also attributed a wide range of functions to the AF, reinforcing its crucial role in aphasia outcome. For example, tract-specific analyses performed at the chronic stage of stroke have reported that damage to the AF has been shown to correlate with rate, informativeness, and efficiency of speech (Marchina et al., 2011), fluency (Basilakos et al., 2014; Fridriksson et al., 2013), and other various measures of speech (Geva et al., 2015). One notable study by Hillis et al. (2018) acquired acute DWI scans <48 hours post-stroke and found that lesion load to the posterior superior temporal gyrus and the AF was highly predictive of improvement in object naming 6

months afterwards. In terms of voxel-based studies with early imaging data to predict chronic outcome, Ramsey et al. (2017) investigated language recovery in a large cohort of patients using lesion location from brain imaging performed within 2 weeks post stroke; they showed that worse aphasia at 3 months was associated with lesions of the superior and medial temporal gyri and the white matter corresponding to posterior regions of the AF, which improved prediction beyond lesion size, age, education level, physiotherapy dose, and baseline behavioral measurements.

As we are the first to report day 1 changes in AD of the AF related to chronic aphasia, it is difficult to compare our results to other studies. In fact, there are few studies reporting acute (<1 week post-stroke) changes in diffusivity for future aphasia outcome. In one investigation similar to ours, Hosomi et al. (2009) acquired DTI data at 2 days post-stroke in thirteen patients and reported that the FA of the AF was unable to distinguish between aphasic and non-aphasic patients at discharge. Unfortunately, this study did not provide information on any other diffusivity parameter, such as AD. Nevertheless, acute FA has repeatedly been shown to be a poor marker of acute neuronal damage and long-term motor and global outcome (Doughty et al., 2016; Groisser et al., 2014; Moulton et al., 2019, 2015); thus, a similar relationship would also be expected for language outcome. More similar to the present study, Zavanone et al. (2018) reported a significant link between acute changes in diffusivity with chronic language outcome using apparent diffusion coefficient (ADC) maps at day 1 post-stroke and ART scores at 6 months post-stroke. They found that lower ADC values in the posterior superior and middle temporal gyri, and the underlying white matter corresponding to the AF, ILF, and IFOF significantly correlated with worse aphasia outcome.

More importantly, not only have we confirmed that initial aphasia severity is crucial to predict long-term language outcome (Lazar et al., 2010; Pedersen et al., 2004), but we have also demonstrated that the AD of the AF contains additive information for improving prognosis. Moreover, this variable lead to a clinically relevant increase of 12.9% in explained variance with respect to a purely clinical model. This extra variability in aphasia outcome captured by a DTI imaging protocol suggests that this radiological exam can provide clinicians with the pertinent information as early as day 1 post-stroke to make accurate predictions for mild-to-severe stroke patients.

Despite the many candidate fasciculi and clinical variables entered in the step-wise regression to capture the variability in chronic aphasia, the final model only explained 66.6% of the variance in language outcome. In fact, the complementarity of the tract-specific and voxel-based analyses suggest that all of the pertinent predictors of aphasia outcome – here, the rAD of the AF, age, and initial aphasia severity – were well accounted for. One logical follow-up question, therefore, is: what could be responsible for the remaining unexplained variance? The answer may lie in an unaccounted clinical, imaging, or more profound neuroanatomical features such as aphasia type, damage to cortical regions outside the scope of

our analysis, hemispheric dominance, or wide-range network measures (Forkel et al., 2014; Fridriksson et al., 2018; Watila and Balarabe, 2015).

4.3. Limitations

A small caveat of the motor cohort was the unbalanced side of lesions. Indeed, in our stroke unit, the day 1 follow-up DTI protocol is only part of the imaging clinical routine for patients who receive thrombolysis treatment in order to closely monitor efficacy of the treatment and potential complications. This imbalance could be explained by the fact that aphasic patients (usually afflicted by left-sided lesions) are known to seek medical help earlier than non-aphasic patients (which, in large part, suffer from right-sided lesions) and are therefore more prone to arrive within the therapeutic window of 4.5 hours (Engelter et al., 2006).

Second, since we limited prognosis to mild-to-severe stroke patients, our findings will likely not generalize to minor stroke or aphasia. Indeed, in these patients, initial severity is a very strong indicator of near-perfect outcome or complete recovery, leaving little variance left to be explained by imaging variables (Lazar et al., 2010; Pedersen et al., 2004). Consequently, future research may aim to refine cutoff values of initial aphasia severity in order to determine which patients could benefit from a DTI scan at 24 hours post-stroke to improve the certainty of prognosis.

5. Conclusion

In summary, our study has shown that acute changes in AD measured as early as 24 hours post-stroke in crucial white matter pathways are independent predictors of not only motor but also aphasia outcome in mild-to-severe stroke patients. With respect to previous research, our findings demonstrate that damage to the CST predicts better than initial motor severity and that the AD of the AF adds a clinically relevant improvement to the prediction made by baseline clinical variables.

While the sample size of our cohorts may be considered small, we have purposefully limited our analysis to patients for whom prognosis is difficult to predict, which we believe constitutes a noteworthy strength of the current investigation. As MRI acceleration techniques continue to progress, acquiring DTI data in emergency stroke units, as is done in ours, may allow these markers of motor and language outcome to be easily incorporable in clinical trials at the hyperacute and acute stages of stroke. Moreover, that AD strongly correlates with outcome in two functionally and anatomically separate domains suggests that all future investigations employing DTI at the acute stroke stage should quantify early brain damage with AD. Finally, our results have important implications for salvaging brain areas critical for motor and aphasia outcome and can aid clinicians in weighing the costs, benefits, and risks for thrombolysis or thrombectomy treatments at the acute stroke stage.

Acknowledgements

Sources of Funding

The Pitié-Salpêtrière registry was supported by the French Ministry of Health grant EVALUSINV PHRC AOM 03 008. The research leading to these results has received funding from “Investissements d'avenir” ANR- 10-IAIHU-06 and ANR-11-INBS-0006.

The Fondation AVC granted part of the salary of EM.

Disclosures

None

References

Abraham, A., Pedregosa, F., Eickenberg, M., Gervais, P., Mueller, A., Kossaifi, J., Gramfort, A., Thirion, B., Varoquaux, G., 2014. Machine learning for neuroimaging with scikit-learn. Front. Neuroinform. 8, 1–10. https://doi.org/10.3389/fninf.2014.00014

Andersson, J.L.R., Graham, M.S., Zsoldos, E., Sotiropoulos, S.N., 2016. Incorporating outlier detection and replacement into a non-parametric framework for movement and distortion correction of diffusion MR images. Neuroimage 141, 556–572. https://doi.org/10.1016/j.neuroimage.2016.06.058

Andersson, J.L.R., Sotiropoulos, S.N., 2016. An integrated approach to correction for off-resonance effects and subject movement in diffusion MR imaging. Neuroimage 125, 1063–1078. https://doi.org/10.1016/j.neuroimage.2015.10.019

Azuar, C., Leger, A., Arbizu, C., Henry-Amar, F., Chomel-Guillaume, S., Samson, Y., 2013. The Aphasia Rapid Test: an NIHSS-like aphasia test. J. Neurol. 260, 2110–7. https://doi.org/10.1007/s00415-013-6943-x

Baron, C.A. lla., Kate, M., Gioia, L., Butcher, K., Emery, D., Budde, M., Beaulieu, C., 2015. Reduction of Diffusion-Weighted Imaging Contrast of Acute Ischemic Stroke at Short Diffusion Times. Stroke. 46, 2136–2141. https://doi.org/10.1161/STROKEAHA.115.008815

Basilakos, A., Fillmore, P.T., Rorden, C., Guo, D., Bonilha, L., Fridriksson, J., 2014. Regional White Matter Damage Predicts Speech Fluency in Chronic Post-Stroke Aphasia. Front. Hum. Neurosci. 8, 1–9. https://doi.org/10.3389/fnhum.2014.00845

Basser, P.J., Mattiello, J., LeBihan, D., 1994. Estimation of the effective self-diffusion tensor from the NMR spin echo. J. Magn. Reson. B 103, 247–54.

Bhagat, Y. a, Hussain, M.S., Stobbe, R.W., Butcher, K.S., Emery, D.J., Shuaib, A., Siddiqui, M.M., Maheshwari, P., Al-Hussain, F., Beaulieu, C., 2008. Elevations of diffusion anisotropy are associated with hyper-acute stroke: a serial imaging study. Magn. Reson. Imaging 26, 683–93. https://doi.org/10.1016/j.mri.2008.01.015

Boyd, L.A., Hayward, K.S., Ward, N.S., Stinear, C.M., Rosso, C., Fisher, R.J., Carter, A.R., Leff, A.P., Copland, D.A., Carey, L.M., Cohen, L.G., Basso, D.M., Maguire, J.M., Cramer, S.C., Basso, M., Maguire, J.M., Cramer, S.C., 2017. Biomarkers of stroke recovery: Consensus-based core recommendations from the Stroke Recovery and Rehabilitation Roundtable. Int. J. Stroke 12, 480–493. https://doi.org/10.1177/1747493017714176

Budde, M.D., Frank, J.A., 2010. Neurite beading is sufficient to decrease the apparent diffusion coefficient after ischemic stroke. Proc. Natl. Acad. Sci. 107, 14472–14477. https://doi.org/10.1073/pnas.1004841107

Budisavljevic, S., Acqua, F.D., Zanatto, D., Begliomini, C., Miotto, D., Motta, R., Castiello, U., 2016. Asymmetry and Structure of the Fronto-Parietal Networks Underlie Visuomotor Processing in Humans. Cereb. Cortex 1–13. https://doi.org/10.1093/cercor/bhv348

Byblow, W.D., Stinear, C.M., Barber, P.A., Petoe, M.A., Ackerley, S.J., 2015. Proportional recovery after

stroke depends on corticomotor integrity. Ann. Neurol. 78, 848–859. https://doi.org/10.1002/ana.24472

Catani, M., Thiebaut de Schotten, M., 2008. A diffusion tensor imaging tractography atlas for virtual in vivo dissections. Cortex. 44, 1105–32. https://doi.org/10.1016/j.cortex.2008.05.004

Cloutman, L., Gottesman, R., Chaudhry, P., Davis, C., Kleinman, J.T., Pawlak, M., Herskovits, E.H., Kannan, V., Lee, A., Newhart, M., Heidler-Gary, J., Hillis, A.E., 2009. Where (in the brain) do semantic errors come from? Cortex 45, 641–649. https://doi.org/10.1016/j.cortex.2008.05.013

Dick, A.S., Tremblay, P., 2012. Beyond the arcuate fasciculus: consensus and controversy in the connectional anatomy of language. Brain 135, 3529–50. https://doi.org/10.1093/brain/aws222

Doughty, C., Wang, J., Feng, W., Hackney, D., Pani, E., Schlaug, G., 2016. Detection and Predictive Value of Fractional Anisotropy Changes of the Corticospinal Tract in the Acute Phase of a Stroke. Stroke 47, 1520–1526. https://doi.org/10.1161/STROKEAHA.115.012088

El Hachioui, H., Lingsma, H.F., Van De Sandt-Koenderman, M.W.M.E., Dippel, D.W.J., Koudstaal, P.J., Visch-Brink, E.G., 2013. Long-term prognosis of aphasia after stroke. J. Neurol. Neurosurg. Psychiatry 84, 310–315. https://doi.org/10.1136/jnnp-2012-302596

Engelter, S.T., Gostynski, M., Papa, S., Frei, M., Born, C., Ajdacic-Gross, V., Gutzwiller, F., Lyrer, P.A., 2006. Epidemiology of aphasia attributable to first ischemic stroke: Incidence, severity, fluency, etiology, and thrombolysis. Stroke 37, 1379–1384. https://doi.org/10.1161/01.STR.0000221815.64093.8c

Feng, W., Wang, J., Chhatbar, P.Y., Doughty, C., Landsittel, D., Lioutas, V.A., Kautz, S.A., Schlaug, G., 2015. Corticospinal tract lesion load: An imaging biomarker for stroke motor outcomes. Ann. Neurol. 78, 860–870. https://doi.org/10.1002/ana.24510

Forkel, S.J., De Schotten, M.T., Dell'Acqua, F., Kalra, L., Murphy, D.G.M., Williams, S.C.R., Catani, M., 2014. Anatomical predictors of aphasia recovery: A tractography study of bilateral perisylvian language networks. Brain 137, 2027–2039. https://doi.org/10.1093/brain/awu113

Fridriksson, J., den Ouden, D.-B., Hillis, A.E., Hickok, G., Rorden, C., Basilakos, A., Yourganov, G., Bonilha, L., 2018. Anatomy of aphasia revisited. Brain 141, 848–862. https://doi.org/10.1093/brain/awx363

Fridriksson, J., Guo, D., Fillmore, P., Holland, A., Rorden, C., 2013. Damage to the anterior arcuate fasciculus predicts non-fluent speech production in aphasia. Brain 136, 3451–3460. https://doi.org/10.1093/brain/awt267

Fridriksson, J., Kjartansson, O., Morgan, P.S., Hjaltason, H., Magnusdottir, S., Bonilha, L., Rorden, C., 2010. Impaired Speech Repetition and Left Parietal Lobe Damage. J. Neurosci. 30, 11057–11061. https://doi.org/10.1523/JNEUROSCI.1120-10.2010

Geva, S., Correia, M.M., Warburton, E.A., 2015. Contributions of bilateral white matter to chronic aphasia symptoms as assessed by diffusion tensor MRI. Brain Lang. 150, 117–128. https://doi.org/10.1016/j.bandl.2015.09.001

Glasser, M.F., Rilling, J.K., 2008. DTI tractography of the human brain's language pathways. Cereb.

Cortex 18, 2471–2482. https://doi.org/10.1093/cercor/bhn011

Groisser, B.N., Copen, W.A., Singhal, A.B., Hirai, K.K., Schaechter, J.D., 2014. Corticospinal tract diffusion abnormalities early after stroke predict motor outcome. Neurorehabil. Neural Repair 28, 751–60. https://doi.org/10.1177/1545968314521896

Hickok, G., Poeppel, D., 2007. The cortical organization of speech processing. Nat. Rev. Neurosci. 8, 393–402. https://doi.org/10.1038/nrn2113

Hillis, A.E., Beh, Y.Y., Sebastian, R., Breining, B., Tippett, D.C., Wright, A., Saxena, S., Rorden, C., Bonilha, L., Basilakos, A., Yourganov, G., Fridriksson, J., 2018. Predicting recovery in acute poststroke aphasia. Ann. Neurol. 83, 612–622. https://doi.org/10.1002/ana.25184

Hosomi, A., Nagakane, Y., Yamada, K., Kuriyama, N., Mizuno, T., Nishimura, T., Nakagawa, M., 2009. Assessment of arcuate fasciculus with diffusion-tensor tractography may predict the prognosis of aphasia in patients with left middle cerebral artery infarcts. Neuroradiology 51, 549–555. https://doi.org/10.1007/s00234-009-0534-7

Jauch, E.C., Saver, J.L., Adams, H.P., Bruno, A., Connors, J.J., Demaerschalk, B.M., Khatri, P., McMullan, P.W., Qureshi, A.I., Rosenfield, K., Scott, P.A., Summers, D.R., Wang, D.Z., Wintermark, M., Yonas, H., 2013. Guidelines for the Early Management of Patients With Acute Ischemic Stroke: A Guideline for Healthcare Professionals From the American Heart Association/American Stroke Association. Stroke 44, 870–947. https://doi.org/10.1161/STR.0b013e318284056a

Jayakumar, H., Samivel, B., Janarthanam, M., Shanmuga, S.N., Ranganathan, L., Kuppusamy, K., Gowthaman, K., 2018. Aphasia Rapid Test - Quantification and assessment of Aphasia in Stroke (P3.230). Neurology 90.

Jebsen, R.H., Taylor, N., Trieschmann, R.B., Trotter, M.J., Howard, L.A., 1969. An objective and standardized test of hand function. Arch. Phys. Med. Rehabil. https://doi.org/10.1002/acr.20631

Kümmerer, D., Hartwigsen, G., Kellmeyer, P., Glauche, V., Mader, I., Klöppel, S., Suchan, J., Karnath, H.-O.O., Weiller, C., Saur, D., 2013. Damage to ventral and dorsal language pathways in acute aphasia. Brain 136, 619–629. https://doi.org/10.1093/brain/aws354

Lazar, R.M., Minzer, B., Antoniello, D., Festa, J.R., Krakauer, J.W., Marshall, R.S., 2010. Improvement in aphasia scores after stroke is well predicted by initial severity. Stroke 41, 1485–1488. https://doi.org/10.1161/STROKEAHA.109.577338

Liu, G., Peng, K., Dang, C., Tan, S., Chen, H., Xie, C., Xing, S., Zeng, J., 2018. Axial diffusivity changes in the motor pathway above stroke foci and functional recovery after subcortical infarction. Restor. Neurol. Neurosci. 36, 173–182. https://doi.org/10.3233/RNN-170747

Marchina, S., Zhu, L.L., Norton, A., Zipse, L., Wan, C.Y., Schlaug, G., 2011. Impairment of speech production predicted by lesion load of the left arcuate fasciculus. Stroke 42, 2251–2256. https://doi.org/10.1161/STROKEAHA.110.606103

Meyer, S., Karttunen, A.H., Thijs, V., Feys, H., Verheyden, G., 2014. How Do Somatosensory Deficits in the Arm and Hand Relate to Upper Limb Impairment, Activity, and Participation Problems After Stroke? A Systematic Review. Phys. Ther. 94, 1220–1231. https://doi.org/10.2522/ptj.20130271

Meyer, S., Kessner, S.S., Cheng, B., Bönstrup, M., Schulz, R., Hummel, F.C., De Bruyn, N., Peeters, A., Van Pesch, V., Duprez, T., Sunaert, S., Schrooten, M., Feys, H., Gerloff, C., Thomalla, G., Thijs, V., Verheyden, G., 2016. Voxel-based lesion-symptom mapping of stroke lesions underlying somatosensory deficits. NeuroImage Clin. 10, 257–266. https://doi.org/10.1016/j.nicl.2015.12.005

Moulton, E., Amor-Sahli, M., Perlbarg, V., Pires, C., Crozier, S., Galanaud, D., Valabregue, R., Yger, M., Baronnet-Chauvet, F., Samson, Y., Dormont, D., Rosso, C., 2015. Axial diffusivity of the corona radiata at 24 hours post-stroke: A new biomarker for motor and global outcome. PLoS One 10, 1–16. https://doi.org/10.1371/journal.pone.0142910

Moulton, E., Valabrègue, R., Díaz, B., Kemlin, C., Leder, S., Lehéricy, S., Samson, Y., Rosso, C., Valabregue, R., Díaz, B., Kemlin, C., Leder, S., Lehéricy, S., Samson, Y., Rosso, C., 2018. Comparison of spatial normalization strategies of diffusion MRI data for studying motor outcome in subacute-chronic and acute stroke. Neuroimage 183, 186–199. https://doi.org/10.1016/j.neuroimage.2018.08.002

Moulton, E., Valabregue, R., Lehéricy, S., Samson, Y., Rosso, C., 2019. Multivariate Prediction of Functional Outcome using Lesion Topography Characterized by Acute Diffusion Tensor Imaging. Submitted.

Muñoz Maniega, S., Bastin, M.E., Armitage, P.A., Farrall, A.J., Carpenter, T.K., Hand, P.J., Cvoro, V., Rivers, C.S., Wardlaw, J.M., 2004. Temporal evolution of water diffusion parameters is different in grey and white matter in human ischaemic stroke. J. Neurol. Neurosurg. Psychiatry 75, 1714–1718. https://doi.org/10.1136/jnnp.2003.033852

Park, C.-H., Kou, N., Boudrias, M.-H., Playford, E.D., Ward, N.S., 2013. Assessing a standardised approach to measuring corticospinal integrity after stroke with DTI. NeuroImage. Clin. 2, 521–33. https://doi.org/10.1016/j.nicl.2013.04.002

Pedersen, P.M., Vinter, K., Olsen, T.S., 2004. Aphasia after stroke: Type, severity and prognosis: The Copenhagen aphasia study. Cerebrovasc. Dis. 17, 35–43. https://doi.org/10.1159/000073896

Plowman, E., Hentz, B., Ellis, C., 2012. Post-stroke aphasia prognosis: A review of patient-related and stroke-related factors. J. Eval. Clin. Pract. 18, 689–694. https://doi.org/10.1111/j.1365-2753.2011.01650.x

Prabhakaran, S., Zarahn, E., Riley, C., Speizer, A., Chong, J.Y., Lazar, R.M., Marshall, R.S., Krakauer, J.W., 2008. Inter-individual variability in the capacity for motor recovery after ischemic stroke. Neurorehabil. Neural Repair 22, 64–71. https://doi.org/10.1177/1545968307305302

Ramsey, L.E., Siegel, J.S., Lang, C.E., Strube, M., Shulman, G.L., Corbetta, M., 2017. Behavioural clusters and predictors of performance during recovery from stroke. Nat. Hum. Behav. 1, 38. https://doi.org/10.1038/s41562-016-0038

Roelofs, A., 2014. A dorsal-pathway account of aphasic language production: The WEAVER++/ARC model. Cortex 59, 33–48. https://doi.org/10.1016/j.cortex.2014.07.001

Rojkova, K., Volle, E., Urbanski, M., Humbert, F., Dell'Acqua, F., Thiebaut de Schotten, M., 2016. Atlasing the frontal lobe connections and their variability due to age and education: a spherical deconvolution

tractography study. Brain Struct. Funct. 221, 1751–1766. https://doi.org/10.1007/s00429-015-1001-3

Rondina, J.M., Park, C.H., Ward, N.S., 2017. Brain regions important for recovery after severe post-stroke upper limb paresis. J. Neurol. Neurosurg. Psychiatry 88, 737–743. https://doi.org/10.1136/jnnp-2016-315030

Schulz, R., Koch, P., Zimerman, M., Wessel, M., Bönstrup, M., Thomalla, G., Cheng, B., Gerloff, C., Hummel, F.C., 2015. Parietofrontal motor pathways and their association with motor function after stroke. Brain 138, 1949–1960. https://doi.org/10.1093/brain/awv100

Scott, S.H., 2004. Optimal feedback control and the neural basis of volitional motor control. Nat. Rev. Neurosci. 5, 532–546. https://doi.org/10.1038/nrn1427

Smith, S.M., 2002. Fast robust automated brain extraction. Hum. Brain Mapp. 17, 143–155. https://doi.org/10.1002/hbm.10062

Smith, S.M., Jenkinson, M., Woolrich, M.W., Beckmann, C.F., Behrens, T.E.J., Johansen-Berg, H., Bannister, P.R., De Luca, M., Drobnjak, I., Flitney, D.E., Niazy, R.K., Saunders, J., Vickers, J., Zhang, Y., De Stefano, N., Brady, J.M., Matthews, P.M., 2004. Advances in functional and structural MR image analysis and implementation as FSL. Neuroimage 23 Suppl 1, S208-19. https://doi.org/10.1016/j.neuroimage.2004.07.051

Spampinato, M.V., Chan, C., Jensen, J.H., Helpern, J.A., Bonilha, L., Kautz, S.A., Nietert, P.J., Feng, W., 2017. Diffusional Kurtosis Imaging and Motor Outcome in Acute Ischemic Stroke. Am. J. Neuroradiol. 1–7. https://doi.org/10.3174/ajnr.A5180

Sun, S.-W., Liang, H.-F., Le, T.Q., Armstrong, R.C., Cross, A.H., Song, S.-K., 2006. Differential sensitivity of in vivo and ex vivo diffusion tensor imaging to evolving optic nerve injury in mice with retinal ischemia. Neuroimage 32, 1195–204. https://doi.org/10.1016/j.neuroimage.2006.04.212

Tábuas-Pereira, M., Freitas, S., Beato-Coelho, J., Ribeiro, J., Parra, J., Martins, C., Silva, M., Matos, M.A., Nogueira, A.R., Silva, F., Sargento-Freitas, J., Cordeiro, G., Cunha, L., Santana, I., 2018. Aphasia Rapid Test: Estudos de Tradução, Adaptação e Validação para a População Portuguesa. Acta Med. Port. 31, 265. https://doi.org/10.20344/amp.9090

Ueno, T., Saito, S., Rogers, T.T., Lambon Ralph, M.A., 2011. Lichtheim 2: Synthesizing aphasia and the neural basis of language in a neurocomputational model of the dual dorsal-ventral language pathways. Neuron 72, 385–396. https://doi.org/10.1016/j.neuron.2011.09.013

Veraart, J., Fieremans, E., Novikov, D.S., 2016a. Diffusion MRI noise mapping using random matrix theory. Magn. Reson. Med. 76, 1582–1593. https://doi.org/10.1002/mrm.26059

Veraart, J., Novikov, D.S., Christiaens, D., Ades-aron, B., Sijbers, J., Fieremans, E., 2016b. Denoising of diffusion MRI using random matrix theory. Neuroimage 142, 394–406. https://doi.org/10.1016/j.neuroimage.2016.08.016

Watila, M.M., Balarabe, B., 2015. Factors predicting post-stroke aphasia recovery. J. Neurol. Sci. 352, 12–18. https://doi.org/10.1016/j.jns.2015.03.020

Yang, Q., Tress, B.M., Barber, P. a., Desmond, P.M., Darby, D.G., Gerraty, R.P., Li, T., Davis, S.M., Barber, ; P Alan, Desmond, P.M., Darby, D.G., Gerraty, R.P., Li, T., Davis, S.M., 1999. Serial Study

of Apparent Diffusion Coefficient and Anisotropy in Patients With Acute Stroke. Stroke 30, 2382–2390. https://doi.org/10.1161/01.STR.30.11.2382

Zavanone, C., Samson, Y., Arbizu, C., Dupont, S., Dormont, D., Rosso, C., 2018. Critical brain regions related to post-stroke aphasia severity identified by early diffusion imaging are not the same when predicting short- and long-term outcome. Brain Lang. 186, 1–7. https://doi.org/10.1016/j.bandl.2018.08.005

Zhang, Y., Brady, M., Smith, S., 2001. Segmentation of brain MR images through a hidden Markov random field model and the expectation-maximization algorithm. IEEE Trans. Med. Imaging 20, 45–57. https://doi.org/10.1109/42.906424

7.3 Conclusion

The last study of the current thesis revealed two effective and simple imaging biomarkers of long-term motor and language outcome. Not only did we confirm that acute AD of the corticospinal tract is associated with chronic motor impairment, but we have demonstrated this relationship to be valid at the very early time point of 24 hours post-stroke. However, the most novel result of this investigation was the first-time report of the AD of the arcuate fasciculus as an independent predictor of chronic aphasia severity. Moreover, these tract-specific results were confirmed in a subsequent voxel-based analysis in which – without any *a priori* assumptions – white matter regions corresponding to these same fasciculi naturally emerged and remained significant even after adjusting for age, lesion volume, and initial impairment. Importantly, our results showed that damage to the corticospinal tract alone – that is, with no contribution of the initial motor deficit – was an independent predictor of motor outcome. For aphasia outcome, on the other hand, initial severity still remained a significant predictor, yet the AD of the arcuate fasciculus explained a clinically relevant increase in the variability of patient outcome. Finally, since the entire analysis – from processing the raw data to the extraction of axial diffusivity in these two fasciculi using the normalization strategy proposed in chapter 5 – was entirely automized, these biomarkers of acute damage could be easily implemented in clinical practice.

Part III

General Discussion and Conclusion

Chapter 8

Discussion, Conclusions, and Perspectives

Contents

The present thesis benefits from robust image processing techniques and a mixture of machine learning and classical statistical analyses to respond to a lack of reliable diffusion tensor imaging (DTI) biomarkers at the acute stage of stroke for long-term global, motor, and language outcome. More precisely, the objectives of the current doctoral work were threefold: (1) determine a spatial normalization strategy for diffusion MRI data of acute stroke patients that preserves anatomical overlap of crucial white matter structures, (2) assess which diffusion parameters accurately capture acute stroke damage related to long-term functional outcome, and (3) conclude whether acute ischemic damage to major white matter fasciculi, quantified with DTI, can bring to light simple and independent biomarkers of long-term motor and language outcome. Using a unique dataset to conduct the proper research to achieve these objectives, the present thesis led to three major contributions to the scientific community in the form of one publication and two submitted articles. The results of the present work strongly support the use of AD for quantifying early brain damage and also its use within crucial brain regions such as the corona radiata, the corticospinal tract, and the arcuate fasciculus for prognosis. The current discussion reviews the strengths and limitations concerning the implementation of the DTI protocol, the practicality of its use in clinical trials, and perspectives for future work.

8.1 Implementation in Clinical Practice

Above all, it is important to reflect on the remarkable dataset that drove the investigations of the current thesis: thrombolyzed patients who underwent a diffusion-weighted imaging protocol with 30 diffusion-encoding directions at the very early time point of 24 hours post-stroke. From a clinical perspective, this dataset is truly unique in its kind with respect to previously reported results. The inclusion of this imaging modality in clinical routine allowed for a large number of patients to be scanned: from September 2013 to April 2018, analyzable images and the associated behavioral evaluations from 131 patients became available, of which 69 were used in the first publication, 87 in the second, and 18 & 28 in the third in order to achieve the precise objectives of the doctoral thesis. This cohort enabled us to reliably determine a proper spatial normalization strategy to analyze not only this large cohort but any stroke cohort at any stage. Using this reliable strategy, we were able to (1) demonstrate that axial diffusivity is truly the best parameter – more than any other diffusion tensor imaging parameter – to study acute neuronal damage and (2)

propose effective biomarkers of motor and language outcome at one of the earliest moments post-stroke.

Nevertheless, the current dataset suffers from several drawbacks, the vast majority of which stem from the practical and realistic logistics of its implementation. In particular, such an imaging sequence could not overly interfere with the natural order of the emergency stroke unit of the Salpêtrière Hospital. Since thrombolyzed patients require careful monitoring of the evolution of their stroke, the DTI protocol was added to a routine imaging exam at 24 hours post-stroke already in place for this population. The use of thrombolyzed patients in the current investigations thus led to uncontrolable shortcomings. First, there was a marginally significant imbalance in left-to-right (2:1) lesions. Indeed, it has been reported that aphasic patients (mostly suffering from left-hemisphere lesions) are more likely to arrive in the therapeutic window of thrombolysis than non-aphasics[13] (which constitute almost all right-sided stroke cases). A second consequence of studying thrombolyzed patients was their long-term outcome. Since thrombolysis is an effective recanalization therapy, many of the studied patients at follow-up had few discernable deficits, slightly skewing our analyses and results towards patients with good outcome. Perhaps the largest limitation of the current thesis was the difficulty in obtaining exploitable imaging data. Indeed, while 131 analyzable images were available after the study period, 146 thrombolyzed patients during the same time window did not receive the follow-up DTI protocol (see Fig 1 in the Introduction). In fact, the MRI scanner required over 6 minutes to obtain diffusion-weighted images in all 30 directions. At 24 hours post-stroke, a large percentage of patients are disoriented or aphasic and are thus too severe to endure or remain still during the entire length of the scan. For this reason, the radiologists at our emergency stroke unit sometimes did not perform the scan after weighing the benefits and costs for patients in such a critical state. That being said, for those patients who did receive the DTI protocol, only a small percentage (6.7%) were not able to be analyzed, suggesting that incorporating this modality in clinical routine can feasibly yield useful biomarkers. In addition, despite the great feat it is to obtain DTI data in an emergency stroke unit at 24 hours post-stroke, from a purely image processing point of view, 30 diffusion-weighted directions is considered rather low according to today's standards. However, as MRI acceleration techniques continue to progress, acquiring DTI data in emergency stroke units, as is done in ours, may allow the biomarkers highlighted in this thesis to be easily incorporable in clinical trials at the hyperacute and acute stages of stroke. In fact, current MRI

scanners are now able to obtain DWI data with twice the angular resolution in half the time. Furthermore, it is important to consider that all of the predictions – from raw imaging data to a final prognosis – relied on completely automated analyses, suggesting that this practice could be easily integrated in clinical workflow.

8.2 Clinical Practicality

An important reflection of this conclusion concerns the practicality of the use of the models proposed within the current manuscript. To summarize, this thesis puts forth three particular models using day 1 AD in crucial white matter structures for predicting various outcome measures at 3 months post-stroke: (1) one for autonomy *vs.* dependence on external aid with 82.8% accuracy, (2) a second for motor outcome explaining 53.7% of the variance in outcome, and (3) a third for aphasia outcome explaining 66.6% of the variance in outcome. From a research perspective, these models are either on par with or better than those based on other imaging markers used in the literature; however, from a clinical standpoint, one can wonder whether these models are reliable enough to fulfill the major objectives of prognostic models[20]: (A) informing patients, family, caregivers, and clinicians, (B) evaluating the effectiveness of treatment, and (C) planning the future course of rehabilitation therapy. The current section serves to contemplate the clinical utility of the models of this thesis for each of these purposes with an emphasis on the repercussions of false predictions.

The models proposed in this thesis are likely most appropriate for informing patients. Indeed, informing patients and their entourage of expected outcomes is already common practice and currently relies on easily measurable clinical factors such as, initial severity, age, and lesion volume. Since these "reference" predictions are prone to high error rates, from a clinical perspective, any increase in accuracy or certainty can be considered useful and low risk. Moreover, the cost-benefit ratio of additional MRI time *vs.* the increase in prediction accuracy with respect to non-imaging clinical variables seems advantageous. In our case, for patient autonomy, while our model would correctly identify a high percentage of 82.8% of patients, 17.2% (1 out of 6) would receive an incorrect prognosis. The harm in erroneously predicting patient outcome is rather insignificant; however, care would need to be taken for such early predictions to not affect decisions regarding standard rehabilitation or patient motivation.

The use of acute AD in critical brain regions for the two remaining objectives is more nuanced. First of all, its benefit can be imagined in several situations. For example, early neuroprotective clinical trials aiming to diminish the deleterious effects of stroke – perhaps intervening at admission in an emergency stroke unit – could use measures of AD within crucial brain regions and fasciculi as early as the following day to assess their efficacy on long-term outcome. For this scenario, using our early predictive models as opposed to waiting several months to record true outcome may result in a larger sample size by reducing the dropout rate of patients. Alternatively, similar AD measures may be used as a means to stratify patients in therapeutic trials for later stages of stroke targeting those with damage to specific critical structures. Indeed, by considering expected outcomes for patients, clinicians and researchers can deduce their recovery potential and propose adaptive rehabilitative strategies. Similarly, deviations from expected outcomes *vs.* true outcome after a therapeutic trial may be used to evaluate their effectiveness. However, in all of these cases, the limitations of the implementation of our proposed models lies within the effectiveness of the trials themselves. In other words, the effect sizes of any intervention would need to exceed the non-negligible error rates in order for the biomarkers proposed in this thesis to be clinically useful. It is therefore difficult to judge the clinical relevance of early AD in crucial brain structures and whether this marker is ready to be used in clinical trials as it is case-dependent. For example, concerning our model for patient autonomy *vs.* dependence on external aid, one may envision a clinical trial aimed at improving outcome in patients who are attributed a poor prognosis. Patient inclusion would hypothetically occur at 24 hours post-stroke when all determining factors are available; however, 1 out of every 6 patients would be incorrectly placed in this group. These patients, even if they do not respond to the proposed therapy, will still evolve towards a good outcome, which could alter the preceived efficacy of the trial on a group level. With this in mind, our models – as they stand today – could be used for evaluating trial effectiveness or founding stratification strategies but should be employed with caution.

8.3 Perspectives

As discussed in the previous section, the biomarkers from the models proposed in this thesis could be tested in clinical trials. However, despite the high accuracies of our models – both absolute and relative to other studies – a non-negligible amount of

error remains. While the most obvious solution is to include more patients (possibly, from other hospital centers) to increase the certainty of our predictions, the associated error may not necessarily improve. Rather, new features are likely to account for the unexplained variability in outcome.

One promising research avenue is to include an extra follow-up imaging exam as longitudinal data are considerably more sensitive than cross-sectional measures. For instance, previous research has suggested that changes in diffusion parameters from the first to the second week post-stroke are highly predictive of long-term outcome[157]. We could therefore imagine incorporating a second scan at one week post-stroke to investigate short-term changes in AD of crucial brain structures for the prediction of long-term outcome. Scanning at the first week seems ideal also from a neurophysiological point of view since substantial changes in absolute AD occur during this time. However, a large limitation of this type of implementation would be that a prognosis would not be available before the second scan, and dropout rates may be rather high.

One crucial factor that was not taken into account in this thesis is the contribution of brain function in predicting outcome. While damage to the white matter is a large determinant of the deficits patients can experience, functional reorganization – through functional connectivity measured at rest – has been shown to play a significant role, especially for language outcome[232]. Two modalities are possible in a clinical setting: functional MRI or electroencephalography (EEG). Functional MRI is not only costly but also requires more time than DTI sequences. EEG data, on the other hand, can be easily obtained while patients are in bed. Such data could also be acquired as early as 24 hours post-stroke and benefit from automatic data processing methods, making their implementation with MRI data rather easy. The combination of structural and functional imaging methods could not only improve upon the proposed prediction models of the current thesis but also bring to light new subgroups of patients for distinct outcome profiles.

Beyond prognostic models in and of themselves, the research in the current thesis strongly emphasizes the importance of white matter pathways in patient outcome. This result alone could therefore generate new avenues for neuroprotective therapies aimed at preserving white matter following stroke. Similarly, our results also support the use of non-invasive stimulation techniques to reinforce the neuronal integrity of crucial white matter fasciculi involved in global, motor, and language outcome. While other imaging or clinical parameters may be preferred for patient stratification

or for evaluating the effectiveness of such trials, from a neuroscientific point of view, our research supports the clinical relevance of these fasciculi.

In conclusion, the research contained in the present manuscript serves to lay a foundation for quantifying early brain damage with diffusion tensor imaging. Its implementation in clinical practice is already feasible and imaginable in emergency stroke units on a large scale. Markers derived from this research should be better understood either through subsequent investigations, in clinical trials as secondary surrogate markers of hyperacute treatment effectiveness, or as a stratification tool for therapies expecting large effect sizes.

Bibliography

1. Warlow, C., Sudlow, C., Dennis, M., Wardlaw, J. & Sandercock, P. Stroke. *Lancet* **362,** 1211–1224 (2003).
2. WHO. *Global Health Estimates 2016: Disease burden by Cause, Age, Sex, by Country and by Region, 2000-2016* 2018.
3. Feigin, V. L., Norrving, B. & Mensah, G. A. Global Burden of Stroke. *Circulation Research* **120,** 439–448 (2017).
4. Benjamin, E. J. *et al.* Heart disease and stroke statistics - 2018 update: A report from the American Heart Association. *Circulation* **137,** E67–E492 (2018).
5. Bousser, M. & Mas, J. *Accidents Vasculaires Cérébraux* 61–76 (Doin Editions, 2009).
6. Phan, T. G. *et al.* Development of a new tool to correlate stroke outcome with infarct topography: A proof-of-concept study. *NeuroImage* **49,** 127–133 (2010).
7. Murphy, T. H. & Corbett, D. Plasticity during stroke recovery: From synapse to behaviour. *Nature Reviews Neuroscience* **10,** 861–872 (2009).
8. Bernhardt, J. *et al.* Agreed Definitions and a Shared Vision for New Standards in Stroke Recovery Research: The Stroke Recovery and Rehabilitation Roundtable Taskforce. *Neurorehabilitation and Neural Repair* **31,** 793–799 (2017).
9. Stinear, C. M. & Byblow, W. D. Predicting and accelerating motor recovery after stroke. *Current Opinion in Neurology* **27,** 624–630 (2014).
10. Hatem, S. M. *et al.* Rehabilitation of Motor Function after Stroke: A Multiple Systematic Review Focused on Techniques to Stimulate Upper Extremity Recovery. *Frontiers in Human Neuroscience* **10,** 1–22 (2016).
11. Katan, M. & Luft, A. Global Burden of Stroke. *Seminars in neurology* **38,** 208–211 (2018).
12. Flowers, H. L. *et al.* Poststroke Aphasia Frequency, Recovery, and Outcomes: A Systematic Review and Meta-Analysis. *Archives of Physical Medicine and Rehabilitation* **97,** 2188–2201.e8 (2016).

13. Engelter, S. T. *et al.* Epidemiology of aphasia attributable to first ischemic stroke: Incidence, severity, fluency, etiology, and thrombolysis. *Stroke* **37,** 1379–1384 (2006).

14. Flowers, H. L., Silver, F. L., Fang, J., Rochon, E. & Martino, R. The incidence, co-occurrence, and predictors of dysphagia, dysarthria, and aphasia after first-ever acute ischemic stroke. *Journal of communication disorders* **46,** 238–48 (2013).

15. Buxbaum, L. J. *et al.* Hemispatial neglect: Subtypes, neuroanatomy, and disability. *Neurology* **62,** 749–56 (2004).

16. Appelros, P., Karlsson, G. M., Seiger, Å. & Nydevik, I. Prognosis for patients with neglect and anosognosia with special reference to cognitive impairment. *Journal of Rehabilitation Medicine* **35,** 254–258 (2003).

17. Corbetta, M. *et al.* Common behavioral clusters and subcortical anatomy in stroke. *Neuron* **85,** 927–941 (2015).

18. Riestra, A. R. & Barrett, A. M. Rehabilitation of spatial neglect. *Handbook of Clinical Neurology* **110,** 347–355 (2013).

19. Boyd, L. A. *et al.* Biomarkers of stroke recovery: Consensus-based core recommendations from the Stroke Recovery and Rehabilitation Roundtable. *International Journal of Stroke* **12,** 480–493 (2017).

20. Stinear, C. M. *et al.* Proportional Motor Recovery after Stroke: Implications for Trial Design. *Stroke* **48,** 795–798 (2017).

21. Stinear, C. M., Byblow, W. D., Ackerley, S. J., Barber, P. A. & Smith, M. C. Predicting Recovery Potential for Individual Stroke Patients Increases Rehabilitation Efficiency. *Stroke* **48,** 1011–1019 (2017).

22. Rosso, C. *et al.* Contribution of corticospinal tract and functional connectivity in hand motor impairment after stroke. *PloS one* **8,** e73164 (2013).

23. Saur, D. *et al.* Dynamics of language reorganization after stroke. *Brain : a journal of neurology* **129,** 1371–84 (2006).

24. Thiebaut de Schotten, M. *et al.* Damage to White Matter Pathways in Subacute and Chronic Spatial Neglect: A Group Study and 2 Single-Case Studies with Complete Virtual "In Vivo" Tractography Dissection. *Cerebral Cortex* **24,** 691–706 (2014).

25. Hope, T. M. H. *et al.* Recovery after stroke: not so proportional after all? *Brain* **11,** 1–22 (2018).

26. Yoo, A. J. *et al.* Combining acute diffusion-weighted imaging and mean transmit time lesion volumes with National Institutes of Health Stroke Scale Score improves the prediction of acute stroke outcome. *Stroke; a journal of cerebral circulation* **41,** 1728–35 (2010).

27. Weimar, C., König, I. R., Kraywinkel, K., Ziegler, A. & Diener, H. C. Age and National Institutes of Health Stroke Scale Score within 6 hours after onset are accurate predictors of outcome after cerebral ischemia: development and external validation of prognostic models. *Stroke; a journal of cerebral circulation* **35,** 158–162 (2004).

28. Prabhakaran, S. *et al.* Inter-individual variability in the capacity for motor recovery after ischemic stroke. *Neurorehabilitation and Neural Repair* **22,** 64–71 (2008).

29. Pedersen, P. M., Vinter, K. & Olsen, T. S. Aphasia after stroke: Type, severity and prognosis: The Copenhagen aphasia study. *Cerebrovascular Diseases* **17,** 35–43 (2004).

30. Jeffers, M. S., Karthikeyan, S. & Corbett, D. Does Stroke Rehabilitation Really Matter? Part A: Proportional Stroke Recovery in the Rat. *Neurorehabilitation and Neural Repair* **32,** 3–6 (2018).

31. Kwakkel, G., Kollen, B. & Twisk, J. Impact of time on improvement of outcome after stroke. *Stroke* **37,** 2348–2353 (2006).

32. Brott, T. *et al.* Measurements of acute cerebral infarction: a clinical examination scale. *Stroke* **20,** 864–870 (1989).

33. Veerbeek, J. M., Kwakkel, G., Van Wegen, E. E., Ket, J. C. & Heymans, M. W. Early prediction of outcome of activities of daily living after stroke: A systematic review. *Stroke* **42,** 1482–1488 (2011).

34. Bang, O. Y. *et al.* Predicting the Long-Term Outcome after Subacute Stroke within the Middle Cerebral Artery Territory. *Journal of clinical neurology (Seoul, Korea)* **1,** 148–58 (2005).

35. Saposnik, G., Guzik, A. K., Reeves, M., Ovbiagele, B. & Johnston, S. C. Stroke Prognostication using Age and NIH Stroke Scale: SPAN-100. *Neurology* **80,** 21–28 (2013).

36. Le Bouc, R. *et al.* Efficacy of Endovascular Therapy in Acute Ischemic Stroke Depends on Age and Clinical Severity. *Stroke* **49,** 1686–1694 (2018).

37. Group, T. N. I. o. N. D. & rt PA Stroke Study, S. Tissue Plasminogen Activator for Acute Ischemic Stroke. *New England Journal of Medicine* **333,** 1581–1588 (1995).

38. Duncan, P. W., Goldstein, L. B., Matchar, D., Divine, G. W. & Feussner, J. Measurement of motor recovery after stroke. Outcome assessment and sample size requirements. *Stroke* **23,** 1084–1089 (1992).

39. Byblow, W. D., Stinear, C. M., Barber, P. A., Petoe, M. A. & Ackerley, S. J. Proportional recovery after stroke depends on corticomotor integrity. *Annals of Neurology* **78,** 848–859 (2015).

40. Veerbeek, J. M., Winters, C., van Wegen, E. E. & Kwakkel, G. Is the proportional recovery rule applicable to the lower limb after a first-ever ischemic stroke? *PLoS ONE* **13** (2018).

41. Lazar, R. M. *et al.* Improvement in aphasia scores after stroke is well predicted by initial severity. *Stroke* **41,** 1485–1488 (2010).

42. Winters, C., Van Wegen, E. E., Daffertshofer, A. & Kwakkel, G. Generalizability of the Maximum Proportional Recovery Rule to Visuospatial Neglect Early Poststroke. *Neurorehabilitation and Neural Repair* **31,** 334–342 (2017).

43. Krakauer, J. W. & Marshall, R. S. The proportional recovery rule for stroke revisited. *Annals of neurology* **78,** 845–7 (2015).

44. Groisser, B. N., Copen, W. a., Singhal, A. B., Hirai, K. K. & Schaechter, J. D. Corticospinal tract diffusion abnormalities early after stroke predict motor outcome. *Neurorehabilitation and neural repair* **28,** 751–60 (2014).

45. Marchina, S. *et al.* Impairment of speech production predicted by lesion load of the left arcuate fasciculus. *Stroke* **42,** 2251–2256 (2011).

46. Purves, D. *et al. Neuroscience 3rd edition* (2004).

47. Lo, R., Gitelman, D., Levy, R., Hulvershorn, J. & Parrish, T. Identification of critical areas for motor function recovery in chronic stroke subjects using voxel-based lesion symptom mapping. *NeuroImage* **49,** 9–18 (2010).

48. Schulz, R. *et al.* Assessing the integrity of corticospinal pathways from primary and secondary cortical motor areas after stroke. *Stroke* **43,** 2248–51 (2012).

49. Schulz, R. *et al.* Parietofrontal motor pathways and their association with motor function after stroke. *Brain* **138,** 1949–1960 (2015).

50. Schulz, R. *et al.* White matter integrity of premotor-motor connections is associated with motor output in chronic stroke patients. *NeuroImage: Clinical* **7,** 82–86 (2015).

51. Hoshi, E. & Tanji, J. Differential involvement of neurons in the dorsal and ventral premotor cortex during processing of visual signals for action planning. *Journal of neurophysiology* **95,** 3596–616 (2006).

52. Nachev, P., Kennard, C. & Husain, M. Functional role of the supplementary and pre-supplementary motor areas. *Nature Reviews Neuroscience* **9,** 856–869 (2008).

53. Hepp-Reymond, M. C. & Wiesendanger, M. Unilateral pyramidotomy in monkeys: Effect on force and speed of a conditioned precision grip. *Brain Research* **36,** 117–131 (1972).

54. Koch, P., Schulz, R. & Hummel, F. C. Structural connectivity analyses in motor recovery research after stroke. *Annals of Clinical and Translational Neurology* **3,** 233–244 (2016).

55. Rüber, T., Schlaug, G. & Lindenberg, R. Compensatory role of the cortico-rubrospinal tract in motor recovery after stroke. *Neurology* **79,** 515–522 (2012).

56. Lindenberg, R *et al.* Structural integrity of corticospinal motor fibers predicts motor impairment in chronic stroke. *Neurology* **74,** 280–7 (2010).

57. Schulz, R. *et al.* Synergistic but independent: The role of corticospinal and alternate motor fibers for residual motor output after stroke. *NeuroImage: Clinical* **15,** 118–124 (2017).

58. Schulz, R. *et al.* Interactions Between the Corticospinal Tract and Premotor-Motor Pathways for Residual Motor Output After Stroke. *Stroke,* STROKEAHA.117.016834 (2017).

59. Lindenberg, R., Zhu, L. L., Rüber, T. & Schlaug, G. Predicting functional motor potential in chronic stroke patients using diffusion tensor imaging. *Human Brain Mapping* **33,** 1040–51 (2012).

60. Pollock, A. *et al.* Cochrane Overview Interventions for Improving Upper Limb Function After Stroke. *Stroke* **46,** e57–e58 (2015).

61. Corbetta, M., Siegel, J. S. & Shulman, G. L. *On the low dimensionality of behavioral deficits and alterations of brain network connectivity after focal injury* 2018.

62. Beebe, J. A. & Lang, C. E. Relationships and responsiveness of six upper extremity function tests during the first six months of recovery after stroke. *Journal of Neurologic Physical Therapy* **33,** 96–103 (2009).

63. Santisteban, L. *et al.* Upper limb outcome measures used in stroke rehabilitation studies: A systematic literature review. *PLoS ONE* **11** (2016).

64. Fugl-Meyer, A. R., Jääskö, L, Leyman, I, Olsson, S & Steglind, S. The post-stroke hemiplegic patient. 1. a method for evaluation of physical performance. *Scandinavian journal of rehabilitation medicine* **7,** 13–31 (1975).

65. See, J. *et al.* A standardized approach to the Fugl-Meyer assessment and its implications for clinical trials. *Neurorehabilitation and Neural Repair* **27,** 732–741 (2013).

66. Kwakkel, G. *et al.* Standardized measurement of sensorimotor recovery in stroke trials: Consensus-based core recommendations from the Stroke Recovery and Rehabilitation Roundtable. *International journal of stroke : official journal of the International Stroke Society* **12,** 451–461 (2017).

67. Yelnik, A. P. *et al.* AMOBES (Active Mobility Very Early After Stroke). *Stroke* **48,** 400–405 (2017).

68. Jebsen, R. H., Taylor, N, Trieschmann, R. B., Trotter, M. J. & Howard, L. A. *An objective and standardized test of hand function.* 1969.

69. Fridriksson, J. *et al.* Anatomy of aphasia revisited. *Brain : a journal of neurology* **141,** 848–862 (2018).

70. Price, C. J. A review and synthesis of the first 20years of PET and fMRI studies of heard speech, spoken language and reading. *NeuroImage* **62,** 816–847 (2012).

71. Dick, A. S. & Tremblay, P. Beyond the arcuate fasciculus: consensus and controversy in the connectional anatomy of language. *Brain : a journal of neurology* **135,** 3529–50 (2012).

72. Dick, A. S., Bernal, B. & Tremblay, P. The language connectome: New pathways, new concepts. *Neuroscientist* **20,** 453–467 (2014).

73. Tremblay, P. & Dick, A. S. Broca and Wernicke are dead, or moving past the classic model of language neurobiology. *Brain and Language* **162,** 60–71 (2016).

74. Broca, P. Localisation des fonctions cérébrales. *Bulletin of the Society of Anthropology (Paris)* **4,** 200–203 (1863).

75. Wernicke, C. Lehrbuch der gehirnkrankheiten fur aerzte und studirende. *Kassel Theodor Fischer* **2,** 229–242 (1881).

76. Geschwind, N. Disconnexion syndromes in animals and man. I. *Brain : a journal of neurology* **88,** 237–94 (1965).

77. Geschwind, N. Disconnexion syndromes in animals and man. II. *Brain : a journal of neurology* **88,** 585–644 (1965).

78. Hickok, G. & Poeppel, D. The cortical organization of speech processing. *Nature reviews. Neuroscience* **8,** 393–402 (2007).

79. Martino, J. *et al.* Cortex-sparing fiber dissection: An improved method for the study of white matter anatomy in the human brain. *Journal of Anatomy* **219,** 531–541 (2011).

80. Glasser, M. F. & Rilling, J. K. DTI tractography of the human brain's language pathways. *Cerebral Cortex* **18,** 2471–2482 (2008).

81. Bernal, B. & Ardila, A. *The role of the arcuate fasciculus in conduction aphasia* 2009.

82. Bernal, B. & Altman, N. The connectivity of the superior longitudinal fasciculus: A tractography DTI study. *Magnetic Resonance Imaging* **28,** 217–225 (2010).

83. Catani, M. & Thiebaut de Schotten, M. A diffusion tensor imaging tractography atlas for virtual in vivo dissections. *Cortex; a journal devoted to the study of the nervous system and behavior* **44,** 1105–32 (2008).

84. Hau, J. *et al.* Cortical Terminations of the Inferior Fronto-Occipital and Uncinate Fasciculi: Anatomical Stem-Based Virtual Dissection. *Frontiers in Neuroanatomy* **10,** 1–14 (2016).

85. Ffytche, D. H. & Catani, M. Beyond localization: from hodology to function. *Philosophical transactions of the Royal Society of London. Series B, Biological sciences* **360,** 767–779 (2005).

86. Yagmurlu, K, Middlebrooks, E. H., Tanriover, N & Rhoton Jr., A. L. Fiber tracts of the dorsal language stream in the human brain. *J Neurosurg*, 1–10 (2015).

87. Sarubbo, S., De Benedictis, A., Maldonado, I. L., Basso, G. & Duffau, H. Frontal terminations for the inferior fronto-occipital fascicle: Anatomical dissection, DTI study and functional considerations on a multi-component bundle. *Brain Structure and Function* **218,** 21–37 (2013).

88. Saygin, Z. M. *et al.* Anatomical connectivity patterns predict face selectivity in the fusiform gyrus. *Nature neuroscience* **15,** 321–7 (2012).

89. Osher, D. E. *et al.* Structural Connectivity Fingerprints Predict Cortical Selectivity for Multiple Visual Categories across Cortex. *Cerebral Cortex* **26,** 1668–1683 (2016).

90. Saygin, Z. M. *et al.* Connectivity precedes function in the development of the visual word form area. *Nature neuroscience* **19,** 1250–5 (2016).

91. Ueno, T., Saito, S., Rogers, T. T. & Lambon Ralph, M. A. Lichtheim 2: Synthesizing aphasia and the neural basis of language in a neurocomputational model of the dual dorsal-ventral language pathways. *Neuron* **72,** 385–396 (2011).

92. Roelofs, A. A dorsal-pathway account of aphasic language production: The WEAVER++/ARC model. *Cortex* **59,** 33–48 (2014).

93. Duffau, H., Moritz-Gasser, S. & Mandonnet, E. A re-examination of neural basis of language processing: Proposal of a dynamic hodotopical model from data provided by brain stimulation mapping during picture naming. *Brain and Language* **131,** 1–10 (2014).

94. Fridriksson, J. *et al.* Revealing the dual streams of speech processing. *Proceedings of the National Academy of Sciences* **113,** 15108–15113 (2016).

95. Geschwind, N. The organization of language and the brain. *Science (New York, N.Y.)* **170,** 940–4 (1970).

96. Catani, M. The rises and falls of disconnection syndromes. *Brain* **128,** 2224–2239 (2005).

97. Martino, J., Brogna, C., Robles, S. G., Vergani, F. & Duffau, H. Anatomic dissection of the inferior fronto-occipital fasciculus revisited in the lights of brain stimulation data. *Cortex* **46,** 691–699 (2010).

98. Von Der Heide, R. J., Skipper, L. M., Klobusicky, E. & Olson, I. R. Dissecting the uncinate fasciculus: Disorders, controversies and a hypothesis. *Brain* **136,** 1692–1707 (2013).

99. Duffau, H. Stimulation mapping of white matter tracts to study brain functional connectivity. *Nature Reviews Neurology* **11,** 255–265 (2015).

100. Catani, M., Jones, D. K. & Ffytche, D. H. Perisylvian language networks of the human brain. *Annals of Neurology* **57,** 8–16 (2005).

101. Hillis, A. E. *et al.* Predicting recovery in acute poststroke aphasia. *Annals of Neurology* **83,** 612–622 (2018).

102. Turken, U & Dronkers, N. F. The neural architecture of the language comprehension network: converging evidence from lesion and connectivity analyses. *Frontiers in systems neuroscience* **5,** 1 (2011).

103. Rosso, C. *et al.* Aphasia severity in chronic stroke patients: a combined disconnection in the dorsal and ventral language pathways. *Neurorehabilitation and neural repair* **29,** 287–95 (2015).

104. Griffis, J. C., Nenert, R., Allendorfer, J. B. & Szaflarski, J. P. Damage to white matter bottlenecks contributes to language impairments after left hemispheric stroke. *NeuroImage: Clinical* **14,** 552–565 (2017).

105. El Hachioui, H. *et al.* Screening tests for aphasia in patients with stroke: a systematic review. *Journal of Neurology* **264,** 211–220 (2017).

106. Butler, R. A., Lambon Ralph, M. A. & Woollams, A. M. Capturing multidimensionality in stroke aphasia: mapping principal behavioural components to neural structures. *Brain* **137,** 3248–3266 (2014).

107. Goodglass, H., & Kaplan, E. in *Boston diagnostic aphasia examination booklet* (1983).

108. Azuar, C *et al.* The Aphasia Rapid Test: an NIHSS-like aphasia test. *Journal of neurology* **260,** 2110–7 (2013).

109. Lyden, P. Using the National Institutes of Health Stroke Scale. *Stroke* **48,** 513–519 (2017).

110. Cheng, B. *et al.* Influence of stroke infarct location on functional outcome measured by the modified rankin scale. *Stroke* **45,** 1695–1702 (2014).

111. Wu, O. *et al.* Role of Acute Lesion Topography in Initial Ischemic Stroke Severity and Long-Term Functional Outcomes. *Stroke* **46,** 2438–2444 (2015).

112. Rosso, C. *et al.* Tissue at risk in the deep middle cerebral artery territory is critical to stroke outcome. *Neuroradiology* **53,** 763–71 (2011).

113. Ernst, M. *et al.* Impact of Ischemic Lesion Location on the mRS Score in Patients with Ischemic Stroke: A Voxel-Based Approach. *AJNR. American journal of neuroradiology,* 1–6 (2018).

114. Cuingnet, R. *et al.* Spatial regularization of SVM for the detection of diffusion alterations associated with stroke outcome. *Medical Image Analysis* **15,** 729–737 (2011).

115. Rosso, C. *et al.* Hyperglycaemia, Insulin Therapy and Critical Penumbral Regions for Prognosis in Acute Stroke: Further Insights from the INSULINFARCT Trial. *PloS one* **10,** e0120230 (2015).

116. Duncan, P. W., Jorgensen, H. S. & Wade, D. T. Outcome measures in acute stroke trials: a systematic review and some recommendations to improve practice. *Stroke* **31,** 1429–38 (2000).

117. Broderick, J. P., Adeoye, O. & Elm, J. Evolution of the Modified Rankin Scale and Its Use in Future Stroke Trials. *Stroke* **48,** 2007–2012 (2017).

118. Assaf, Y., Johansen-Berg, H. & Thiebaut de Schotten, M. The role of diffusion MRI in neuroscience. *NMR in Biomedicine,* e3762 (2017).

119. Le Bihan, D. & Breton, E. *Imagerie de diffusion in-vivo par résonance magnetique nucléaire* 1985.

120. Basser, P. J., Mattiello, J & LeBihan, D. Estimation of the effective self-diffusion tensor from the NMR spin echo. *Journal of magnetic resonance. Series B* **103,** 247–54 (1994).

121. Bastiani, M. & Roebroeck, A. Unraveling the multiscale structural organization and connectivity of the human brain: the role of diffusion MRI. *Frontiers in Neuroanatomy* **9,** 1–15 (2015).

122. Bihan, D. L. Molecular diffusion, tissue microdynamics and microstructure. *NMR in Biomedicine* **8,** 375–386 (1995).

123. Le Bihan, D. Looking into the functional architecture of the brain with diffusion MRI. *Nature Reviews Neuroscience* **4,** 469–480 (2003).

124. Le Bihan, D. & Van Zijl, P. From the diffusion coefficient to the diffusion tensor. *NMR in Biomedicine* **15,** 431–434 (2002).

125. Bihan, D. L. & Johansen-Berg, H. Diffusion MRI at 25 : Exploring brain tissue structure and function Diffusion MRI principles. *Neuroimage* **61,** 324–341 (2012).

126. Uluğ, A. M., Beauchamp, N., Bryan, R. N. & Van Zijl, P. C. Absolute quantitation of diffusion constants in human stroke. *Stroke* **28,** 483–490 (1997).

127. Basser, P. J. Inferring microstructural features and the physiological state of tissues from diffusion-weighted images. *NMR in biomedicine* **8,** 333–44 (1995).

128. Beaulieu, C. The basis of anisotropic water diffusion in the nervous system - a technical review. *NMR in biomedicine* **15,** 435–55 (2002).

129. Chong, J *et al.* Diffusion-weighted MR of acute cerebral infarction: comparison of data processing methods. *AJNR. American journal of neuroradiology* **19,** 1733–9 (1998).

130. Pierpaoli, C., Jezzard, P, Basser, P. J., Barnett, A & Di Chiro, G. Diffusion tensor MR imaging of the human brain. *Radiology* **201,** 637–48 (1996).

131. Sharman, M. A. *et al.* Impact of outliers on diffusion tensor and Q-ball imaging: Clinical implications and correction strategies. *Journal of Magnetic Resonance Imaging* **33,** 1491–1502 (2011).

132. Jeurissen, B., Leemans, A., Tournier, J. D., Jones, D. K. & Sijbers, J. Investigating the prevalence of complex fiber configurations in white matter tissue with diffusion magnetic resonance imaging. *Human Brain Mapping* **34,** 2747–2766 (2013).

133. Volz, L. J., Cieslak, M. & Grafton, S. T. A probabilistic atlas of fiber crossings for variability reduction of anisotropy measures. *Brain Structure and Function* **223,** 635–651 (2018).

134. Dubois, J *et al.* The early development of brain white matter: a review of imaging studies in fetuses, newborns and infants. *Neuroscience* **276,** 48–71 (2014).

135. Jones, D. K., Knösche, T. R. & Turner, R. White matter integrity, fiber count, and other fallacies: the do's and don'ts of diffusion MRI. *NeuroImage* **73,** 239–54 (2013).

136. Dell'Acqua, F. & Tournier, J. D. Modelling white matter with spherical deconvolution: How and why? *NMR in Biomedicine,* 1–18 (2018).

137. Tournier, J.-D. D., Calamante, F., Gadian, D. G. & Connelly, A. Direct estimation of the fiber orientation density function from diffusion-weighted MRI data using spherical deconvolution. *NeuroImage* **23,** 1176–1185 (2004).

138. Tournier, J. D., Calamante, F. & Connelly, A. Determination of the appropriate b value and number of gradient directions for high-angular-resolution diffusion-weighted imaging. *NMR in Biomedicine* **26,** 1775–1786 (2013).

139. Jeurissen, B., Descoteaux, M., Mori, S. & Leemans, A. Diffusion MRI fiber tractography of the brain. *NMR in biomedicine,* 1–22 (2017).

140. Mukherjee, P, Berman, J. I., Chung, S. W., Hess, C. P. & Henry, R. G. Diffusion tensor MR imaging and fiber tractography: theoretic underpinnings. *AJNR. American journal of neuroradiology* **29,** 632–41 (2008).

141. Tournier, J.-D., , F. Calamante & a. Connelly. Improved probabilistic streamlines tractography by 2 nd order integration over fibre orientation distributions. *Ismrm* **88,** 2010 (2010).

142. Cox, S. R. *et al.* Ageing and brain white matter structure in 3,513 UK Biobank participants. *Nature Communications* **7,** 1–13 (2016).

143. Alexander, A. L., Lee, J. E., Lazar, M. & Field, A. S. Diffusion Tensor Imaging of the Brain. *Neurotherapeutics* **4,** 316–329 (2007).

144. Bennett, I. J., Madden, D. J., Vaidya, C. J., Howard, D. V. & Howard, J. H. Age-related differences in multiple measures of white matter integrity: A diffusion tensor imaging study of healthy aging. *Human Brain Mapping* **31,** 378–390 (2010).

145. Liang, D., Bhatta, S., Gerzanich, V. & Simard, J. M. Cytotoxic edema: mechanisms of pathological cell swelling. *Neurosurgical focus* **22,** E2 (2007).

146. Liu, Y. *et al.* Serial diffusion tensor MRI after transient and permanent cerebral ischemia in nonhuman primates. *Stroke* **38,** 138–145 (2007).

147. Pitkonen, M. *et al.* Long-term evolution of diffusion tensor indices after temporary experimental ischemic stroke in rats. *Brain Research* **1445,** 103–110 (2012).

148. Bhagat, Y. a. *et al.* The relationship between diffusion anisotropy and time of onset after stroke. *Journal of cerebral blood flow and metabolism : official journal of the International Society of Cerebral Blood Flow and Metabolism* **26,** 1442–50 (2006).

149. Kambiz Nael *et al.* White Matter Ischemic Changes in Hyperacute Ischemic Stroke. *Stroke* **46,** 413–418 (2015).

150. Bhagat, Y. a. *et al.* Elevations of diffusion anisotropy are associated with hyperacute stroke: a serial imaging study. *Magnetic resonance imaging* **26,** 683–93 (2008).

151. Yang, Q. *et al.* Serial Study of Apparent Diffusion Coefficient and Anisotropy in Patients With Acute Stroke. *Stroke* **30,** 2382–2390 (1999).

152. Sun, S.-W. *et al.* Differential sensitivity of in vivo and ex vivo diffusion tensor imaging to evolving optic nerve injury in mice with retinal ischemia. *NeuroImage* **32,** 1195–204 (2006).

153. Muñoz Maniega, S. *et al.* Temporal evolution of water diffusion parameters is different in grey and white matter in human ischaemic stroke. *Journal of Neurology, Neurosurgery and Psychiatry* **75,** 1714–1718 (2004).

154. Schlaug, G, Siewert, B, Benfield, a, Edelman, R. R. & Warach, S. Time course of the apparent diffusion coefficient (ADC) abnormality in human stroke. *Neurology* **49,** 113–9 (1997).

155. Schwamm, L. H. *et al.* Time course of lesion development in patients with acute stroke: serial diffusion- and hemodynamic-weighted magnetic resonance imaging. *Stroke; a journal of cerebral circulation* **29,** 2268–76 (1998).

156. Lansberg, M. G. *et al.* Evolution of apparent diffusion coefficient, diffusion-weighted, and T2-weighted signal intensity of acute stroke. *AJNR. American journal of neuroradiology* **22,** 637–44 (2001).

157. Yu, C. *et al.* A longitudinal diffusion tensor imaging study on Wallerian degeneration of corticospinal tract after motor pathway stroke. *NeuroImage* **47,** 451–8 (2009).

158. Waller, A. Experiments on the Section of the Glossopharyngeal and Hypoglossal Nerves of the Frog, and Observations of the Alterations Produced Thereby in the Structure of Their Primitive Fibres. *Philosophical Transactions of the Royal Society of London* **140,** 423–429 (1850).

159. Doughty, C. *et al.* Detection and Predictive Value of Fractional Anisotropy Changes of the Corticospinal Tract in the Acute Phase of a Stroke. *Stroke* **47,** 1520–1526 (2016).

160. Thomalla, G. *et al.* Diffusion tensor imaging detects early Wallerian degeneration of the pyramidal tract after ischemic stroke. *NeuroImage* **22,** 1767–74 (2004).

161. DeVetten, G. *et al.* Acute corticospinal tract Wallerian degeneration is associated with stroke outcome. *Stroke; a journal of cerebral circulation* **41,** 751–6 (2010).

162. Liu, G. *et al.* Axial diffusivity changes in the motor pathway above stroke foci and functional recovery after subcortical infarction. *Restorative Neurology and Neuroscience* **36,** 173–182 (2018).

163. Stinear, C. M. *et al.* Functional potential in chronic stroke patients depends on corticospinal tract integrity. *Brain : a journal of neurology* **130,** 170–80 (2007).

164. Park, C.-H., Kou, N., Boudrias, M.-H., Playford, E. D. & Ward, N. S. Assessing a standardised approach to measuring corticospinal integrity after stroke with DTI. *NeuroImage. Clinical* **2,** 521–33 (2013).

165. Vargas, P. *et al.* Assessment of corticospinal tract (CST) damage in acute stroke patients: comparison of tract-specific analysis versus segmentation of a CST template. *Journal of magnetic resonance imaging : JMRI* **37,** 836–45 (2013).

166. Radlinska, B *et al.* Diffusion tensor imaging, permanent pyramidal tract damage, and outcome in subcortical stroke. *Neurology* **75,** 1048–54 (2010).

167. Bonilha, L., Rorden, C. & Fridriksson, J. Assessing the clinical effect of residual cortical disconnection after ischemic strokes. *Stroke* **45,** 988–993 (2014).

168. Yourganov, G., Fridriksson, J., Rorden, C., Gleichgerrcht, E. & Bonilha, L. Multivariate Connectome-Based Symptom Mapping in Post-Stroke Patients: Networks Supporting Language and Speech. *The Journal of Neuroscience* **36,** 6668–6679 (2016).

169. Peters, D. M. *et al.* Cortical disconnection of the ipsilesional primary motor cortex is associated with gait speed and upper extremity motor impairment in chronic left hemispheric stroke. *Human Brain Mapping* **39,** 120–132 (2018).

170. Zhu, L. L., Lindenberg, R., Alexander, M. P. & Schlaug, G. Lesion load of the corticospinal tract predicts motor impairment in chronic stroke. *Stroke; a journal of cerebral circulation* **41,** 910–5 (2010).

171. Petoe, M. A. *et al.* A template-based procedure for determining white matter integrity in the internal capsule early after stroke. *NeuroImage: Clinical* **4,** 695–700 (2014).

172. Hirai, K. K., Groisser, B. N., Copen, W. A., Singhal, A. B. & Schaechter, J. D. Comparing prognostic strength of acute corticospinal tract injury measured by a new diffusion tensor imaging based template approach versus common approaches. *Journal of Neuroscience Methods* **257,** 204–213 (2016).

173. Chen, J. L. & Schlaug, G. Resting state interhemispheric motor connectivity and white matter integrity correlate with motor impairment in chronic stroke. *Frontiers in Neurology* **4 NOV,** 1–7 (2013).

174. Hua, K. *et al.* Tract probability maps in stereotaxic spaces: Analyses of white matter anatomy and tract-specific quantification. *NeuroImage* **39,** 336–347 (2008).

175. Varentsova, A., Zhang, S. & Arfanakis, K. Development of a high angular resolution diffusion imaging human brain template. *NeuroImage* **91,** 177–186 (2014).

176. Raffelt, D. *et al.* Symmetric diffeomorphic registration of fibre orientation distributions. *NeuroImage* **56,** 1171–1180 (2011).

177. Zhang, Y. *et al.* Atlas-guided tract reconstruction for automated and comprehensive examination of the white matter anatomy. *NeuroImage* **52,** 1289–1301 (2010).

178. Zhang, S. & Arfanakis, K. Role of standardized and study-specific human brain diffusion tensor templates in inter-subject spatial normalization. *Journal of magnetic resonance imaging : JMRI* **37,** 372–81 (2013).

179. Mori, S. *et al.* Stereotaxic white matter atlas based on diffusion tensor imaging in an ICBM template. *NeuroImage* **40,** 570–82 (2008).

180. Avants, B. B. *et al.* A reproducible evaluation of ANTs similarity metric performance in brain image registration. *NeuroImage* **54,** 2033–2044 (2011).

181. Rondina, J. M., Park, C.-h. H. & Ward, N. S. Brain regions important for recovery after severe post-stroke upper limb paresis. *Journal of Neurology, Neurosurgery and Psychiatry* **88,** 737–743 (2017).

182. Friston, K. in *Statistical Parametric Mapping: The Analysis of Functional Brain Images* 10–31 (2007). arXiv: 1802.08624.

183. Mateos-Pérez, J. M. *et al.* Structural neuroimaging as clinical predictor: A review of machine learning applications. *NeuroImage: Clinical* **20,** 506–522 (2018).

184. Abraham, A. *et al.* Machine learning for neuroimaging with scikit-learn. *Frontiers in Neuroinformatics* **8,** 1–10 (2014).

185. Varoquaux, G. *et al.* Assessing and tuning brain decoders: Cross-validation, caveats, and guidelines. *NeuroImage* **145,** 166–179 (2017).

186. Price, C. J., Hope, T. M. & Seghier, M. L. Ten problems and solutions when predicting individual outcome from lesion site after stroke. *NeuroImage* **145,** 200–208 (2017).

187. Varoquaux, G. Cross-validation failure: Small sample sizes lead to large error bars. *NeuroImage* **180,** 68–77 (2018).

188. Archer, D. B., Patten, C. & Coombes, S. A. Free-water and free-water corrected fractional anisotropy in primary and premotor corticospinal tracts in chronic stroke. *Human Brain Mapping* **4562,** 4546–4562 (2017).

189. Kunimatsu, A. *et al.* Three-dimensional white matter tractography by diffusion tensor imaging in ischaemic stroke involving the corticospinal tract. *Neuroradiology* **45,** 532–535 (2003).

190. Newton, J. M. *et al.* Non-invasive mapping of corticofugal fibres from multiple motor areas - Relevance to stroke recovery. *Brain* **129,** 1844–1858 (2006).

191. Phan, T. G. *et al.* Impact of corticofugal fibre involvement in subcortical stroke. *BMJ Open* **3** (2013).

192. Zhang, H., Yushkevich, P. a., Alexander, D. C. & Gee, J. C. Deformable registration of diffusion tensor MR images with explicit orientation optimization. *Medical image analysis* **10,** 764–85 (2006).

193. Wang, Y. *et al.* DTI registration in atlas based fiber analysis of infantile Krabbe disease. *NeuroImage* **55,** 1577–86 (2011).

194. Brett, M. Spatial Normalization of Brain Images with Focal Lesions Using Cost Function Masking. *NeuroImage* **14,** 486–500 (2001).

195. Renard, F., Urvoy, M. & Jaillard, A. in *MICCAI, Brain lesion workshop* 91–103 (2016).

196. Ripollés, P *et al.* Analysis of automated methods for spatial normalization of lesioned brains. *NeuroImage* **60,** 1296–1306 (2012).

197. Andersen, S. M., Rapcsak, S. Z. & Beeson, P. M. Cost function masking during normalization of brains with focal lesions: Still a necessity? *NeuroImage* **53,** 78–84 (2010).

198. Nachev, P., Coulthard, E., Jäger, H. R., Kennard, C. & Husain, M. Enantiomorphic normalization of focally lesioned brains. *NeuroImage* **39,** 1215–1226 (2008).

199. Van Gelderen, P. *et al.* Water diffusion and acute stroke. *Magnetic Resonance in Medicine* **31,** 154–163 (1994).

200. Thijs, V. N. *et al.* Is early ischemic lesion volume on diffusion-weighted imaging an independent predictor of stroke outcome? A multivariable analysis. *Stroke* **31,** 2597–2602 (2000).

201. Johnston, K. C. *et al.* Validation of an acute ischemic stroke model: does diffusion-weighted imaging lesion volume offer a clinically significant improvement in prediction of outcome? *Stroke; a journal of cerebral circulation* **38,** 1820–5 (2007).

202. Johnston, K. C., Barrett, K. M., Ding, Y. H. & Wagner, D. P. Clinical and imaging data at 5 days as a surrogate for 90-day outcome in ischemic stroke. *Stroke; a journal of cerebral circulation* **40,** 1332–3 (2009).

203. Habegger, S. *et al.* Relating Acute Lesion Loads to Chronic Outcome in Ischemic Stroke–An Exploratory Comparison of Mismatch Patterns and Predictive Modeling. *Frontiers in Neurology* **9,** 737 (2018).

204. Ramsey, L. E. *et al.* Behavioural clusters and predictors of performance during recovery from stroke. *Nature Human Behaviour* **1,** 0038 (2017).

205. Watila, M. M. & Balarabe, B. Factors predicting post-stroke aphasia recovery. *Journal of the Neurological Sciences* **352,** 12–18 (2015).

206. Feng, W. *et al.* Corticospinal tract lesion load: An imaging biomarker for stroke motor outcomes. *Annals of Neurology* **78,** 860–870 (2015).

207. Etherton, M. R., Rost, N. S. & Wu, O. Infarct topography and functional outcomes. *Journal of Cerebral Blood Flow and Metabolism* **38,** 1517–1532 (2018).

208. Sperber, C. & Karnath, H. O. Topography of acute stroke in a sample of 439 right brain damaged patients. *NeuroImage: Clinical* **10,** 124–128 (2016).

209. Lövblad, K. O. *et al.* Ischemic lesion volumes in acute stroke by diffusion-weighted magnetic resonance imaging correlate with clinical outcome. *Annals of Neurology* **42,** 164–170 (1997).

210. Gaudinski, M. R. *et al.* Establishing final infarct volume: Stroke lesion evolution past 30 days is insignificant. *Stroke* **39,** 2765–2768 (2008).

211. Geva, S., Baron, J. C., Jones, P. S., Price, C. J. & Warburton, E. A. A comparison of VLSM and VBM in a cohort of patients with post-stroke aphasia. *NeuroImage: Clinical* **1,** 37–47 (2012).

212. Pillay, S. B., Binder, J. R., Humphries, C., Gross, W. L. & Book, D. S. Lesion localization of speech comprehension deficits in chronic aphasia (2017).

213. Seghier, M. L. *et al.* The PLORAS Database: A data repository for Predicting Language Outcome and Recovery After Stroke. *NeuroImage* **124,** 1208–1212 (2016).

214. Karnath, H. O. & Rennig, J. Investigating structure and function in the healthy human brain: validity of acute versus chronic lesion-symptom mapping. *Brain Structure and Function* **222,** 2059–2070 (2017).

215. Liu, G. *et al.* Motor Recovery Prediction With Clinical Assessment and Local Diffusion Homogeneity After Acute Subcortical Infarction. *Stroke* (2017).

216. Wang, P. *et al.* Development and validation of a deep-learning algorithm for the detection of polyps during colonoscopy. *Nature Biomedical Engineering* **2,** 741–748 (2018).

217. Takenobu, Y. *et al.* Motor recovery and microstructural change in rubro-spinal tract in subcortical stroke. *NeuroImage. Clinical* **4,** 201–8 (2014).

218. Henseler, I., Regenbrecht, F. & Obrig, H. Lesion correlates of patholinguistic profiles in chronic aphasia: Comparisons of syndrome-, modality-and symptom-level assessment. *Brain* **137,** 918–930 (2014).

219. Kümmerer, D. *et al.* Damage to ventral and dorsal language pathways in acute aphasia. *Brain : a journal of neurology* **136,** 619–629 (2013).

220. Cloutman, L. *et al.* Where (in the brain) do semantic errors come from? *Cortex* **45,** 641–649 (2009).

221. Fridriksson, J. Preservation and modulation of specific left hemisphere regions is vital for treated recovery from anomia in stroke. *The Journal of neuroscience : the official journal of the Society for Neuroscience* **30,** 11558–64 (2010).

222. Payabvash, S., Taleb, S. & Qureshi, A. I. Cerebral regions preserved by successful endovascular recanalization of acute M1 segment occlusions: A voxel based analysis. *British Journal of Radiology* **90** (2017).

223. Munsch, F. *et al.* Stroke location is an independent predictor of cognitive outcome. *Stroke* **47,** 66–73 (2016).

224. Fridriksson, J., Guo, D., Fillmore, P., Holland, A. & Rorden, C. Damage to the anterior arcuate fasciculus predicts non-fluent speech production in aphasia. *Brain* **136,** 3451–3460 (2013).

225. Basilakos, A. *et al.* Regional White Matter Damage Predicts Speech Fluency in Chronic Post-Stroke Aphasia. *Frontiers in Human Neuroscience* **8,** 1–9 (2014).

226. Geva, S., Correia, M. M. & Warburton, E. A. Contributions of bilateral white matter to chronic aphasia symptoms as assessed by diffusion tensor MRI. *Brain and Language* **150,** 117–128 (2015).

227. Zavanone, C. *et al.* Critical brain regions related to post-stroke aphasia severity identified by early diffusion imaging are not the same when predicting short- and long-term outcome. *Brain and Language* **186,** 1–7 (2018).

228. Forkert, N. D. *et al.* Multiclass support vector machine-based lesion mapping predicts functional outcome in ischemic stroke patients. *PLoS ONE* **10** (2015).

229. Payabvash, S., Taleb, S., Benson, J. C. & Mckinney, A. M. Acute Ischemic Stroke Infarct Topology : Association with and Discharge. *American Journal of Neuroradiology* **38,** [Epub ahead of print] (2017).

230. Rosso, C. *et al.* Early ADC changes in motor structures predict outcome of acute stroke better than lesion volume. *Journal of neuroradiology. Journal de neuroradiologie* **38,** 105–12 (2011).

231. Moulton, E. *et al.* Axial diffusivity of the corona radiata at 24 hours post-stroke: A new biomarker for motor and global outcome. *PLoS ONE* **10,** 1–16 (2015).

232. Siegel, J. S. *et al.* Disruptions of network connectivity predict impairment in multiple behavioral domains after stroke. *Proceedings of the National Academy of Sciences of the United States of America* **113,** E4367–76 (2016).

Appendix A

Fugl-Meyer Arm Motor Assessment

Echelle de Fugl-Meyer

A. Epaule/ Coude/ Avant-bras en position assise

I. Motricité volontaire en synergie

a. Synergie en flexion : porter la main à l'oreille ipsi-latérale avec l'avant-bras en supination, le coude en flexion, et l'épaule en abduction à 90°, rotation externe, rétropulsion et élévation.

Epaule	Rétropulsion	_____
	Elévation	_____
	Abduction	_____
	Rotation externe	_____
Coude	Flexion	_____
Avant-bras	Supination	_____

b. Synergie en extension de la position ci-dessus, porter la main en direction du genou coté sain avec l'épaule en rotation interne et adduction, le coude en extension, l'avant-bras en pronation.

Epaule	Adduction/rotation int	_____
Coude	Extension	_____
Avant-bras	Pronation	_____

0 = non effectué
1 = partiellement effectué
2 = complètement effectué

Total (max = 18) _____

II. Motricité volontaire associant des synergies en flexion et en extension

a. Main/lombes _____

0 = non effectué
1 = dépasse l'épine iliaque
2 = complètement effectué

b. Flexion de l'épaule de 0° à 90° _____

(coude en extension complète et avant-bras en pronation/supination neutre)

0 = bras en abduction et coude fléchi dès le début du mouvement
1 = bras en abduction et coude fléchi en cours de mouvement
2= complètement effectué

c. Prono-supination de l'avant-bras _____

(épaule à 0° de flexion et coude en flexion à 90°)

0 = position d'épaule et de coude incorrecte et/ou aucune prono-supination
1 = position d'épaule et de coude correcte mais prono-supination limitée
2 = complètement effectué

Total (max = 6) _____

III. Motricité volontaire avec peu ou pas de synergies

a. Abduction d'épaule de 0° à 90) _____

(coude en extension complète, avant bras en pronation)

0 = flexion du coude ou perte de la pronation dès le début du mouvement

1 = abduction partielle, ou perte de l'extension du coude, ou de la pronation en cours de mouvement

2 = complètement effectué

b. Flexion de l'épaule de 90° à 180° _____

(coude en extension complète et avant bras en position neutre)

0 = bras en abduction ou coude fléchi dès le début du mouvement

1 = bras en abduction ou coude fléchi en cours de mouvement

2 = complètement effectué

c. Prono-supination de l'avant-bras _____

(épaule entre 30° et 90° de flexion et coude en extension complète)

0 = position d'épaule et de coude incorrecte et/ou aucun prono-supination

1 = position d'épaule et de coude correcte mais prono-supination limitée

2 = complètement effectué

Total (max = 6)_____

B. Poignet

I. Stabilité du poignet : _____
Maintenir le poignet en dorsiflexion à 15°
(épaule à 0° de flexion, coude à 90° de flexion et avant-bras en pronation)

0 = ne peut amener le poignet à 15° de dorsiflexion
1 = atteint 15° de dorsiflexion mais ne peut maintenir cette position contre résistance
2 = atteint 15° de dorsiflexion et peut maintenir cette position contre certaine (légère) résistance

II. Flexion/extension de poignet : _____
Mouvements répétés de flexion/extension dans toute l'amplitude avec la position d'épaule et de coude décrite en I (l'avant-bras peut être soutenu)

0 = pas de mouvement volontaire
1 = mouvement possible mais pas dans toute l'amplitude
2= mouvement complètement effectué

III. Stabilité du poignet : _____
Maintenir le poignet en dorsiflexion à 15° (épaule en flexion et/ou abduction, coude en extension complète et avant-bras en pronation ; le bras peut être soutenu)

0 = ne peut pas amener le poignet à 15° de dorsiflexion
1 = atteint 15° de dorsiflexion mais ne peut maintenir cette position contre résistance
2 = atteint 15° de dorsiflexion et peut maintenir cette position contre une certaine (légère) résistance.

IV. Flexion/extension de poignet : _____
Mouvements répétés de flexion/extension dans toute l'amplitude avec la position d'épaule et de coude décrite en III.

0 = pas de mouvement volontaire
1 = mouvement possible mais pas dans toute l'amplitude
2 = mouvement complètement effectué

V. Circumduction (position épaule-coude non précisée) _____

0 = aucune circumduction
1 = circumduction incomplète ou avec des ressauts
2 = circumduction complète

Total (max = 10) _____

C. Main

I. Flexion globale _____
(L'examinateur peut aider en soutenant le coude à 90°, sans toucher le poignet)
Flexion de tous les doigts

0 = aucune flexion volontaire
1 = flexion volontaire partielle
2 = flexion volontaire complète (par rapport au coté sain)

II. Extension globale _____
De la position de flexion active ou passive complète, extension de tous les doigts

0 = aucune extension volontaire
1 = peut relâcher une position de flexion globale active
2 = extension volontaire complète par rapport au coté opposé

III. Préhension A (préhension en crochet) _____
Extension des articulations métacarpophalangiennes et flexion des articulations interphalangiennes proximales et distales des doigts II à V ; tester la préhension contre résistance

0 = la position ne peut être atteinte
1 = la préhension est faible
2 = la position est maintenue contre une résistance importante

IV. Préhension B _____
Pouce contre la face latérale du 2ème métacarpe

0 = non effectuée
1 = un papier placé entre le pouce et le 2ème métacarpe peut être tenu mais pas contre résistance
2 = le papier est tenu correctement contre résistance

V. Préhension C (pince pouce/index) _____
Opposition de la pulpe du pouce contre la pulpe de l'index et un crayon est interposé

0 = non effectuée
1 = le crayon peut être tenu, mais pas contre résistance
2 = le crayon est tenu correctement contre résistance

VI. Préhension D (tenir un cylindre) _____
Le pouce contre l'index

0 = non effectuée
1 = le cylindre peut être tenu, mais pas contre résistance
2 = le cylindre est tenu correctement contre résistance

VII. Préhension E (préhension sphérique : balle de tennis) _____

0 = non effectuée
1 = l'objet peut être tenu, mais pas contre résistance
2 = l'objet est tenu correctement contre résistance

Total (max = 14) _____

D. Coordination/Vitesse

Doigt/nez rapidement, 5 fois, les yeux fermés. Mesurer le temps de réalisation et comparer au côté opposé.

I. Tremblement _____

0 = tremblement marqué
1 = léger tremblement
2 = pas de tremblement

II. Dysmétrie _____

0 = dysmétrie prononcée ou non systématisée
1 = dysmétrie légère ou systématisée
2 = pas de dysmétrie

III. Vitesse (par rapport au coté sain) _____

0 = au moins 6 secondes de plus
1 = 2 à 5 secondes de plus
2 = moins de 2 secondes de différence

Total (max = 6)_____

Total membre supérieur (max 60)

Appendix B

Aphasia Severity Rating Scale

5	Minimal discernible speech handicap
4	Obvious loss of fluency or facility of comprehension
3	Conversation about certain topics difficult/impossible
2	Conversation about familiar subjects possible with help
1	Fragmentary expression
0	No usable speech or auditory comprehension

Appendix C

Aphasia Rapid Test

Aphasia Rapid Test (ART)

	Cotation
1a. Exécution d'ordres simples : *« Ouvrez et fermez les yeux. »* *« Donnez-moi la main gauche. »* **1b. Exécution d'ordre complexe :** *« Mettez votre main gauche sur votre oreille droite. »*	0 = exécute les 2 ordres correctement. 1 = exécute 1 seul ordre correctement. 2 = n'exécute aucun des 2 ordres. 0 = exécute l'ordre en moins de 10 secondes. 1 = exécute l'ordre en plus de 10 secondes ou nécessité d'un rappel de la consigne. 2 = exécute partiellement l'ordre : passe la ligne médiane ou exécute mais avec erreur de côté. 3 = n'exécute pas l'ordre : ne passe pas la ligne médiane ou pas de mouvement.
2. Répétition de mots : **2a.** *« anneau »* **2b***. « macaron »* **2c.** *« bagage »*	Chaque mot est côté de 0 à 2 (total de 0 à 6), avec pour chacun: 0 = répétition parfaite. 1 = mot reconnaissable. 2 = mot non reconnaissable.
3. Répétition de phrase : *« Le garçon chante dans les bois.»*	0 = répétition parfaite. 1 = phrase reconnaissable. 2 = phrase non reconnaissable.
4. Dénomination d'objets : **4a.** *« montre »* **4b.** *« stylo »* **4c***. « blouse »*	Chaque mot est côté de 0 à 2 (total de 0 à 6), avec pour chacun: 0 = dénomination parfaite. 1 = mot reconnaissable. 2 = mot non reconnaissable.
5. Evaluation de la dysarthrie :	0 = pas de dysarthrie. 1 = dysarthrie minime. 2 = dysarthrie modérée, compréhensible. 3 = dysarthrie sévère, incompréhensible.
6. Fluence catégorielle : *« Dites le plus de noms d'animaux en 1minute.* »	0 = plus de quinze mots. 1 = entre onze et quinze mots. 2 = entre six et dix mots. 3 = entre trois et cinq mots. 4 = entre zéro et deux mots.
Score total	***/*26**

Appendix D

Aphasia Handicap Scale

0 Normal Language

1 Minor difficulties of language without disability (no impact on normal life)

2 Mild language-related disability (without restrictions in the autonomy of verbal communication in daily life)

3 Moderate language-related disability (restricted autonomy of verbal communication)

4 Severe language-related disability (lack of effective verbal communication)

5 Mutism or total loss of verbal expression and comprehension

Appendix E

National Institute of Health Stroke Scale

Score NIHSS

Item	Intitulé	cotation	score
la	**vigilance**	**0** vigilance normale, réactions vives **1** trouble léger de la vigilance : obnubilation, éveil plus ou moins adapté aux stimulations environnantes **2** coma ; réactions adaptées aux stimulations nociceptives **3** coma grave : réponse stéréotypée ou aucune réponse motrice	
Ib	**orientation** (mois, âge)	**0** deux réponses exactes **1** une seule bonne réponse **2** pas de bonne réponse	
lc	**commandes** (ouverture des yeux, ouverture du poing)	**0** deux ordres effectués **1** un seul ordre effectué **2** aucun ordre effectué	
2	**oculomotricité**	**0** oculomotricité normale **1**ophtalmoplégie partielle ou déviation réductible du regard **2** ophtalmoplégie horizontale complète ou déviation forcée du regard	
3	**champ visuel**	**0** champ visuel normal **1** quadranopsie latérale homonyme ou hémianopsie incomplète ou négligence visuelle unilatérale **2** hémianopsie latérale homonyme franche **3** cécité bilatérale ou coma (la=3)	
4	**paralysie faciale**	**0** motricité faciale normale **1** asymétrie faciale modérée (paralysie faciale unilatérale incomplète) **2** paralysie faciale unilatérale centrale franche **3** paralysie faciale périphérique ou diplégie faciale	
5	**motricité membre supérieur**	**0** pas de déficit moteur proximal **1** affaissement dans les 10 secondes, mais sans atteindre le plan du lit. **2** effort contre la pesanteur, mais le membre chute dans les 10 secondes sur le plan du lit. **3** pas d'effort contre la pesanteur (le membre chute mais le patient peut faire un mouvement tel qu'une flexion de hanche ou une adduction.) **4** absence de mouvement (coter 4 si le patient ne fait aucun mouvement volontaire) **X** cotation impossible (amputation, arthrodèse)	**Dt G**
6	**motricité membre inférieur**	**0** pas de déficit moteur proximal **1** affaissement dans les 5 secondes, mais sans atteindre le plan du lit. **2** effort contre la pesanteur, mais le membre chute dans les 5 secondes sur le plan du lit. **3** pas d'effort contre la pesanteur (le membre chute mais le patient peut faire un mouvement tel qu'une flexion de hanche ou une adduction.) **4** absence de mouvement (le patient ne fait aucun mouvement volontaire) **X** cotation impossible (amputation, arthrodèse)	**Dt G**
7	**ataxie**	**0** ataxie absente **1** ataxie présente pour 1 membre **2** ataxie présente pour 2 membres ou plus	
8	**sensibilité**	**0** sensibilité normale **1** hypoesthésie minime à modérée **2** hypoesthésie sévère ou anesthésie	
9	**langage**	**0** pas d'aphasie **1** aphasie discrète à modérée : communication informative **2** aphasie sévère **3** mutisme ; aphasie totale	
10	**dysarthrie**	**0** normal **1** dysarthrie discrète à modérée **2** dysarthrie sévère **X** cotation impossible	
11	**extinction, négligence**	**0** absence d'extinction et de négligence **1** extinction dans une seule modalité, visuelle ou sensitive, ou négligence partielle auditive, spatiale ou personnelle. **2** négligence sévère ou anosognosie ou extinction portant sur plus d'une modalité sensorielle	
		TOTAL	

Appendix F

modified Rankin Scale

0 No symptoms

1 No significant disability. Able to carry out all usual activities, despite some symptoms

2 Slight disability. Able to look after own affairs without assistance, but unable to carry out all previous activities

3 Moderate disability. Requires some help, but able to walk unassisted

4 Moderately severe disability. Unable to attend to own bodily needs without assistance, and unable to walk unassisted

5 Severe disability. Requires constant nursing care and attention, bedridden, incontinent

6 Dead

Appendix G

Supplementary Materials for Study I

SUPPLEMENTARY MATERIALS

Comparison of Spatial Registration Strategies of Diffusion MRI Data for Studying Motor Outcome in Acute and Chronic Stroke

Eric Moulton, Romain Valabregue, Belén Díaz, Claire Kemlin, Sara Leder, Stéphane Lehéricy, Yves Samson, Charlotte Rosso

Creation of the Study-Specific Templates and Tractography

Twenty-four healthy controls (10 females, age=31.7±10.4 years) from the same protocol as the subacute-chronic stroke cohort were included in this study to create the different image templates for normalization. We note that, while our healthy controls are younger than the studied stroke patients ($p<0.0001$), the templates constructed from these data are similar to existing open source FA and FOD templates, such as the IIT Human Brain Atlas v4.1 (https://www.nitrc.org/projects/iit/) (Varentsova et al., 2014).

We began by creating a FOD template through iterative non-linear warping and averaging of FOD volumes using MRtrix's *population_template* function (http://www.mrtrix.org) (Raffelt et al., 2011). The final resolution of the template was $2x2x2mm^3$.

The deformation fields obtained from the previous step were applied to the subjects' respective FA maps and brain masks. The resulting summed FA map was divided by the summed brain mask in order to create a voxel-wise average FA template reflecting the correct overlap of subjects due to differences in brain extraction masks or partial brainstem coverage.

In order to create a T1 template, the T1 images of healthy controls from the subacute-chronic cohort were first nonlinearly registered to the corresponding FA map using Advanced Normalization Tools (ANTs) and then normalized and averaged with the FOD-estimated deformation fields as for the FA template (Avants et al., 2008). We opted for a non-linear registration between the native T1 and native FA maps for several reasons. We found that affine transformations between these two images did not yield a perfectly satisfactory overlap, likely due to the strong susceptibility distortions caused by the high b-value of 1500 s/mm^2 despite the TOPUP and EDDY preprocessing steps as in other studies (Schulz et al., 2015). While we could have created a separate T1 population template using ANTs's *buildtemplateparallel.sh* function, we wanted to have all of our templates in the same reference frame and of the same size to avoid any bias. Furthermore, we wanted to avoid a suboptimal T1 template due to imperfect registrations between the T1 and FA images.

We performed whole brain probabilistic tractography on the FOD template using the second-order integration over fiber orientation distribution (iFOD2) algorithm with the following parameters (number of streamlines=100 million, max length=250mm, step size=1mm, max angle=45°) (Tournier and , F. Calamante, 2010). Streamlines were subsequently filtered down to 10 million using the SIFT algorithm (Smith et al., 2013).

We virtually dissected the corticofugal tracts emanating from the primary motor cortex (M1) using carefully segmented landmarks as described in (Geyer et al., 2000; Newton et al., 2006). The cortex of M1 is composed of the central sulcus, the paracentral lobule on the medial convexity and the exposed cortical surface of the precentral gyrus. The rostral border on the pre-central gyrus is delimited by a line joining the vertex of the precentral sulcus at the longitudinal cerebral fissure to the vertex of the central sulcus at the level of the junction of the superior frontal sulcus with the precentral sulcus. We further included an inclusion mask in the cerebral peduncles in addition to appropriate exclusion masks to remove aberrant fibers. Finally, streamlines of the corticospinal tract (CST) were converted to a density map.

Supplementary Tables for ANOVA analyses

Repeated measures ANOVA were performed for DTI parameters extracted from the corticospinal tract of the unaffected and affected hemisphere as well as their ratio and lesion load. Presented below for each parameter are the descriptive statistics, within-subject effects, post-hoc tests for significant factors and interactions where applicable, and individual paired t-tests between each pair of strategies.

Fractional Anisotropy of the Unaffected Hemisphere (FA_{unaff})

STRATEGY	MASKING	Mean	SD
ANTs-T1	Masking	0.524	0.033
	No_Masking	0.524	0.033
ANTs-FA	Masking	0.532	0.034
	No_Masking	0.533	0.033
FOD-lmax2	Masking	0.521	0.035
	No_Masking	0.521	0.035
FOD-lmax4	Masking	0.516	0.036
	No_Masking	0.516	0.036

Table S1. Descriptive statistics for FA_{unaff}. SD = Standard Deviation.

Post Hoc Comparisons - STRATEGY

		Mean Difference	SE	t	p_{bonf}
ANTs-T1	ANTs-FA	-0.009	0.002	-5.482	< .001
	FOD-lmax2	0.003	0.002	1.751	0.527
	FOD-lmax4	0.007	0.002	4.012	0.002
ANTs-FA	FOD-lmax2	0.012	0.001	9.175	< .001
	FOD-lmax4	0.016	0.001	11.706	< .001
FOD-lmax2	FOD-lmax4	0.004	4.246e -4	9.797	< .001

Table S2. Post-hoc t-tests for main effect of STRATEGY. For each comparison, the mean difference, standard error (SE), t statistic, and Bonferroni-corrected p-value (p_{bonf}) are shown.

Individual Paired Samples T-Test

		t	df	p_{bonf}	Mean Difference	SE Difference
ANTs-T1_Masking	- ANTs-T1_No_Masking	0.013	39	1	4.510e -6	3.478e -4
ANTs-FA_Masking	- ANTs-FA_No_Masking	-2.113	39	0.657	-0.001	5.426e -4
FOD-lmax2_Masking	- FOD-lmax2_No_Masking	-1.941	39	0.953	-4.917e -5	2.534e -5
FOD-lmax4_Masking	- FOD-lmax4_No_Masking	-0.150	39	1	-1.568e -6	1.046e -5
ANTs-T1_Masking	- ANTs-FA_Masking	-5.085	39	< .001	-0.008	0.002
ANTs-T1_Masking	- FOD-lmax2_Masking	1.786	39	1	0.003	0.002
ANTs-T1_Masking	- FOD-lmax4_Masking	4.032	39	0.004	0.007	0.002
ANTs-FA_Masking	- FOD-lmax2_Masking	8.067	39	< .001	0.012	0.001
ANTs-FA_Masking	- FOD-lmax4_Masking	10.490	39	< .001	0.016	0.001
FOD-lmax2_Masking	- FOD-lmax4_Masking	9.749	39	< .001	0.004	4.243e -4
ANTs-T1_No_Masking	- ANTs-FA_No_Masking	-5.713	39	< .001	-0.010	0.002
ANTs-T1_No_Masking	- FOD-lmax2_No_Masking	1.701	39	1	0.003	0.002
ANTs-T1_No_Masking	- FOD-lmax4_No_Masking	3.955	39	0.005	0.007	0.002
ANTs-FA_No_Masking	- FOD-lmax2_No_Masking	10.082	39	< .001	0.013	0.001
ANTs-FA_No_Masking	- FOD-lmax4_No_Masking	12.647	39	< .001	0.017	0.001
FOD-lmax2_No_Masking	- FOD-lmax4_No_Masking	9.837	39	< .001	0.004	4.254e -4

Table S3. Individual paired t-tests between each strategy. For each comparison, the t-statistic, degrees of freedom (df), Bonferroni-corrected p-value (p_{bonf}), mean difference, and standard error (SE) are shown.

Fractional Anisotropy of the Affected Hemisphere (FA_{aff})

STRATEGY	MASKING	Mean	SD
ANTs-T1	Masking	0.430	0.070
	No_Masking	0.440	0.065
ANTs-FA	Masking	0.440	0.069
	No_Masking	0.450	0.065
FOD-lmax2	Masking	0.419	0.077
	No_Masking	0.425	0.075
FOD-lmax4	Masking	0.412	0.076
	No_Masking	0.416	0.076

Table S4. Descriptive statistics for FA_{aff}. SD = Standard Deviation.

Post Hoc Comparisons - STRATEGY

		Mean Difference	SE	t	p_{bonf}
ANTs-T1	ANTs-FA	-0.010	0.002	-6.398	< .001
	FOD-lmax2	0.013	0.003	4.871	< .001
	FOD-lmax4	0.021	0.003	7.166	< .001
ANTs-FA	FOD-lmax2	0.023	0.003	8.989	< .001
	FOD-lmax4	0.031	0.003	10.408	< .001
FOD-lmax2	FOD-lmax4	0.008	7.401e -4	10.751	< .001

Table S5. Post-hoc t-tests for main effect of STRATEGY. For each comparison, the mean difference, standard error (SE), t statistic, and Bonferroni-corrected p-value (p_{bonf}) are shown.

Post Hoc Comparisons - MASKING

		Mean Difference	SE	t	p_{bonf}
Masking	No_Masking	-0.008	0.001	-6.363	< .001

Table S6. Post-hoc t-tests for main effect of MASKING. The mean difference, standard error (SE), t statistic, and Bonferroni-corrected p-value (p_{bonf}) are shown.

Post Hoc Comparisons - STRATEGY*MASKING Interaction

		Mean Difference	SE	t	p_{bonf}
ANTs-T1	ANTs-FA	0.0006	0.0015	0.437	1
	FOD-lmax2	-0.0032	0.0015	-3.631	0.257
	FOD-lmax4	-0.0055	0.0015	-2.094	0.005
ANTs-FA	FOD-lmax2	-0.0038	0.0016	-3.983	0.149
	FOD-lmax4	-0.0061	0.0015	-2.333	0.002
FOD-lmax2	FOD-lmax4	-0.0023	0.0007	-3.405	0.009

Table S7. Post-hoc t-tests for the STRATEGY*MASKING interaction, representing the comparison of the effect of MASKING on each strategy (i.e., ΔFA_{aff} from MASKING). The mean difference, standard error (SE), t statistic, and Bonferroni-corrected p-value (p_{bonf}) are shown.

Individual Paired Samples T-Test

		t	df	p_{bonf}	Mean Difference	SE Difference
ANTs-T1_Masking	- ANTs-T1_No_Masking	-6.232	39	< .001	-0.010	0.002
ANTs-FA_Masking	- ANTs-FA_No_Masking	-6.302	39	< .001	-0.010	0.002
FOD-lmax2_Masking	- FOD-lmax2_No_Masking	-4.053	39	0.004	-0.007	0.002
FOD-lmax4_Masking	- FOD-lmax4_No_Masking	-3.866	39	0.007	-0.004	0.001
ANTs-T1_Masking	- ANTs-FA_Masking	-5.798	39	< .001	-0.010	0.002
ANTs-T1_Masking	- FOD-lmax2_Masking	4.633	39	< .001	0.012	0.003
ANTs-T1_Masking	- FOD-lmax4_Masking	6.657	39	< .001	0.018	0.003
ANTs-FA_Masking	- FOD-lmax2_Masking	8.306	39	< .001	0.022	0.003
ANTs-FA_Masking	- FOD-lmax4_Masking	9.559	39	< .001	0.028	0.003
FOD-lmax2_Masking	- FOD-lmax4_Masking	10.993	39	< .001	0.007	6.202e -4
ANTs-T1_No_Masking	- ANTs-FA_No_Masking	-5.817	39	< .001	-0.011	0.002
ANTs-T1_No_Masking	- FOD-lmax2_No_Masking	4.784	39	< .001	0.015	0.003
ANTs-T1_No_Masking	- FOD-lmax4_No_Masking	7.236	39	< .001	0.024	0.003
ANTs-FA_No_Masking	- FOD-lmax2_No_Masking	8.847	39	< .001	0.025	0.003
ANTs-FA_No_Masking	- FOD-lmax4_No_Masking	10.593	39	< .001	0.034	0.003

Individual Paired Samples T-Test

		t	df	p_{bonf}	Mean Difference	SE Difference
FOD-lmax2_No_Masking	- FOD-lmax4_No_Masking	9.408	39	< .001	0.009	9.668e -4

Table S8. Individual paired t-tests between each strategy. For each comparison, the t-statistic, degrees of freedom (df), Bonferroni-corrected p-value (p_{bonf}), mean difference, and standard error (SE) are shown.

FA_{aff}/FA_{unaff} (rFA)

STRATEGY	MASKING	Mean	SD
ANTs-T1	Masking	0.821	0.122
	No_Masking	0.840	0.114
ANTs-FA	Masking	0.827	0.121
	No_Masking	0.845	0.112
FOD-lmax2	Masking	0.804	0.138
	No_Masking	0.817	0.136
FOD-lmax4	Masking	0.798	0.141
	No_Masking	0.806	0.139

Table S9. Descriptive statistics for rFA. SD = Standard Deviation.

Post Hoc Comparisons - STRATEGY

		Mean Difference	SE	t	p_{bonf}
ANTs-T1	ANTs-FA	-0.005	0.002	-2.269	0.173
	FOD-lmax2	0.020	0.005	4.365	< .001
	FOD-lmax4	0.029	0.005	5.466	< .001
ANTs-FA	FOD-lmax2	0.025	0.005	5.229	< .001
	FOD-lmax4	0.034	0.006	5.893	< .001
FOD-lmax2	FOD-lmax4	0.008	0.002	5.378	< .001

Table S10. Post-hoc t-tests for main effect of STRATEGY. For each comparison, the mean difference, standard error (SE), t statistic, and Bonferroni-corrected p-value (p_{bonf}) are shown.

Post Hoc Comparisons - MASKING

		Mean Difference	SE	t	p_{bonf}
Masking	No_Masking	-0.014	0.002	-6.044	< .001

Table S11. Post-hoc t-tests for main effect of MASKING. The mean difference, standard error (SE), t statistic, and Bonferroni-corrected p-value (p_{bonf}) are shown.

Post Hoc Comparisons - STRATEGY*MASKING Interaction

		Mean Difference	SE	t	p_{bonf}
ANTs-T1	ANTs-FA	-0.0013	0.0029	-0.465	1
	FOD-lmax2	-0.0062	0.0029	-2.163	0.221
	FOD-lmax4	-0.0106	0.0029	-3.688	0.004
ANTs-FA	FOD-lmax2	-0.0049	0.0032	-1.536	0.796
	FOD-lmax4	-0.0092	0.0028	-3.241	0.015
FOD-lmax2	FOD-lmax4	-0.0044	0.0013	-3.350	0.011

Table S12. Post-hoc t-tests for the STRATEGY*MASKING interaction, representing the comparison of the effect of MASKING on each strategy (i.e., ΔrFA from MASKING). The mean difference, standard error (SE), t statistic, and Bonferroni-corrected p-value (p_{bonf}) are shown.

Individual Paired Samples T-Test

		t	df	p_{bonf}	Mean Difference	SE Difference
ANTs-T1_Masking	- ANTs-T1_No_Masking	-6.068	39	< .001	-0.019	0.003
ANTs-FA_Masking	- ANTs-FA_No_Masking	-5.881	39	< .001	-0.018	0.003
FOD-lmax2_Masking	- FOD-lmax2_No_Masking	-3.952	39	0.005	-0.013	0.003
FOD-lmax4_Masking	- FOD-lmax4_No_Masking	-3.797	39	0.008	-0.008	0.002
ANTs-T1_Masking	- ANTs-FA_Masking	-2.141	39	0.618	-0.006	0.003
ANTs-T1_Masking	- FOD-lmax2_Masking	3.966	39	0.005	0.017	0.004
ANTs-T1_Masking	- FOD-lmax4_Masking	4.720	39	< .001	0.023	0.005
ANTs-FA_Masking	- FOD-lmax2_Masking	4.818	39	< .001	0.023	0.005
ANTs-FA_Masking	- FOD-lmax4_Masking	5.303	39	< .001	0.029	0.006
FOD-lmax2_Masking	- FOD-lmax4_Masking	4.424	39	0.001	0.006	0.001
ANTs-T1_No_Masking	- ANTs-FA_No_Masking	-1.695	39	1	-0.004	0.003
ANTs-T1_No_Masking	- FOD-lmax2_No_Masking	4.377	39	0.001	0.023	0.005
ANTs-T1_No_Masking	- FOD-lmax4_No_Masking	5.778	39	< .001	0.034	0.006
ANTs-FA_No_Masking	- FOD-lmax2_No_Masking	5.125	39	0.001	0.028	0.005
ANTs-FA_No_Masking	- FOD-lmax4_No_Masking	6.111	39	< .001	0.039	0.006

Individual Paired Samples T-Test

			t	df	p_{bonf}	Mean Difference	SE Difference
FOD-lmax2_No_Masking	-	FOD-lmax4_No_Masking	5.479	39	< .001	0.011	0.002

Table S13. Individual paired t-tests between each strategy. For each comparison, the t-statistic, degrees of freedom (df), Bonferroni-corrected p-value (p_{bonf}), mean difference, and standard error (SE) are shown.

Weighted Lesion Load (wLL) of the Corticospinal Tract

STRATEGY	MASKING	Mean	SD
ANTs-T1	Masking	0.158	0.100
	No_Masking	0.124	0.083
ANTs-FA	Masking	0.158	0.093
	No_Masking	0.129	0.083
FOD-lmax2	Masking	0.175	0.104
	No_Masking	0.166	0.102
FOD-lmax4	Masking	0.177	0.103
	No_Masking	0.172	0.102

Table S14. Descriptive statistics for wLL. SD = Standard Deviation.

Post Hoc Comparisons - STRATEGY

		Mean Difference	SE	t	p_{bonf}
ANTs-T1	ANTs-FA	-0.003	0.003	-1.135	1.000
	FOD-lmax2	-0.030	0.004	-7.076	< .001
	FOD-lmax4	-0.034	0.004	-7.522	< .001
ANTs-FA	FOD-lmax2	-0.027	0.005	-5.430	< .001
	FOD-lmax4	-0.031	0.005	-5.787	< .001
FOD-lmax2	FOD-lmax4	-0.004	0.001	-2.816	0.046

Table S15. Post-hoc t-tests for main effect of STRATEGY. For each comparison, the mean difference, standard error (SE), t statistic, and Bonferroni-corrected p-value (p_{bonf}) are shown.

Post Hoc Comparisons - MASKING

		Mean Difference	SE	t	p_{bonf}
Masking	No_Masking	0.019	0.003	6.869	< .001

Table S16. Post-hoc t-tests for main effect of MASKING. The mean difference, standard error (SE), t statistic, and Bonferroni-corrected p-value (p_{bonf}) are shown.

Post Hoc Comparisons - STRATEGY*MASKING Interaction

		Mean Difference	SE	t	p_{bonf}
ANTs-T1	ANTs-FA	0.0049	0.0063	0.776	1
	FOD-lmax2	0.0256	0.0048	4.437	<.001
	FOD-lmax4	0.0287	0.0052	5.012	<.001
ANTs-FA	FOD-lmax2	0.0208	0.0058	4.317	0.001
	FOD-lmax4	0.0238	0.0057	4.579	<.001
FOD-lmax2	FOD-lmax4	0.0030	0.0011	2.690	0.063

Table S17. Post-hoc t-tests for the STRATEGY*MASKING interaction, representing the comparison of the effect of MASKING on each strategy (i.e., ΔwLL from MASKING). The mean difference, standard error (SE), t statistic, and Bonferroni-corrected p-value (p_{bonf}) are shown.

Individual Paired Samples T-Test

		t	df	p_{bonf}	Mean Difference	SE Difference
ANTs-T1_Masking	- ANTs-T1_No_Masking	6.051	39	< .001	0.034	0.006
ANTs-FA_Masking	- ANTs-FA_No_Masking	5.211	39	< .001	0.029	0.006
FOD-lmax2_Masking	- FOD-lmax2_No_Masking	3.653	39	0.012	0.008	0.002
FOD-lmax4_Masking	- FOD-lmax4_No_Masking	3.642	39	0.013	0.005	0.001
ANTs-T1_Masking	- ANTs-FA_Masking	-0.194	39	1	-6.317e -4	0.003
ANTs-T1_Masking	- FOD-lmax2_Masking	-3.843	39	0.007	-0.017	0.004
ANTs-T1_Masking	- FOD-lmax4_Masking	-3.999	39	0.004	-0.019	0.005
ANTs-FA_Masking	- FOD-lmax2_Masking	-4.607	39	< .001	-0.016	0.004
ANTs-FA_Masking	- FOD-lmax4_Masking	-5.013	39	< .001	-0.019	0.004
FOD-lmax2_Masking	- FOD-lmax4_Masking	-2.041	39	0.769	-0.002	0.001
ANTs-T1_No_Masking	- ANTs-FA_No_Masking	-1.132	39	1	-0.005	0.005
ANTs-T1_No_Masking	- FOD-lmax2_No_Masking	-7.455	39	< .001	-0.043	0.006
ANTs-T1_No_Masking	- FOD-lmax4_No_Masking	-8.358	39	< .001	-0.048	0.006

Individual Paired Samples T-Test

			t	df	p_{bonf}	Mean Difference	SE Difference
ANTs-FA_No_Masking	-	FOD-lmax2_No_Masking	-5.387	39	< .001	-0.037	0.007
ANTs-FA_No_Masking	-	FOD-lmax4_No_Masking	-5.705	39	< .001	-0.043	0.007
FOD-lmax2_No_Masking	-	FOD-lmax4_No_Masking	-3.081	39	0.060	-0.005	0.002

Table S18. Individual paired t-tests between each strategy. For each comparison, the t-statistic, degrees of freedom (df), Bonferroni-corrected p-value (p_{bonf}), mean difference, and standard error (SE) are shown.

Axial Diffusivity of the Unaffected Hemisphere (AD_{unaff})

STRATEGY	MASKING	Mean	SD
ANTs-FA	Masking	1.395	0.074
	No_Masking	1.392	0.068
FOD-lmax2	Masking	1.389	0.075
	No_Masking	1.389	0.075
FOD-lmax4	Masking	1.408	0.084
	No_Masking	1.408	0.084

Table S19. Descriptive statistics for AD_{unaff}. SD = Standard Deviation.

Post Hoc Comparisons - STRATEGY

		Mean Difference	SE	t	p_{bonf}
ANTs-FA	FOD-lmax2	0.005	0.004	1.405	0.494
	FOD-lmax4	-0.014	0.005	-3.033	0.010
FOD-lmax2	FOD-lmax4	-0.019	0.002	-9.171	< .001

Table S20. Post-hoc t-tests for main effect of STRATEGY. For each comparison, the mean difference, standard error (SE), t statistic, and Bonferroni-corrected p-value (p_{bonf}) are shown.

Individual Paired Samples T-Test

		t	df	p_{bonf}	Mean Difference	SE Difference
ANTs-FA_Masking	- ANTs-FA_No_Masking	1.378	68	1	0.003	0.002
FOD-lmax2_Masking	- FOD-lmax2_No_Masking	2.499	68	0.134	7.072e -5	2.830e -5
FOD-lmax4_Masking	- FOD-lmax4_No_Masking	0.587	68	1	4.040e -5	6.882e -5
ANTs-FA_Masking	- FOD-lmax2_Masking	1.556	68	1	0.007	0.004
ANTs-FA_Masking	- FOD-lmax4_Masking	-2.444	68	0.154	-0.013	0.005
FOD-lmax2_Masking	- FOD-lmax4_Masking	-9.177	68	< .001	-0.019	0.002
ANTs-FA_No_Masking	- FOD-lmax2_No_Masking	1.077	68	1	0.004	0.003
ANTs-FA_No_Masking	- FOD-lmax4_No_Masking	-3.534	68	0.007	-0.016	0.005
FOD-lmax2_No_Masking	- FOD-lmax4_No_Masking	-9.162	68	< .001	-0.019	0.002

Table S21. Individual paired t-tests between each strategy. For each comparison, the t-statistic, degrees of freedom (df), Bonferroni-corrected p-value (p_{bonf}), mean difference, and standard error (SE) are shown.

Axial Diffusivity of the Affected Hemisphere (AD_{aff})

STRATEGY	MASKING	Mean	SD
ANTs-FA	Masking	1.344	0.095
	No_Masking	1.345	0.091
FOD-lmax2	Masking	1.340	0.100
	No_Masking	1.343	0.097
FOD-lmax4	Masking	1.359	0.106
	No_Masking	1.362	0.104

Table S22. Descriptive statistics for AD_{aff}. SD = Standard Deviation.

Post Hoc Comparisons - STRATEGY

		Mean Difference	SE	t	p_{bonf}
ANTs-FA	FOD-lmax2	0.003	0.003	1.050	0.892
	FOD-lmax4	-0.016	0.004	-4.237	< .001
FOD-lmax2	FOD-lmax4	-0.019	0.002	-10.178	< .001

Table S23. Post-hoc t-tests for main effect of STRATEGY. For each comparison, the mean difference, standard error (SE), t statistic, and Bonferroni-corrected p-value (p_{bonf}) are shown.

Post Hoc Comparisons - MASKING

		Mean Difference	SE	t	p_{bonf}
Masking	No_Masking	-0.002	6.899e -4	-2.853	0.006

Table S24. Post-hoc t-tests for main effect of MASKING. The mean difference, standard error (SE), t statistic, and Bonferroni-corrected p-value (p_{bonf}) are shown.

Individual Paired Samples T-Test

		t	df	p_{bonf}	Mean Difference	SE Difference
ANTs-FA_Masking	- ANTs-FA_No_Masking	-0.374	68	1	-5.429e -4	0.001
FOD-lmax2_Masking	- FOD-lmax2_No_Masking	-4.534	68	< .001	-0.003	6.179e -4
FOD-lmax4_Masking	- FOD-lmax4_No_Masking	-5.204	68	< .001	-0.003	4.918e -4
ANTs-FA_Masking	- FOD-lmax2_Masking	1.362	68	1	0.004	0.003
ANTs-FA_Masking	- FOD-lmax4_Masking	-3.845	68	0.002	-0.015	0.004
FOD-lmax2_Masking	- FOD-lmax4_Masking	-10.217	68	< .001	-0.020	0.002
ANTs-FA_No_Masking	- FOD-lmax2_No_Masking	0.655	68	1	0.002	0.003
ANTs-FA_No_Masking	- FOD-lmax4_No_Masking	-4.508	68	< .001	-0.017	0.004
FOD-lmax2_No_Masking	- FOD-lmax4_No_Masking	-10.105	68	< .001	-0.019	0.002

Table S25. Individual paired t-tests between each strategy. For each comparison, the t-statistic, degrees of freedom (df), Bonferroni-corrected p-value (p_{bonf}), mean difference, and standard error (SE) are shown.

AD_{aff}/AD_{unaff} (rAD)

STRATEGY	MASKING	Mean	SD
ANTs-FA	Masking	0.964	0.059
	No_Masking	0.966	0.054
FOD-lmax2	Masking	0.965	0.053
	No_Masking	0.967	0.051
FOD-lmax4	Masking	0.966	0.054
	No_Masking	0.968	0.052

Table 26 Descriptive statistics for rAD. SD = Standard Deviation.

Post Hoc Comparisons - MASKING

		Mean Difference	SE	t	p_{bonf}
Masking	No_Masking	-0.002	6.131e -4	-3.408	0.001

Table S27. Post-hoc t-tests for main effect of MASKING. The mean difference, standard error (SE), t statistic, and Bonferroni-corrected p-value (p_{bonf}) are shown.

Individual Paired Samples T-Test

			t	df	p_{bonf}	Mean Difference	SE Difference
ANTs-FA_Masking	-	ANTs-FA_No_Masking	-1.835	68	1	-0.002	0.001
FOD-lmax2_Masking	-	FOD-lmax2_No_Masking	-4.644	68	< .001	-0.002	4.497e -4
FOD-lmax4_Masking	-	FOD-lmax4_No_Masking	-5.222	68	< .001	-0.002	3.578e -4
ANTs-FA_Masking	-	FOD-lmax2_Masking	-0.591	68	1	-0.001	0.002
ANTs-FA_Masking	-	FOD-lmax4_Masking	-0.837	68	1	-0.002	0.002
FOD-lmax2_Masking	-	FOD-lmax4_Masking	-0.615	68	1	-6.333e -4	0.001
ANTs-FA_No_Masking	-	FOD-lmax2_No_Masking	-0.603	68	1	-9.512e -4	0.002
ANTs-FA_No_Masking	-	FOD-lmax4_No_Masking	-0.771	68	1	-0.001	0.002
FOD-lmax2_No_Masking	-	FOD-lmax4_No_Masking	-0.403	68	1	-4.134e -4	0.001

Table S28. Individual paired t-tests between each strategy. For each comparison, the t-statistic, degrees of freedom (df), Bonferroni-corrected p-value (p_{bonf}), mean difference, and standard error (SE) are shown.

Weighted Lesion Load (wLL) of the Corticospinal Tract

STRATEGY	MASKING	Mean	SD
ANTs-FA	Masking	0.051	0.076
	No_Masking	0.047	0.068
FOD-lmax2	Masking	0.055	0.074
	No_Masking	0.051	0.069
FOD-lmax4	Masking	0.054	0.072
	No_Masking	0.051	0.068

Table S29. Descriptive statistics for wLL. SD = Standard Deviation.

Post Hoc Comparisons - STRATEGY

		Mean Difference	SE	t	p_{bonf}
ANTs-FA	FOD-lmax2	-0.004	0.002	-2.529	0.041
	FOD-lmax4	-0.004	0.002	-1.810	0.224
FOD-lmax2	FOD-lmax4	5.764e -4	6.421e -4	0.898	1.000

Table S30. Post-hoc t-tests for main effect of STRATEGY. For each comparison, the mean difference, standard error (SE), t statistic, and Bonferroni-corrected p-value (p_{bonf}) are shown.

Post Hoc Comparisons - MASKING

		Mean Difference	SE	t	p_{bonf}
Masking	No_Masking	0.004	0.001	3.567	< .001

Table S31. Post-hoc t-tests for main effect of MASKING. The mean difference, standard error (SE), t statistic, and Bonferroni-corrected p-value (p_{bonf}) are shown.

Individual Paired Samples T-Test

			t	df	p_{bonf}	Mean Difference	SE Difference
ANTs-FA_Masking	-	ANTs-FA_No_Masking	1.985	68	0.461	0.004	0.002
FOD-lmax2_Masking	-	FOD-lmax2_No_Masking	4.718	68	< .001	0.004	8.507e -4
FOD-lmax4_Masking	-	FOD-lmax4_No_Masking	4.386	68	< .001	0.003	6.764e -4
ANTs-FA_Masking	-	FOD-lmax2_Masking	-1.874	68	0.587	-0.004	0.002
ANTs-FA_Masking	-	FOD-lmax4_Masking	-1.242	68	1	-0.003	0.003
FOD-lmax2_Masking	-	FOD-lmax4_Masking	1.629	68	0.972	0.001	6.753e -4
ANTs-FA_No_Masking	-	FOD-lmax2_No_Masking	-3.326	68	0.013	-0.004	0.001
ANTs-FA_No_Masking	-	FOD-lmax4_No_Masking	-2.582	68	0.108	-0.004	0.002
FOD-lmax2_No_Masking	-	FOD-lmax4_No_Masking	0.079	68	1	5.288e -5	6.712e -4

Table S32. Individual paired t-tests between each strategy. For each comparison, the t-statistic, degrees of freedom (df), Bonferroni-corrected p-value (p_{bonf}), mean difference, and standard error (SE) are shown.

Correlations between ΔwLL and ΔFA/ΔAD due to lesion masking

Subacute-Chronic Stroke Cohort

Strategy	ρ (CI)	p_{bonf}
ANTs-T1	-0.783 (-0.864;-0.644)	<.001
ANTs-FA	-0.762 (-0.901;-0.526)	<.001
FOD-*lmax2*	-0.395 (-0.694;-0.028)	0.046
FOD-*lmax4*	-0.432 (-0.701;-0.103)	0.021

Table S33. Spearman correlations between the difference (Δ) in weighted lesion load (wLL) and Fractional Anisotropy (FA) due to lesion masking. Shown are Spearman's ρ with the 95% confidence interval (CI) and the Bonferroni-corrected p-value.

Acute Stroke Cohort

Strategy	ρ (CI)	p_{bonf}
ANTs-FA	-0.663 (-0.808;-0.461)	<.001
FOD-*lmax2*	-0.802 (-0.875;-0.671)	<.001
FOD-*lmax4*	-0.742 (-0.842;-0.597)	<.001

Table S34. Spearman correlations between the difference (Δ) in weighted lesion load (wLL) and Axial Diffusivity (AD) due to lesion masking. Shown are Spearman's ρ with the 95% confidence interval (CI) and the Bonferroni-corrected p-value.

Supplementary Tables for Correlation Comparisons

Paired Samples T-Test (Subacute-Chronic)

			p	Difference
ANTs-T1_Masking	-	ANTs-T1_No_Masking	0.059	0.041
ANTs-FA_Masking	-	ANTs-FA_No_Masking	0.009	0.057
FOD-lmax2_Masking	-	FOD-lmax2_No_Masking	< .001	0.075
FOD-lmax4_Masking	-	FOD-lmax4_No_Masking	0.003	0.027
ANTs-T1_Masking	-	ANTs-FA_Masking	0.671	0.011
ANTs-T1_Masking	-	FOD-lmax2_Masking	< .001	-0.105
ANTs-T1_Masking	-	FOD-lmax4_Masking	< .001	-0.114
ANTs-FA_Masking	-	FOD-lmax2_Masking	< .001	-0.116
ANTs-FA_Masking	**-**	**FOD-lmax4_Masking**	**< .001**	**-0.125**
FOD-lmax2_Masking	-	FOD-lmax4_Masking	0.215	-0.009
ANTs-T1_No_Masking	-	ANTs-FA_No_Masking	0.315	0.027
ANTs-T1_No_Masking	-	FOD-lmax2_No_Masking	0.005	-0.071
ANTs-T1_No_Masking	-	FOD-lmax4_No_Masking	< .001	-0.128
ANTs-FA_No_Masking	-	FOD-lmax2_No_Masking	< .001	-0.098
ANTs-FA_No_Masking	**-**	**FOD-lmax4_No_Masking**	**< .001**	**-0.155**
FOD-lmax2_No_Masking	-	FOD-lmax4_No_Masking	< .001	-0.057

Table S35. Permutation tests for comparing the correlation strength (Spearman's ρ) between the rFA extracted with each STRATEGY and the composite motor score. The largest differences between strategies where lesion masking was and was not employed are in bold.

Permutation Tests (Acute)

			p	Difference
ANTs-FA_Masking	-	ANTs-FA_No_Masking	0.452	0.008
FOD-lmax2_Masking	-	FOD-lmax2_No_Masking	< .001	0.013
FOD-lmax4_Masking	-	FOD-lmax4_No_Masking	< .001	0.019
ANTs-FA_Masking	-	FOD-lmax2_Masking	0.683	-0.009
ANTs-FA_Masking	-	FOD-lmax4_Masking	0.084	0.010
FOD-lmax2_Masking	**-**	**FOD-lmax4_Masking**	**0.174**	**0.019**
ANTs-FA_No_Masking	-	FOD-lmax2_No_Masking	0.865	0.004
ANTs-FA_No_Masking	-	FOD-lmax4_No_Masking	0.364	-0.021
FOD-lmax2_No_Masking	**-**	**FOD-lmax4_No_Masking**	**0.699**	**0.025**

Table S36. Permutation tests for comparing the correlation strength (Spearman's ρ) between the rAD extracted with each STRATEGY and the NIHSS7 MOT. The largest differences between strategies where lesion masking was and was not employed are in bold.

Supplementary Analysis with CST template from Archer et al. 2018 Cerebral Cortex

In order to superimpose the CST template from Archer et al., (2018) on our normalized images, we estimated non-linear transformations with ANTs between our FA template and the FMRIB58_FA template for which Archer et al. (2018)'s CST template was constructed. We then extracted the unweighted FA and AD from both hemispheres in the subacute-chronic and acute stroke cohorts, respectively. We observed that the previously observed trends for FA, AD, rFA, rAD, lesion load, and correlations globally stayed the same (see figures below for this response); however, the correlation strength of the unweighted DTI-parameters were much less.

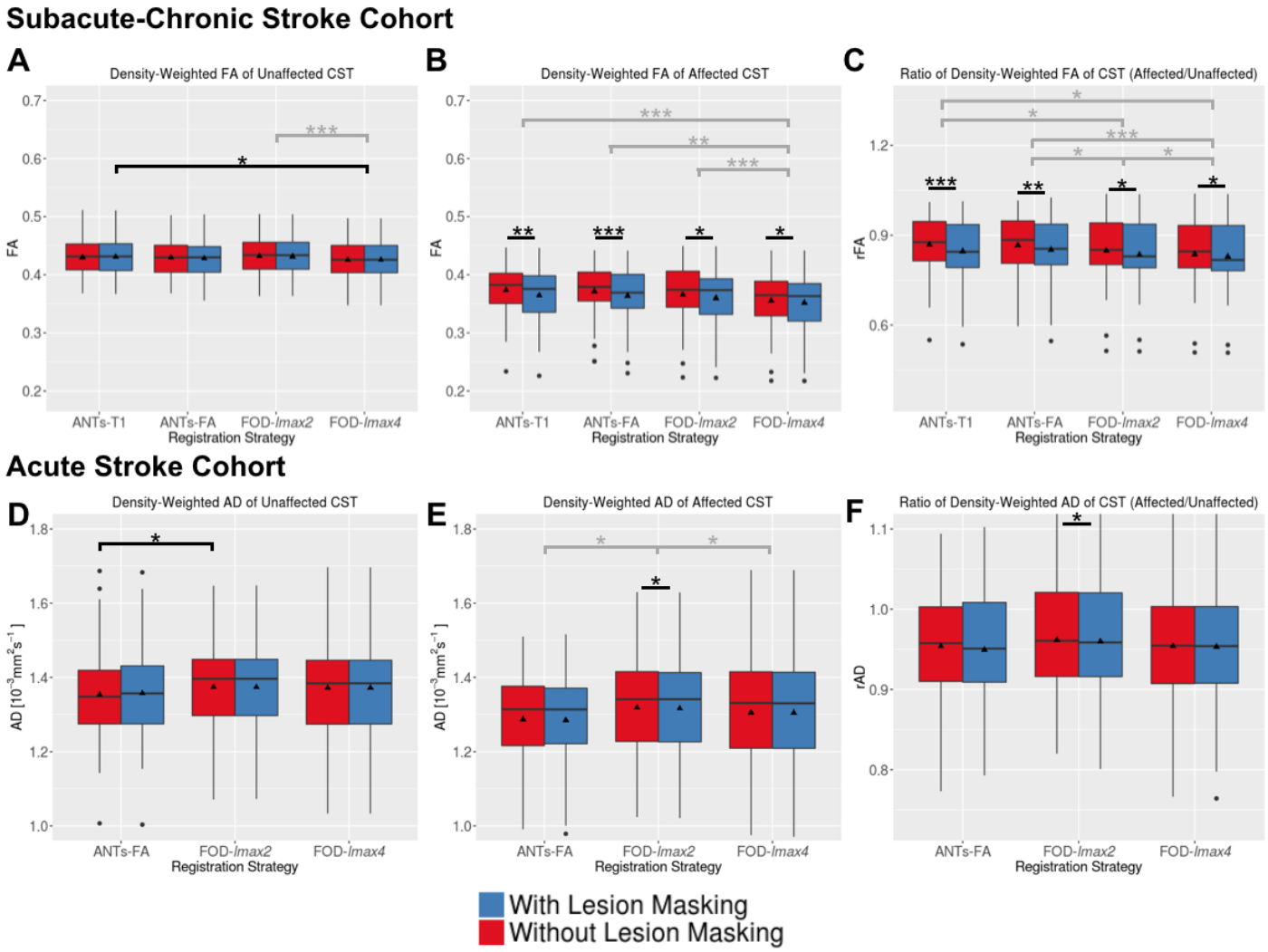

Figure S1. Effect of registration strategy and lesion masking on DTI parameter extraction of the corticospinal tract (CST) template from Archer et al. 2018 Cerebral Cortex.

*Fractional Anisotropy (FA) of the subacute-chronic stroke cohort (top row) and Axial Diffusivity (AD of the acute stroke cohort (bottom row) of the unaffected (left column) and affected (middle column) CST as well as the ratio (right column). Boxes display the median and interquartile range, whiskers show the range of values, dots reflect outliers, and triangles represent the mean value. For tidiness, black-colored comparisons reflect significant differences between two registration strategies (hooks over interquartile lines), whereas grey-colored comparisons reflect significant differences between two software packages for both lesion masking and without lesion masking (hooks in between blue and red boxplots). Black bars at the top of the whiskers reflect significant differences for lesion masking for a given software. *p<0.05, **p<0.001, ***p<0.0001 Bonferroni-corrected from individual paired t-tests.*

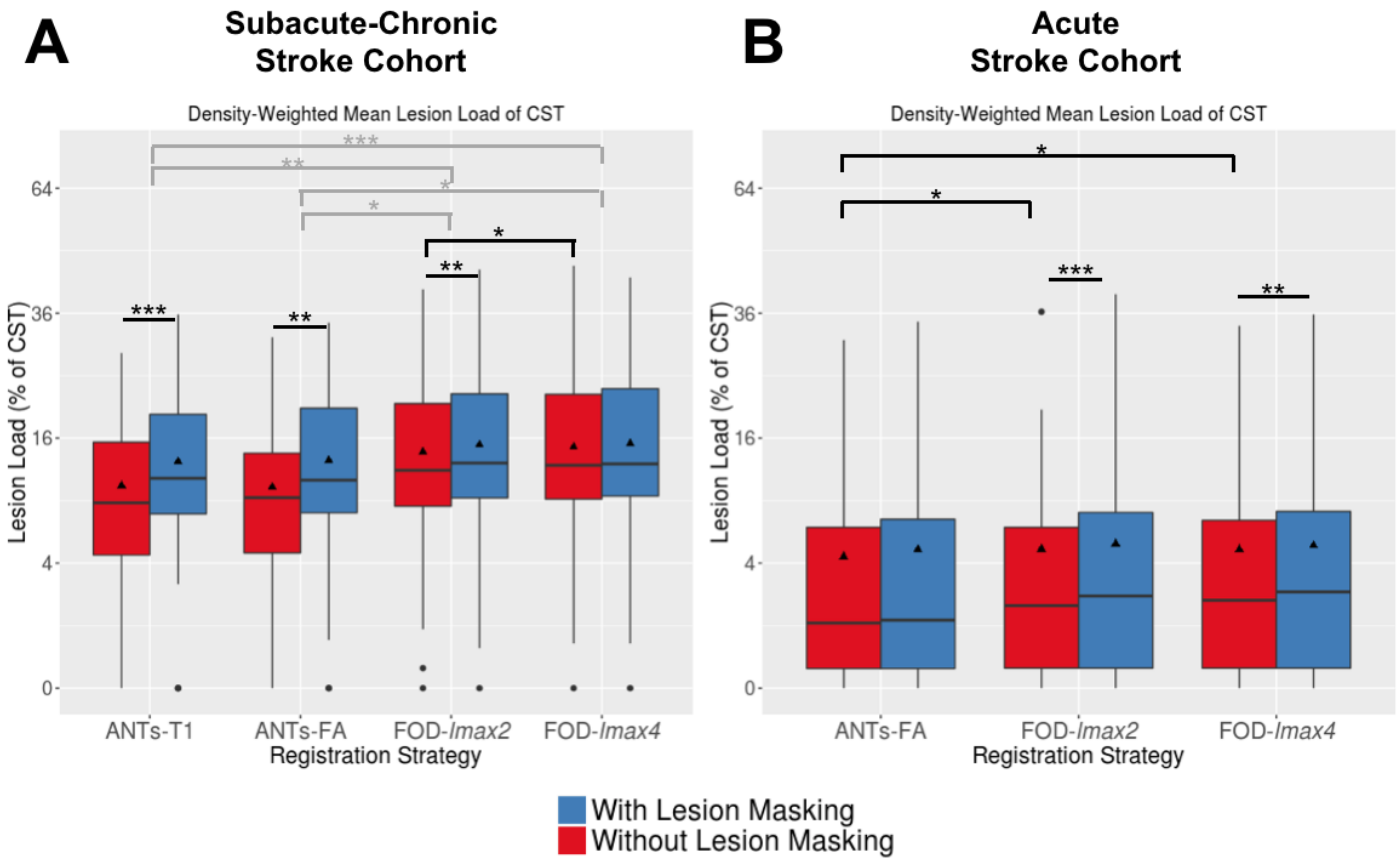

*Figure S2. Lesion load analysis using the CST template from Archer et al. 2018 Cerebral Cortex. Lesion load for the subacute-chronic stroke cohort (A) and the acute stroke cohort (B). Note that the y-axis scales as y^2 to facilitate visualization between both groups. Boxes display the median and interquartile range, whiskers show the range of values, dots reflect outliers, and triangles represent the mean value. For tidiness, black-colored comparisons reflect significant differences between two registration strategies (hooks over interquartile lines), whereas grey-colored comparisons reflect significant differences between two software packages for both lesion masking and without lesion masking (hooks in between blue and red boxplots). Black bars at the top of the whiskers reflect significant differences for lesion masking for a given software. *p<0.05, **p<0.001, ***p<0.0001 Bonferroni-corrected from individual paired t-tests.*

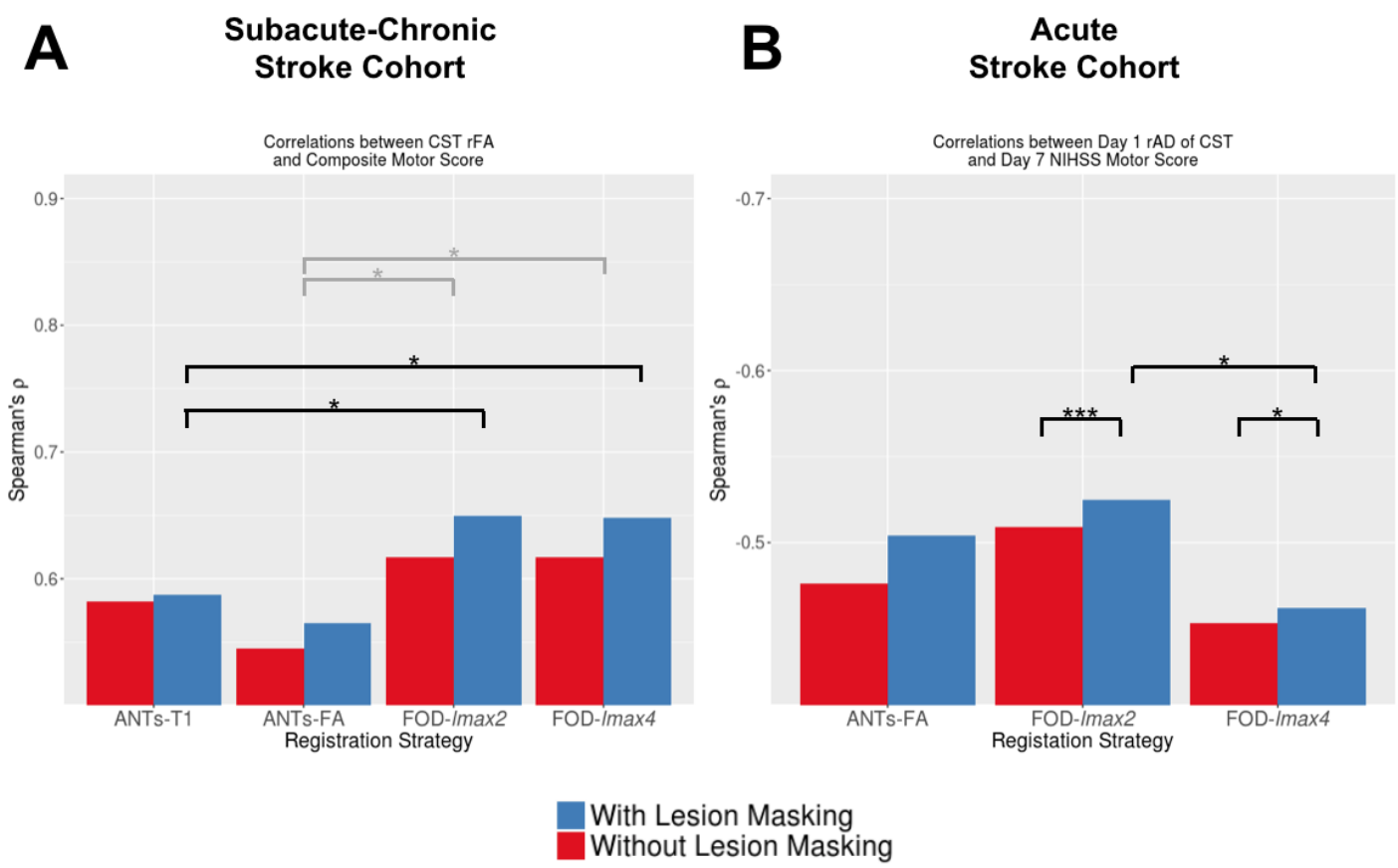

Figure S3. Spearman correlations between clinical scores and DTI parameters of the CST from Archer et al. 2018 Cerebral Cortex for each registration strategy.

*(A) Correlations were performed between ratios of the fractional anisotropy (rFA; affected/unaffected) and the composite motor score for the subacute-chronic stroke cohort. (B) Correlations were performed between ratios of day 1 post-stroke radial diffusivity (rAD) and the NIHSS motor score at day 7 post-stroke. Spearman's ρ for each correlation is shown on the y-axis and each strategy with lesion masking (blue) and without lesion masking (red) is shown on the x-axis. The upper limit for the y-axis is the same as in the manuscript to facilitate visual comparison. For tidiness, black-colored comparisons reflect significant differences between two registration strategies (hooks over center of bars), whereas grey-colored comparisons reflect significant differences between two software packages for both lesion masking and without lesion masking (hooks in between blue and red bars). Permutation test significance: *p<0.05, *p<0.001, *p<0.0001*

Supplementary Analysis using imaging and CST templates from healthy controls from the acute stroke cohort MRI scanner

Data from sixteen healthy controls (mean±std age 33.8±6.5 years old, 9 female) who had undergone a DWI sequence acquired with the same MRI scanner as the acute stroke cohort, were retrospectively used to create the imaging and CST templates. The imaging protocol for the controls was very similar to the acute stroke cohort (TR=14s, TE=83.2, voxel size=1.09x1.09x3mm^3, no phase encoding, 50 directions, b=1000s/mm^2).

Before any preprocessing steps, we only retained the 30 diffusion-encoding directions from the DWI sequence of the healthy controls which were most aligned with those of the acute stroke cohort (mean ± standard deviation difference in bvec axes: 7.6+/-3.0°). As with the acute stroke patients, we applied the following steps: denoising, eddy without topup, DTIFIT and MSMT-CSD FOD with intensity normalization. The healthy control FODs were used to make a population template using MRtrix's *population_template* function, and the resulting warp fields were applied to the FA maps to recreate the corresponding FA template. As with the acute stroke patient population, there were no T1 images available. Whole brain tractography with SIFT with the same regions of interest were used to reconstruct the CST of both hemispheres as described above.

The patient data from the acute stroke cohort (and the subacute-chronic stroke cohort as a control) were renormalized to the new template with and without lesion masking, and the warp fields were applied to the different DTI parameter maps, and the weighted average value within the CST was extracted. We then reran the same statistical analyses.

As can be seen from the graphs below, the general trends were very similar for both the acute and subacute-chronic stroke cohort.

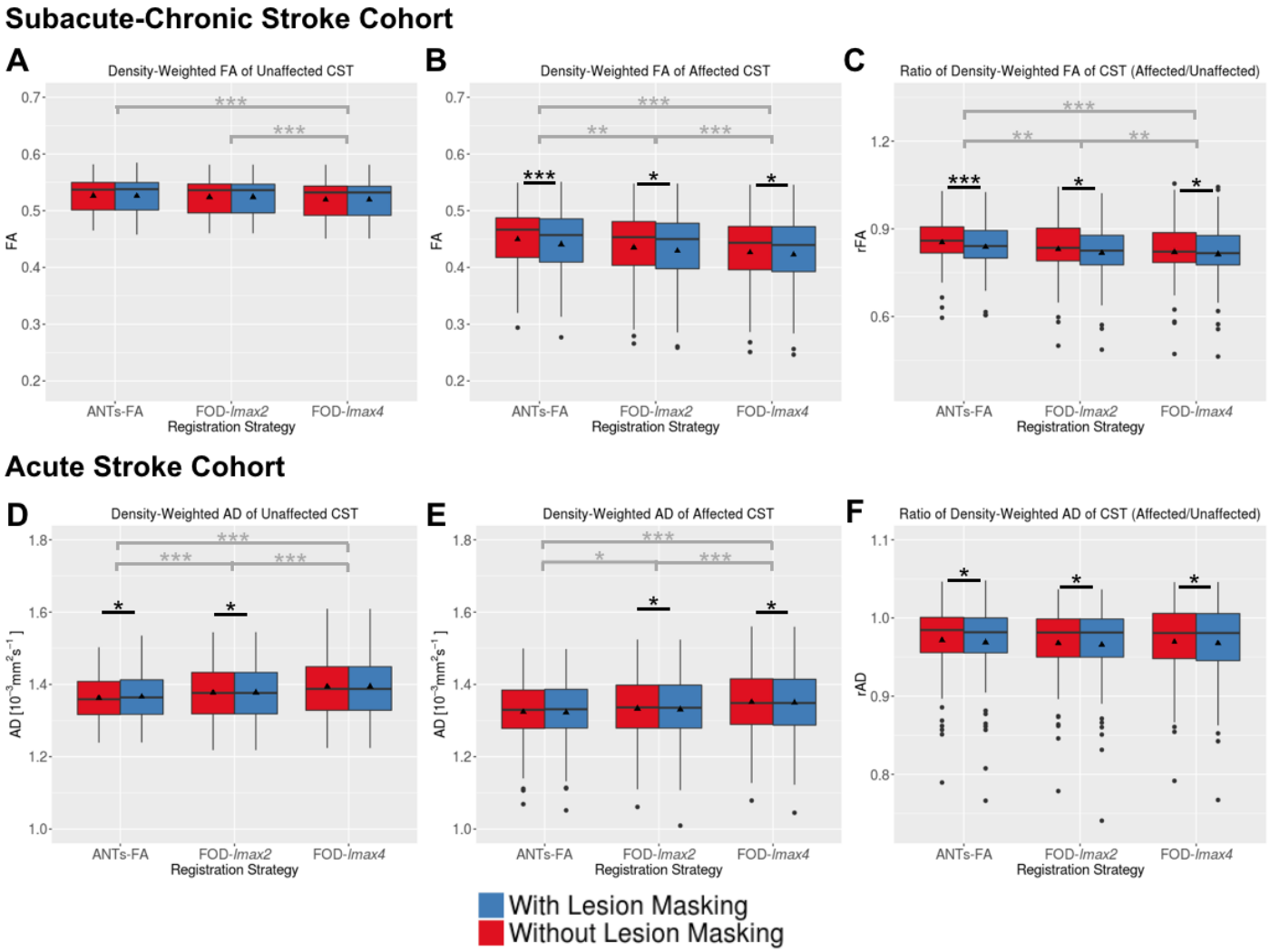

Figure S4. Effect of registration strategy and lesion masking on DTI parameter extraction of the corticospinal tract (CST) template the second healthy control cohort.

Fractional Anisotropy (FA) of the subacute-chronic stroke cohort (top row) and Axial Diffusivity (AD of the acute stroke cohort (bottom row) of the unaffected (left column) and affected (middle column) CST as well as the ratio (right

*column). Boxes display the median and interquartile range, whiskers show the range of values, dots reflect outliers, and triangles represent the mean value. For tidiness, black-colored comparisons reflect significant differences between two registration strategies (hooks over interquartile lines), whereas grey-colored comparisons reflect significant differences between two software packages for both lesion masking and without lesion masking (hooks in between blue and red boxplots). Black bars at the top of the whiskers reflect significant differences for lesion masking for a given software. *p<0.05, **p<0.001, ***p<0.0001 Bonferroni-corrected from individual paired t-tests.*

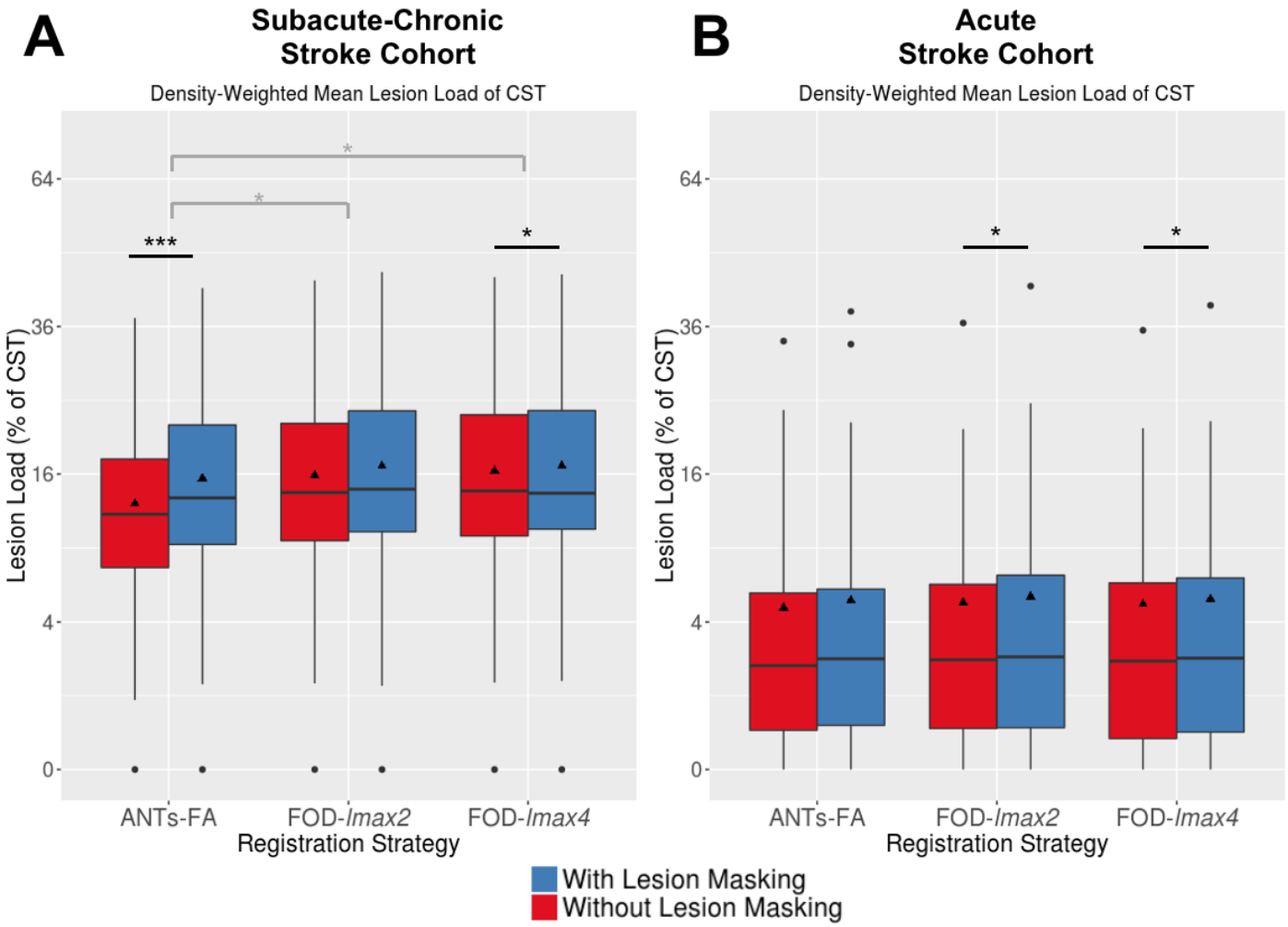

*Figure S5. Lesion load analysis using the CST template from the second healthy control cohort. Lesion load for the subacute-chronic stroke cohort (A) and the acute stroke cohort (B). Note that the y-axis scales as y2 to facilitate visualization between both groups. Boxes display the median and interquartile range, whiskers show the range of values, dots reflect outliers, and triangles represent the mean value. For tidiness, black-colored comparisons reflect significant differences between two registration strategies (hooks over interquartile lines), whereas grey-colored comparisons reflect significant differences between two software packages for both lesion masking and without lesion masking (hooks in between blue and red boxplots). Black bars at the top of the whiskers reflect significant differences for lesion masking for a given software. *p<0.05, **p<0.001, ***p<0.0001 Bonferroni-corrected from individual paired t-tests.*

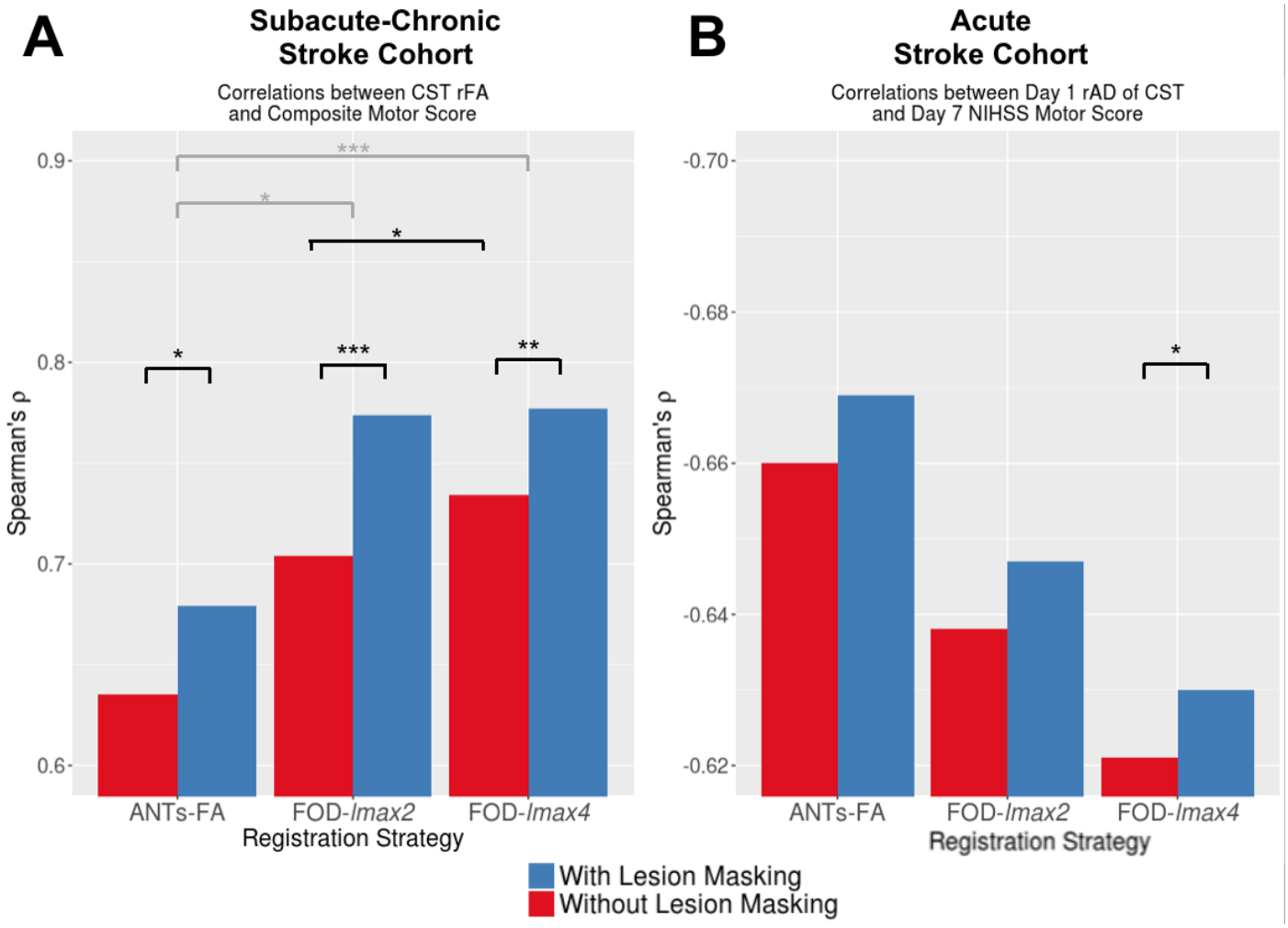

Figure S6. Spearman correlations between clinical scores and DTI parameters of the CST from the second healthy control cohort for each registration strategy.

*(A) Correlations were performed between ratios of the fractional anisotropy (rFA; affected/unaffected) and the composite motor score for the subacute-chronic stroke cohort. (B) Correlations were performed between ratios of day 1 post-stroke radial diffusivity (rAD) and the NIHSS motor score at day 7 post-stroke. Spearman's ρ for each correlation is shown on the y-axis and each strategy with lesion masking (blue) and without lesion masking (red) is shown on the x-axis. The upper limit for the y-axis is the same as in the manuscript to facilitate visual comparison. For tidiness, black-colored comparisons reflect significant differences between two registration strategies (hooks over center of bars), whereas grey-colored comparisons reflect significant differences between two software packages for both lesion masking and without lesion masking (hooks in between blue and red bars). Permutation test significance: *p<0.05, *p<0.001, *p<0.0001*

All correlations with DTI parameters and subacute-chronic/acute outcome

Parameter	Strategy	Masking	ρ	CI_lower	CI_upper
rFA	ANTs-FA	Masking	0.692*	0.446	0.839
rFA	ANTs-FA	No_Masking	0.635*	0.361	0.813
rFA	ANTs-T1	Masking	0.703*	0.471	0.841
rFA	ANTs-T1	No_Masking	0.662*	0.41	0.817
rFA	FOD-lmax2	Masking	0.808*	0.634	0.901
rFA	FOD-lmax2	No_Masking	0.733*	0.512	0.859
rFA	FOD-lmax4	Masking	0.817*	0.653	0.907
rFA	FOD-lmax4	No_Masking	0.790*	0.606	0.89
rMD	ANTs-FA	Masking	-0.673*	-0.814	-0.437
rMD	ANTs-FA	No_Masking	-0.655*	-0.815	-0.379
rMD	ANTs-T1	Masking	-0.651*	-0.803	-0.399
rMD	ANTs-T1	No_Masking	-0.653*	-0.813	-0.392
rMD	FOD-lmax2	Masking	-0.732*	-0.837	-0.536
rMD	FOD-lmax2	No_Masking	-0.730*	-0.846	-0.527
rMD	FOD-lmax4	Masking	-0.718*	-0.83	-0.516
rMD	FOD-lmax4	No_Masking	-0.737*	-0.844	-0.542
rAD	ANTs-FA	Masking	-0.315*	-0.548	-0.029
rAD	ANTs-FA	No_Masking	-0.239	-0.516	0.065
rAD	ANTs-T1	Masking	-0.259	-0.517	0.041
rAD	ANTs-T1	No_Masking	-0.150	-0.447	0.178
rAD	FOD-lmax2	Masking	-0.371*	-0.582	-0.099
rAD	FOD-lmax2	No_Masking	-0.309	-0.551	-0.016
rAD	FOD-lmax4	Masking	-0.383*	-0.587	-0.111
rAD	FOD-lmax4	No_Masking	-0.341*	-0.556	-0.064
rRD	ANTs-FA	Masking	-0.755*	-0.867	-0.554
rRD	ANTs-FA	No_Masking	-0.722*	-0.859	-0.494
rRD	ANTs-T1	Masking	-0.732*	-0.859	-0.522
rRD	ANTs-T1	No_Masking	-0.709*	-0.849	-0.48
rRD	FOD-lmax2	Masking	-0.837*	-0.902	-0.701
rRD	FOD-lmax2	No_Masking	-0.844*	-0.912	-0.707
rRD	FOD-lmax4	Masking	-0.805*	-0.882	-0.661
rRD	FOD-lmax4	No_Masking	-0.821*	-0.891	-0.676

Table S37. Correlation coefficients of the ratio (r) of Fractional Anisotropy (FA), Mean Diffusivity (MD), Axial Diffusivity (AD), and Radial Diffusivity (RD) of the affected over the unaffected CST. Correlation coefficients (ρ) and confidence intervals (CI) were computed with each registration strategy with and without masking. * $p<0.05$, uncorrected

Parameter	Strategy	Masking	ρ	CI_lower	CI_upper
rFA	ANTs-FA	Masking	-0.451*	-0.632	-0.233
rFA	ANTs-FA	No_Masking	-0.446*	-0.618	-0.243
rFA	FOD-lmax2	Masking	-0.431*	-0.614	-0.217
rFA	FOD-lmax2	No_Masking	-0.387*	-0.575	-0.162
rFA	FOD-lmax4	Masking	-0.398*	-0.592	-0.172
rFA	FOD-lmax4	No_Masking	-0.384*	-0.571	-0.165
rMD	ANTs-FA	Masking	-0.550*	-0.704	-0.355
rMD	ANTs-FA	No_Masking	-0.550*	-0.709	-0.347
rMD	FOD-lmax2	Masking	-0.547*	-0.722	-0.323
rMD	FOD-lmax2	No_Masking	-0.533*	-0.713	-0.304
rMD	FOD-lmax4	Masking	-0.535*	-0.697	-0.325
rMD	FOD-lmax4	No_Masking	-0.511*	-0.686	-0.287
rAD	ANTs-FA	Masking	-0.668*	-0.777	-0.516
rAD	ANTs-FA	No_Masking	-0.660*	-0.777	-0.498
rAD	FOD-lmax2	Masking	-0.677*	-0.784	-0.519
rAD	FOD-lmax2	No_Masking	-0.664*	-0.775	-0.51
rAD	FOD-lmax4	Masking	-0.658*	-0.769	-0.498
rAD	FOD-lmax4	No_Masking	-0.639*	-0.759	-0.473
rRD	ANTs-FA	Masking	-0.411*	-0.598	-0.185
rRD	ANTs-FA	No_Masking	-0.430*	-0.612	-0.207
rRD	FOD-lmax2	Masking	-0.430*	-0.638	-0.181
rRD	FOD-lmax2	No_Masking	-0.425*	-0.631	-0.179
rRD	FOD-lmax4	Masking	-0.406*	-0.606	-0.168
rRD	FOD-lmax4	No_Masking	-0.408*	-0.604	-0.168

Table S38. Correlation coefficients of the ratio (r) of Fractional Anisotropy (FA), Mean Diffusivity (MD), Axial Diffusivity (AD), and Radial Diffusivity (RD) of the affected over the unaffected CST. Correlation coefficients (ρ) and confidence intervals (CI) were computed with each registration strategy with and without masking. * p<0.05, uncorrected

References for Supplementary Materials

Archer, D.B., Vaillancourt, D.E., Coombes, S.A., 2018. A Template and Probabilistic Atlas of the Human Sensorimotor Tracts using Diffusion MRI. Cereb. Cortex 28, 1685–1699. https://doi.org/10.1093/cercor/bhx066

Avants, B.B., Epstein, C.L., Grossman, M., Gee, J.C., 2008. Symmetric diffeomorphic image registration with cross-correlation: Evaluating automated labeling of elderly and neurodegenerative brain. Med. Image Anal. 12, 26–41. https://doi.org/10.1016/j.media.2007.06.004

Geyer, S., Matelli, M., Luppino, G., Zilles, K., 2000. Functional neuroanatomy of the primate isocortical motor system. Anat. Embryol. (Berl). https://doi.org/10.1007/s004290000127

Newton, J.M., Ward, N.S., Parker, G.J.M., Deichmann, R., Alexander, D.C., Friston, K.J., Frackowiak, R.S.J., 2006. Non-invasive mapping of corticofugal fibres from multiple motor areas - Relevance to stroke recovery. Brain 129, 1844–1858. https://doi.org/10.1093/brain/awl106

Raffelt, D., Tournier, J.D., Fripp, J., Crozier, S., Connelly, A., Salvado, O., 2011. Symmetric diffeomorphic registration of fibre orientation distributions. Neuroimage 56, 1171–1180. https://doi.org/10.1016/j.neuroimage.2011.02.014

Schulz, R., Koch, P., Zimerman, M., Wessel, M., Bönstrup, M., Thomalla, G., Cheng, B., Gerloff, C., Hummel, F.C., 2015. Parietofrontal motor pathways and their association with motor function after stroke. Brain 138, 1949–1960. https://doi.org/10.1093/brain/awv100

Smith, R.E., Tournier, J.D., Calamante, F., Connelly, A., 2013. SIFT: Spherical-deconvolution informed filtering of tractograms. Neuroimage 67, 298–312. https://doi.org/10.1016/j.neuroimage.2012.11.049

Tournier, J.-D., , F. Calamante, and a. C., 2010. Improved probabilistic streamlines tractography by 2 nd order integration over fibre orientation distributions. Ismrm 88, 2010.

Varentsova, A., Zhang, S., Arfanakis, K., 2014. Development of a high angular resolution diffusion imaging human brain template. Neuroimage 91, 177–186. https://doi.org/10.1016/j.neuroimage.2014.01.009

Appendix H

Supplementary Materials for Study II

SUPPLEMENTARY MATERIALS

Multivariate Prediction of Functional Outcome using Lesion Topography Characterized by Acute Diffusion Tensor Imaging

Eric Moulton, Romain Valabregue, Stephane Lehéricy, Yves Samson, Charlotte Rosso

Supplementary Methods

Creation of in-house study-specific template as described in Moulton et al. 2018

The following procedure is as described in Moulton et al. (2018). Data from twenty-four healthy controls (10 females, age=31.7±10.4 years) acquired with a different imaging protocol were used to create the in-house templates for image normalization. Subjects were scanned with a 3T MRI (Siemens, VERIO) with a 32-channel head coil. A multi-shell Diffusion Weighted Imaging (DWI) sequence (3 b-value shells obtained with both posterior to anterior (PA) and anterior to posterior (AP) phase encoding: 60 non-collinear diffusion encoding gradients at b=1500s/mm^2,30 at b=700s/mm^2, and 8 at b=300 s/mm^2, TR=4000 ms, TE=87.8 ms, matrix size=110×110, slice number=66, voxel size=2×2×2mm^3, acquisition time=16:16 min).

Image processing was the same as the stroke cohort in the current paper, with the exception of FSL's TOPUP as an additional step to take advantage of the opposite phase-encoded images.

Fiber Orientation Distribution (FOD) volumes were computed by estimating response functions for the GM, WM, and CSF tissues (Dhollander et al., 2016) for multi-shell multi-tissue constrained spherical deconvolution (MSMT-CSD) using a lmax of 4 (Jeurissen et al., 2014).

We began by creating a FOD template through iterative non-linear warping and averaging of FOD volumes using MRtrix's *population_template* function (http://www.mrtrix.org)(Raffelt et al., 2011). The final resolution of the template was 2x2x2mm^3.

The deformation fields obtained from the previous step were applied to the subjects' respective FA maps and brain masks. The resulting summed FA map was divided by the summed brain mask in order to create a voxel-wise average FA template reflecting the correct overlap of subjects due to differences in brain extraction masks or partial brainstem coverage.

Tractography analysis with the group template

A tractography analysis was used to visualize the white matter tracts passing through regions of the brain with the most influence on long-term outcome. We performed whole brain probabilistic tractography on the FOD template using the second-order integration over fiber orientation distribution (iFOD2) algorithm with the following parameters (number of streamlines=100 million, max length=250mm, step size=1mm, max angle=45°) (Tournier and , F. Calamante, 2010). Streamlines were subsequently filtered down to 10 million using the SIFT algorithm (Smith et al., 2013).

Adhering to the procedures outlined in Rojkova et al. (2016) and Catani and Thiebaut de Schotten (2008), we dissected the following well-known long-range tracts: (1) the three branches of the superior longitudinal fasciculus (SLF), (2) cingulum, (3) uncinate fasciculus, (4) the anterior, long, and posterior segment of the arcuate fasciculus (AF), (5) inferior fronto-occipital fasciculus (IFOF), (6), inferior longitudinal fasciculus (ILF) (7) frontal aslant tract (FAT), (8) corticospinal tract (CST), and (9) the corpus callosum (CC). Tracts were converted into density maps and the most probable regions (at least 10% maximum tract density) were retained. We created a region of interest (ROI) composed of

the largest connected component of voxels with the strongest weights (95th percentile) associated with larger decreases in diffusivity or higher lesion incidence in patients with poor outcome, depending on the winning model. We then investigated which of the dissected long-range fasciculi passed through this area.

Supplementary Figures

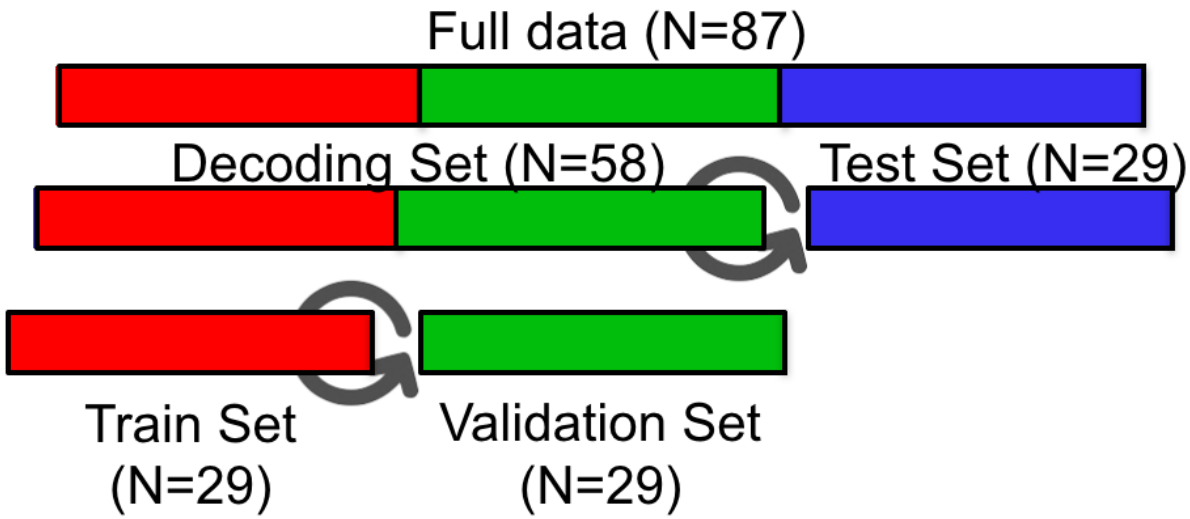

Supplementary Figure 1. Cross-validation scheme
The full dataset is initially split into the decoding set and test set. The decoding set is split again into a training and validation set. Multiple models, each with a unique set of hyperparameters, are built with data in the training set and evaluated on the independent, validation set. The best set of hyperparameters are chosen for the final model, reconstructed with the decoding set. A final, unbiased evaluation is performed on the test set.

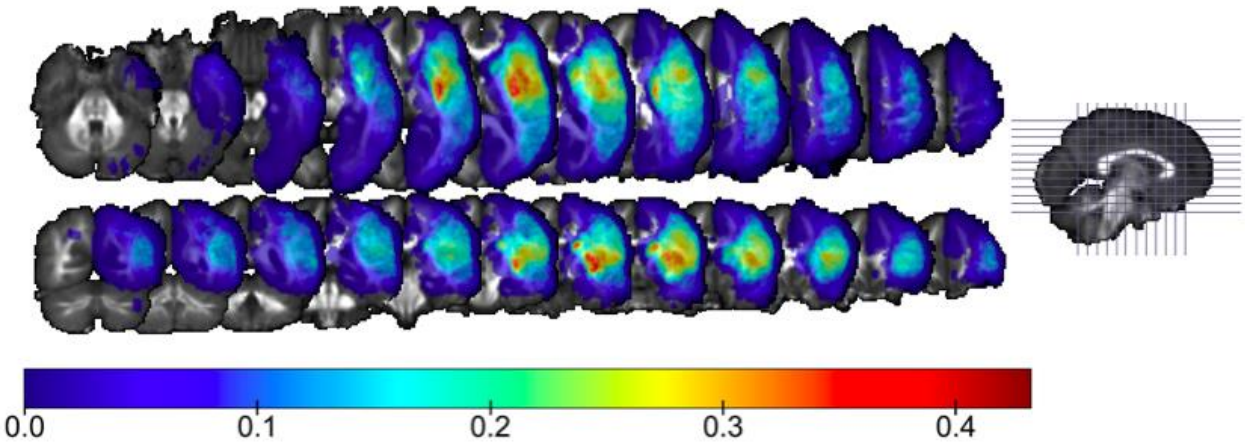

Supplementary Figure 2. Lesion Probability Maps
Lesion probability maps overlaid on selected axial (top) and coronal (bottom) slices of the in-house FA template. The colormap reflects the percentage of lesioned voxels over the studied cohort. Right-sided lesions were flipped onto the left hemisphere, and normalization was performed again to warp the lesion.

Supplementary References

Catani, M., Thiebaut de Schotten, M., 2008. A diffusion tensor imaging tractography atlas for virtual in vivo dissections. Cortex. 44, 1105–32. https://doi.org/10.1016/j.cortex.2008.05.004

Dhollander, T., Raffelt, D., Connelly, A., 2016. Unsupervised 3-tissue response function estimation from single-shell or multi-shell diffusion MR data without a co-registered T1 image, in: ISMRM Workshop on Breaking the Barriers of Diffusion MRI. p. 5.

Jeurissen, B., Tournier, J.D., Dhollander, T., Connelly, A., Sijbers, J., 2014. Multi-tissue constrained spherical deconvolution for improved analysis of multi-shell diffusion MRI data. Neuroimage 103, 411–426. https://doi.org/10.1016/j.neuroimage.2014.07.061

Moulton, E., Valabrègue, R., Díaz, B., Kemlin, C., Leder, S., Lehéricy, S., Samson, Y., Rosso, C., Valabregue, R., Díaz, B., Kemlin, C., Leder, S., Lehéricy, S., Samson, Y., Rosso, C., 2018. Comparison of spatial normalization strategies of diffusion MRI data for studying motor outcome in subacute-chronic and acute stroke. Neuroimage 183, 186–199. https://doi.org/10.1016/j.neuroimage.2018.08.002

Raffelt, D., Tournier, J.D., Fripp, J., Crozier, S., Connelly, A., Salvado, O., 2011. Symmetric diffeomorphic registration of fibre orientation distributions. Neuroimage 56, 1171–1180. https://doi.org/10.1016/j.neuroimage.2011.02.014

Rojkova, K., Volle, E., Urbanski, M., Humbert, F., Dell'Acqua, F., Thiebaut de Schotten, M., 2016. Atlasing the frontal lobe connections and their variability due to age and education: a spherical deconvolution tractography study. Brain Struct. Funct. 221, 1751–1766. https://doi.org/10.1007/s00429-015-1001-3

Smith, R.E., Tournier, J.D., Calamante, F., Connelly, A., 2013. SIFT: Spherical-deconvolution informed filtering of tractograms. Neuroimage 67, 298–312. https://doi.org/10.1016/j.neuroimage.2012.11.049

Tournier, J.-D., , F. Calamante, and a. C., 2010. Improved probabilistic streamlines tractography by 2 nd order integration over fibre orientation distributions. Ismrm 88, 2010.

Appendix I

Supplementary Materials for Study III

SUPPLEMENTARY MATERIALS

Acute diffusivity biomarkers for prediction of motor and language outcome in moderate-to-severe stroke patients

Eric Moulton, Romain Valabregue, Stephane Lehéricy, Yves Samson, Charlotte Rosso

Supplementary Methods

Creation of in-house study-specific template as described in Moulton et al. 2018

The following procedure is as described in Moulton et al. (2018). Data from twenty-four healthy controls (10 females, age=31.7±10.4 years) acquired with a different imaging protocol were used to create the in-house templates for image normalization. Subjects were scanned with a 3T MRI (Siemens, VERIO) with a 32-channel head coil. A multi-shell Diffusion Weighted Imaging (DWI) sequence (3 b-value shells obtained with both posterior to anterior (PA) and anterior to posterior (AP) phase encoding: 60 non-collinear diffusion encoding gradients at b=1500s/mm^2,30 at b=700s/mm^2, and 8 at b=300 s/mm^2, TR=4000 ms, TE=87.8 ms, matrix size=110×110, slice number=66, voxel size=2×2×2mm^3, acquisition time=16:16 min).

Image processing was the same as the stroke cohort in the current paper, with the exception of FSL's TOPUP as an additional step to take advantage of the opposite phase-encoded images.

Fiber Orientation Distribution (FOD) volumes were computed by estimating response functions for the GM, WM, and CSF tissues (Dhollander et al., 2016) for multi-shell multi-tissue constrained spherical deconvolution (MSMT-CSD) using a lmax of 4 (Jeurissen et al., 2014).

We began by creating a FOD template through iterative non-linear warping and averaging of FOD volumes using MRtrix's *population_template* function (http://www.mrtrix.org)(Raffelt et al., 2011). The final resolution of the template was 2x2x2mm^3.

The deformation fields obtained from the previous step were applied to the subjects' respective FA maps and brain masks. The resulting summed FA map was divided by the summed brain mask in order to create a voxel-wise average FA template reflecting the correct overlap of subjects due to differences in brain extraction masks or partial brainstem coverage.

Tractography analysis with the group template

A tractography analysis was used to virtually dissect major white matter fasciculi of the visuomotor and language networks. We performed whole brain probabilistic tractography on the FOD template using the second-order integration over fiber orientation distribution (iFOD2) algorithm with the following parameters (number of streamlines=100 million, max length=250mm, step size=1mm, max angle=45°) (Tournier and , F. Calamante, 2010). Streamlines were subsequently filtered down to 10 million using the SIFT algorithm (Smith et al., 2013).

Adhering to the procedures outlined in Rojkova et al. (2016) and Catani and Thiebaut de Schotten (2008), we virtually dissected the (1) the second and (2) third branches of the superior longitudinal fasciculus (SLF) and (3) the corticopinal tract (CST) as part of the visuomotor network in addition to the (A) arcuate fasciculus (AF), (B) inferior fronto-occipital fasiculus (IFOF), (C) inferior longitudinal fasciculus (ILF), and (D) the unciate fasciculus (UNC) as part of the language network.

Supplementary References

Catani, M., Thiebaut de Schotten, M., 2008. A diffusion tensor imaging tractography atlas for virtual in vivo dissections. Cortex. 44, 1105–32. https://doi.org/10.1016/j.cortex.2008.05.004

Dhollander, T., Raffelt, D., Connelly, A., 2016. Unsupervised 3-tissue response function estimation from single-shell or multi-shell diffusion MR data without a co-registered T1 image, in: ISMRM Workshop on Breaking the Barriers of Diffusion MRI. p. 5.

Jeurissen, B., Tournier, J.D., Dhollander, T., Connelly, A., Sijbers, J., 2014. Multi-tissue constrained spherical deconvolution for improved analysis of multi-shell diffusion MRI data. Neuroimage 103, 411–426. https://doi.org/10.1016/j.neuroimage.2014.07.061

Moulton, E., Valabrègue, R., Díaz, B., Kemlin, C., Leder, S., Lehéricy, S., Samson, Y., Rosso, C., Valabregue, R., Díaz, B., Kemlin, C., Leder, S., Lehéricy, S., Samson, Y., Rosso, C., 2018. Comparison of spatial normalization strategies of diffusion MRI data for studying motor outcome in subacute-chronic and acute stroke. Neuroimage 183, 186–199. https://doi.org/10.1016/j.neuroimage.2018.08.002

Raffelt, D., Tournier, J.D., Fripp, J., Crozier, S., Connelly, A., Salvado, O., 2011. Symmetric diffeomorphic registration of fibre orientation distributions. Neuroimage 56, 1171–1180. https://doi.org/10.1016/j.neuroimage.2011.02.014

Rojkova, K., Volle, E., Urbanski, M., Humbert, F., Dell'Acqua, F., Thiebaut de Schotten, M., 2016. Atlasing the frontal lobe connections and their variability due to age and education: a spherical deconvolution tractography study. Brain Struct. Funct. 221, 1751–1766. https://doi.org/10.1007/s00429-015-1001-3

Smith, R.E., Tournier, J.D., Calamante, F., Connelly, A., 2013. SIFT: Spherical-deconvolution informed filtering of tractograms. Neuroimage 67, 298–312. https://doi.org/10.1016/j.neuroimage.2012.11.049

Tournier, J.-D., , F. Calamante, and a. C., 2010. Improved probabilistic streamlines tractography by 2 nd order integration over fibre orientation distributions. Ismrm 88, 2010.